INFORMATION TO USERS

This manuscript has been reproduced from the microfilm master. UMI films the text directly from the original or copy submitted. Thus, some thesis and dissertation copies are in typewriter face, while others may be from any type of computer printer.

The quality of this reproduction is dependent upon the quality of the copy submitted. Broken or indistinct print, colored or poor quality illustrations and photographs, print bleedthrough, substandard margins, and improper alignment can adversely affect reproduction.

In the unlikely event that the author did not send UMI a complete manuscript and there are missing pages, these will be noted. Also, if unauthorized copyright material had to be removed, a note will indicate the deletion.

Oversize materials (e.g., maps, drawings, charts) are reproduced by sectioning the original, beginning at the upper left-hand corner and continuing from left to right in equal sections with small overlaps. Each original is also photographed in one exposure and is included in reduced form at the back of the book.

Photographs included in the original manuscript have been reproduced xerographically in this copy. Higher quality 6" x 9" black and white photographic prints are available for any photographs or illustrations appearing in this copy for an additional charge. Contact UMI directly to order.

UMI

A Bell & Howell Information Company
300 North Zeeb Road, Ann Arbor MI 48106-1346 USA
313/761-4700 800/521-0600

Structure and Reactivity of Dinuclear Complexes of Iridium

by

David Andrew Fine

A dissertation submitted in partial fulfillment
of the requirements for the degree of

Doctor of Philosophy

University of Washington

1996

Approved by D M. Heinekey
(Chairperson of Supervisory Committee)

Program Authorized
to Offer Degree Chemistry

Date 12/10/96

Doctoral Dissertation

In presenting this dissertation in partial fulfillment of the requirements for the Doctoral degree at the University of Washington, I agree that the Library shall make its copies freely available for inspection. I further agree that extensive copying of this dissertation is allowable only for scholarly purposes, consistent with "fair use" as prescribed in the U.S. Copyright Law. Requests for copying or reproduction of this dissertation may be referred to University Microfilms, 1490 Eisenhower Place, P.O. Box 975, Ann Arbor, MI 48106, to whom the author has granted "the right to reproduce and sell (a) copies of the manuscript in microfilm and/or (b) printed copies of the manuscript made from microform."

Signature David G Fair

Date 12/10/96

University of Washington

Abstract

Structure and Reactivity of Dinuclear Complexes of Iridium

by David Andrew Fine

Chairperson of the Supervisory Committee: Professor Dennis Michael Heinekey
Department of Chemistry

Reaction of $Cp^*Ir(CO)H_2$ ($Cp^* = \eta^5\text{-}C_5Me_5$) with triflic acid ($HOSO_2CF_3$) generates hydrogen and the hydride bridged dimer $[Cp^*Ir(CO)H]_2(\mu\text{-}H)^+$. Variable temperature (VT) ^1H NMR spectroscopy reveals that the bridging and terminal hydride ligands rapidly exchange at room temperature. Deprotonation of the trihydride cation dimer affords $[Cp^*Ir(CO)H]_2$. The hydride ligands rapidly permute between the iridium atoms at room temperature, as demonstrated by VT ^1H NMR of the isotopically labelled $[Cp^*Ir(^{13}CO)H]_2$. VT ^1H NMR of the lower symmetry analogue, $[Cp\text{^}Ir(CO)H]_2$ ($Cp\text{^} = \eta^5\text{-}C_5Me_4Et$), indicates that the chiral iridium centers are configurationally unstable. The dihydride dimers exist as unequal mixtures of two isomers, which rapidly interconvert at room temperature. X-ray structure determinations of $[Cp^*Ir(CO)H]_2$ and $[Cp^*Ir(CO)H]_2(\mu\text{-}H)^+$ indicate that the Ir-Ir bond length increases by 0.198 Å upon protonation.

The monomers $Cp^*Ir(CO)R_2$ (R = H, Me) both exhibit substantial thermal stability, though the dihydride slowly incorporates deuterium from C_6D_6 into its Cp^* methyl groups. Thermolysis of $[Cp^*Ir(CO)H]_2$ in the solid state or in methylcyclohexane-d_{14} leads to extrusion of H_2 and exclusive formation of $[Cp^*Ir(\mu\text{-}CO)]_2$, whereas thermolysis in C_6D_6 or CD_2Cl_2 is complicated by the co-generation of $Cp^*Ir(CO)H_2$. Photolysis of $[Cp^*Ir(CO)H]_2$ leads to clean fragmentation of the dimer to form $Cp^*Ir(CO)H_2$ and $[Cp^*Ir(\mu\text{-}CO)]_2$ in a 2:1 ratio. Chemical oxidation of both the dihydride monomer and dimer induces proton transfer reactions.

Reaction of $[Cp^*Ir(\mu\text{-}CO)]_2$ with one equivalent of $HBAr'_4\bullet(Et_2O)_2$ (Ar' = 3,5-$(CF_3)_2C_6H_3$) generates $[Cp^*Ir(CO)]_2(\mu\text{-}H)^+$. The mono-protonated dimer reacts instantaneously at room temperature with a variety of reagents, including H_2 and CO. Addition of a second equivalent of acid yields the dication $[Cp^*Ir(CO)]_2(\mu\text{-}H)_2^{2+}$.

The dimethyl dimer, $[Cp^*Ir(\mu\text{-}CO)Me]_2$, was generated by two different routes, the most successful of which involved reduction with Na/K alloy followed by alkylation with MeCl. Efforts to separate $[Cp^*Ir(\mu\text{-}CO)Me]_2$ from the persistent byproduct, $[Cp^*Ir(\mu\text{-}CO)]_2$, have found limited success.

TABLE OF CONTENTS

LIST OF FIGURES

Chapter 1

Chapter 2

Chapter 3

Chapter 4

LIST OF SCHEMES

Chapter 2

Chapter 3

Chapter 4

Chapter 5

LIST OF TABLES

Chapter 2

Chapter 4

ABBREVIATIONS AND SYMBOLS

Ar	aryl
BAr'_4	$B(3,5\text{-}(CF_3)_2C_6H_3)_4^-$
BDE	bond dissociation energy
br	broad
COD	1,5-cyclooctadiene
Cp	cyclopentadienyl, $(\eta^5\text{-}C_5H_5)^-$
Cp^*	pentamethylcyclopentadienyl, $(\eta^5\text{-}C_5(CH_3)_5)^-$
Cp^	ethyltetramethylcyclopentadienyl, $(\eta^5\text{-}C_5(CH_3)_4(CH_2CH_3))^-$
Cy	cyclohexyl
d	doublet
δ	chemical shift in ppm (NMR)
$\Delta G^{\ddagger}_{298}$	free energy of activation at specified temperature (K)
ΔG°_{298}	free energy of reaction at specified temperature (K)
$\Delta H^{\ddagger}$	enthalpy of activation
ΔH°	enthalpy of reaction
$\Delta S^{\ddagger}$	entropy of activation
ΔS°	entropy of reaction
dppm	1,2-bis(diphenylphosphino)methane, $Ph_2PCH_2PPh_2$
EI	electron impact (mass spectrometry)
eq	equation
equiv	equivalents
Et	ethyl
η	hapticity
eu	entropy units (cal mol^{-1} K^{-1})

h	hour
HOMO	highest occupied molecular orbital
HOTf	trifluoromethanesulfonic acid (triflic acid, $HOSO_2CF_3$)
IPA	isopropanol
^{i}Pr	isopropyl
IR	infrared spectroscopy
J	coupling constant
k	rate constant
L	ligand, neutral 2-electron donor
λ	wavelength
LUMO	lowest unoccupied molecular orbital
m	multiplet
M	molarity or metal atom
Me	methyl
MS	mass spectrometry
μ	descriptor for ligand bridging two metal atoms
NMR	nuclear magnetic resonance
ν	vibrational frequency
ORTEP	Oak Ridge thermal ellipsoid projection
OTf	trifluoromethanesulfonate (triflate, $SO_3CF_3^-$)
P	pressure
Ph	phenyl
PMDT	N, N, N', N", N"-pentamethyldiethylenetriamine
[PPN]Cl	$[(PPh_3)_2N]^+Cl^-$
q	quartet
R	alkyl

s	singlet (NMR) or strong absorbance (IR)
t	triplet
$t_{1/2}$	half-life
T_1	spin-lattice relaxation time
τ	lifetime
THF	tetrahydrofuran
TMS	tetramethylsilane
UV/Vis	ultra-violet/visible spectroscopy
VT	variable temperature (NMR)
w	weak spectral intensity

ACKNOWLEDGMENTS

Though only my name appears on the front of this dissertation, it is certainly not my accomplishment alone. This work is the result of the contributions of many people to whom I owe a great debt of gratitude. First, I would like to thank Prof. D. Michael Heinekey for his guidance, encouragement, and sense of humor. It was a pleasure working for Mike and a tremendous learning experience.

A large part of the enjoyment of working in the Heinekey group was due to interactions with the other members of the group –Beth Schomber, Greg Harper, Warren Oldham, Mark Voges, Amber Hinkle, Cathy Radzewich, Tom Luther, Mirjam van Roon, Diane Nagahara, Jack Wiley, and Heather Mellows– whose friendship and support were invaluable. I would especially like to thank Mark Voges for his careful review of the drafts of this thesis and for his *ki*, and Warren Oldham for sharing an office and a vacuum line with me and for flying across country to be at my defense.

The Inorganic division as a whole also enjoys a great camaraderie. I had many fruitful discussions over the years with members of the Mayer, Kovacs, and Goldberg groups, in particular Sam Tahmassebi, Seth Brown, Steve Shoner, and Jeff Ellison.

I would also like to thank Professor James Mayer for his valuable editorial comments on this and other documents, and for enlightening me on many aspects of chemistry.

Significant technical assistance was lent by Tom Pratum (NMR spectroscopy), Dave Barnhart (X-ray crystallography), and Jim Roe (mass spectrometry).

Sam Tahmassebi and Dave Kuhns are due special thanks for their enduring friendship and their ability to make me laugh during those times when it often would have been easier to scream.

The long road to this degree began with the love and support of my parents and

my sister, for which I am grateful. And the successful negotiation of the long final section of the often bumpy and circuitous road was achieved in large part due to the love, strength, and caring of my wife Betsy, for whom this work is dedicated.

CHAPTER 1

Introduction to Polynuclear Transition Metal Compounds

The theory that bonds can exist between metal atoms in a complex has been developed and validated only relatively recently in the history of chemistry. Until the 1960's the predominant model for the molecular structure of transition metal compounds was based upon the concepts of Alfred Werner developed around the turn of the century. This paradigm consisted of a central, ionized metal surrounded in a regular geometry by neutral or anionic ligands. Polynuclear transition metal compounds were known at the time but could be accommodated in the Wernerian scheme as mononuclear complexes joined exclusively through shared ligand atoms, which is correct for the majority of these compounds. However, there were a few compounds whose behavior could not be accounted for using Werner's model.

As early as 1844, Eugene Peligot reported[1] that addition of sodium or potassium acetate to a bright blue aqueous solution of chromium(II) ions produced red crystals, later to be identified as hydrated chromous acetate, $Cr_2(O_2CCH_3)_4(H_2O)_2$ (**1**), a compound believed to have a Cr-Cr quadruple bond. Over a century after Peligot's experiment, King and Garner (1950)[2] made magnetic susceptibility measurements that showed the compound to be diamagnetic, which along with its color and solubility were unusual when compared to other known chromium(II) salts. With the publication[3] of the crystal structure in 1970, the Cr-Cr bond of **1** was finally accepted and added to the burgeoning list of compounds containing metal-metal multiple bonds.

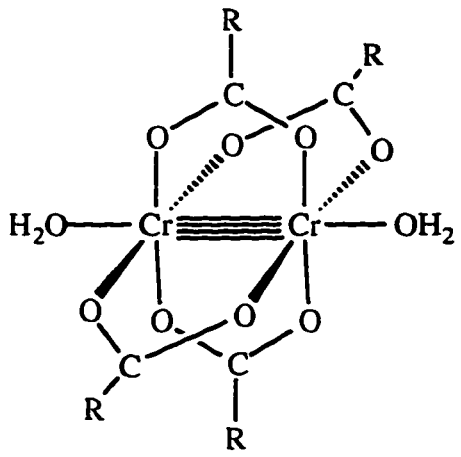

1

It was not until the advent of X-ray crystallography that many in the scientific community began to question Werner's model. In 1935,[4] and again in 1946,[5] Brosset found that the tungsten atoms in $K_3W_2Cl_9$, and then the molybdenum atoms in the lower chlorides of molybdenum, were separated by distances shorter than those found in the pure metal, though this provoked little discussion. Finally, in 1963, with the discovery[6,7] that $[Re_3Cl_{12}]^-$ consists of three $ReCl_4^-$ units in a triangular arrangement with Re-Re distances (2.47 Å) far shorter than those found in metallic Re (2.75 Å), metal cluster chemistry became a prominent area of research. Careful structural and electronic analysis lead the investigators to conclude that the rhenium atoms were connected by double bonds, the first explicit recognition of metal-metal multiple bonds.

Since these seminal investigations, the synthesis and study of compounds containing metal-metal bonds has developed into a large and active field of transition metal research.[1,8] A motivation for much of this work derives from the expectation that compounds containing metal-metal bonds might have access to reaction pathways unavailable to their monomeric counterparts. For example, the binding of a ligand to one metal center might induce enhanced reactivity at another bonded to it through electronic

or steric effects ("cooperativity"). The capacity to transfer ligands between metal centers can provide sites of coordinative unsaturation. Ligand-bridged metal centers can constrain a geometry that promotes stereoselective reactivity. In addition, adjacent metals can act as a template for the assembly of molecules, by holding reactive fragments (ligands) in proximity.

Another impetus for research of di- and polynuclear organometallic complexes is their proposed utility as discrete molecular models for metal surface chemistry.[9-13] To determine the nature of the bonding of small molecules to a metal surface, as well as elucidate the mechanism of reactions of those molecules, can be exceedingly difficult. Insight gained from structural, and perhaps mechanistic studies of the homogeneous chemistry of polynuclear compounds might be applicable to the heterogeneous chemistry of a metal surface. The structural analogy is compelling; Somorjai has noted[12] that "For every surface species where structure and atomic location have been determined, there is at least one or more equivalent organometallic complexes that exhibit the same structure and bonding behavior." Some known examples of this correspondence are shown in Figure 1.1.

An additional parallel between polynuclear organometallic compounds and metal surfaces is the ability of ligands like H or CO to migrate between metal centers.[9] The activation barrier for hydrogen atom diffusion on tungsten or nickel surfaces is only 6 to 10 kcal/mol.[9] Migration of hydride ligands between metal centers in polynuclear complexes typically encounter activation barriers of a comparable magnitude. For example, the free energy of activation (298 K) for bridge-terminal hydride ligand exchange in $[Cp^*Ir(CO)H]_2(\mu\text{-}H)^+$ (see Chapter 2) is 8.8 kcal/mol.

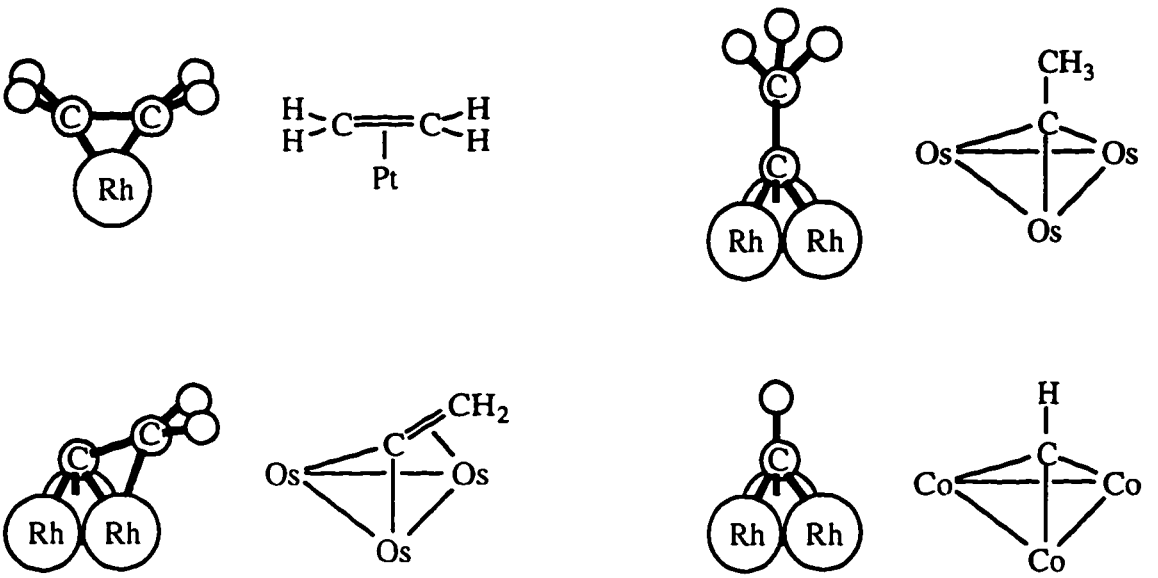

Figure 1.1. Bonding of hydrocarbon species to a rhodium surface and in organometallic complexes.[12,14] The small spheres without labels represent hydrogen atoms. Ancillary ligands in the organometallic complexes have been omitted for clarity.

Mechanistic comparisons are not yet as well documented, though there are a growing number of examples. Maitlis and co-workers recently reported[13] studies of a series of rhodium dimers which seem to shed new light on the mechanism of C-C coupling reactions in heterogeneous Fischer-Tropsch catalysis (Figure 1.2). Decomposition of $[Cp^*Rh(\mu\text{-}CH_2)Me]_2$ in the presence of a one electron oxidant generates propene and methane and is believed to proceed via coupling of a σ-vinyl ligand with a bridging methylene group. Further work lead them to propose an "alkenyl" mechanism for the C-C couplings of the Fischer-Tropsch reaction.

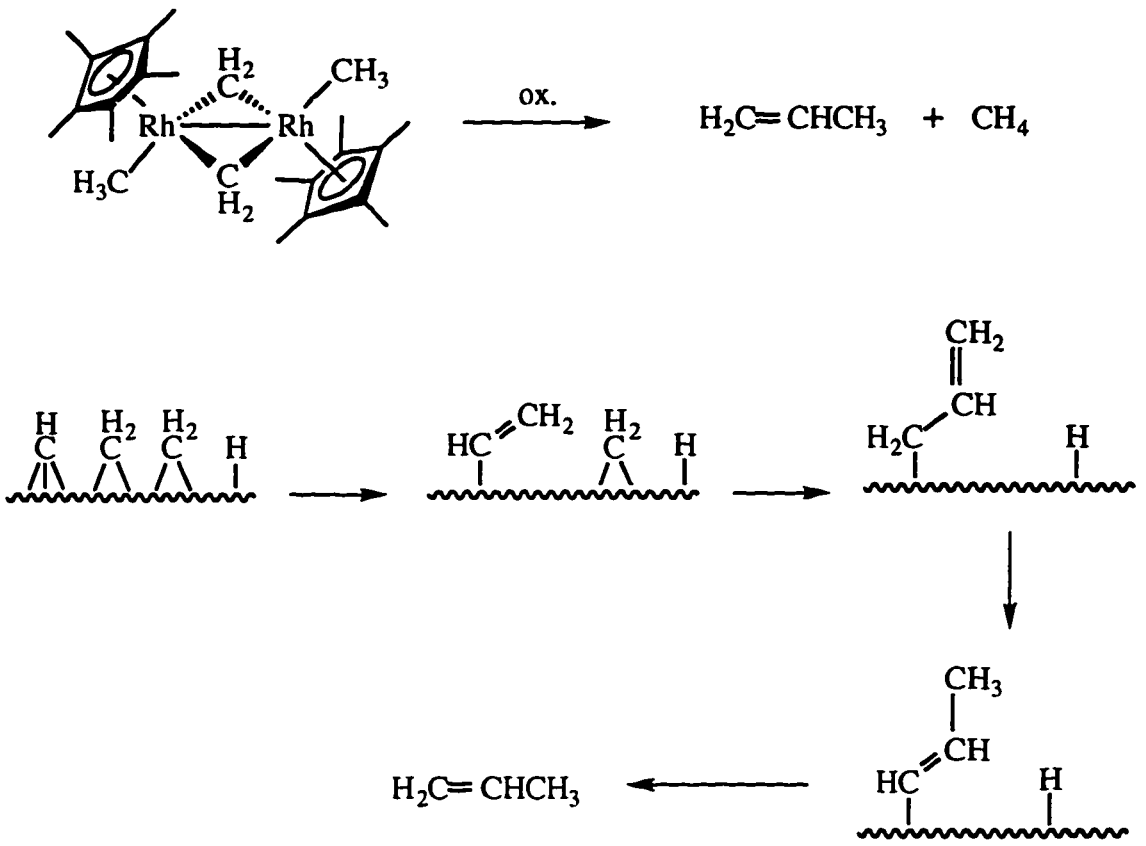

Figure 1.2. Decomposition of $[Cp^*Rh(\mu\text{-}CH_2)Me]_2$ to propene and methane (top) and the analogous mechanism proposed for C-C bond making at a metal surface during Fischer-Tropsch catalysis.

Notes to Chapter 1

(1) Cotton, F. A.; Walton, R. A. *Multiple Bonds between Metal Atoms;* 2nd ed.; Clarendon: Oxford, 1993, and references therein.

(2) King Jr., W. R.; Garner, C. S. *J. Chem. Phys.* **1950**, *18*, 689-691.

(3) Cotton, F. A.; DeBoer, B. G.; LaPrade, M. D.; Pipal, J. R.; Ucko, D. A. *J. Am. Chem. Soc.* **1970**, *92*, 2926-2927.

(4) Brosset, C. *Nature* **1935**, *135*, 874.

(5) Brosset, C. *Arkiv for Kemi, Miner. Geol.* **1946**, *A22*(11).

(6) Bertrand, J. A.; Cotton, F. A.; Dollase, W. A. *J. Am. Chem. Soc.* **1963**, *85*, 1349-1350.

(7) Robinson, W. T.; Fergusson, J. E.; Penfold, B. R. *Proc. Chem. Soc.* **1963**, 116.

(8) *Reactivity of Metal-Metal Bonds*; Chisholm, M. H., Ed.; ACS Symposium Series 155; American Chemical Society: Washington, D.C., 1981.

(9) Muetterties, E. L.; Rhodin, T. N.; Band, E.; Brucker, C. F.; Pretzer, W. R. *Chem. Rev.* **1979**, *79*, 91-137.

(10) Muetterties, E. L.; Krause, M. J. *Angew. Chem. Int. Ed. Engl.* **1983**, *22*, 135-148.

(11) Marks, T. *Acc. Chem. Res.* **1992**, *25*, 57-65.

(12) Somorjai, G. A. In *Perspectives in Catalysis*; Thomas, J. M. and Zamaraev, K. I., Eds.; Blackwell Scientific: Oxford, 1992; pp 147-167.

(13) Maitlis, P. M.; Long, H. C.; Quyoum, R.; Turner, M. L.; Wang, Z.-Q. *J. Chem. Soc., Chem. Commun.* **1996**, 1-8.

(14) Somorjai, G. A. *Pure Appl. Chem.* **1988**, *60*, 1499-1516.

CHAPTER 2

Dihydride Dimers Of Iridium: Synthesis, Structure, and Dynamics of $[(C_5Me_4R)Ir(CO)H]_2$ (R = Me, Et)[1]

Introduction

There is a vast literature regarding the preparation and chemistry of monomeric transition metal compounds containing hydride ligands.[2-4] In contrast, investigations directed at hydride dimers are comparatively few. One contributing factor is the lack of general synthetic methodologies. Indeed, a large percentage of bimetallic complexes containing hydride ligands were obtained unintentionally in attempts to prepare hydride monomers.[5] A route that we have found particularly useful employs condensation of monomeric hydride complexes induced by protonation to afford dinuclear compounds in excellent yield (equation 2.1).

(2.1)

The special fluxionality of hydride ligands bound to transition metal monomers, clusters, and bulk metal surfaces, is well documented.[2,6] The migration of hydride ligands between metal centers is often quite facile, and is indicative of their proclivity to change binding from terminal to bridging modes. The inclination of hydrides to adopt a bridging position in complexes containing metal-metal bonds is manifest by the paucity of dinuclear compounds containing only terminal hydrides. The only well-characterized examples of dimers containing terminal hydride ligands with unsupported metal-metal bonds are the osmium carbonyl dimers $H_2Os_2(CO)_8$,[7] $H_2Os_2(CO)_6(PPh_3)_2$,[8] and $H(Me)Os_2(CO)_8$,[9] and more recently $[CpIr(P(OPh)_3)H]_2$[1] (Cp = η^5-C_5H_5) (vide infra).

An iron analogue,[10] $H_2Fe_2(CO)_8$, is less well characterized but is thought to have terminal hydride ligands based upon the ^1H NMR chemical shift value for the hydrides.

The facility with which hydride ligands permute in transition metal complexes can lead to changes in chirality at the metal center(s). A classic example is the stereochemical nonrigidity in complexes of the form, $CpMo(CO)_2(L)H$ (L = various phosphines), investigated by Faller and Anderson.[11,12] The ground state structure can best be described as square pyramidal with the Cp ligand occupying the apical position. These compounds can undergo relatively facile intramolecular cis-trans isomerizations ($\Delta G^{\ddagger}_{298}$ = 13 kcal mol^{-1}) (Scheme 2.1).

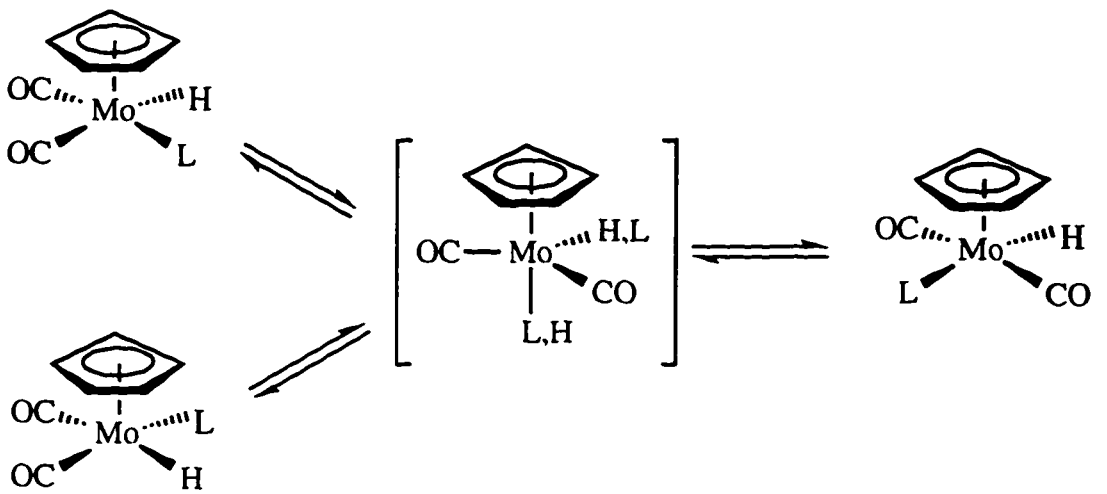

Scheme 2.1

Moreover, variable temperature (VT) NMR studies reveal an even lower energy rearrangement process. The cis isomer is chiral and rapid interconversion of the cis enantiomers occurs prior to any cis-trans isomerization. Both processes are believed to proceed via a trigonal bipyramidal transition state, though it is unclear whether the hydride occupies an axial or equatorial position. Similar rearrangements do occur when the hydride is replaced by alkyls or halides, however, the kinetic barriers become much greater ($\Delta G^{\ddagger}_{298}$ = 20-25 kcal mol^{-1} for cis-trans interconversion).

Previously in the Heinekey group,[13] monomeric trihydride cations of the form $CpIrLH_3^+$ (L = various phosphines) were prepared in order to investigate their unusual NMR properties. It was subsequently found[14] that thermolysis of $CpIr(P(OPh)_3)H_3^+$, generated in situ from $CpIr(P(OPh)_3)H_2$ and triflic acid (HOTf), affords the trihydride cation dimer $[CpIr(P(OPh)_3)H]_2(\mu\text{-}H)^+$ (**5**). Deprotonation of **5** yields the neutral dihydride dimer $[CpIr(P(OPh)_3)H]_2$ (**8**), which exhibits complex VT NMR behavior.[1]

To further investigate the fluxionality of cyclopentadienyl hydride dimers of iridium, we have prepared the carbonyl analogues $[Cp^*Ir(CO)H]_2$ (**6**) ($Cp^* = \eta^5\text{-}C_5Me_5$) and $[Cp^\wedge Ir(CO)H]_2$ (**7**) ($Cp^\wedge = \eta^5\text{-}C_5Me_4Et$). This chapter details the synthesis, VT NMR analysis, and X-ray diffraction study of complexes **6** and **7**. In addition, the fluxionality of the protonated precursors to **6** and **7**, $[Cp^*Ir(CO)H]_2(\mu\text{-}H)^+$ (**3**) and $[Cp^\wedge Ir(CO)H]_2(\mu\text{-}H)^+$ (**4**), is discussed. A solid-state structure determination of **3** by X-ray diffraction is presented. Solution-state dynamics of **3**, **4**, **6**, and **7**, are compared to that of the corresponding $Cp/P(OPh_3)$ analogues (**5** and **8**).

Results

Synthesis.

Our preparation[15] of $Cp^*Ir(CO)Cl_2$ from $[Cp^*IrCl_2]_2$ is a slight modification of the reported method.[16] A solution of $[Cp^*IrCl_2]_2$ in methylene chloride is stirred under an atmosphere of carbon monoxide. The solution is transferred into cold, stirring heptane, precipitating the bright yellow $Cp^*Ir(CO)Cl_2$.

Reaction of $Cp^*Ir(CO)Cl_2$ with zinc in acetic acid/methanol affords the monomeric dihydride $Cp^*Ir(CO)H_2$ (**1**), which is recovered via sublimation as low-melting, air-sensitive, pale yellow crystals (Scheme 2.2). The dihydride can also be recovered by crystallization from cold (-78 °C) pentane. Well resolved ^1H NMR spectra

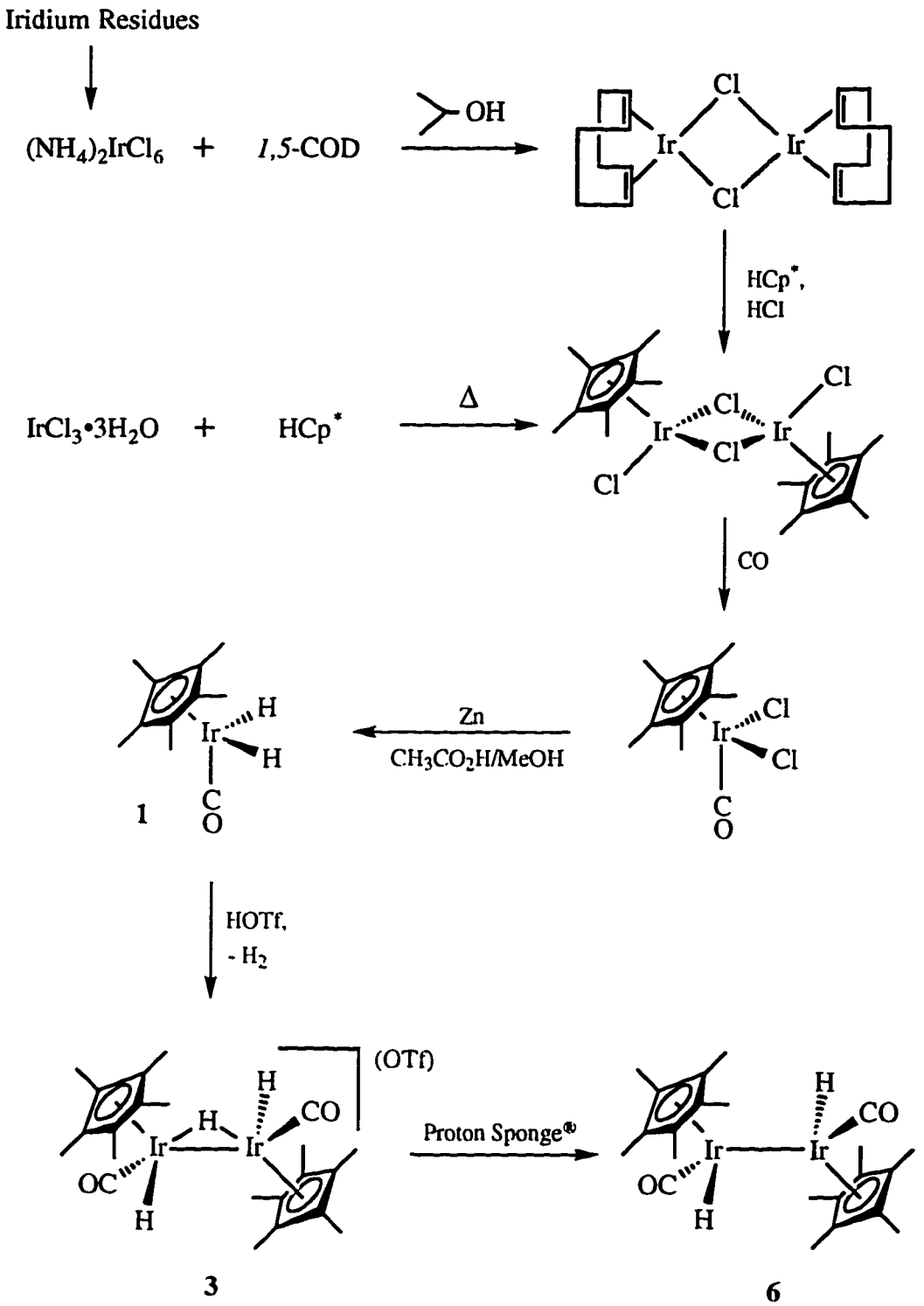
Iridium Residues
(NH4)2IrCl6 + 1,5-COD
OH
Cl
Ir
Ir
Cl
HCp*,
HCl
IrCl3•3H2O + HCp*
Δ
Cl
Ir
Cl
Ir
Cl
Cl
CO
Zn
CH3CO2H/MeOH
H
Ir
H
C
O
1
Cl
Ir
Cl
C
O
HOTf,
- H2
(OTf)
H
CO
H
Ir
Ir
OC
H
Proton Sponge®
H
CO
Ir
Ir
OC
H
3
6

Scheme 2.2

of **1** reveal fine splitting of the Cp^* and hydride resonances, evidence of a small 4-bond coupling (J = 0.7 - 0.8 Hz) between the two.[17]

Protonation of **1** in CH_2Cl_2 at low temperature (CO_2/IPA bath) is effected with triflic acid ($HOSO_2CF_3$, 0.5 equiv). Upon warming to room temperature, the pale yellow solution becomes deep orange-yellow and H_2 is generated. A ^1H NMR spectrum of the reaction run in CD_2Cl_2 seems to show that no reaction has occurred: a single resonance in the Cp^* region and another upfield in the hydride region appear at approximately the same chemical shifts as are found for the starting dihydride (δ 2.22, -16.46 as compared to δ 2.22, -16.48 for **1**). Closer examination of the spectrum reveals that the ratio of the Cp^* to hydride intensities is now 10:1, rather than 7.5:1. The greater chemical shift range of a $^{13}C\{^1H\}$ NMR spectrum confirms that a new compound has been formed. An IR spectrum of the isolated solid (Nujol mull) exhibits two strong absorbances at 2020 and 1990 cm^{-1}, characteristic of terminal CO stretches,[18] and a weak absorbance at 2111 cm^{-1} indicative of a terminal Ir-H stretch.[4] These data, together with X-ray diffraction and low temperature NMR experiments (vide infra), support the formulation of this compound as the dimeric cation $\{[Cp^*Ir(CO)H]_2(\mu\text{-}H)\}OTf$ (**3**).

Complex **3** is readily deprotonated by relatively mild bases such as 1,8-bis(dimethylamino)naphthalene (Proton Sponge®) to afford the neutral dimer $[Cp^*Ir(CO)H]_2$ (**6**). An IR spectrum of **6** (Nujol) reveals two strong absorbances characteristic of terminal CO stretches (1971, 1942 cm^{-1}), and a weak absorbance at 2180 cm^{-1} indicative of a terminal Ir-H stretch. Single crystal X-ray diffraction (vide infra) confirms the unusual solid-state structure of **6**, which possesses neither bridging carbonyls nor bridging hydrides to support the Ir-Ir bond. The dihydride dimer (**6**) is an air-stable solid and sublimes readily at 95 °C under static vacuum. Sealed solutions of **6** are light-sensitive and decompose over the course of several weeks in room light (see

Chapter 3). The structural dynamics of **6** in solution, as revealed by variable temperature NMR spectroscopy, proved to be quite complex, as described below.

The same synthetic path was followed in the preparation of ^{13}C labelled derivatives of the Cp* complexes. Reaction of $[Cp^*IrCl_2]_2$ with ^{13}CO gives $Cp^*Ir(^{13}CO)Cl_2$. Subsequent transformations were carried out as detailed above for the unlabelled analogues.

An additional probe of the stereodynamics of these complexes is available in the lower symmetry derivatives prepared with the ethyltetramethylcyclopentadienyl ligand Cp^ (Cp^ = η^5-C_5Me_4Et). $[Cp^{\wedge}IrCl_2]_2$ has been prepared previously[19] from NaCp^ and $IrCl_3 \cdot 3H_2O$, but the reported yield was only 16%. We find that the procedure developed by El Amouri and co-workers[20] for the preparation of the Cp* analogue, $[Cp^*IrCl_2]_2$, from $[(COD)IrCl]_2$, gives much better yields (56%). $\{[Cp^{\wedge}Ir(CO)H]_2(\mu\text{-}H)\}OTf$ (**4**) and $[Cp^{\wedge}Ir(CO)H]_2$ (**7**) were prepared from $Cp^{\wedge}Ir(CO)H_2$ (**2**) by the procedures outlined in Scheme 2.2. Compounds **2** and **4** are recovered as oils, whereas complex **7** precipitates from heptane as bright yellow crystals suitable for X-ray diffraction.

Solid State Structures of $\{[Cp^*Ir(CO)H]_2(\mu\text{-}H)\}BAr'_4$ (3-BAr'_4), $[Cp^*Ir(CO)H]_2$ (6), and $[Cp^{\wedge}Ir(CO)H]_2$ (7).

Summaries of the crystallographic data are given in Tables 2.1 and 2.2. ORTEP diagrams are shown in Figures 2.1-2.4. Selected bond lengths and angles are given in Table 2.3. Tables of atomic coordinates, and isotropic and anisotropic displacement coefficients are presented in the appendix.

Table 2.1 Summary of Crystal Data for $\{[Cp^*Ir(CO)H]_2(\mu\text{-}H)\}BAr'_4$ (**3-BAr'$_4$**)

Empirical Formula	$C_{54}H_{45}BF_{24}Ir_2O_2$
Color; Habit	Green trapezoid
Crystal Size (mm)	0.12 x 0.28 x 0.40
Crystal System	Triclinic
Space Group	P1(bar)
Unit Cell Dimensions	a = 12.873 (3) Å
	b = 21.209 (4) Å
	c = 22.364 (4) Å
	α = 67.02 (3)°
	β = 86.61 (3)°
	γ = 83.91 (3)°
Volume	5589 (3) Å^3
Z	4
Formula Weight	1577.2
Density (calc.)	1.856 mg/m^3
Absorption Coefficient	4.878 mm^{-1}
F(000)	2980
Radiation	MoKα (λ = 0.71073 Å)
Temperature (K)	183
Monochromator	Highly oriented graphite crystal
2θ Range	2 to 45°
Scan Type	ω
Scan Speed	Variable; 1.5 to 5.5°/min. in ω
Scan Range (ω)	0.80 + 0.35(tan θ)°
Reflections Collected	15318
Independent Reflections	14536 (R_{int} = 2.58 %)
Observed Reflections	10793 (F > 4.0σ(F))
Number of Parameters Refined	1496
Final R Indices (obs. data)	R = 4.48 %, wR = 6.51 %
R Indices (all data)	R = 6.78 %, wR = 7.45 %
Goodness of Fit	1.11

Table 2.2 Summary of Crystal Data for $[Cp^*Ir(CO)H]_2$ (**6**), and $[Cp^\wedge Ir(CO)H]_2$ (**7**).

	6	**7**
Empirical Formula	$C_{22}H_{32}Ir_2O_2$	$C_{24}H_{36}Ir_2O_2$
Color; Habit	Yellow needle	Clear yellow rhomb.
Crystal Size (mm)	0.1 x 0.1 x 0.3	0.25 x 0.30 x 0.35
Crystal System	Orthorhombic	Monoclinic
Space Group	Pbca	C2/c
Unit Cell Dimensions	a = 15.107 (2) Å	a = 20.262 (2) Å
	b = 16.165 (2) Å	b = 7.913 (2) Å
	c = 17.853 (3) Å	c = 16.771 (3) Å
		β = 117.52 (2)°
Volume	4359.9 (1) Å^3	2369.7 (5) Å^3
Z	8	4
Formula Weight	712.9	741.0
Density (calc.)	2.172 mg/m^3	2.077 mg/m^3
Absorption Coefficient	12.209 mm^{-1}	11.236 mm^{-1}
F(000)	2672	1400
Radiation	MoKα (λ = 0.71073 Å)	
Temperature (K)	183	183
Monochromator	Highly oriented graphite crystal	
2θ Range	2.0 to 50.0°	2.0 to 50.0°
Scan Type	2θ-ω	2θ-θ
Scan Speed	Constant; 1.5 to 5.5°/min.	Variable; 1.5 to 5.5°/min. in ω
Scan Range (ω)	0.80 + 0.35(tan θ)°	0.80 + 0.35(tan θ)°
Reflections Collected	4127	3976
Independent Reflections	3817 (R_{int} = 2.60 %)	2084 (R_{int} = 9.11 %)
Observed Reflections	2275 (F > 4.0σ(F))	1753 (F > 4.0σ(F))
Number of Parameters Refined	236	132
Final R Indices (obs. data)	R = 3.75%, wR = 4.55%	R = 2.98%, wR = 3.77%
R Indices (all data)	R = 9.21%, wR = 6.70%	R = 4.67%, wR = 8.00%
Goodness of Fit	1.04	1.03

Table 2.3 Selected Bond Distances and Angles for $\{[Cp^*Ir(CO)H]_2(\mu\text{-}H)\}BAr'_4$ (**3-BAr'$_4$**), $[Cp^*Ir(CO)H]_2$ (**6**), and $[Cp^{\wedge}Ir(CO)H]_2$ (**7**).

	3[a]	**3**[a]	**6**	**7**[b]
Bond Length (Å)				
Ir(1)-Ir(2)	2.935(1)[d]	2.921(1)	2.730(1)	2.724(1)
Ir(1)-C(1)	1.897(17)	1.887(12)	1.817(16)	1.828(7)
Ir(2)-C(2)	1.883(14)	1.856(16)	1.829(15)	
Ir(1)-Cp(1)[c]	1.881	1.883	1.908	1.909
Ir(2)-Cp(2)	1.878	1.867	1.897	
C(1)-O(1)	1.099(20)	1.135(15)	1.158(19)	1.146(8)
C(2)-O(2)	1.119(17)	1.175(19)	1.150(18)	
Bond Angle (°)				
Ir(1)-Ir(2)-Cp(2)	131.6	132.2	128.8	128.4
Ir(2)-Ir(1)-Cp(1)	131.8	130.6	129.9	
Ir(1)-Ir(2)-C(2)	77.8(4)	78.5(4)	85.1(5)	85.5(3)
Ir(2)-Ir(1)-C(1)	80.9(4)	82.0(4)	85.4(5)	
Ir(1)-C(1)-O(1)	179.4(15)	176.8(11)	179.0(6)	178.5(5)
Ir(2)-C(2)-O(2)	177.6(10)	176.6(11)	177.8(13)	
Cp(1)-Ir(1)-C(1)	130.6	130.4	136.2	137.0
Cp(2)-Ir(2)-C(2)	134.0	131.6	136.0	
Dihedral Angle (°)				
Cp(1)-Ir(1)-Ir(2)-Cp(2)	153.1	158.2	142.9	122.8
C(1)-Ir(1)-Ir(2)-C(2)	70.3	72.8	83.0	64.5

[a]Crystal structure of **3** consists of two unique molecules per asymmetric unit. [b]Crystal structure of **7** possesses molecular center of inversion. [c]Cp(1) refers to the centroid of Cp attached to Ir(1). [d]Standard deviations in the least significant figures are enclosed in parentheses following the value.

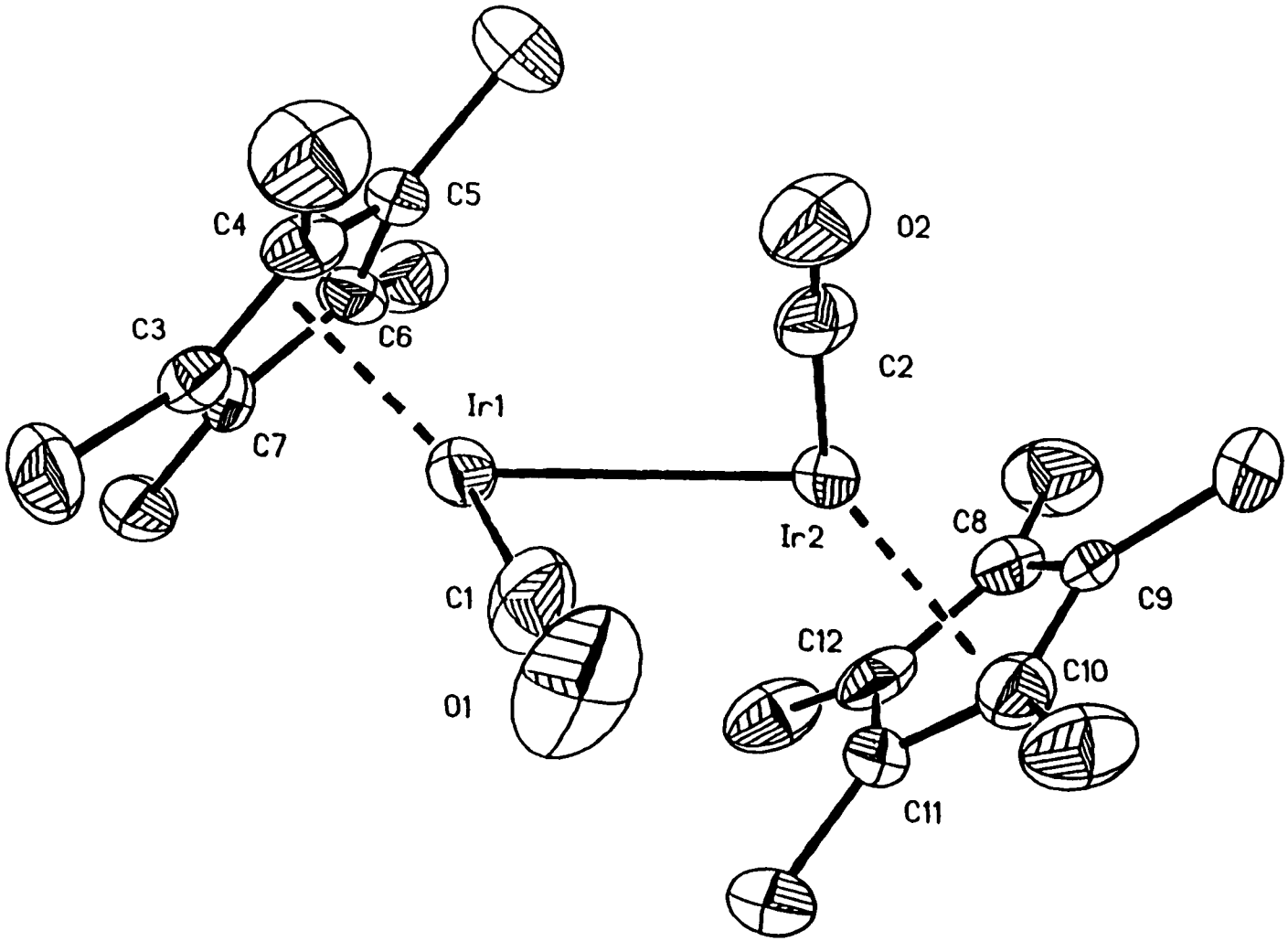

Figure 2.1. ORTEP representation of $\{[Cp^*Ir(CO)H]_2(\mu\text{-}H)\}BAr'_4$ (**3-BAr'$_4$**). Thermal ellipsoids are shown at 50% probability. Hydrogen atoms are omitted for clarity. Hydride ligands were not located. The BAr'_4 anion is not pictured.

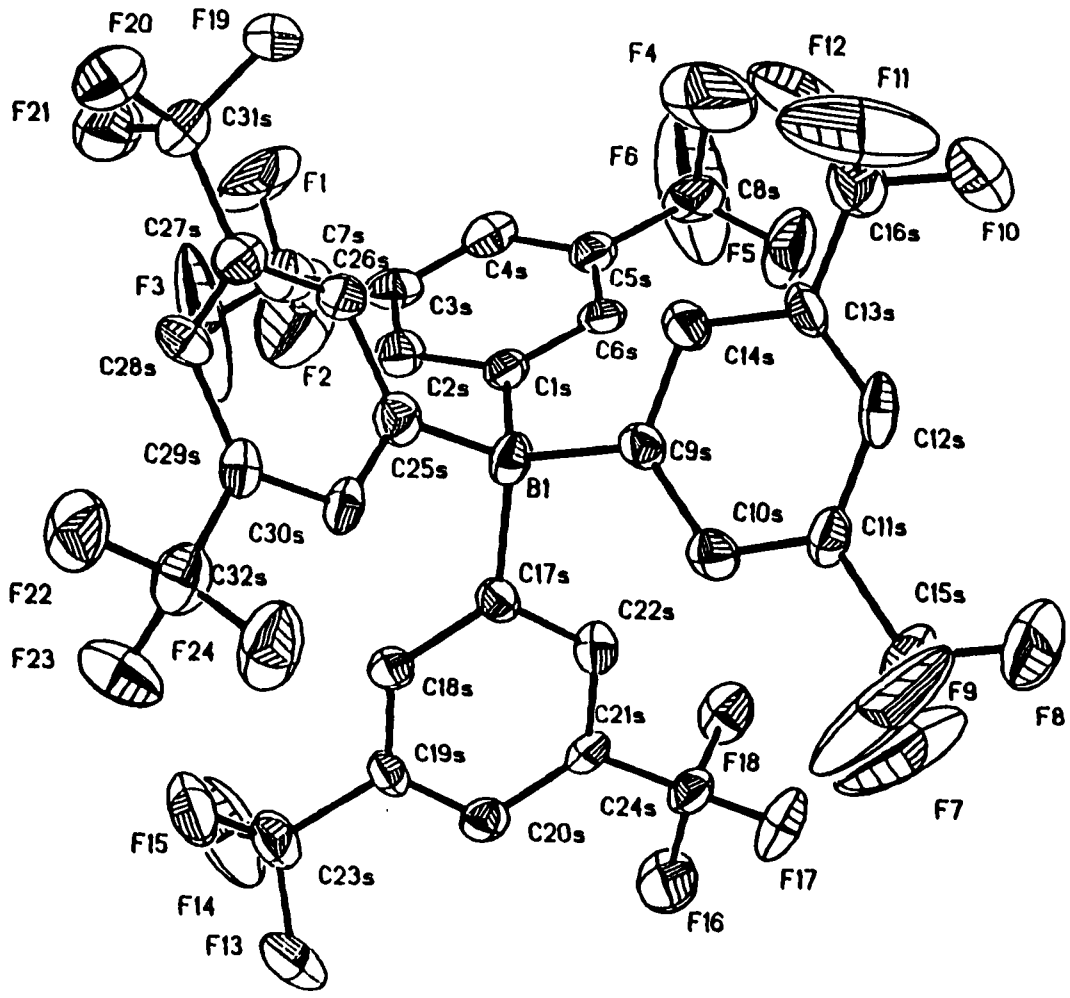

Figure 2.2. ORTEP representation of the BAr'_4 anion of **3**. Thermal ellipsoids are shown at 50% probability. Hydrogen atoms are omitted for clarity.

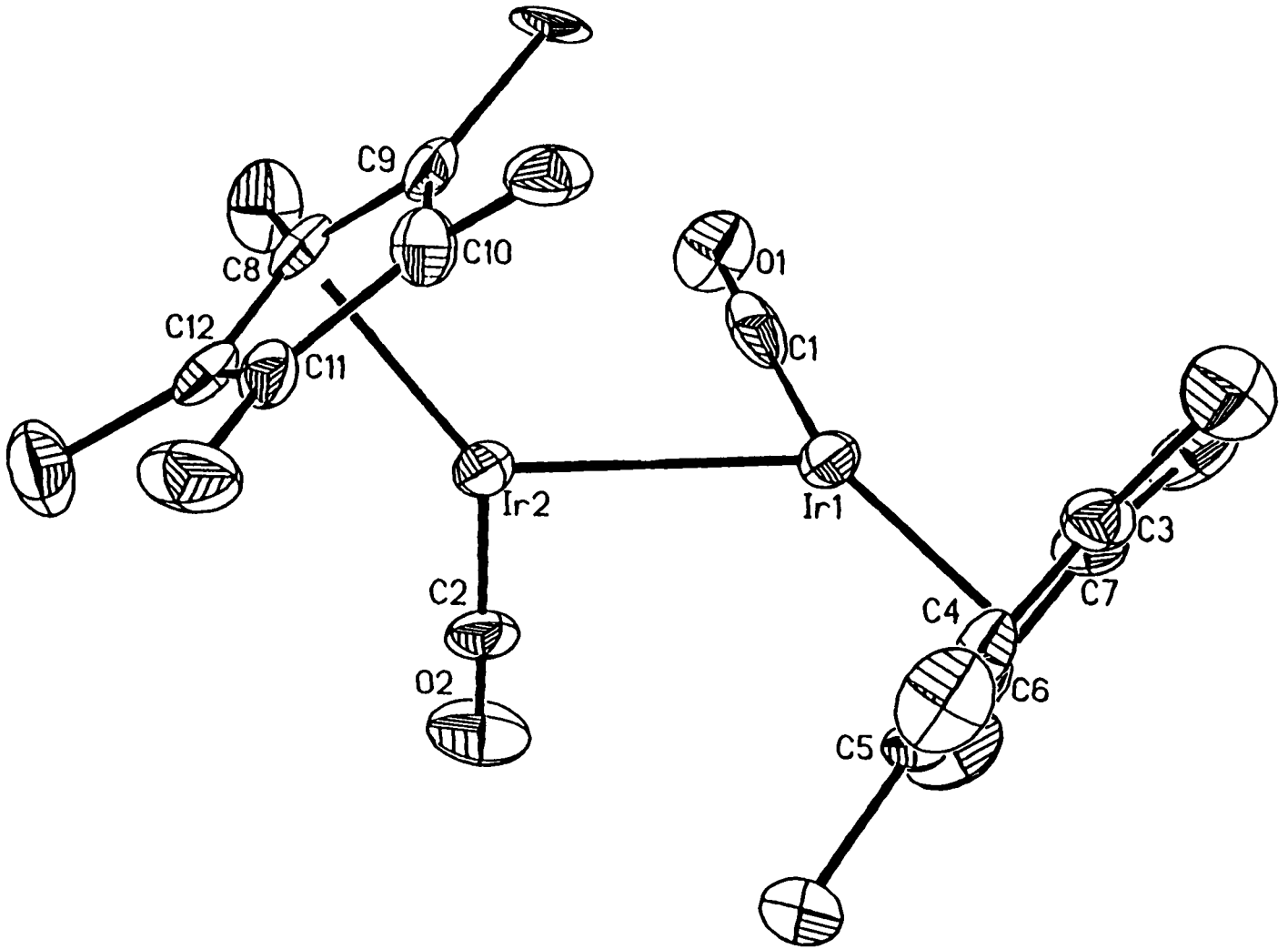

Figure 2.3. ORTEP representation of $[Cp^*Ir(CO)H]_2$ (**6**). Thermal ellipsoids are shown at 50% probability. Hydrogen atoms are omitted for clarity. Hydride ligands were not located.

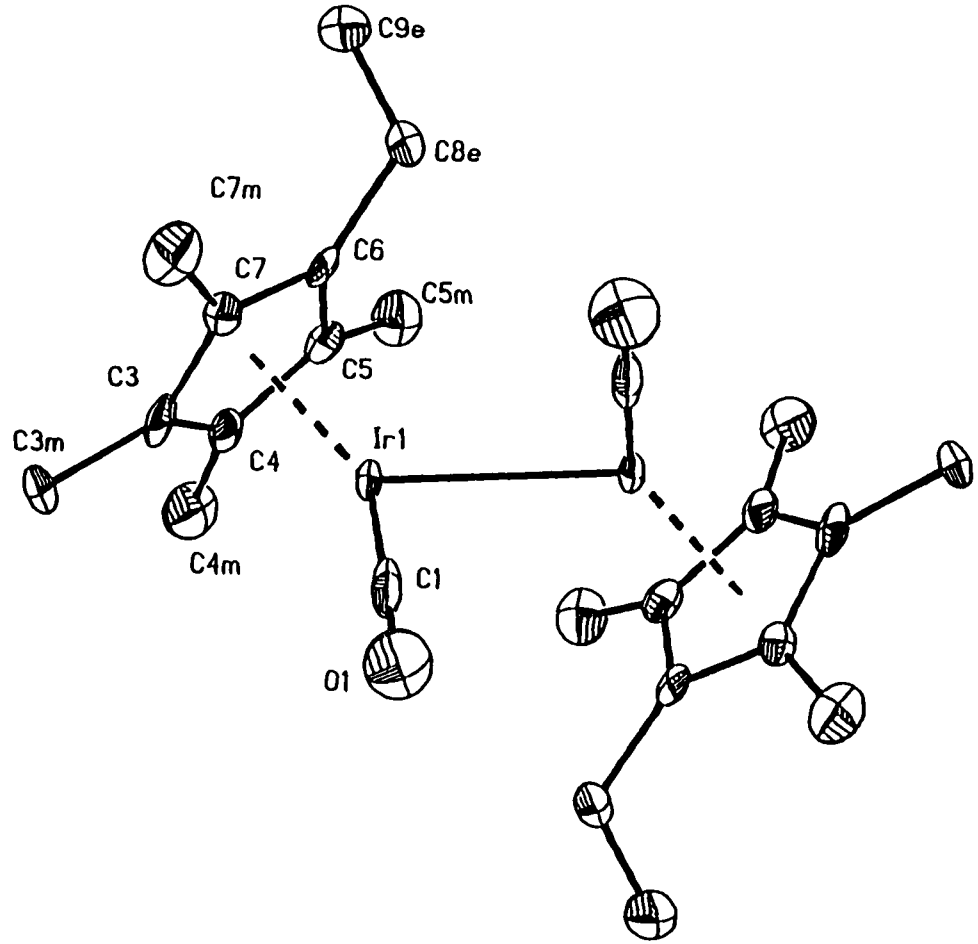

Figure 2.4. ORTEP representation of $[Cp^{\wedge}Ir(CO)H]_2$ (7). Thermal ellipsoids are shown at 50% probability. Hydrogen atoms are omitted for clarity. Hydride ligands were not located.

Variable Temperature (VT) NMR Spectroscopy of $[Cp'Ir(CO)H]_2(\mu\text{-}H)^+$ (Cp' = Cp^* (3), Cp^ (4)).

The room temperature ^1H NMR spectrum of $\{[Cp^*Ir(CO)H]_2(\mu\text{-}H)\}OTf$ (**3**) in $CDFCl_2$ exhibits a single sharp resonance in the Cp^* region at 2.23 ppm and another in the hydride region at −16.44 ppm. At lower temperatures, the hydride singlet decoalesces into two broad resonances. Even at the lowest attainable temperature, a static limit ^1H NMR spectrum could not be obtained. At 138 K in $CDFCl_2$ (500 MHz), the two broad resonances are observed at −15.3 and −18.1 ppm, with approximate integrals in the ratio of 2:1. The ^1H NMR spectrum of the ^{13}CO substituted analogue of **3**, $[Cp^*Ir(^{13}CO)H]_2(\mu\text{-}H)^+$ (**3***), exhibits a broad resonance in the hydride region at ambient temperature. Selective homonuclear decoupling of the Cp^* resonance removes the small 4-bond coupling and resolves the broad hydride lump into a sharp triplet ($^2J_{H\text{-}C}$ = 3.4 Hz). At low temperature in $CDFCl_2$, the two hydride peaks are too broad to resolve coupling.

The Cp^ analogue, $[Cp^\wedge Ir(CO)H]_2(\mu\text{-}H)^+$ (**4**), similarly shows a single sharp hydride resonance in the ^1H NMR spectrum at room temperature, which broadens at lower temperatures. These observations, together with those for the $CpIr(P(OPh_3))$ analogue,[1,14] $[CpIr(P(OPh)_3)H]_2(\mu\text{-}H)^+$ (**5**), indicate that the ground state structures of **3**, **4**, and **5**, each have two terminal hydride ligands and one bridging hydride ligand and that a rapid rearrangement process causes site exchange. In these trihydride cation dimers, the downfield peak is assigned to the two terminal hydride ligands and the upfield peak is attributed to the bridging hydride ligand.

The inability to freeze out the facile bridge-terminal hydride migration in **3** or **4** precludes the determination of the activation parameters for the exchange using NMR line shape analysis. However, a static limit ^1H NMR spectrum of the hydride region of **5** was obtained previously.[14] We prepared **5** according to the reported[1,14] method.

Lineshape analysis of spectra obtained in the temperature range 153-210 K furnished rate constants, from which were derived the following activation parameters by means of an Eyring plot (Figure 2.5): $\Delta G^{\ddagger}_{298} = 8.8 \pm 0.6$ kcal mol^{-1} , $\Delta H^{\ddagger} = 6.8 \pm 0.2$ kcal mol^{-1} and $\Delta S^{\ddagger} = -6.8 \pm 1.2$ cal mol^{-1} K^{-1}.

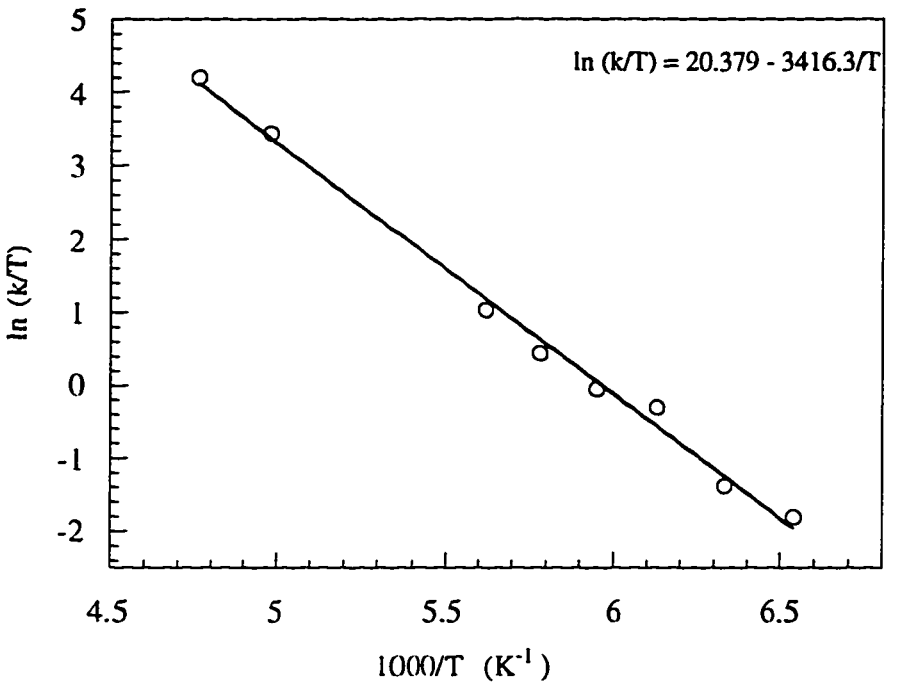

Figure 2.5. Eyring plot for hydride migration between terminal and bridging positions in $[CpIr(P(OPh)_3)H]_2(\mu\text{-}H)^+$ (**5**).

The trihydride cation dimers **3**, **4**, and **5**, each contain two chiral iridium centers. The ethyltetramethylcyclopentadienyl (Cp^) ligands of compound **4** are useful probes of stereochemistry (Figure 2.6). The Cp^ methyl groups, ring carbons, and methylene protons are diastereotopic (chemically inequivalent) if the Cp^ ligand is attached (η^5) to a stereochemically rigid chiral metal center. If the Cp^ ligand is connected to a chiral metal center that is configurationally unstable on the NMR timescale, i.e. undergoing rapid

racemization, then the methylene protons, and methyl groups and ring carbons on opposite sides of the ring, are rendered equivalent. A room temperature ^1H NMR spectrum of **4** shows only two singlets for the Cp^ methyl groups (δ 2.22, 12 H; δ 2.20, 12 H) and a simple quartet for the methylene protons. A $^{13}C\{^1H\}$ NMR spectrum of **4** at ambient temperature reveals two resonances for the methyl groups (δ 10.6, 10.5) and two resonances for the ring carbons bonded to the methyl groups (δ 102.1, 101.4). These data indicate that the iridium centers in **4** (and undoubtedly **3** and **5**) are stereochemically nonrigid in solution at room temperature. This is not surprising given the facile hydride exchange in these compounds. Alternatively, it is possible that the iridium centers of **4** are not fluxional but that the chemical shift differences for the diastereotopic protons and carbons are too small to resolve. However, this seems unlikely, since stereochemically rigid chiral metal centers with attached Cp^ ligands are known in which the diastereotopic peaks were resolved by ^1H NMR spectroscopy,[19,21] including the low temperature spectra of the neutral dihydride dimer $[Cp^{\wedge}Ir(CO)H]_2$ (**7**) (vide infra).

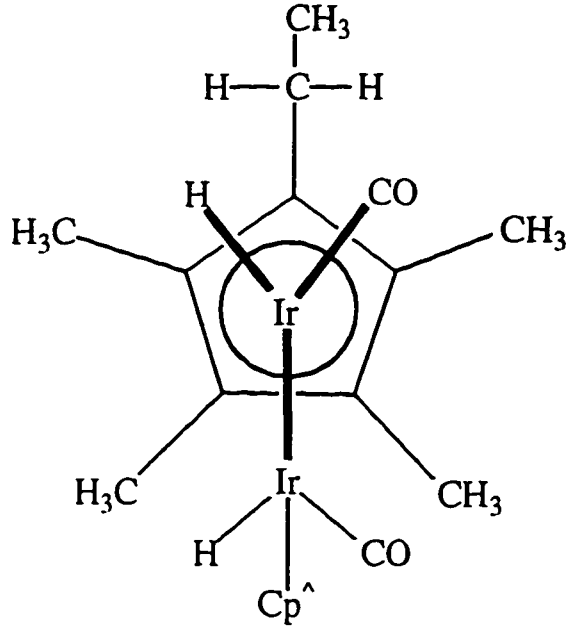

Figure 2.6. Newman projection of $[Cp^{\wedge}Ir(CO)H]_2$ (**7**) looking down an Ir-Cp^(centroid) axis.

VT NMR Spectroscopy of [Cp'Ir(CO)H]$_2$ (Cp' = Cp* (6), Cp$^\wedge$ (7)).

The room temperature ^{1}H NMR spectrum ($CDFCl_2$, 500 MHz) of [Cp*Ir(CO)H]$_2$ (**6**) consists of a single sharp resonance in the Cp* region at 2.15 ppm and another in the hydride region at −16.22 ppm. Lowering the temperature to 263 K results in substantial line broadening of the hydride signal. At 229 K, the broad hydride resonance has decoalesced into a sharp signal at −16.0 ppm and a weak, broad peak at −19.2 ppm. The ratio of the two peaks was determined by integration to be 12.3:1. Continued cooling decreases the peak linewidths and shifts the ratio to 2.2:1 at 168 K. All spectral changes with temperature are fully reversible. Like the hydride resonance, the Cp* peak also broadens and decoalesces into two new singlets whose relative intensities change reversibly with temperature (though the smaller $\Delta\delta$ makes reliable integration difficult). A van't Hoff plot of the relative populations of the two species (as measured by peak integration of the hydride resonances), determined at six temperatures between 168 and 229 K (Figure 2.7), yields the thermodynamic parameters for the interconversion of the minor to major species: ΔH° = 1.98 ± 0.23 kcal mol^{-1}, ΔS° = 13.3 ± 1.2 cal mol^{-1} K^{-1}, ΔG°_{298} = −1.98 ± 0.43 kcal mol^{-1}. Extrapolation of the linear fit (R^2 = 0.95) to T = 298 K yields K_{eq} = 29. The activation energy for the interconversion was estimated from the coalescence temperature (T_c) and the predicted chemical shifts and populations at T_c, using the method of Shanan-Atidi and Bar-Eli.[22] This procedure allows for the calculation of $\Delta G^\ddagger$ for interconversion of two species of unequal population. At T_c (240 ± 10 K), $\Delta G^\ddagger$ = 11.2 ± 0.6 kcal mol^{-1} for the conversion of the major to the minor species, and $\Delta G^\ddagger$ = 10.0 ± 0.4 kcal mol^{-1} for the reverse reaction. The difference in free energy between the two species at T_c (ΔG°_{240} = 1.2 kcal mol^{-1}), derived from the difference in $\Delta G^\ddagger$ for the forward and reverse reactions, is identical (within experimental error) to that obtained from the van't Hoff plot above.

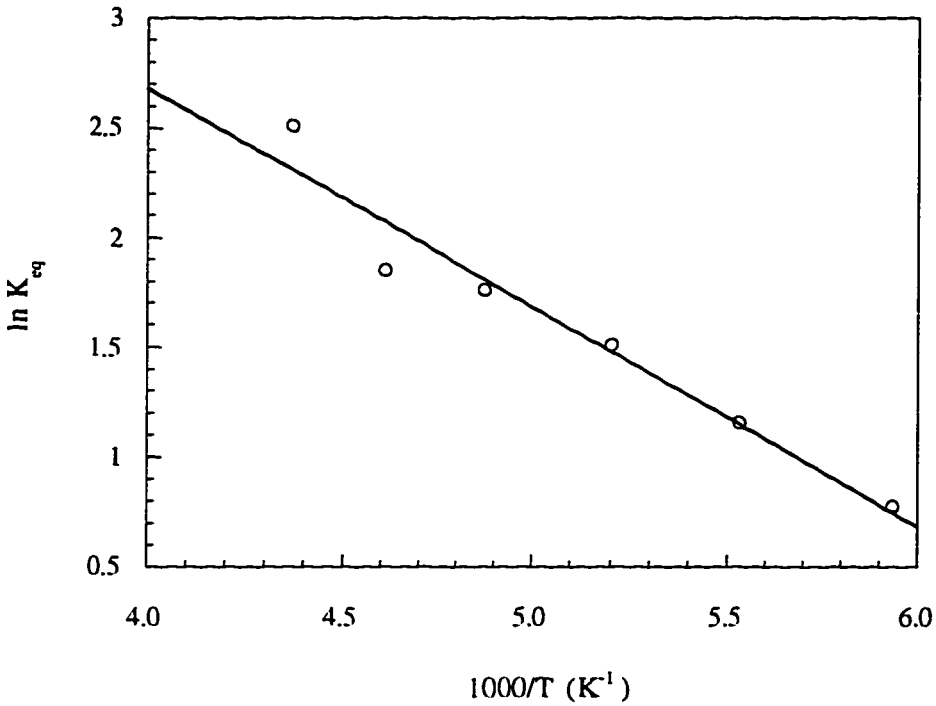

Figure 2.7. Ratio of the equilibrium populations of the two isomers of $[Cp^*Ir(CO)H]_2$ (**6**) as a function of temperature.

In order to probe for a dynamic process which would exchange the two terminal hydride ligands in **6**, the complex was prepared with ^{13}C labelling in the carbonyl groups, i.e. $[Cp^*Ir(^{13}CO)H]_2$ (**6***). The ^1H NMR spectrum of **6*** in $CDFCl_2$ exhibits a poorly resolved triplet hydride resonance ($J_{H\text{-}C}$ = 4.5 Hz) at room temperature (Figure 2.8). As is the case for **3***, selective decoupling of the Cp^* resonance is required in order to resolve hydride-^{13}C coupling. As the temperature is lowered, the hydride resonance decoalesces into two resonances, as was observed for **6**. At 145 K, the major resonance at −15.89 ppm is a doublet ($J_{H\text{-}C}$ = 7.9 Hz), and the minor resonance at -19.04 ppm is a triplet ($J_{H\text{-}C}$ = 6.0 Hz). The VT NMR behavior of the hydride resonance of **6** is similar to that reported for the $CpIr(P(OPh_3))$ analogue,[1,14] $[CpIr(P(OPh)_3)H]_2$ (**8**). These

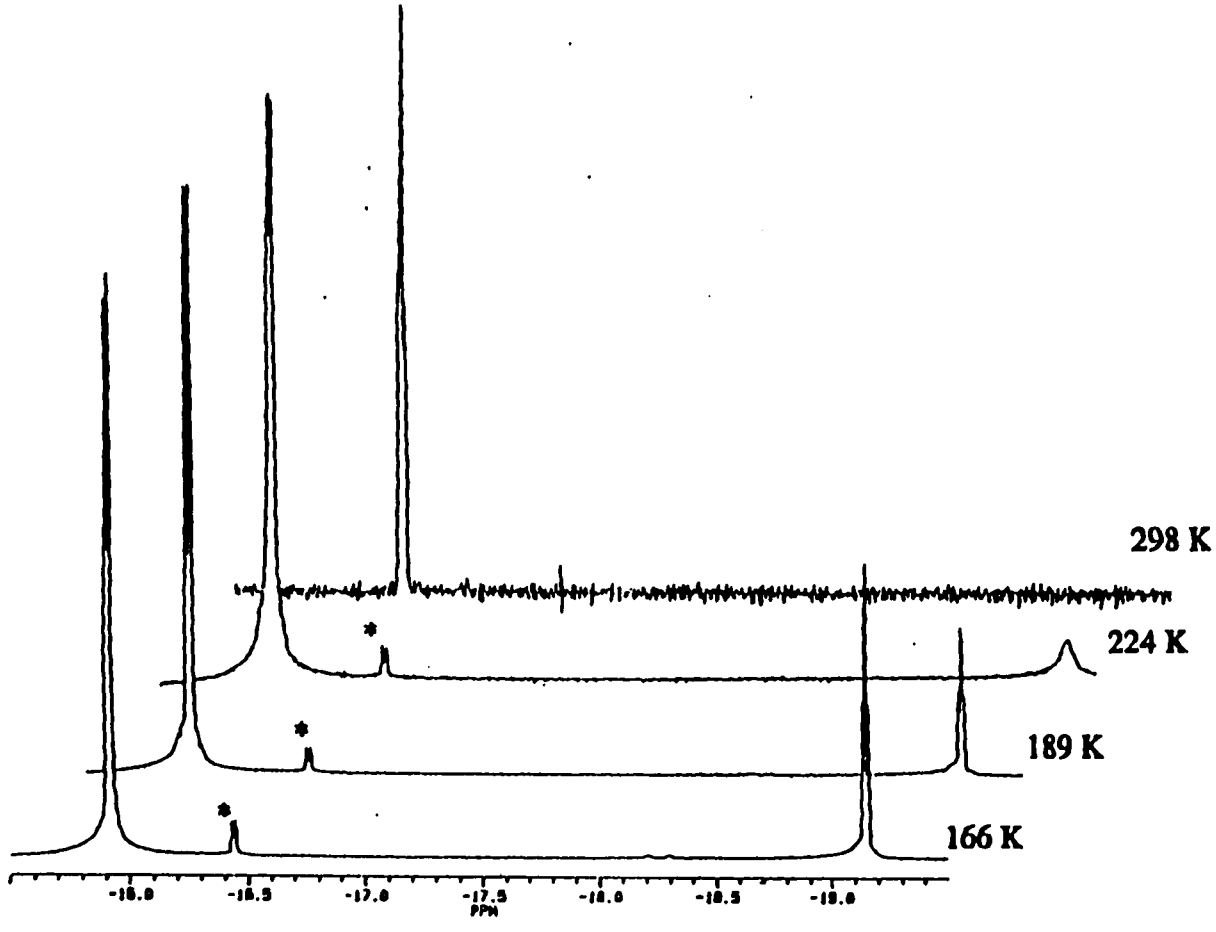

Figure 2.8. Variable temperature ^1H NMR (500 MHz) spectra of the hydride region of $[Cp^*Ir(^{13}CO)H]_2$ (6*) in $CDCl_2F$. Cp^* resonances are selectively decoupled. Asterisks indicate resonance due to $Cp^*Ir(^{13}CO)H_2$ impurity.

observations on the fluxionality of compounds **6** and **8** suggest that they each exist as a mixture of two isomers that rapidly interconvert at room temperature.

The variable temperature ^{1}H NMR spectra of [Cp^Ir(CO)H]$_2$ (**7**) in the hydride region are similar to that described above for complex **6**. Interconversion between a major and minor species is frozen out at low temperature. However, due to technical problems, the inability to determine accurate integral ratios over a sufficiently large temperature range for **7** precluded the derivation of precise ΔH° and ΔS° values by NMR. Nevertheless, rough thermodynamic parameters calculated for the interconversion of the major and minor species of **7** (ΔH° = 1.8 kcal mol^{-1}, ΔS° = 14 cal mol^{-1} K^{-1}, ΔG°_{298} = −2.4 kcal mol^{-1}) are the same as those derived for **6** within experimental error. The ^{1}H NMR spectrum of the Cp^ region at ambient temperature exhibits two distinct methyl resonances (Figure 2.9). At 212 K, the two methyl resonances have split into a total of four peaks (major species), and a small lump (minor species) is visible just upfield. At 177 K, the minor species has grown in and appears as a somewhat broadened pair of singlets. Like the trihydride cation dimers **3**, **4**, and **5**, the neutral dihydride dimers **6**, **7**, and **8** each possess two chiral iridium centers. The VT NMR data for **7** are consistent with a dynamic process which causes rapid racemization of the iridium centers at room temperature.

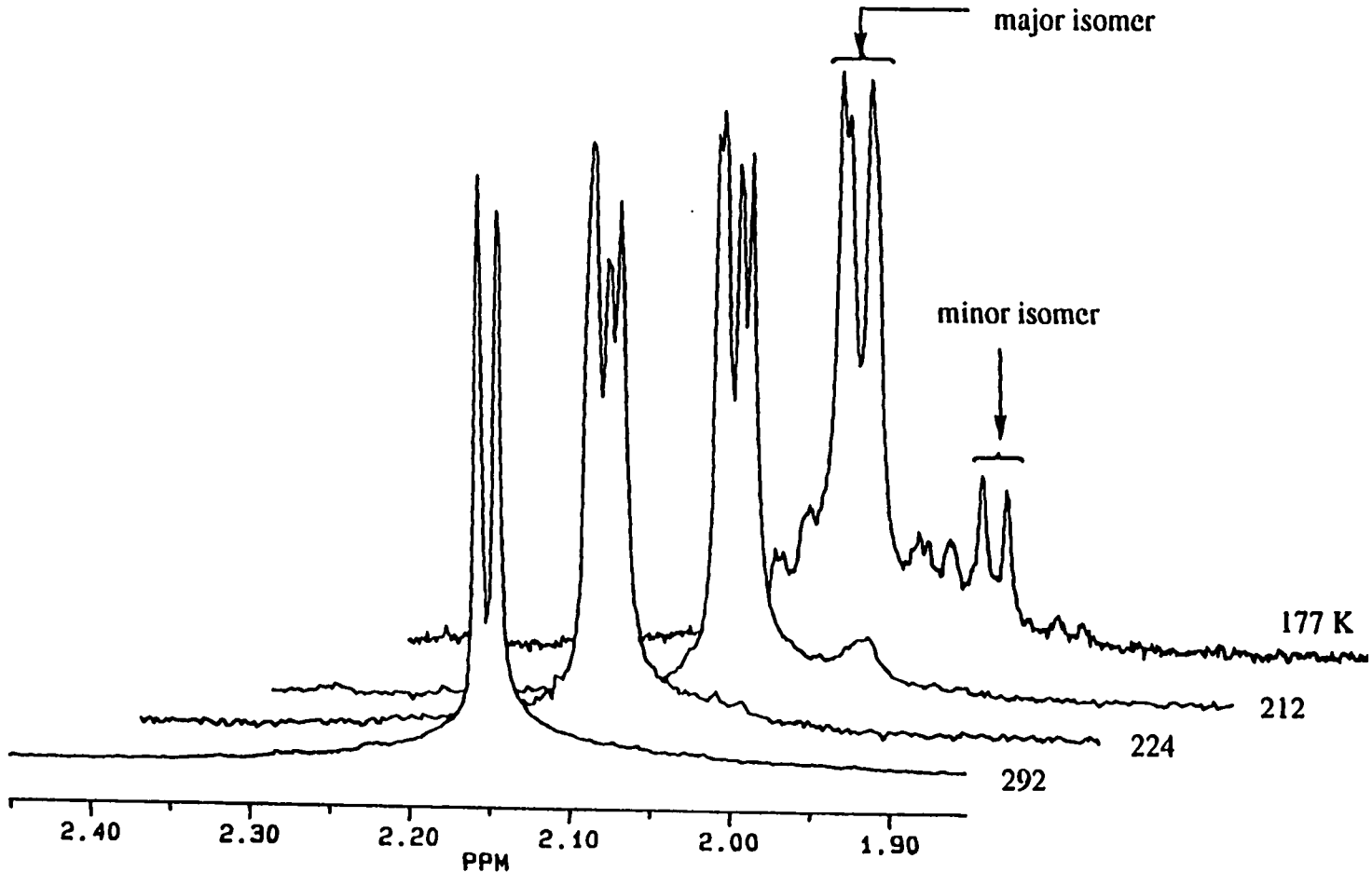

Figure 2.9. Variable temperature ^{1}H NMR (500 MHz) spectra of the Cp^-methyl region of $[Cp^{\wedge}Ir(CO)H]_2$ (7) in $CDCl_2F$.

Discussion

Synthesis.

The reaction of Maitlis' tetrachloride dimer, $[Cp^*IrCl_2]_2$, with a wide variety of reagents is the starting point for the synthesis of many iridium compounds with pentamethylcyclopentadienyl (Cp^*) ligands. Previously in our group, $[Cp^*IrCl_2]_2$ was prepared in good yield from $IrCl_3 \cdot 3H_2O$ and pentamethylcyclopentadiene by the published method.[23] We find that an alternate route[20,24] via $[(COD)IrCl]_2$ (COD = 1,5-cyclooctadiene), despite requiring an extra step, is advantageous because it allows us to recycle our iridium residues while maintaining excellent yields (Scheme 2.2). Iridium containing solids can be converted to black crystals of $(NH_4)_2IrCl_6$ via a process reported by Kauffman and Meyers.[25]

The reduction of an organometallic dihalide to the corresponding dihydride employing zinc dust in an acetic acid/methanol solution was first communicated by Moss and Graham for the conversion of $Os_3(CO)_{12}Br_2$ to $Os_3CO)_{12}H_2$.[7] The same method was used successfully by Shapley and co-workers to convert $CpIr(CO)Br_2$ to $CpIr(CO)H_2$.[26] Several brief reports regarding the chemistry of the Cp^* analogue, $Cp^*Ir(CO)H_2$ (1), have appeared previously,[26-28] but a procedure for its preparation was not published until our recent article.[1]

Protonation of the neutral metal dihydride complex $CpRh(P^iPr_3)H_2$ was reported by Werner and Wolf[29] to generate H_2 and a cationic dimeric species formulated as $[CpRh(P^iPr_3)]_2(\mu\text{-}H)_3^+$. In the case of similar iridium complexes, Bergman and Gilbert reported[30] that protonation of $Cp^*Ir(PMe_3)H_2$ affords the monomeric cation $Cp^*Ir(PMe_3)H_3^+$. Hydrogen loss from this cationic species does not occur readily. The dimeric iridium species identified as $[Cp^*Ir(PMe_3)H]_2(\mu\text{-}H)^+$ was prepared[30] however by reaction of $[Cp^*Ir]_2(\mu\text{-}H)_3^+$ with PMe_3. We find[1] that protonation of $CpIr(P(OPh)_3)H_2$ in methylene chloride heated to reflux cleanly affords the dimeric cation

$[CpIr(P(OPh)_3)H]_2(\mu\text{-}H)^+$ (**5**). This reaction also works well for $Cp^*Ir(CO)H_2$ (**1**), though no heating is required. The dimer formation reaction depicted in equation 2.2 proceeds via initial protonation of the neutral dihydrides to afford the cationic trihydride monomers. In the case of L = $P(OPh)_3$ (as well as several other phosphines), this

$$Cp^*Ir(CO)H_2 \;(\mathbf{1}) \underset{}{\overset{H^+}{\rightleftharpoons}} Cp^*Ir(CO)H_3^+ \xrightarrow[-\,H_2]{> -78\ ^\circ C} \left[Cp^*Ir(CO)H^+\right] \xrightarrow{Cp^*Ir(CO)H_2\,(\mathbf{1})} [Cp^*Ir(CO)H]_2(\mu\text{-}H)^+ \;(\mathbf{3}) \tag{2.2}$$

complex is isolable and has been previously reported.[13] When L = CO, hydrogen loss is facile, and the monomeric trihydride complex has only been observed at very low temperatures.[15] Elimination of H_2 from $Cp^*Ir(CO)H_3^+$ generates a coordinatively unsaturated species which rapidly reacts with another equivalent of **1** to afford $[Cp^*Ir(CO)H]_2(\mu\text{-}H)^+$ (**3**). This condensation methodology is very efficient. When the progress of the reaction between **1** and triflic acid is monitored by ^1H NMR spectroscopy, the yield of dimer is quantitative. Isolated yields are somewhat diminished by losses during manipulation. The relative facility with which these various $(\eta^5\text{-}C_5R_5)Ir(L)H_3^+$ compounds lose H_2 and hence undergo the condensation to dimers (i.e. $Cp^*Ir(PMe_3)H_2$ << $CpIr(P(OPh)_3)H_2$ < $Cp^*Ir(CO)H_2$) correlates well with the decreasing electron density at the metal. The combination of a hydride donor (e.g. $Cp^*Ir(CO)H_2$) with a coordinatively unsaturated hydride acceptor (e.g. $[Cp^*Ir(CO)H^+]$) is a standard method for the formation of hydride-bridged dimers.[5]

Deprotonation of the carbonyl dimers $[Cp^*Ir(CO)H]_2(\mu\text{-}H)^+$ (**3**) and $[Cp^\wedge Ir(CO)H]_2(\mu\text{-}H)^+$ (**4**) is readily effected by mild bases such as 1,8-bis(dimethylamino)naphthalene (Proton Sponge). While quantitative pKa data have not

yet been obtained, it is clear that the phosphite complex, $[CpIr(P(OPh)_3)H]_2(\mu\text{-}H)^+$ (**5**), is a much weaker acid than the cationic carbonyl dimers. A stronger base, such as lithium diisopropylamide (LDA), is required to carry out the deprotonation in this case. This is consistent with lower electron density at the metal centers in the carbonyl containing complexes.

Solid State Structures of $\{[Cp^*Ir(CO)H]_2(\mu\text{-}H)\}BAr'_4$ (3-BAr'$_4$), $[Cp^*Ir(CO)H]_2$ (6), and $[Cp^\wedge Ir(CO)H]_2$ (7).

A single crystal X-ray structure determination confirmed the dimeric nature of $[Cp^*Ir(CO)H]_2$ (**6**), with an Ir-Ir bond length of 2.730 Å and terminal carbonyl ligands (Figure 2.3). While the hydride ligands could not be definitively located in the structure determination, the infrared spectrum indicates the presence of terminal hydride and terminal carbonyl ligands. The results of investigations of **6**, **7**, and **8** by VT NMR spectroscopy indicate that the ground state structure of the major isomer (and possibly the minor isomer) has terminal hydrides (see below). Intraligand angles in **6** are similar to those observed[31] in closely related pseudo-octahedral monomeric complexes such as $Cp^*Ir(PMe_3)(Cy)H$, in which, for example, the angles between the Cp^* centroid (referred to as Cp^*_{cent}) and the phosphine, and between Cp^*_{cent} and the cyclohexyl carbon are 131° and 129° respectively. The comparable angles in **6** between Cp^*_{cent} and the carbonyl group and between Cp^*_{cent} and the distant iridium atom (Cp^*_{cent}-Ir-Ir) are 136° and 129° respectively. These angles are slightly greater than the 125° angle between Cp^*_{cent} and the ancillary ligands expected for perfect octahedral geometry, whereby the Cp^* ligand is considered to occupy three facially related vertices of the octahedron. The slightly enlarged angles are most likely the result of the Cp^* rings bending away from the proximate carbonyl and the distant iridium and toward the less sterically demanding proximate hydride. This hypothesis is corroborated in $Cp^*Ir(PMe_3)(Cy)H$, in which the

Cp^*_{cent}-Ir-H angle is only 121°. The Cp^* rings of **6** are disposed in a transoid fashion, though the dihedral angle (142.9°) is somewhat less than 180°, perhaps due to some steric interaction between the Cp^* methyl groups and the carbonyl attached to the distant iridium atom. The Ir-C-O angles are essentially linear (179.0° and 177.8°).

X-ray diffraction analysis of $[Cp^{\wedge}Ir(CO)H]_2$ (**7**) (Figure 2.4) reveals a solid-state structure that is quite similar to that of **6** (see Table 2.3). The Ir-Ir bond length is 2.724 Å in **7**, as compared to 2.730 Å in **6**. As in the case of **6**, the hydride ligands of **7** were not located, though again, IR and NMR data support a terminal hydride description. The major difference between the structures of **7** and **6**, is the smaller dihedral angle between the two cyclopentadienyl rings (**7** = 122.8°, **6** = 142.9°) and between the two carbonyls (**7** = 64.5°, **6** = 83.0°). We propose that the reason for the smaller $Cp^{\wedge}_{cent}$-Ir-Ir-$Cp^{\wedge}_{cent}$ dihedral angle of **7** is due to the slightly more pronounced steric interaction between the $Cp^{\wedge}$ rings and the vicinal carbonyl ligands.

There are few structurally characterized examples of unbridged Ir-Ir single bonds in the literature.[32-36] Examples include a distance of 2.717 Å reported[32] in 1973 for $Ir_2(NO)_4(PPh_3)_2$ and a distance of 2.839 Å reported[35] for the dication $[Cp^*Ir(CO)_2]_2^{2+}$. A closely related complex with bridging carbonyl ligands and a formal Ir=Ir double bond is $[Cp^*Ir(\mu\text{-}CO)]_2$, which has an Ir=Ir distance of 2.554 Å.[23] Structural characterization of $[Cp^*Os(CO)(\mu\text{-}H)]_2$, an isoelectronic complex of osmium, indicates that the two hydride ligands are bridging the Os=Os double bond.[37] Significantly, in $[Cp^*Os(CO)(\mu\text{-}H)]_2$, unlike in $[Cp^*Ir(CO)H]_2$ (**6**) or $[Cp^{\wedge}Ir(CO)H]_2$ (**7**), the metal atoms, the carbonyl carbons, and the ring centroids all form a plane.

Placement of the hydride ligands in their expected positions based on pseudo-octahedral geometry about the iridium atoms, reveals that both **6** and **7** have crystallized as the racemic diastereomer (RR/SS enantiomeric pair). Solution NMR spectroscopy data, discussed below, suggest that there may be a rapidly established equilibrium

between the racemic and meso forms of these dihydride dimers (**6** and **7**). It has not yet been determined whether the crystal structures represent the major or minor isomer.

Determination of the structure of $\{[Cp^*Ir(CO)H]_2(\mu\text{-}H)\}BAr'_4$ (**3-BAr'$_4$**) (BAr'_4 = $B(3,5\text{-}(CF_3)_2C_6H_3)_4$) by X-ray diffraction analysis (Figs. 2.1, 2.2) provides a unique opportunity to evaluate the effect of protonation upon the length of an unsupported metal-metal bond. To our knowledge this has not been determined previously for iridium. The crystal structure of **3-BAr'$_4$** consists of two independent molecules, so mean values of the two will be used for comparison. The Ir-Ir bond length in **3-BAr'$_4$** is 2.928 Å, which is significantly longer (by 0.198 Å) than that in $[Cp^*Ir(CO)H]_2$ (**6**). Churchill and co-workers were first to make the generalization that protonation of an unsupported metal-metal bond leads to an increase in the length of that metal-metal bond.[38] This is what we would expect based upon conversion from a 2-center-2-electron bond to a delocalized 3-center-2-electron bond. There are few examples in the literature wherein a complex containing an unsupported metal-metal bond and the corresponding complex containing the protonated metal-metal bond are both structurally characterized by diffraction methods. One of the first X-ray diffraction studies of polynuclear transition metal complexes containing a bridging hydride involved a pair of chromium dimers, $[Cr_2(CO)_{10}]^{2-}$ and $[Cr_2(CO)_{10}(\mu\text{-}H)]^-$, which revealed a marked 0.44 Å increase in the Cr-Cr bond length upon protonation.[39] A complex containing a third row metal, $[(\mu\text{-}H)Re_3(CO)_{12}]^{2-}$, possesses a triangular metal core, with one hydrogen bridged Re-Re bond.[40] The Re-Re bond bridged by the hydride ligand is 0.14 Å longer than each of the unbridged Re-Re bonds, which is closer to the change in metal-metal bond length we find in our system for iridium. However, the non-hydride bridged Re-Re bonds are not truly "unsupported" as they are bridged by the third Re atom, and it is unclear what effect this has on the Re-Re bond lengths.

Again, as for structures **6** and **7**, the hydride ligands of **3** were not located. It should be noted that this is not an uncommon occurrence in X-ray diffraction studies of transition metal hydrides; the small X-ray scattering cross-section of a hydrogen atom is often lost next to the relatively large metal atom to which it is bonded.[41]

The ligand bond angles of **3-BAr'$_4$** are similar to those of **6** and **7**. The carbonyl carbons of **3-BAr'$_4$** are bent slightly more towards the Ir-Ir bond (Ir(1)-Ir(2)-C(2) = 78.2° and Ir(2)-Ir(1)-C(1) = 81.4°). The Cp* rings of **3-BAr'$_4$** are disposed in a more nearly trans geometry (dihedral angle = 155.6°). The bonds between the iridium atoms and the carbonyl carbons of **3-BAr'$_4$** are longer than the corresponding bonds in **6** and **7**, which is consistent with its positive charge, and hence its lesser ability to back-donate electron density form the iridium atoms to the carbonyl π^* orbitals. There appears to be no interaction between the BAr'$_4$ anion and the iridium centers (closest contact > 5 Å). This structure determination is also a rare example of a well-resolved structure containing the BAr'$_4$ anion, which historically has proven to be a difficult counterion with which to obtain suitable X-ray quality crystals.

The structure of **3-BAr'$_4$** can profitably be compared to that of the trimethylphosphine analogue, $\{[Cp^*Ir(PMe_3)H]_2(\mu\text{-}H)\}PF_6$.[42] The Ir-Ir bond length in $[Cp^*Ir(PMe_3)H]_2(\mu\text{-}H)^+$ is 2.983 Å, slightly longer than the Ir-Ir bond of **3-BAr'$_4$** (2.928 Å), and the hydrides were located, confirming the presence of two terminal and one bridging hydride. The configuration of the ligands around the iridium atoms in **3-BAr'$_4$** is very similar to that of the phosphine analogue (Figure 2.10).

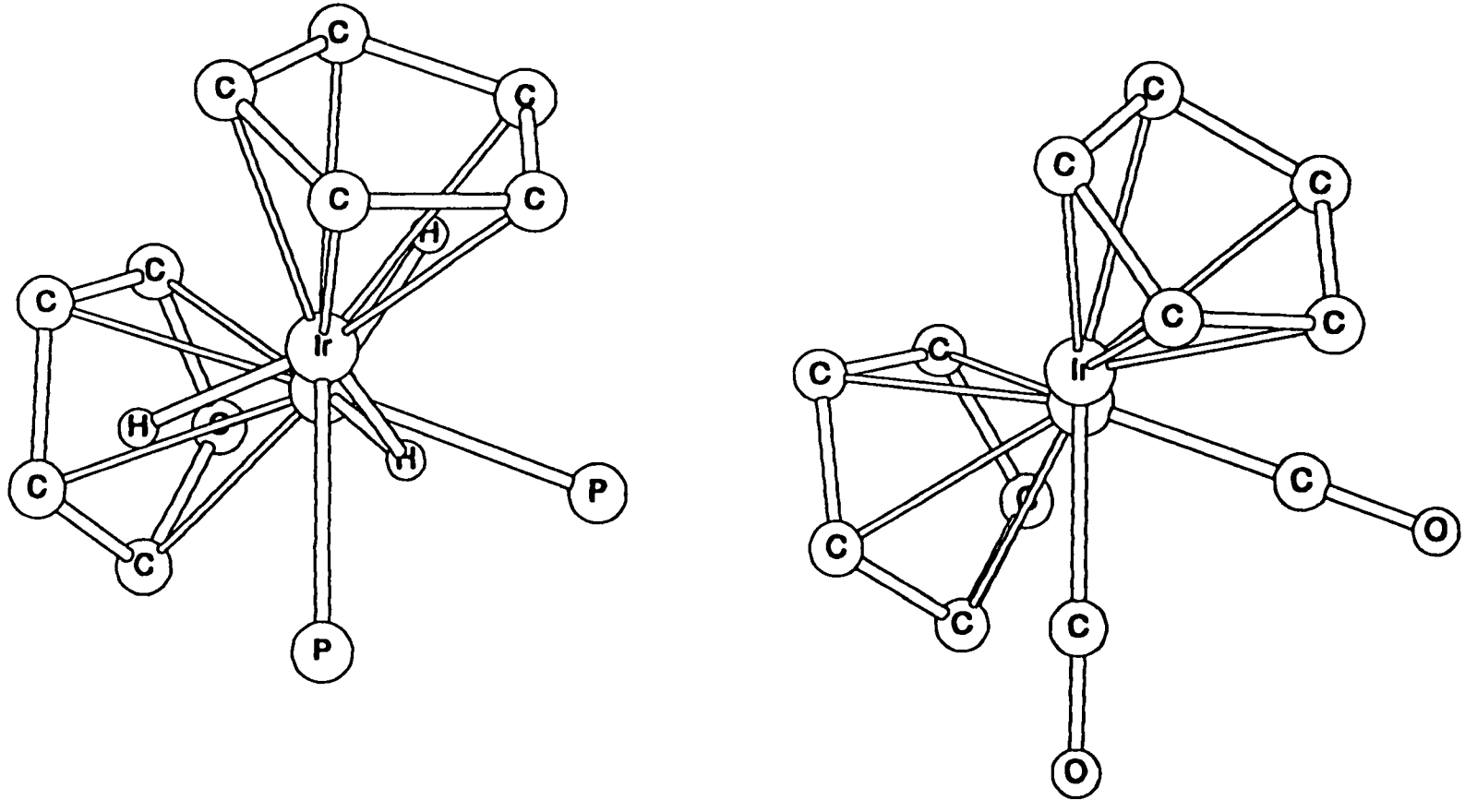

Figure 2.10. Comparison of solid state structures of $[Cp^*Ir(PMe_3)H]_2(\mu\text{-}H)^+$ and $[Cp^*Ir(CO)H]_2(\mu\text{-}H)^+$ (**3**) as determined by X-ray diffraction. Representations were created with CAChe™ Scientific software using X-ray crystal data. Cp^* and PMe_3 methyl groups are omitted for clarity. Counterions are not pictured. Hydride ligands were not located for **3**.

Again, placement of the terminal hydride ligands in their expected positions based on pseudo-octahedral geometry (ignoring the bridging hydride ligand) about the iridium atoms (and based on comparison to $[Cp^*Ir(PMe_3)H]_2(\mu\text{-}H)^+$), reveals that **3-BAr'$_4$**, like **6** and **7**, has crystallized as the racemic diastereomer (RR/SS enantiomeric pair). Solution NMR spectroscopy data obtained for the Cp^ analogue, $[Cp^\wedge Ir(CO)H]_2(\mu\text{-}H)^+$ (**4**), suggest that the chiral iridium centers in these trihydride cation dimers undergo rapid racemization at room temperature (vide infra).

Dynamics of $[Cp'Ir(CO)H]_2(\mu\text{-}H)^+$ (Cp' = Cp* (3), Cp^ (4)).

The variable temperature (VT) NMR spectroscopy of the trihydride cation dimers **3** and **4** is consistent with the presence of one bridging and two terminal hydride ligands. A rapid dynamic process is operational in these complexes which allows site exchange of the terminal and bridging hydrides. In the case of $[CpIr(P(OPh)_3)H]_2(\mu\text{-}H)^+$ (**5**), this process is indicated by the observation of a single triplet resonance ($J_{H\text{-}P}$ = 18 Hz) in the hydride region of the ^1H NMR spectrum at room temperature. This observation would also be consistent with a triply bridging structure, as suggested by Werner and Wolf[29] for the related dimeric trihydride complex which results from the reaction of $CpRh(P^iPr_3)H_2$ with acid. However, the appearance of two distinct hydride resonances in the intensity ratio 2:1 in the low temperature ^1H NMR spectrum favors the less symmetrical, singly bridged structure for **5**. The coupling to ^{31}P is in agreement with this structure, in that the resonance corresponding to one hydride is a triplet, while the signal corresponding to two hydrides is a doublet. This same structure was found by Bergman and Gilbert[30] for the closely related trimethylphosphine complex $[Cp^*Ir(PMe_3)H]_2(\mu\text{-}H)^+$, as indicated by VT NMR spectroscopy and confirmed by an X-ray diffraction study.[42] Complex **5** differs from the previously reported PMe_3 complex in having a somewhat lower barrier to the dynamic process which permutes the bridging and terminal hydride ligands: $\Delta G^{\ddagger}_{298}$ = 8.8

± 0.6 kcal mol^{-1} for **5**, $\Delta G^{\ddagger}_{298}$ = 10.96 ± 0.04 kcal mol^{-1} for the Cp*-PMe_3 analogue. The entropy of activation of the two compounds is essentially the same however: $\Delta S^{\ddagger}$ = −6.8 ± 1.2 cal mol^{-1} K^{-1} for **5**, $\Delta S^{\ddagger}$ = −6.4 ± 1.2 cal mol^{-1} K^{-1} for $[Cp^*Ir(PMe_3)H]_2(\mu\text{-}H)^+$. A transition state geometry with two or three hydrides adopting bridging positions would be consistent with the increase in order required by the slightly negative entropy of activation for these compounds. A very similar situation was reported by Werner and co-workers[43] for the bis-Cp bridged compound $\{[CH_2(\eta^5\text{-}C_5H_4)_2][RhH(P^iPr_3)]_2(\mu\text{-}H)\}^+$. In this case, the presence of bridging and terminal hydride ligands was indicated crystallographically, but the bridge/terminal exchange process was too facile to be frozen out by low temperature NMR spectroscopy.

Qualitatively similar observations were made for $[Cp^*Ir(CO)H]_2(\mu\text{-}H)^+$ (**3**). The structural assignment here is less definitive, since ^{31}P coupling is not available to aid in the differentiation of terminal and bridging hydride ligands. In an attempt to verify that the dynamic behavior of **3** is analogous to that of $[CpIr(P(OPh)_3)H]_2(\mu\text{-}H)^+$ (**5**), we prepared complex **3** with ^{13}C labels in the carbonyl carbon atoms (referred to as **3***). At ambient temperature, the ^1H NMR spectrum for **3*** shows a triplet hydride resonance with $J_{H\text{-}C}$ = 3.4 Hz (Cp* selectively decoupled). The expected doublet and triplet H-C couplings in the low temperature spectra of **3*** were not resolvable.

Room temperature ^1H and $^{13}C\{^1H\}$ NMR spectra of the Cp^ analogue, $[Cp^{\wedge}Ir(CO)H]_2(\mu\text{-}H)^+$ (**4**), reveal that the chiral iridium centers are fluxional on the NMR timescale. The most likely mechanism for the racemization of the iridium centers in these trihydride cation dimers (**3**, **4**, **5**) proceeds via the rapid bridge/terminal hydride exchange. We can envisage an alternate possibility that invokes rapid dissociation/association of the carbonyl or phosphine ligands. However, this would necessarily result in a loss of phosphorus (for **5**) or ^{13}C (for **3***) coupling to the hydride and Cp or Cp* ligands, which is contrary to the observed couplings.

Since *both* metal centers in dimers such as **3**, **4**, and **5**, are chiral, two diastereomers are possible: the racemic form (RR/SS enantiomeric pair) and the meso structure (RS or SR) (Scheme 2.3). An extension of Cahn-Ingold-Prelog sequence rules to organometallic compounds is used to denote the configuration at the metal centers (ignoring the bridging hydride).[44] Note that the ^1H and $^{13}C\{^1H\}$ NMR spectra of **4**, which reveal the stereochemical nonrigidity of the iridium centers of these dimers, does not distinguish racemization (e.g. RR to SS conversion) from epimerization (e.g. RR to RS conversion). The fact that only one set of resonances is observed in the ^1H NMR spectra of these dimers at all temperatures suggests three possible explanations: 1) The dimers each exist as a static mixture of diastereomers, but the differences in chemical shifts between the diastereomers are too small to be resolved; 2) The dimers each exist as a dynamic mixture of diastereomers, but the interconversion is so facile that the epimerization cannot be frozen out at low temperature; or 3) The formation of the dimers via acid-induced condensation of monomeric dihydride units is diastereoselective, that is only one diastereomer is preferentially formed.

The first explanation seems unlikely based upon related dimers with two chiral metal centers which show significant ^1H NMR chemical shift differences between diastereomers. For example, cyclopentadienyl ruthenium dimers of the form $[CpRu(CO)L]_2(\mu\text{-}H)^+$ (L = PMe_3, PMe_2Ph, PPh_3), exist as two configurationally stable (on the NMR timescale) diastereomers which exhibit hydride resonances that differ by 1.43 to 3.74 ppm.[45] A similar rhenium dimer, $[CpRe(CO)(NO)]_2(\mu\text{-}H)^+$, also exists in solution as two diastereomers, whose hydride resonances are separated by 0.30 ppm in the room temperature ^1H NMR spectrum.[46] To be consistent with our observation that the iridium centers in $[Cp^{\wedge}Ir(CO)H]_2(\mu\text{-}H)^+$ (**4**) are configurationally unstable, this explanation necessitates that the rapid intramolecular hydride migration in these trihydride cation dimers leads to racemization, but not epimerization.

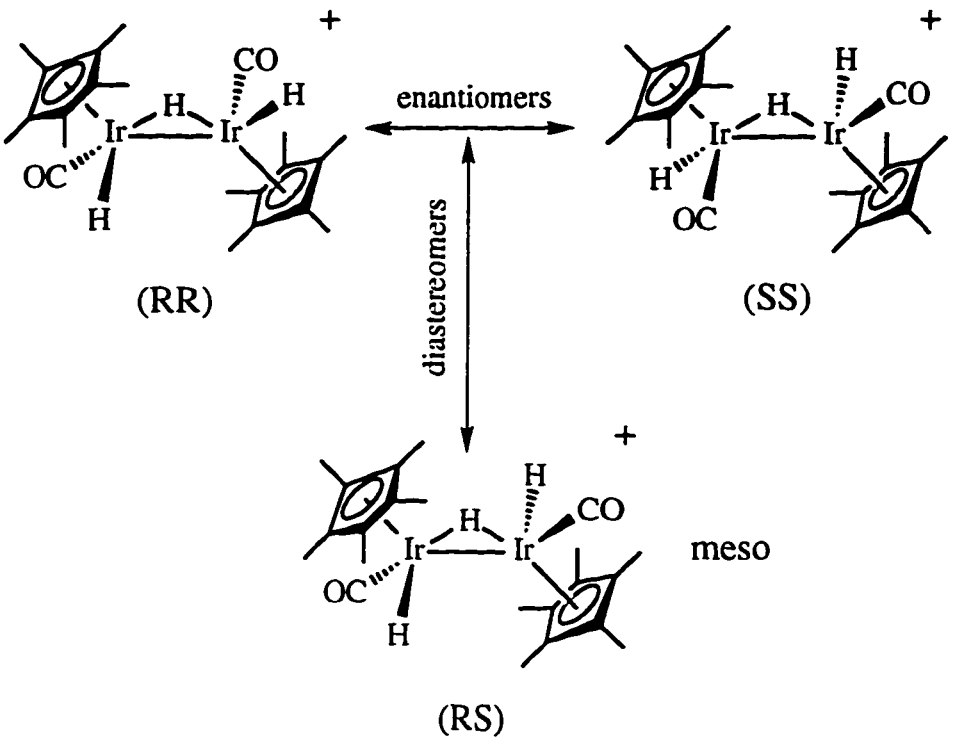

Scheme 2.3

The second explanation appears to be unusual based upon literature precedent. Commonly, there is a fairly significant kinetic barrier to interconversion of diastereomers. Indeed, a classical method employed by organic chemists to separate enantiomers involves conversion to the corresponding diastereomers. To our knowledge, there is no organometallic example of rapid epimerization (on the NMR timescale) at room temperature. The most facile epimerizations include the observations of Heinekey and Chinn, that an isolated, single diastereomer of $[CpRu(CO)(PMe_3)]_2(\mu\text{-}H)^+$, after standing at 23 °C in CD_3CN for 65 hours, had been partially converted (20%) to its epimer.[45] Royo and co-workers[47] reported that an isolated isomer of the bis-Cp bridged dimer with chiral molybdenum centers, *RR*- or *SS*-$[Mo(CO)(\eta^2\text{-}MeCCMe)(PPh_3)]_2(\mu\text{-}(\eta^5\text{-}C_5H_4)_2SiMe_2)^{2+}$, transforms to the RS diastereomer in $CDCl_3$ in a process that reaches equilibrium in several hours. Though dissociative or associative routes for the

epimerization are not strictly ruled out, the authors believed the most plausible mechanism to be intramolecular. Nevertheless, the NMR spectra of **4** demonstrate that the chiral iridium centers of that dimer are rapidly changing configuration at room temperature, though, as stated above, this does not distinguish between racemization and epimerization. An additional complication associated with the second explanation is as follows: if, as seems probable, epimerization is achieved via bridge/terminal hydride exchange, then both diastereomers should be evident by ^{1}H NMR spectroscopy once the exchange is frozen out at low temperature (e.g. for $[CpIr(P(OPh)_3)H]_2(\mu\text{-}H)^+$ (**5**)). However, only one set of resonances is observed in the low temperature spectra of **5**. This observation could still be rationalized if there is a large free energy difference between the diastereomers, such that one diastereomer predominates at low temperature. This then would be a form of diastereoselectivity, which is discussed in the context of the third explanation below.

To evaluate the third explanation, the mechanism of the formation of the trihydride cation dimers (**3**, **4**, **5**) must be considered. As discussed earlier (eq. 2.2), the condensation reaction proceeds via loss of dihydrogen from $Cp^*Ir(L)H_3^+$, to presumably generate the reactive 16-electron intermediate $[Cp^*Ir(L)H^+]$. Reductive elimination of H_2 would be expected to initially produce a chiral $[Cp^*Ir(L)H^+]$ fragment of pyramidal geometry (Scheme 2.4). The symmetry of $Cp^*Ir(L)H_3^+$ dictates that both the *R*-$[Cp^*Ir(L)H^+]$ and *S*-$[Cp^*Ir(L)H^+]$ configurations should be formed in equal amounts. The rate of inversion of configuration of the 16-electron intermediate may be slow relative to the rate of reaction with $Cp^*Ir(L)H_2$. For example, optically active compounds of the form CpMn(L")(L')L can undergo thermal and photochemical substitution reactions which proceed via a dissociative mechanism, and which in some cases result in retention of configuration.[48] We would expect that addition of $Cp^*Ir(CO)H_2$ to

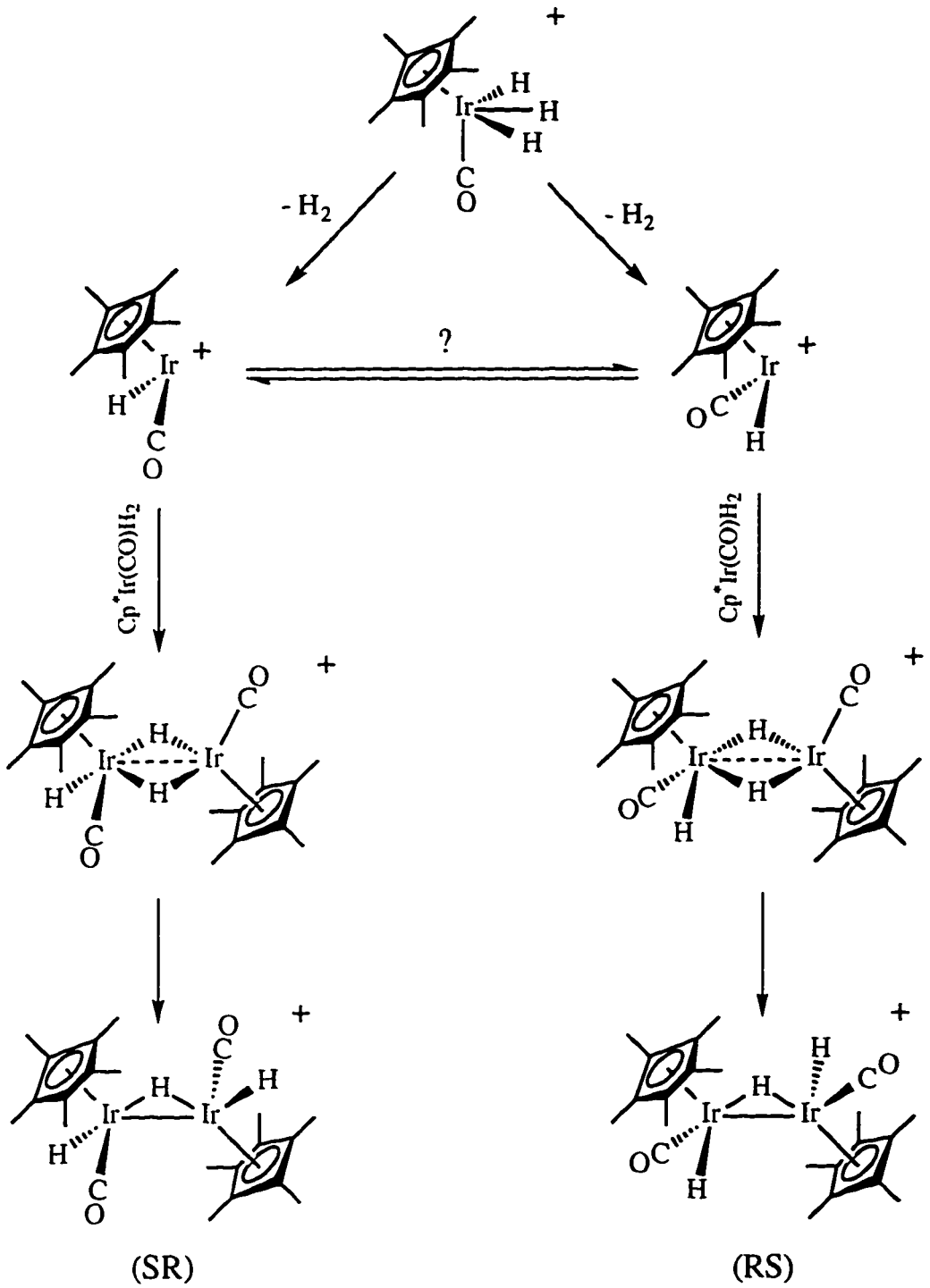

Scheme 2.4

[$Cp^*Ir(L)H^+$] should prefer a transition state wherein the Cp^* rings were disposed in a trans fashion. If then one of the hydride bridges were to open up preferentially, e.g. the one most trans to the terminal hydride, then a single diastereomer would be generated, in this case the meso compound. This outcome seems somewhat unlikely given the facile hydride migration and the rapid racemization of the iridium centers that occurs in these dimers (**3**, **4**, **5**). It is important to note that preparation of $[CpIr(P(OPh)_3)H]_2(\mu\text{-}H)^+$ (**5**) requires 15 h in methylene chloride at reflux; in other words, the barrier to epimerization would have to be fairly substantial. Perhaps a more plausible mechanism for a diastereoselective reaction, would be that both diastereomers are kinetically accessible, but that one diastereomer is greatly preferred thermodynamically. This again would be unusual though, as diastereomers are typically close in energy. For example, the two diastereomers of $[CpRu(CO)(PPh_3)]_2(\mu\text{-}H)^+$ and of $[CpRe(CO)(NO)]_2(\mu\text{-}H)^+$ both form in approximately a 50:50 ratio.[45,46]

Unfortunately, at this point we are unable to distinguish which of the three explanations accounts for our observation of only one set of ^1H NMR resonances for each of the trihydride cation dimers at all temperatures. Given the stereochemical nonrigidity in the neutral dihydride dimers (**6**, **7**, **8**) (vide infra) –the products of deprotonation of **3**, **4**, and **5**– we favor the facile epimerization proposed in the second explanation.

Dynamics of $[Cp'Ir(CO)H]_2$ (Cp' = Cp^* (6), Cp^ (7)).

We propose that the structures of the dihydride dimers **6** and **7** possess two *terminal* hydride ligands. This structural hypothesis is based upon the observation of terminal Ir-H stretches in the infrared spectra, the relative positions of the ancillary ligands in the X-ray diffraction studies, and on the couplings between the hydride ligands and adjacent spin active nuclei observed in the ^1H NMR spectra. For example, $[Cp^*Ir(^{13}CO)H]_2$ (**6***) exhibits a triplet signal ($J_{H\text{-}C} \approx 4$ - 5 Hz) for the hydride ligands at

room temperature, due to coupling to two ^{13}C nuclei. While this observation alone is consistent with the presence of bridging hydrides, variable temperature data show that the hydride resonance (of the *major* species, see below) simplifies to a doublet ($J_{H\text{-}C}$ = 7.9 Hz) at low temperature. This is consistent only with a ground state structure having terminal hydride ligands and a rapid permutation process which causes the hydride ligands to exchange. We propose that this process takes place via an intermediate or transition state with two bridging hydride ligands. The observation that the hydride signal of the *minor* species of **6*** remains as a triplet ($J_{H\text{-}C}$ = 6.0 Hz) in the ^1H NMR spectra down to 166 K is consistent with either a ground state structure possessing bridging hydrides, or a ground state structure with terminal hydrides that are still fluxional at this temperature.

In addition to the dynamic process which causes the permutation of the two hydride ligands, VT NMR (^1H) observations of complex **6** indicate the presence of two different species. The relative concentrations of these two species vary reversibly with temperature, consistent with a rapid equilibrium between isomers. We can imagine three possible scenarios (Fig. 2.11) for the isomer pair: A) tautomers, B) rotamers, or C) diastereomers. The relative merits of each of these hypotheses will be discussed further below.

Like the trihydride cation dimers (**3**, **4**, and **5**), the neutral dihydride dimers (**6**, **7**, and **8**) also possess two chiral iridium centers each. Given the stereochemical nonrigidity of the metal centers in $[Cp^{\wedge}Ir(CO)H]_2(\mu\text{-}H)^+$ (**4**), $[Cp^{\wedge}Ir(CO)H]_2$ (**7**) was prepared in order to directly verify whether its iridium centers were also fluxional. As discussed above, the $Cp^{\wedge}$ ($Cp^{\wedge}$ = $\eta^5\text{-}C_5Me_4Et$) ligand is a convenient NMR probe for stereochemical nonrigidity at the metal centers in that the diastereotopic methylene protons, ring carbons and methyl groups are rendered equivalent by a rapid change (on the NMR time scale) of configuration at the metal center. We find that the ^1H NMR

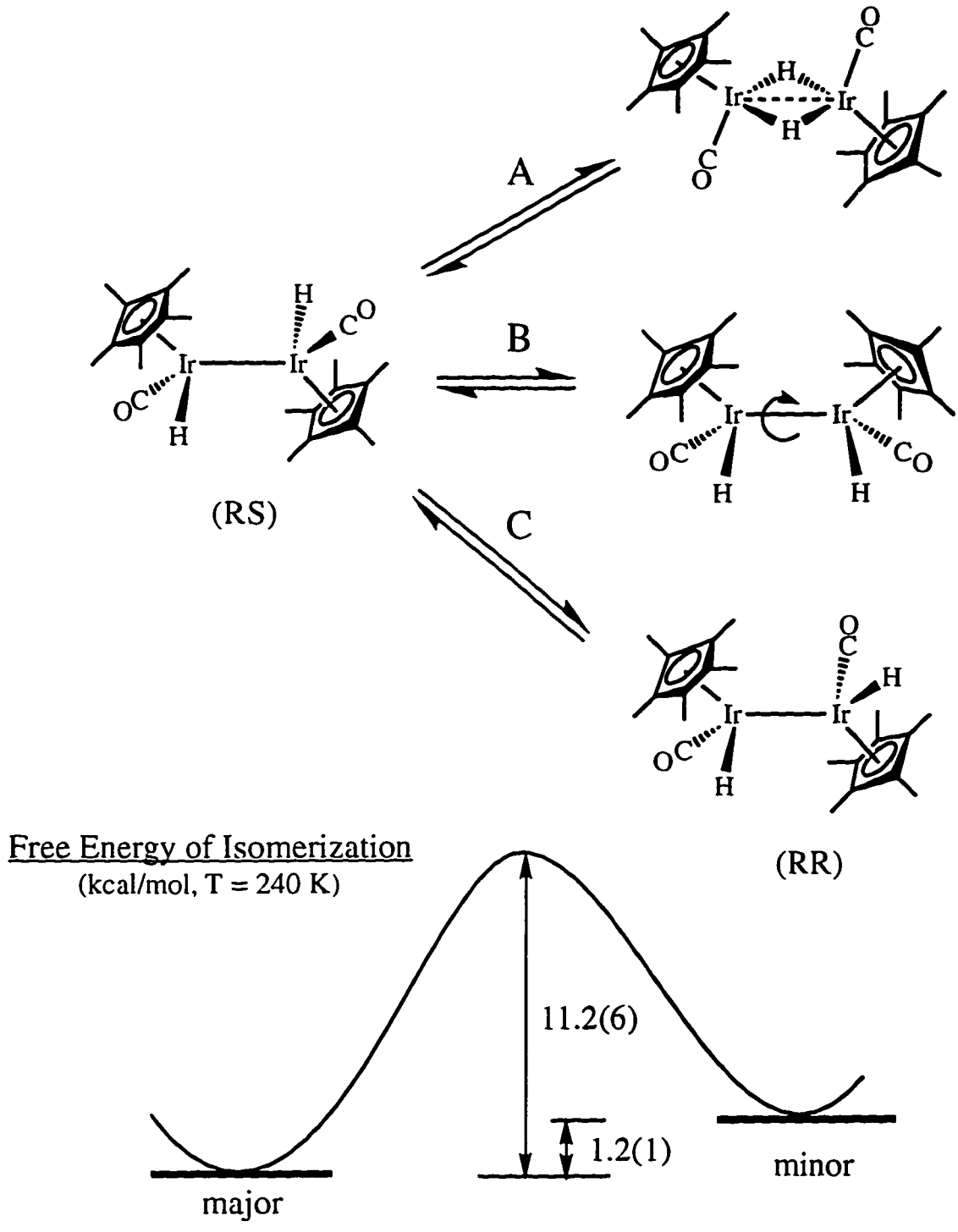

Figure 2.11. Possible relationships for the two isomers of $[Cp^*Ir(CO)H]_2$ (**6**): A) tautomers, B) rotamers, or C) diastereomers. The energy profile shows the difference in free energy between the isomers as well as the activation barrier for the interconversion.

spectrum of **7** at room temperature exhibits a single hydride resonance and only two resonances for the methyl groups attached to the ring carbons (Fig. 2.9). At lower temperatures, two hydride resonances of unequal intensity are observed, similar to the situation observed for $[Cp^*Ir(CO)H]_2$ (**6**). The methyl region of the spectrum also exhibits a major and minor set of resonances. The major species has four distinct methyl resonances, consistent with the freezing out of the configuration at the metal centers. This is in accord with the observation of a doublet resonance for the hydride ligands of the major species at low temperature in the ^1H NMR spectrum of complex **6***. The minor species of complex **7** exhibits only two methyl resonances at all accessible temperatures, indicating that the metal centers are not configurationally stable, or that the minor species adopts a symmetric structure (e.g. doubly hydride bridged). This is again consistent with the observation of a triplet resonance for the hydride ligands of the minor species at all temperatures in the ^1H NMR spectrum of complex **6***.

Similar observations to those for complexes **6** and **7** have been made in the ^1H NMR spectra of $[CpIr(P(OPh)_3)H]_2$ (**8**).[1] The hydride resonance of **8** is a triplet (δ –17.0, $J_{H\text{-}P}$ = 24 Hz) at room temperature in THF-d_8 (Fig. 2.12). Lowering the observation temperature leads to broadening of this triplet resonance and the appearance of a new, very broad signal just upfield at –17.4 ppm. Further cooling causes the new minor resonance to sharpen into a well resolved triplet ($J_{H\text{-}P}$ = 24 Hz). At 200 K, the major signal sharpens into a well resolved doublet at –16.8 ppm ($J_{H\text{-}P}$ = 47 Hz). As observed for **6** and **7**, the predominant isomer is associated with the downfield peak. The low temperature doublet splitting in the major species is consistent with two localized, terminal hydride ligands (the three bond H-P coupling appears to be approximately zero). At higher temperatures, a dynamic process occurs which interchanges these two hydride ligands, leading to a triplet pattern in the ^1H NMR spectrum, with half the coupling observed in the low temperature doublet. Like the minor isomer of $[Cp^*Ir(^{13}CO)H]_2$

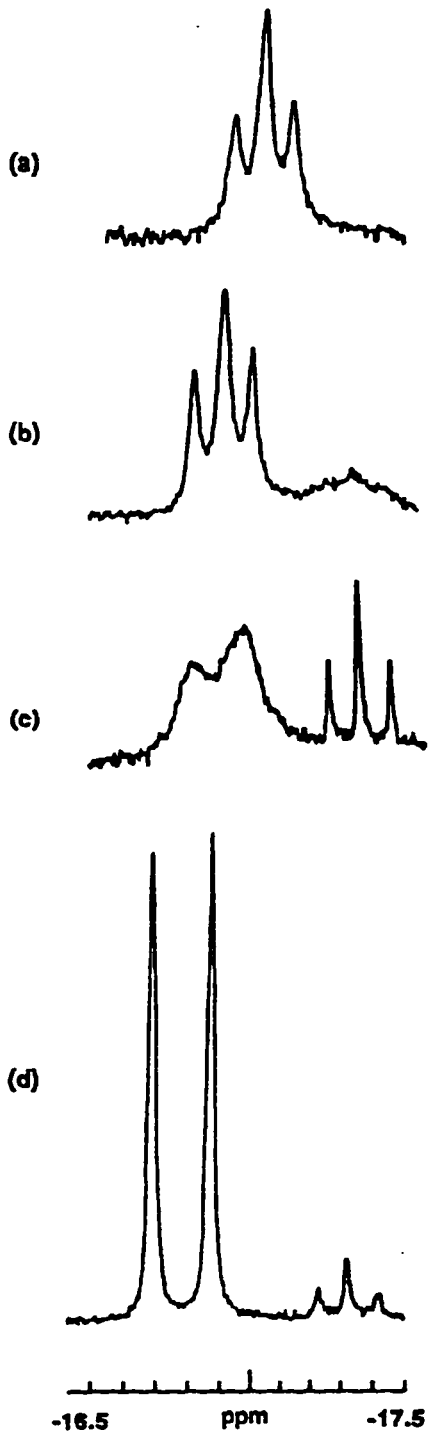

Figure 2.12. Variable temperature ^{1}H NMR (250 MHz) spectra[1,14] of the hydride region of $[CpIr(P(OPh)_3)H]_2$ (**8**) in THF-d_8: (a) 300 K, (b) 257 K, (c) 238 K, (d) 200 K.

(**6***), the minor isomer of **8** remains a triplet resonance down to low temperature. This is again consistent with either a facile hydride exchange that is not frozen out at 200 K, or a static hydride bridged structure. Integration of the hydride resonances at low temperature indicates a ratio of the major doublet to the minor triplet resonance of 4.2:1. This ratio is essentially invariant with temperature, which indicates that the enthalpy difference ($\Delta H°$) between the isomers is approximately zero. This differs from the temperature dependence of the isomer ratio in **6**, for which $\Delta H° = 1.98 \pm 0.23$ kcal mol^{-1}. Variable temperature $^{31}P\{^{1}H\}$ NMR spectra of **8** also exhibit a single resonance at room temperature that decoalesces into a major and a minor species at low temperature. The signals coalesce at 288 K. The activation energy for the interconversion was estimated at T_c: $\Delta G^{\ddagger}_{288} = 13.5 \pm 0.6$ kcal mol^{-1} for the conversion of the major species to the minor species, and $\Delta G^{\ddagger}_{288} = 12.7 \pm 0.5$ kcal mol^{-1} for the reverse reaction. These values are similar to those obtained at T_c for **6**: $\Delta G^{\ddagger}_{240} = 11.2 \pm 0.6$ and 10.0 ± 0.4 kcal mol^{-1}.

The nature of the relationship between the pair of isomers in these dihydride dimers (**6**, **7**, and **8**) warrants further discussion (refer to Fig. 2.11). Tautomers (A) seem reasonable in light of the tendency of hydride ligands to bridge metal-metal bonds. A ground state hydride-bridged structure for the minor isomer is consistent with the observation of a triplet for the upfield hydride resonance in the low temperature ^{1}H NMR spectra of **6*** and **8**. This hydride-bridged structure would have two more valence electrons than the isostructural $[Cp^*Os(CO)(\mu\text{-}H)]_2$,[37] which may be regarded as possessing a diprotonated Os=Os double bond. We might expect the Ir-Ir bonding in the hydride-bridged structure to be similar to a related Re dimer, $[Cp^*Re(CO)_2(\mu\text{-}H)]_2$, which is believed to have four electrons in two delocalized Re(μ-H)Re bonding orbitals and two electrons in a Re-Re antibonding orbital, for a net bond order of one.[49] This structural isomerization is consistent with the increase in entropy ($\Delta S° = 13.3 \pm 1.2$ eu), derived from the van't Hoff plot, for the conversion of the minor to major isomer. There

are certainly many examples of this type of bridge-terminal tautomerism for carbonyl ligands, however, we are unaware of any examples involving hydride ligands.

A complication with this tautomer scenario arises from an observation of the low temperature ^1H NMR spectra of $[CpIr(P(OPh)_3)H]_2$ (**8**) (Figure 2.12). The spectrum at 238 K exhibits a very broad doublet for the major isomer (in this case the isomer with terminal hydrides) and a sharp triplet for the minor isomer (the bridging-hydride isomer) in the hydride region. The broad resonance for the major isomer indicates that the terminal hydride ligands of this isomer are still fluxional, while the sharp triplet for the minor isomer indicates, in the context of this explanation, a static hydride bridged structure. Therefore, the hydride migration in the major isomer must proceed via a transition state that is not the doubly hydride bridged structure of the minor isomer, which seems unlikely if we assume synchronous hydride exchange. We must invoke cis and trans doubly hydride bridged structures in order to circumvent this dilemma. The major isomer could exchange hydride ligands via a hydride bridged geometry with trans Cp^* rings (top row of Scheme 2.5), whereas the minor isomer maintains a static hydride bridged structure with cis Cp^* rings.

Rotamers (B) with respect to the Ir-Ir bond is an alternative hypothesis to explain the observation of two rapidly equilibrating species for **6**, **7**, and **8**. In this scenario, the interconversion of the major to minor species involves simple rotation around the Ir-Ir bond (e.g. Cp^* ligands trans to cis). There are certainly quite a few examples of Cp metal dimers that exist as rotational isomers.[12] Of course, rotation about the Ir-Ir bond does not alter the chirality of the iridium centers. However, hydride migration between Ir atoms within a given rotamer would lead to racemization of those metal centers (top or bottom row of Scheme 2.5) and hence would also render the diastereotopic groups of $[Cp^{\wedge}Ir(CO)H]_2$ (**7**) equivalent. In order to account for the observation of a doublet hydride resonance for the major isomer and a triplet hydride resonance for the minor

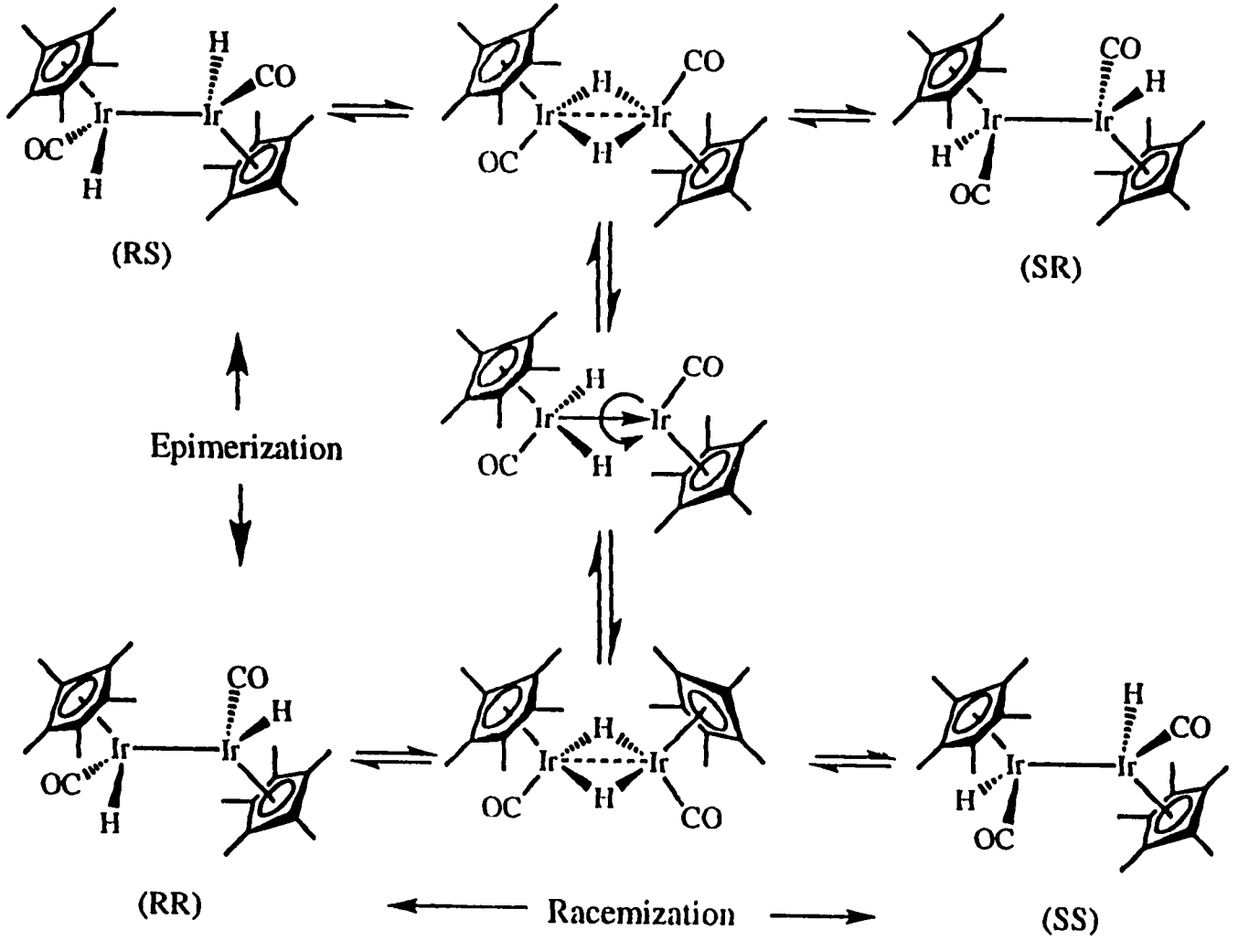

Scheme 2.5

isomer in the low temperature ^{1}H NMR spectra of **6*** and **8**, this scenario requires that the hydride migration in the minor isomer is more facile than that in the major isomer, and that the hydride exchange in the minor isomer cannot be frozen out at the lowest temperatures attained. The rotamer hypothesis (B) also necessitates that only a single diastereomer is present. Hence, the reactions which lead to formation of all the neutral dihydride dimers would be completely diastereoselective. As was discussed earlier, the observation that the ^{1}H NMR spectra of **3**, **4**, and **5**, exhibit only one set of resonances at all temperatures, may indicate that these trihydride cation dimers each exist as a single diastereomer. Therefore, deprotonation of a single diastereomer of a trihydride cation dimer might generate a single diastereomer of the corresponding neutral dihydride dimer (**6**, **7**, or **8**).

Since both metal centers in dimers such as **6**, **7**, and **8** are chiral, the existence of two diastereomers (C) is possible (Scheme 2.5). It is proposed that rapid epimerization occurs, causing equilibration of the two diastereomers (the racemic pair and the meso structure). Note that within a single diastereomer, the hydride site exchange process will lead to synchronous inversion of configuration at both Ir centers (i.e. racemization) *without* epimerization. In order for epimerization to occur, we postulate a mechanism that proceeds via an intermediate in which both hydrides are transiently bound to the same iridium. Rotation (180°) about the Ir-Ir dative bond, reformation of a hydride-bridged structure, followed by synchronous opening of the Ir-(μ-H)-Ir bonds completes the process. A related mechanism has been proposed by Herrmann et al.[50] to account for the change in stereochemistry at Rh in the ring opening of a dimetallacyclopropane (equation 2.3). Protonation of the stereochemically rigid *trans*-[CpRh(CO)]$_2$(μ-CH$_2$)

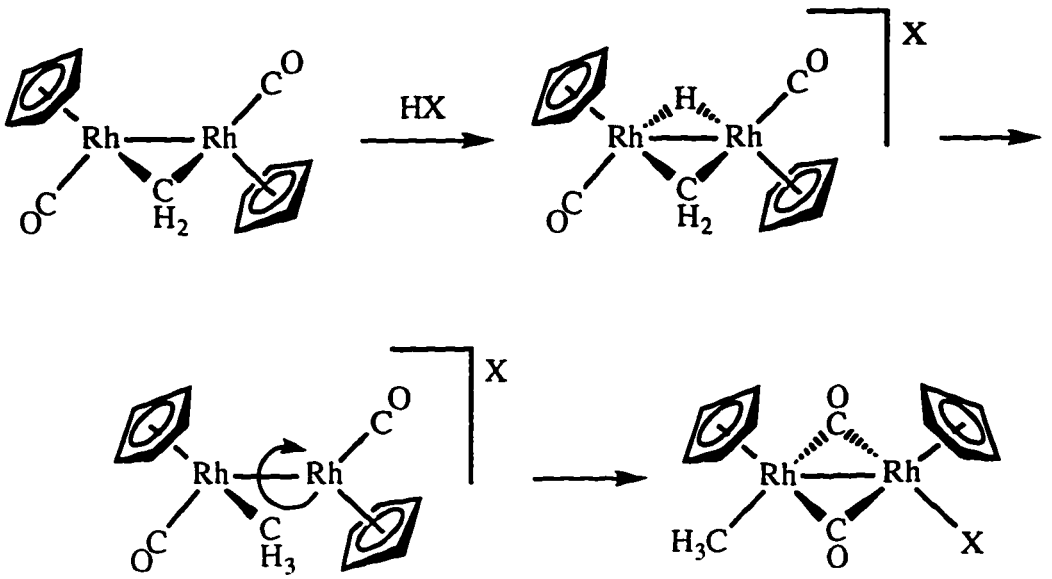

(2.3)

(RR or SS) with HCl or HBr leads to the cis halo methyl product, via rotation about the unbridged Rh-Rh bond. Similarly, Heinekey and Michel[51] speculated that rapid cis/trans isomerization in $[Cp^*Ir(CO)]_2(\mu\text{-}CH_2)(\mu\text{-}H)^+$ proceeds via rotation about the Ir-Ir bond in a methyl tautomer.

The diastereomer theory (C) requires that each diastereomer exist as a single rotamer. As was the case for the rotamer hypothesis, the proposed equilibrium between two diastereomers requires a greater barrier to hydride exchange in the major isomer than in the minor isomer. This may not be unreasonable, based upon similar situations involving carbonyl exchange between metal centers. For example, bridge-terminal carbonyl exchange in $[CpFe(CO)_2]_2$ is much more facile in the trans isomer than in the cis isomer.[12] If we assume, as in the carbonyl case, that the hydrides must be trans to each other in order to exchange in a synchronous fashion, then the permutation in the meso structure (RS or SR) should be more facile than that in the racemic pair (RR/SS) since it allows the sterically demanding Cp^* rings to be disposed in a trans geometry (Figure 2.13). The relatively large free energy difference between the major and minor

isomer of $[Cp^*Ir(CO)H]_2$ (**6**) ($\Delta G°_{298} \approx 2.0$ kcal mol^{-1}, $K_{eq} = 29$) would be somewhat unusual for diastereomers, which are usually quite close in energy.

It should be noted that the suggestion of rapid racemization or epimerization of pseudo-octahedral complexes of iridium is somewhat novel. In closely related monomeric complexes such as $Cp^*Ir(CO)(H)(CH_2CMe_3)$,[52] the diastereotopic methylene protons are distinct in the ^1H NMR spectrum at room temperature, indicating that the metal center is configurationally rigid on the NMR time scale at this temperature. Similar observations have been reported[53] for $Cp^*Ir(PMe_3)(H)(CH_2CMe_3)$.

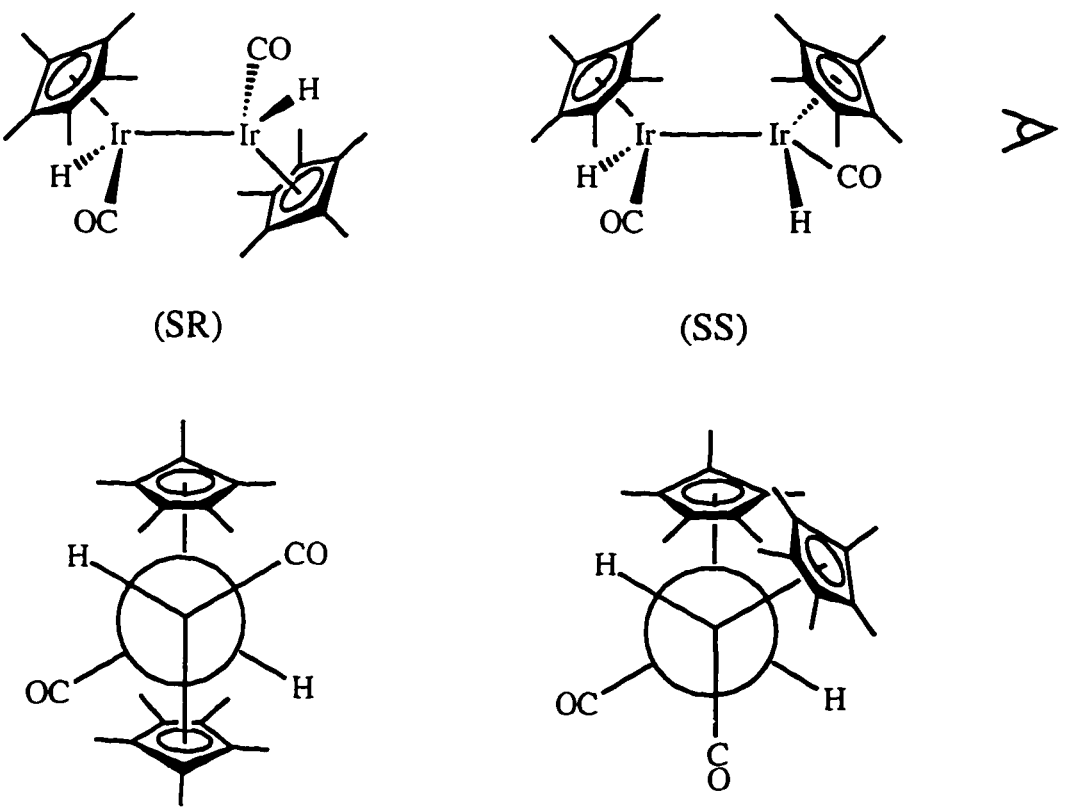

Figure 2.13. Newman projections of the meso (RS or SR) and racemic (RR/SS) diastereomers of $[Cp^*Ir(CO)H]_2$ (**6**).

Conclusion

The protonation of monomeric dihydrides of the form $Cp'Ir(CO)H_2$ ($Cp' = C_5Me_5$ (**1**) or C_5Me_4Et (**2**)) provides an efficient route for the generation of the dinuclear complexes $[Cp'Ir(CO)H]_2(\mu\text{-}H)^+$ (**3** and **4**). The resulting cationic trihydride dimers each exhibit a single resonance in the hydride region of the ^1H NMR spectrum at ambient temperature. Variable temperature ^1H NMR spectroscopy reveals that the ground state structure possesses one bridging and two terminal hydride ligands, which rapidly exchange at room temperature. Compounds **3** and **4** can each achieve two diastereomeric configurations (RR/SS or RS/SR) due to the presence of two chiral iridium centers per molecule. Room temperature ^1H and $^{13}C\{^1H\}$ NMR spectra of the lower symmetry complex, $[Cp^{\wedge}Ir(CO)H]_2(\mu\text{-}H)^+$ (**4**), indicate that the iridium centers are configurationally unstable on the NMR timescale.

Deprotonation of **3** and **4** affords the neutral dihydride dimers $[Cp'Ir(CO)H]_2$ (**6** and **7**). Variable temperature ^1H NMR, IR, and crystallographic analyses indicate that these compounds have terminal hydride and terminal carbonyl ligands, i.e. unsupported Ir-Ir bonds. Very few examples of this structural type have been reported previously. As in **3** and **4**, the hydride ligands of **6** and **7** rapidly permute between chiral iridium centers at room temperature. Although closely related monomeric complexes are configurationally stable on the NMR timescale, these dimers undergo facile racemization. Compounds **6** and **7** each exist as unequal mixtures of two isomers, which rapidly interconvert at room temperature. The relationship between the two isomers has not been unequivocally determined, though epimerization of diastereomers is favored.

Experimental

General Procedures. All manipulations were conducted under argon and nitrogen using standard Schlenk and drybox techniques. Argon and nitrogen were deoxygenated and dried by passage through Chemical Dynamics Corp. R3-11 CuO catalyst followed by Mallinckrodt Aquasorb containing P_2O_5. Air-sensitive compounds were manipulated in an MBraun labmaster 130 glove box equipped with integrated dry train loaded with copper catalyst and molecular sieves. Solvents were purified by distillation from Na/K/benzophenone (except CH_2Cl_2 from P_2O_5) under nitrogen. Deuterated NMR solvents (purchased from Cambridge Isotope Laboratories) were degassed, and stored over the following drying agents: CD_2Cl_2, $CDCl_3$, CD_3NO_2, CD_3CN over CaH_2; C_6D_6, methylcyclohexane-d_{14}, THF-d_8 over Na/K/benzophenone; $(CD_3)_2CO$ over molecular sieves (4 Å). $CDFCl_2$ was prepared according to the reported procedure[54] and stored over CaH_2.

Carbon monoxide-^{13}C (99%) was purchased from Cambridge Isotope Laboratories and adsorbed on activated charcoal (coconut, 8-12 mesh, EM Science) at 77 K. Charcoal was activated by heating to 530 °C in a thick-walled brass tube for 16 hours under dynamic vacuum.

Ethyltetramethylcyclopentadiene ($HCp^{\wedge}$) was prepared according to the procedure for synthesis of pentamethylcyclopentadiene (HCp^*),[55] with substitution of ethyl propionate for ethyl acetate. $[Cp^{\wedge}IrCl_2]_2$ was synthesized from $[(COD)IrCl]_2$ (COD = 1,5-cyclooctadiene) and $Cp^{\wedge}$ according to the method reported[20] for $[Cp^*IrCl_2]_2$. $Cp^*Ir(CO)Cl_2$ was prepared with slight modification to the published procedure.[16] $[CpIr(P(OPh)_3)H]_2(\mu\text{-}H)^+$ and $[CpIr(P(OPh)_3)H]_2$ were prepared by the reported method.[1] Triflic acid ($HOSO_2CF_3$) and 1,8-bis(dimethylamino)naphthalene (Proton Sponge®) were purchased from Aldrich Chemical Co. and used as received. Carbon monoxide (99.99%) was purchased from Airco.

^{1}H NMR spectra were recorded on Bruker AC200, AF300, or WM500 spectrometers and referenced internally to the residual proton resonance of the deuterated solvent or tetramethylsilane (TMS). ^{13}C NMR spectra were collected on the AC200, AF300 and WM500 spectrometers operating at a frequency of 50.32, 75.46 and 125.76 MHz respectively and referenced internally to the solvent. ^{31}P NMR spectra were collected on the AC200 and WM500 spectrometers at frequencies of 81.02 and 202.45 MHz respectively, and referenced externally to 85% H_3PO_4. Variable temperature ^{1}H NMR measurements were performed using the Bruker B-VT1000 temperature control module with a copper/constantan thermocouple. Temperature calibration was obtained by measurement of the chemical shift difference between the $-CH_3$ and -OH peaks of pure methanol using the method of Van Geet [56]. Temperature calibration below the freezing point of methanol was achieved with a copper/constantan thermocouple inserted in the NMR probe sample chamber. Line shape analysis of variable temperature ^{1}H NMR spectra was performed using a modified version of the DYNAMAR program [57]. Proton T_1 measurements were performed using the standard inversion recovery 180°-τ-90° sequence.[58]

Air-sensitive samples to be analyzed by NMR spectroscopy were prepared in Wilmad J. Young® valve NMR tubes (equipped with a threaded Teflon piston, referred to herein as a "screw-cap" NMR tube) or flame-sealed in NMR tubes attached to Kontes high vacuum Teflon stopcocks adapted for vacuum line connection

Infrared spectra were recorded on a Perkin-Elmer Model 1600 Fourier transform spectrophotometer (2.0 cm^{-1} resolution). Samples were examined as solutions in sealable 0.1 mm path length NaCl cells, Nujol mulls, or KBr pellets.

Electron impact mass spectra were obtained using a Kratos Profile HD3 magnetic sector instrument with a direct insertion probe. Data were collected in nominal mode which rounds off results to the nearest mass unit.

UV/Vis spectra were acquired on a Hewlett-Packard HP8452a spectrophotometer. Samples were analyzed in quartz cells (1.0 cm diameter) equipped with Teflon stopcocks.

Elemental analyses were performed by Galbraith Laboratories.

Cp^Ir(CO)Cl$_2$. A vessel fitted with a high vacuum Teflon stopcock was charged with [Cp^IrCl$_2$]$_2$ (0.62 g, 0.75 mmol). Methylene chloride (10 mL) was vacuum transferred onto the solid. The red-orange solution was subjected to three freeze-pump-thaw cycles, pressurized with CO (2.1 atm), and allowed to stir overnight. The solution was transferred via filter cannula into cold stirring heptane, causing immediate precipitation of the product. The yellow powder was collected by filtration through a medium glass frit, washed with heptane, and dried in a desiccator. Yield 0.61 g (92%). Recrystallization from CH_2Cl_2/Et_2O afforded yellow-olive green crystals. ^{1}H NMR ($CDCl_3$): δ 2.31 (q, J = 7.6 Hz, 2 H, $C_5(CH_2CH_3)$); 1.95, 1.90 (s, 6 H each, $C_5(CH_3)$); 1.19 (t, J = 7.6 Hz, 3 H, $C_5(CH_2CH_3)$). IR (Nujol): 2034 cm^{-1} (s, ν_{CO}). Anal. Calcd. for $C_{12}H_{17}Cl_2IrO$: C, 32.73; H, 3.89. Found: C, 32.34; H, 3.95.

Cp*Ir(CO)H$_2$ (1). Methanol (about 20 mL) was added to a Schlenk flask charged with 0.27 g of Cp*Ir(CO)Cl$_2$ (0.64 mmol) and 0.43 g of Zn dust (6.6 mmol). Glacial acetic acid (1.0 mL) was added and the mixture was immediately subjected to three freeze-pump-thaw cycles. The solution was allowed to stir overnight under argon. An aqueous solution of NaOH saturated with NaCl (approx. 15 mL, argon sparged) was transferred via cannula to the deep purple-red solution and stirred for 20 min. The mixture was extracted with 4 x 10 mL of pentane. The extracts were transferred via cannula onto oven-dried $MgSO_4$ and left to stir for one hour. The pale gold-colored liquid was transferred via filter cannula to a sublimation apparatus. The $MgSO_4$ was washed with pentane and this liquid was combined with the previous extracts. The solvent was

removed in vacuo leaving a mostly white crystalline residue, with some brown material. The air-sensitive product was isolated by sublimation (35 °C, dynamic vacuum) into a liquid N_2 cooled Schlenk flask. Low melting, pale yellow crystals were recovered and stored under argon at -30 °C. Yield: 0.23 ± 0.02 g (ca. 100%). $Cp^*Ir(CO)H_2$ also precipitates from concentrated, cold (-78 °C) pentane solutions as large needles. ^1H NMR (CD_2Cl_2): δ 2.22 (s, 15 H, Cp^*), -16.48 (s, 2 H, Ir-H). ^1H NMR (C_6D_6): δ 1.87 (t, $^4J_{H-H}$ = 0.8 Hz, Cp^*); -15.76 (m, $^4J_{H-H}$ = 0.8 Hz, Ir-H). $^{13}C\{^1H\}$ NMR ($CDFCl_2$): δ 98.0 (s, $C_5(CH_3)_5$); 11.1 (s, $C_5(CH_3)_5$). $^{13}C\{^1H\}$ NMR (C_6D_6): δ 97.1 (s, $C_5(CH_3)_5$); 10.6 (s, $C_5(CH_3)_5$). IR (Nujol): 2131 (m, ν_{IrH}) , 2013 (m), 1990 (s), 1945 cm^{-1} (m). Anal. Calcd. for $C_{11}H_{17}IrO$: C, 36.96; H, 4.79. Found: C, 36.60; H, 4.70.

$Cp^*Ir(^{13}CO)H_2$. Prepared as above for $Cp^*Ir(CO)H_2$. ^1H NMR (CD_2Cl_2): δ 2.22 ("q", $^4J_{H-H}$ = 0.7 Hz, $^4J_{H-C}$ = 0.6 Hz, Cp^*); -16.49 (d of m, $^4J_{H-H}$ = 0.7 Hz, $^2J_{H-C}$ = 8.7 Hz, Ir-H). In the $^{13}C\{^1H\}$ NMR (CD_2Cl_2) spectrum of the enriched sample, a singlet resonance for the carbonyl ligand was detected at δ 171.5. IR (Nujol): 2131 (m, ν_{IrH}) , 1964 (sh), 1942 (s), 1900 cm^{-1} (m). IR (heptane): 2137 (m, ν_{IrH}) , 1970 (m), 1950 (s), 1906 cm^{-1} (m).

$Cp^\wedge Ir(CO)H_2$ (2). Prepared as above for $Cp^*Ir(CO)H_2$. Recovered as an air-sensitive pale yellow oil. ^1H NMR (CD_2Cl_2): δ 2.46 (q, J = 7.6 Hz, 2 H, $C_5(CH_2CH_3)$); 2.22, 2.21 (s, 6 H each, $C_5(CH_3)$); 1.07 (t, J = 7.6 Hz, 3 H, $C_5(CH_2CH_3)$); -16.47 (s, 2 H, Ir-H). $^{13}C\{^1H\}$ NMR (CD_2Cl_2): δ 171.5 (s, CO); 103.9 (s, $C(CH_2CH_3)$); 97.7, 97.6 (s, $C(CH_3)$); 18.8 (s, $C(CH_2CH_3)$); 17.7 (s, $C(CH_2CH_3)$); 11.0, 10.8 (s, $C(CH_3)$).

$\{[Cp^*Ir(CO)H]_2(\mu\text{-}H)\}SO_3CF_3$ (3). A small Schlenk flask was charged with 34 mg of $Cp^*Ir(CO)H_2$ (1) (0.094 mmol). Methylene chloride (2-3 mL) was transferred onto the

solids via cannula furnishing a pale yellow solution. With the solution immersed in a CO_2/isopropanol bath, trifluoromethanesulfonic acid (8 μL, 0.09 mmol, 100% stoichiometric excess) was added via syringe. Three freeze/pump/thaw cycles (thaw to -78 °C) were performed and the solution stirred for 30 min at -78 °C. The flask was then transferred to an ice/NaCl bath and the solution stirred for an additional 30 min, becoming deep yellow. The solvent was removed in vacuo and the yellow-brown residue was washed with three aliquots of cold Et_2O. Residual volatiles were removed under vacuum overnight leaving a light brown, air-sensitive solid. Yield: 26 mg (66%). A larger batch was prepared using 274 mg of $Cp^*Ir(CO)H_2$ and 0.74 equiv of triflic acid (yield = 54%). ^1H NMR (CD_2Cl_2): δ 2.22 (s, 30 H, Cp^*); -16.46 (s, 3 H, Ir-H). ^1H NMR ($CDFCl_2$, 300 K): δ 2.23 (s, Cp^*); -16.44 (s, Ir-H); ($CDFCl_2$, 138 K): δ 2.24 (s, Cp^*), -15.35 (br s, 2 H, Ir-$H_{terminal}$); -18.10 (br s, 1 H, Ir-H_{bridge}). $^{13}C\{^1H\}$ NMR ($CDFCl_2$): δ 120.1 (q, J_{C-F} = 317 Hz, SO_3CF_3); 102.0 (s, $C_5(CH_3)_5$); 10.9 (s, $C_5(CH_3)_5$). IR (Nujol): 2111 (w, ν_{Ir-H}); 2020, 1990 cm^{-1} (s, ν_{CO}).

{[Cp*Ir(^{13}CO)H]$_2$(μ-H)}SO_3CF_3 (3*). Prepared using a procedure analogous to that for **3**. ^1H NMR ($CDFCl_2$): δ 2.23 (s, Cp^*); -16.44 (br s, Ir-H). The linewidth of the hydride resonance is increased by an unresolved coupling to the protons of the Cp^* rings. When a spectrum was collected with selective homonuclear decoupling of the Cp^* resonance, the hydride resonance was resolved into a triplet (J_{C-H} = 3.4 Hz). In the $^{13}C\{^1H\}$ NMR ($CDFCl_2$) a singlet resonance for the carbonyl ligands was observed at δ = 166.9.

{[Cp^Ir(CO)H]$_2$(μ-H)}SO_3CF_3 (4). Prepared as above for **3**. Recovered as yellow-brown oil. ^1H NMR (CD_2Cl_2): δ 2.48 (q, J = 7.6 Hz, 4 H, $C_5(CH_2CH_3)$); 2.22, 2.20 (s, 12 H each,); 1.13 (t, J = 7.6 Hz, 6 H, $C_5(CH_2CH_3)$); -16.52 (s, 3 H, Ir-H). $^{13}C\{^1H\}$

NMR (CD_2Cl_2): δ 166.2 (s, CO); 105.7 (s, $C(CH_2CH_3)$); 102.1, 101.4 (s, $C(CH_3)$); 18.7 (s, $C(CH_2CH_3)$); 15.7 (s, $C(CH_2CH_3)$); 10.6, 10.5 (s, $C(CH_3)$).

[Cp*Ir(CO)H]$_2$ (6). Methylene chloride (20 mL) was added via cannula to a Schlenk flask containing 178 mg of **3** (0.207 mmol) and 53.9 mg of proton sponge (0.252 mmol, 1.2 equiv). The solution was subjected to a freeze/pump/thaw cycle and allowed to stir for 2 h. The solvent was removed in vacuo leaving a yellow-brown residue. The residue was extracted with heptane (4 x 10 mL) and the yellow extracts transferred to a clean Schlenk flask via filter cannula. The solution was concentrated in vacuo to 10 mL and storage at -30 °C for 16 h afforded fine yellow needles. The product was washed with cold heptane and dried under vacuum. Yield: 130 mg (88%). [Cp*Ir(CO)H]$_2$ can be sublimed at 95 °C under static vacuum to yield yellow crystals. ^{1}H NMR (CD_2Cl_2): δ 2.13 (s, 30 H, Cp*); -16.30 (s, 2 H, Ir-H). ^{1}H NMR (C_6D_6): δ 2.04 (s, Cp*); -15.91 (s, Ir-H). ^{1}H NMR (C_7D_{14}): δ 2.11 (s, Cp*); -16.31 (s, Ir-H). ^{1}H NMR ($CDFCl_2$, 300 K): δ -16.2 (s, Ir-H); ($CDFCl_2$, 147 K): δ -15.89 (s, Ir-H, major isomer); -19.02 (s, Ir-H, minor isomer). Proton T_1 (298 K, 200 MHz, CD_2Cl_2): 3.62 s (Cp*), 6.55 s (Ir-H). ^{13}C{^{1}H} NMR (CD_2Cl_2): δ 96.82 (s, C_5Me_5); 11.32 (s, C_5Me_5). IR (heptane): 2180 (w, ν_{Ir-H}); 1971, 1942 cm^{-1} (s, ν_{CO}). IR (Nujol): 2177, 2161 (w, ν_{Ir-H}); 1956, 1935, 1929 (s), 1894 (w) cm^{-1} (ν_{CO}). MS (EI): m/e 712 ([(Cp*^{191}Ir(CO)H)-(Cp*^{193}Ir(CO)H)]$^+$). UV/Vis (C_6H_6) [λ_{max}, nm (ε, M^{-1} cm^{-1}]: 320 (1.3 x 10^4), 382 (5.5 x 10^3).

[Cp*Ir(^{13}CO)H]$_2$ (6*). Prepared as above for **6**. The linewidth of the hydride resonances is increased by an unresolved coupling to the protons of the Cp* rings. ^{1}H NMR spectra were collected with selective homonuclear decoupling of the Cp* resonances. ^{1}H NMR ($CDFCl_2$, 300 K): δ 2.15 (s, Cp*); δ -16.22 (br t, J_{C-H} = 4.5 Hz,

Ir-H). ^{1}H NMR ($CDFCl_2$, 145 K): δ −15.89 (d, J = 7.9 Hz); -19.04 (t, J = 6.0 Hz). $^{13}C\{^1H\}$ NMR (CD_2Cl_2): δ 176.5 (s, CO); 11.3 (s, C_5Me_5).

[Cp^Ir(CO)H]$_2$ (7). Prepared as above for **6**. ^{1}H NMR (CD_2Cl_2): δ 2.46 (q, J = 7.6 Hz, 4 H, $C_5(CH_2CH_3)$); 2.13, 2.12 (s, 12 H each,); 1.03 (t, J = 7.6 Hz, 6 H, $C_5(CH_2CH_3)$); -16.24 (s, 2 H, Ir-H). $^{13}C\{^1H\}$ NMR ($CDFCl_2$): δ 97.6, 96.8 (s, $C(CH_3)$); 20.0 (s, $C(CH_2CH_3)$); 16.5 (s, $C(CH_2CH_3)$); 11.5, 11.3 (s, $C(CH_3)$). IR(Nujol): 2202 (w, $\nu_{Ir\text{-}H}$); 1968, 1939 (s), 1921 (sh) cm^{-1} (ν_{CO}). Anal. Calcd. for $C_{24}H_{36}Ir_2O_2$: C, 38.90; H, 4.90. Found: C, 38.40; H, 4.74.

X-ray Structure Determination of [Cp*Ir(CO)H]$_2$ (6). This crystal was generated unintentionally in an attempt to induce reductive elimination of hydrogen from [Cp*Ir(CO)H]$_2$ via solid state thermolysis. An NMR tube equipped with a high vacuum Teflon stopcock was charged with 3.1 mg of [Cp*Ir(CO)H]$_2$ (**6**) in the glove box. The tube was sealed under vacuum and the bottom (ca. 1-2 cm) was submerged in a sand bath at 96 °C. After heating overnight, large yellow crystals of **6** had sublimed onto the sides of the NMR tube, just above the level of the sand bath. The tube was cracked under a flow of argon, and the crystals shaken into a petri dish containing Paratone oil. One such crystal of dimensions 0.10 x 0.10 x 0.30 mm was mounted in a stream of nitrogen gas at 183 K on an Enraf-Nonius CAD-4 diffractometer using MoKα radiation with a graphite monochromator (λ = 0.71073 Å). Systematic absences were consistent with the orthorhombic space group Pbca. A total of 3817 independent reflections were collected with $2\theta \leq 50°$, of which 2275 with $I > 4\sigma(I)$ were used in the refinement. The structure was solved by direct methods which gave the location of the Ir atoms. The remaining non-hydrogen atoms were located from difference Fourier maps. The hydrogen atoms

were placed at calculated positions. Hydrides bound to iridium were not located. The final R factor was 3.75%.

X-ray Structure Determination of [Cp^Ir(CO)H]$_2$ (7). As part of the synthesis of [Cp^Ir(CO)H]$_2$, the heptane extracts containing [Cp^Ir(CO)H]$_2$ were reduced in vacuo in a Schlenk flask, generating bright yellow crystals. The supernatant was transferred to a clean flask via cannula and the crystals exposed briefly to dynamic vacuum to remove residual solvent. Against a strong flow of argon, several crystals were removed using a spatula tipped with a small amount of grease and transferred immediately to a petri dish containing Paratone oil. One such crystal of dimensions 0.25 x 0.30 x 0.35 mm was mounted in a stream of nitrogen gas at 183 K on an Enraf-Nonius CAD-4 diffractometer using MoKα radiation with a graphite monochromator (λ = 0.71073 Å). Systematic absences were consistent with the monoclinic space group C2/c. A total of 2084 independent reflections were collected with $2\theta \leq 50°$, of which 1753 with $I > 4\sigma(I)$ were used in the refinement. The structure was solved by direct methods which gave the location of the Ir atoms. The remaining non-hydrogen atoms were located from difference Fourier maps. The hydrogen atoms were placed at calculated positions. Hydrides bound to iridium were not located. The final R factor was 2.98%.

X-ray Structure Determination of {[Cp*Ir(CO)H]$_2$(μ-H)}BAr'$_4$ (3-BAr'$_4$). Crystals were generated in a sealed NMR tube as described in Chapter 5 (Cp*Ir(CO)H$_2$ + Cp*Ir(CO)(CH$_3$)$_2$ + HBAr'$_4$•(Et$_2$O)$_2$). The tube was cracked under a blanket of argon and the crystals shaken into a petri dish containing Paratone oil. A green trapezoidal plate was selected of dimensions 0.12 x 0.28 x 0.40 mm and mounted in a stream of nitrogen gas at 183 K on an Enraf-Nonius CAD-4 diffractometer using MoKα radiation. The data were collected for a triclinic cell and the assigned space group was P1(bar). The

unit cell contained two unique molecules, with only slight structural differences. A total of 14536 independent reflections were collected with $2\theta \leq 45^{\circ}$, of which 10793 with $I > 4\sigma(I)$ were used in the refinement. The structure was solved primarily from the Patterson map. The remaining non-hydrogen atoms were located from difference Fourier maps. The hydrogen atoms were placed at calculated positions. Hydrides bound to iridium were not located. The final R factor was 4.48%.

Notes to Chapter 2

(1) Portions of this chapter have previously been reported: Heinekey, D. M.; Fine, D. A.; Harper, T. G. P.; Michel, S. T. *Can. J. Chem.* **1995**, *73*, 1116-1125.

(2) *Transition Metal Hydrides*; Muetterties, E. L., Ed.; Marcel Dekker: New York, 1971.

(3) *Transition Metal Hydrides*; Dedieu, A., Ed.; VCH: New York, 1992.

(4) Kaesz, H. D.; Saillant, R. B. *Chem. Rev.* **1972**, *72*, 231-281.

(5) Venanzi, L. M. *Coord. Chem. Rev.* **1982**, *43*, 251-274.

(6) Muetterties, E. L.; Rhodin, T. N.; Band, E.; Brucker, C. F.; Pretzer, W. R. *Chem. Rev.* **1979**, *79*, 91-137.

(7) Moss, J. R.; Graham, W. A. G. *Inorg. Chem.* **1977**, *16*, 75-79.

(8) Moss, J. R.; Graham, W. A. G. *J. Chem. Soc., Dalton Trans.* **1977**, 89-94.

(9) Evans, J.; Okrasinski, S. J.; Pribula, A. J.; Norton, J. R. *J. Am. Chem. Soc.* **1976**, *98*, 4000-4001.

(10) Krusic, P. J.; Jones, D. J.; Roe, D. C. *Organometallics* **1986**, *5*, 456-460.

(11) Faller, J. W.; Anderson, A. S. *J. Am. Chem. Soc.* **1970**, *92*, 5852-5860.

(12) Adams, R. D.; Cotton, F. A. In *Dynamic Nuclear Magnetic Resonance Spectroscopy*; Jackman, L. M. and Cotton, F. A., Eds.; Academic: New York, 1975; pp 489-522.

(13) Heinekey, D. M.; Millar, J. M.; Koetzle, T. F.; Payne, N. G.; Zilm, K. W. *J. Am. Chem. Soc.* **1990**, *112*, 909-919.

(14) Michel, S. Ph.D. Thesis, Yale University, Dec. 1989.

(15) Heinekey, D. M.; Harper, T. G. P. , Yale University, unpublished results.

(16) Kang, J. W.; Maitlis, P. M. *J. Organomet. Chem.* **1971**, *26*, 393-399.

(17) Similar Cp^*-hydride 4-bond coupling has been observed in: a) $Cp^*Ir(CO)(CH_2CMe_3)H$; Hoyano, J. K.; Graham, W. A. G.; *J. Am. Chem. Soc.* **1982**,

104, 3723-3725. b) $Cp^*Ir(PMe_3)(R)H$ (R = cyclohexane, neopentane); Janowicz, A. H.; Bergman, R. G. *J. Am. Chem. Soc.* **1982**, *104*, 352-354. c) $[Cp^*IrCl]_2(\mu\text{-}H)(\mu\text{-}Cl)$; Maitlis, P. M.; White, C.; Oliver, A. J. *J. Chem. Soc., Dalton Trans.* **1973**, 1901-1907. .

(18) Collman, J. P.; Hegedus, L. S.; Norton, J. R.; Finke, R. G. *Principles and Applications of Organotransition Metal Chemistry*; University Science Books: Mill Valley, California, 1987.

(19) Dooley, T.; Fairhurst, G.; Chalk, C. D.; Tabatabaian, K.; White, C. *Transition Met. Chem.* **1978**, *3*, 299-302.

(20) Synthesis of $[Cp^*IrCl_2]_2$ from $[(COD)IrCl]_2$: El Amouri, H.; Gruselle, M.; Jaouen, G. *Synth. React. Inorg. Met.-Org. Chem.* **1994**, *24*(3), 395-400.

(21) Ogilvy, A. E.; Rauchfuss, T. B. *Organometallics* **1988**, *7*, 1884-1885.

(22) Shanan-Atidi, H.; Bar-Eli, K. H. *J. Phys. Chem.* **1970**, *74*(4), 961-963.

(23) Ball, R. G.; Graham, W. A. G.; Heinekey, D. M.; Hoyano, J. K.; McMaster, A. D.; Mattson, B. M.; Michel, S. T. *Inorg. Chem.* **1990**, *29*, 2023-2025.

(24) Synthesis of $[(COD)IrCl]_2$: Crabtree, R. H.; Quirk, J. M. *Synth. React. Inorg. Met.-Org. Chem.* **1982**, *12*(4), 407-413.

(25) Kauffman, G. B.; Meyers, R. D. *Inorg. Synth.* **1978**, *18*, 131-133.

(26) Shapley, J. R.; Adair, P. C.; Lawson, R. J.; Pierpont, C. G. *Inorg. Chem.* **1982**, *21*, 1701-1702.

(27) Graham, W. A. G. *J. Organomet. Chem.* **1986**, *300*, 81-91.

(28) Gilbert, T. M. Ph.D. Thesis, University of California, Berkeley, 1985.

(29) Werner, H.; Wolf, J. *Angew. Chem. Int. Ed. Engl.* **1982**, *21*(4), 296-297.

(30) Gilbert, T. M.; Bergman, R. G. *J. Am. Chem. Soc.* **1985**, *107*, 3502-3507.

(31) The crystal structure of $Cp^*Ir(PMe_3)(Cy)H$ consists of two independent molecules; we report angles herein as mean values of the two. Buchanan, M. J.; Stryker, J. M.; Bergman, R. G. *J. Am. Chem. Soc.* **1986**, *108*, 1537-1550.

(32) Angoletta, M.; Ciani, G.; Manassero, M.; Sansoni, M. *J. Chem. Soc., Chem. Commun.* **1973**, 789-790.

(33) Rasmussen, P. G.; Anderson, J. E.; Bailey, O. H.; Tamres, M. *J. Am. Chem. Soc.* **1985**, *107*, 279-281.

(34) Ciriano, M. A.; Sebastian, S.; Oro, L. A.; Tiripicchio, A.; Tiripicchio Camellini, M.; Lahoz, F. J. *Angew. Chem. Int. Ed. Engl.* **1988**, *27*, 402-403.

(35) Einstein, F. W. B.; Jones, R. H.; Zhang, X.; Yan, X.; Negelkerke, R.; Sutton, D. *J. Chem. Soc., Chem. Commun.* **1989**, 1424-1426.

(36) Beringhelli, T.; Ciani, G.; D'Alfonso, G.; Garlaschelli, L.; Moret, M.; Sironi, A. *J. Chem. Soc., Dalton Trans.* **1992**, 1865-1866.

(37) Hoyano, J. K.; Graham, W. A. G. *J. Am. Chem. Soc.* **1982**, *104*, 3722-3723.

(38) Churchill, M. R.; Deboer, B. G.; Rotella, F. J. *Inorg. Chem.* **1976**, *15*, 1843-1853.

(39) Dahl, L. F. *Ann. N.Y. Acad. Sci.* **1983**, 1-26, and references therein.

(40) Churchill, M. R. *Adv. Chem. Ser.* **1978**, *167*, 36-60.

(41) Bau, R.; Teller, R. G.; Kirtley, S. W.; Koetzle, T. F. *Acc. Chem. Res.* **1979**, *12*, 176-183.

(42) Burns, C. J.; Rutherford, N. M.; Berg, D. J. *Acta Crystallogr., Sect. C* **1987**, *43*, 229-231.

(43) Werner, H.; Treiber, M.; Nessel, A.; Lippert, F.; Betz, P.; Kruger, C. *Chem. Ber.* **1992**, *125*, 337-346.

(44) Sloan, T. E. In *Topics in Inorganic and Organometallic Stereochemistry*; Geoffroy, G. L., Ed.; Wiley: New York, 1981; Vol. 12; pp 1-36.

(45) Chinn, M. S. Ph.D. Thesis, Yale University, 1989.

(46) Sweet, J. R. Ph.D. Thesis, University of Alberta, 1981.

(47) Galakhov, M. V.; Gil, A.; de Jesús, E.; Royo, P. *Organometallics* **1995**, *14*, 3746-3750.

(48) Brunner, H. *Adv. Organomet. Chem.* **1980**, *18*, 151-206.

(49) Casey, C. P.; Sakaba, H.; Hazin, P. N.; Powell, D. R. *J. Am. Chem. Soc.* **1991**, *113*, 8165-8166.

(50) Herrmann, W. A.; Plank, J.; Riedel, D.; Ziegler, M. L.; Weidenhammer, K.; Guggolz, E.; Balbach, B. *J. Am. Chem. Soc.* **1981**, *103*, 63-75.

(51) Heinekey, D. M.; Michel, S. T. *Organometallics* **1989**, *8*, 1241-1246.

(52) Hoyano, J. K.; Graham, W. A. G. *J. Am. Chem. Soc.* **1982**, *104*, 3723-3725.

(53) Janowicz, A. H.; Bergman, R. G. *J. Am. Chem. Soc.* **1983**, *105*, 3929-3939.

(54) Siegel, J. S.; Anet, F. A. L. *J. Org. Chem.* **1988**, *53*, 2629-2630.

(55) Threlkel, R. S.; Bercaw, J. E.; Seidler, P. F.; Stryker, J. M.; Bergman, R. G. *Org. Synth.* **1987**, *65*, 42-45.

(56) Van Geet, A. L. *Anal. Chem.* **1970**, *42*(6), 679-680.

(57) Jesson, J. P.; Meakin, P. *Acc. Chem. Res.* **1973**, *6*, 269-275.

(58) Hamilton, D. G.; Crabtree, R. H. *J. Am. Chem. Soc.* **1988**, *110*, 4126-4133.

CHAPTER 3

Thermolysis, Photolysis, and Oxidation of $Cp^*Ir(CO)R_2$ (R = H, Me) and $[Cp^*Ir(CO)H]_2$: Stability with Respect to Reductive Elimination

Introduction

The reductive elimination of organic products from monomeric transition metal complexes containing hydride and/or alkyl ligands (eq 3.1) is an important final step along the reaction pathway of numerous catalytic and stoichiometric processes and hence, has been an area of intense research. The mechanism of thermal reductive elimination of dihydrogen or alkane from organometallic dihydrides, alkyl hydrides, and dialkyls was the topic of a review by Norton in 1979.[1] He noted that there are relatively few stable monomeric alkyl hydride complexes as compared to the number of dihydride and dialkyl complexes, and addressed this discrepancy in light of his work with the osmium carbonyl compounds, $Os(CO)_4(R)(R')$ (R/R' = H/H, H/Me, Me/Me).

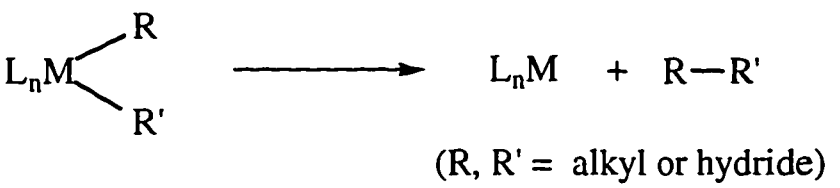

(3.1)

Using standard C-C, C-H, and H-H bond strengths (83, 99, and 104 kcal mol^{-1} respectively), and assuming that the M-H bond strength is greater than that of the M-C bond, simple calculations suggest that there exists a narrow range of M-H and M-C bond dissociation energies (BDE) such that reductive elimination of R-H from $L_nM(R)H$ is thermodynamically favored over elimination of H_2 from $L_nM(H)_2$ and R-R from $L_nM(R)_2$ compounds. Specifically, if $16 > (BDE_{MH} - BDE_{MC}) > 5$, then $\Delta H°$ for R-H elimination will be lowest. This alone seems unlikely to explain the dearth of stable alkyl hydrides. Molecular orbital correlation diagrams for the concerted elimination of R-R

from compounds of the form *cis*-L_4MR_2 reveal that no symmetry constraints exist, and hence, imply no advantage to an unsymmetric R-H elimination.[2] Norton suggests that some compounds of the form $L_nM(R)(R')$ that undergo reductive elimination do so not via an intramolecular route, but rather in a bimolecular fashion, as is the case for certain osmium carbonyl complexes. These alkyl hydrides are particularly well suited to bimolecular reactions since the alkyl group can readily migrate to a carbonyl opening up a site of coordinative unsaturation, and the hydride can bridge the two metal centers prior to reductive elimination (eq 3.2).

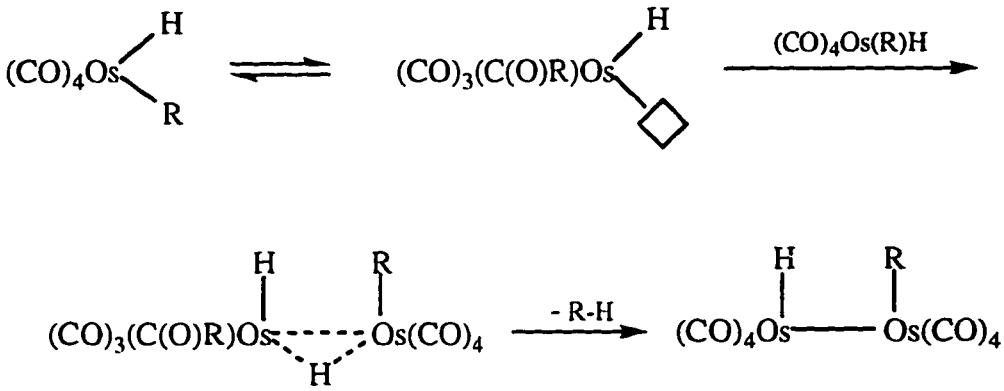

(3.2)

Perhaps a further rationale for the relative instability of alkyl hydrides can be provided by adding a kinetic component to the bond strength arguments discussed above. Dihydrides are often thermodynamically stable with respect to loss of H_2 due to the strength of the M-H bonds. On the other hand dialkyls, despite the fact that M-C bonds are usually weaker than M-H bonds, possess additional *kinetic* stability with respect to elimination of alkane due to the activation energy for the required re-orientation of the directional carbon sp^3 orbitals to form the incipient C-C bond.[3] Alkyl hydrides then often possess sufficient thermodynamic driving force for alkane elimination, without substantial kinetic barriers because of the non-directional hydride *s* orbital.

An important aspect of the energetics of intramolecular reductive elimination is the stability of the metal-bearing product.[4] Due to its coordinative unsaturation, the metal-containing product of reductive elimination is often a high energy species, as is the case for $Os(CO)_4$, and hence alternative, lower energy pathways may be favored. In the case of reductive elimination from dimers (eq 3.3), the metal-bearing product can stabilize its coordinative unsaturation by formation of an additional metal-metal bond, thus providing greater *thermodynamic* driving force. Reductive elimination from

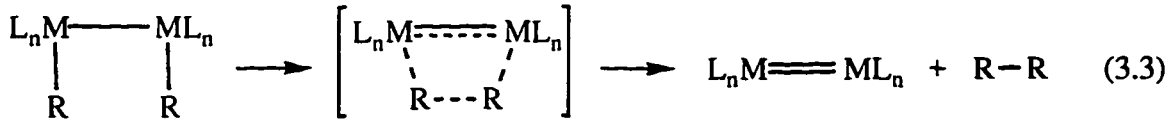

(3.3)

bimetallic species has been less studied than that from monomeric complexes, and proven examples of thermal *intra*molecular reductive elimination from organometallic dimers are rare.[5-9] Indeed, thermal 1,2-dinuclear reductive elimination of H_2 (or R_2) in a concerted fashion is formally "forbidden" according to the principles of orbital symmetry conservation[3] and is isolobal with the similarly forbidden suprafacial elimination of H_2 from ethane.[10] That is, molecular orbital theory predicts a large *kinetic* barrier to concerted, intramolecular, 1,2-reductive elimination from dimers.

The "concertedness" of a reductive elimination reaction is difficult to ascertain. Norton and co-workers[11,12] have committed a great deal of research towards the question of whether the reversible extrusion of ethylene from (μ-1,2-ethanediyl)-octacarbonyldiosmium, a reaction that is similarly symmetry forbidden as a concerted process, proceeds in a concerted manner. Using classic tests for diradical intermediacy from organic chemistry such as retention of stereochemistry (eq 3.4) and introduction of a cyclopropyl substituent at the putative radical center, all results thus far support their contention that the reaction is indeed a concerted process.

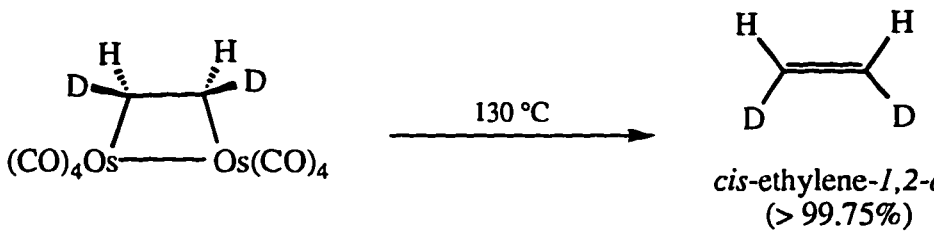

cis-ethylene-*1,2*-d_2
(> 99.75%)

(3.4)

Distinguishing whether a reductive elimination occurs in a *1,2*- versus a *1,1*-dinuclear fashion is also problematic. Stille and co-workers[7] reported that methane reductively eliminates from $Pd(H)Pd(CH_3)(\mu\text{-dppm})_2(\mu\text{-Cl})^+$ (dppm = bis(diphenylphosphino)methane) (eq 3.5). Though it would appear that the H and CH_3 ligands were eliminated from different Pd atoms, observations that the methylene protons of the dppm bridges were equivalent by ^1H NMR and that similar Pt complexes undergo facile A-frame inversion led them to propose a mechanism whereby the terminal hydride exchanged positions with the bridging chloride, providing a path for *1,1*-reductive elimination.

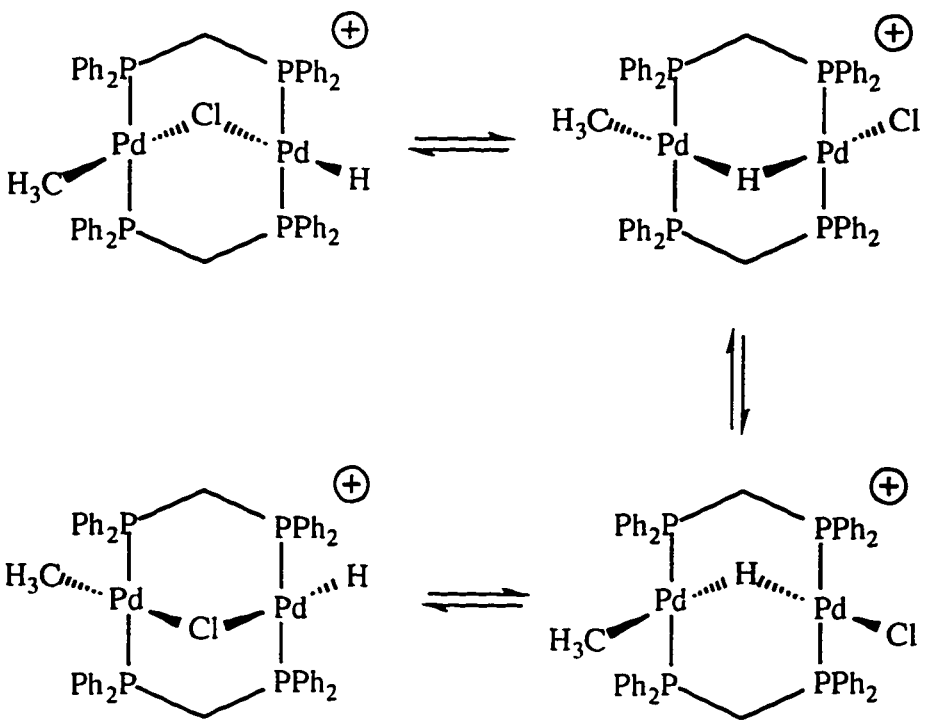

(3.5)

An example of a bimetallic compound that undergoes a thermal reductive elimination reaction, $Os_2(CO)_8(CH_3)H$, is again provided by Norton and co-workers.[13,14] Heating a solution of $Os_2(CO)_8(CH_3)H$ in benzene to 75 °C does indeed generate methane. However, a hint that this reaction may be more complicated than simple intramolecular reductive elimination is provided by the presence of $Os_3(CO)_{12}(CH_3)_2$ among the products. Crossover experiments involving thermolysis of equimolar amounts of $Os_2(CO)_8(CH_3)H$ and $Os_2(CO)_8(CD_3)D$, generated CD_3H and CH_3D, as well as CD_4 and CH_4, indicating that some *inter*molecular reactions had occurred. It is important to note that the putative product of intramolecular reductive elimination, $Os_2(CO)_8$, has never been isolated and is believed to be unstable.

Conversely, $[Cp^*Ir(\mu\text{-}CO)]_2$, a compound that is isolobal with $Os_2(CO)_8$, is isolable and very stable.[15] We proposed that if compounds of the form $[Cp^*Ir(CO)R]_2$ (R = H or alkyl) could be prepared, then perhaps they would have a greater thermodynamic driving force to undergo intramolecular reductive elimination. The syntheses of $[Cp^*Ir(CO)H]_2$ and $[Cp^*Ir(CO)(CH_3)]_2$ are described in Chapters 2 and 5 respectively.

Reductive elimination of hydrogen from organometallic hydride complexes by photochemical means, though not as well studied as the thermal chemistry, has been the subject of a great deal of research over the last three decades. There are now examples of a wide variety of transition metal di- and polyhydride monomers that undergo reductive elimination of H_2 upon irradiation with UV or visible light.[16] In many cases, these reactions do not proceed thermally. An example of great import was the discovery by Bergman and Janowicz that photolysis of $Cp^*Ir(PMe_3)H_2$ led to loss of H_2 and subsequent activation of C-H bonds of saturated hydrocarbons.[17]

As is the case for the thermal chemistry, few examples of photochemical reductive elimination from dimers have been reported.[18-21] The majority of bimetallic

compounds subjected to photolysis undergo homolysis of the metal-metal bond or ligand dissociation in preference to reductive elimination. Unlike the *thermal* 1,2-dinuclear reductive elimination of H_2, the *photochemical* elimination is not subject to orbital symmetry constraints.[3]

In this chapter we examine the thermal, photolytic, oxidation and ligand substitution chemistry of monomers and dimers of the form $Cp^*Ir(CO)R_2$ (R = H (**1**), Me (**2**)) and $[Cp^*Ir(CO)H]_2$ (**3**) and compare their facility to undergo reductive elimination. The syntheses of **1** and **2** are described in Chapters 2 and 5 respectively.

Results

Thermolysis

Heating a pale yellow solution of $Cp^*Ir(CO)H_2$ (**1**) in benzene-d_6 at 100 °C for 4 days generates a minor amount of the dimer, $[Cp^*Ir(\mu\text{-}CO)]_2$ (**4**) (3%, molar basis, calculated as % of total Cp^* resonances in the ^1H NMR spectrum). As the thermolysis progresses, ^1H NMR spectra reveal little change. After 63 days of heating, the dimer, **4**, still accounts for only 4% of the total integration of the Cp^* resonances. The appearance of a 1:1:1 triplet (J = 2.2 Hz) just upfield (18 ppb) of the Cp^* resonance of **1** indicates that deuterium is incorporated from the solvent into the Cp^* methyl groups of the dihydride, **1**, one deuterium atom per methyl group ($C_5(CH_3)_{5-n}(CH_2D)_n$). A 1:1:1 triplet (J = 2.2 Hz) just upfield (18 ppb) of the small Cp^* resonance of **4** similarly indicates that deuterium is incorporated into at least one of its Cp^* methyl groups. Further heating leads to the observation of an additional set of resonances just upfield (16 ppb) of the 1:1:1 triplets of both **1** and **4**. These new multiplets are each 1:2:3:2:1 quintets (J = 2.1 Hz), which overlap with the triplets and are due to the incorporation of a second deuterium atom per methyl group (CHD_2). In a separate experiment, thermolysis of **4** in benzene-d_6 at 100 °C for over 200 days, no deuterium incorporation was evident.

Therefore, during the thermolysis of **1**, deuterium does not transfer directly from the solvent into a Cp^* methyl of **4**, but rather indirectly from the decomposition of **1**.

The monomeric dimethyl, $Cp^*Ir(CO)(CH_3)_2$ (**2**), is also thermally robust: no decomposition is apparent by ^1H NMR when heated in benzene-d_6 at 85 °C for 97 days. In addition, there is no evidence for deuterium incorporation from the solvent.

At room temperature, the neutral dihydride dimer, $[Cp^*Ir(CO)H]_2$ (**3**), is thermally stable with respect to loss of H_2 as a solid or in solution. When a solution of **3** in benzene-d_6 is shielded from light and heated to 100 °C, $[Cp^*Ir(\mu\text{-}CO)]_2$ (**4**) is produced. The reaction is slow, with only 15% conversion (by ^1H NMR) after 2 weeks under these conditions. After an initial period (34 days) in which only **4** was formed (28% conversion), the appearance of a small quantity of monomeric $Cp^*Ir(CO)H_2$ (**1**) was noted. Deuterium incorporation into the Cp^* methyls of **1** and **4** is subsequently observed via ^1H NMR (as described above), though *not* into the starting material **3** (Figs. 3.1, 3.2). This observation is confirmed by a $^{13}C\{^1H\}$ NMR spectrum, which reveals 1:1:1 triplets just upfield of the Cp^* methyl resonances of **1** (J = 20 Hz, $\Delta\delta$ = 0.26 ppm) and **4** (J = 19 Hz, $\Delta\delta$ = 0.25 ppm), but not of **3**. The rate of formation of **4** during the thermolysis of the dihydride dimer, **3**, in C_6D_6 is small, but is still much greater than that from the thermolysis of the monomer, **1**. Hence, the formation of **4** from thermolysis of **3** does not proceed in large part via formation of **1**.

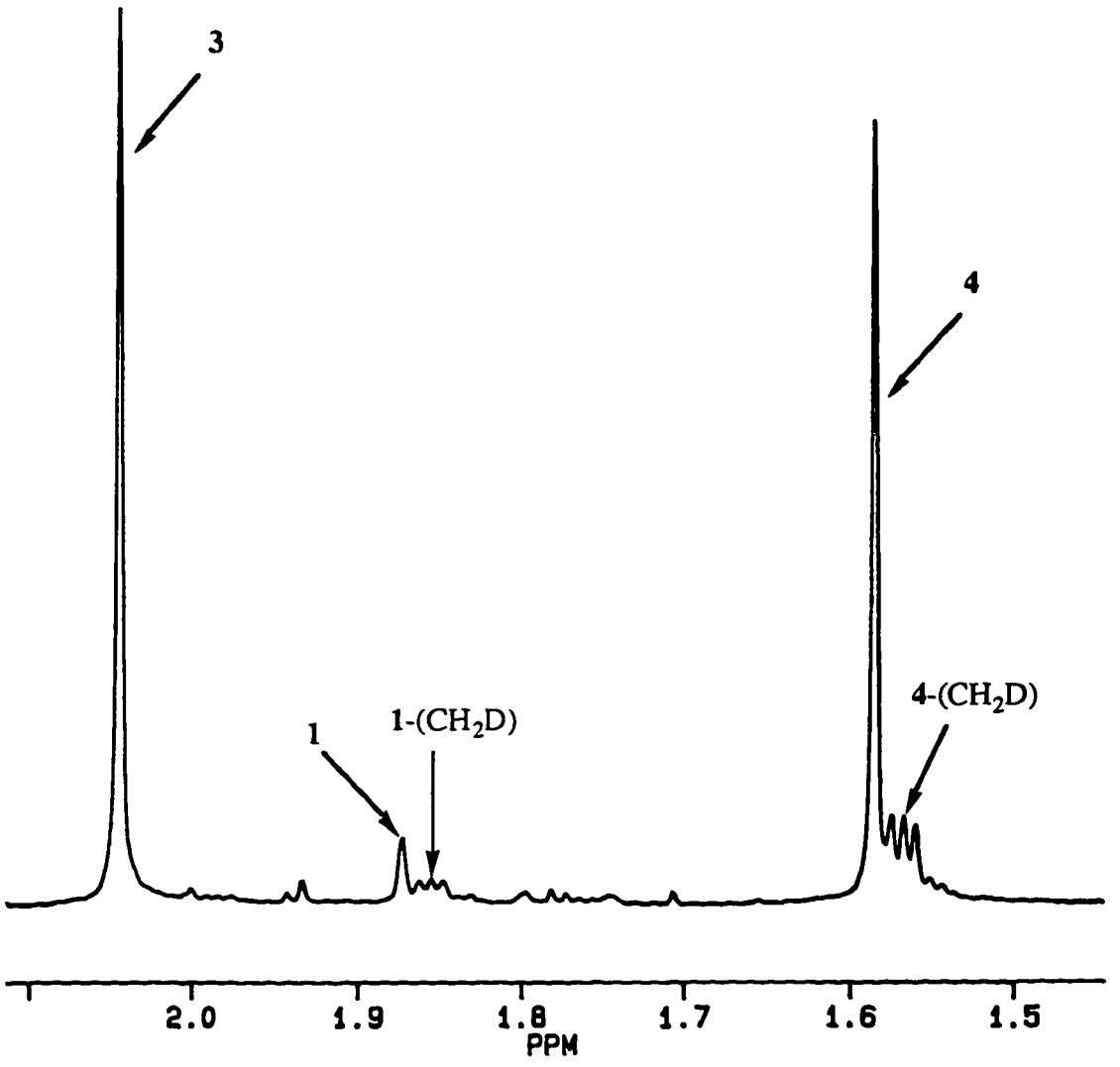

Figure 3.1. Partial ^1H NMR (300 MHz) spectrum (Cp^* region) of a solution of $[Cp^*Ir(CO)H]_2$ (**3**) in C_6D_6, heated to 100 °C for 90 days.

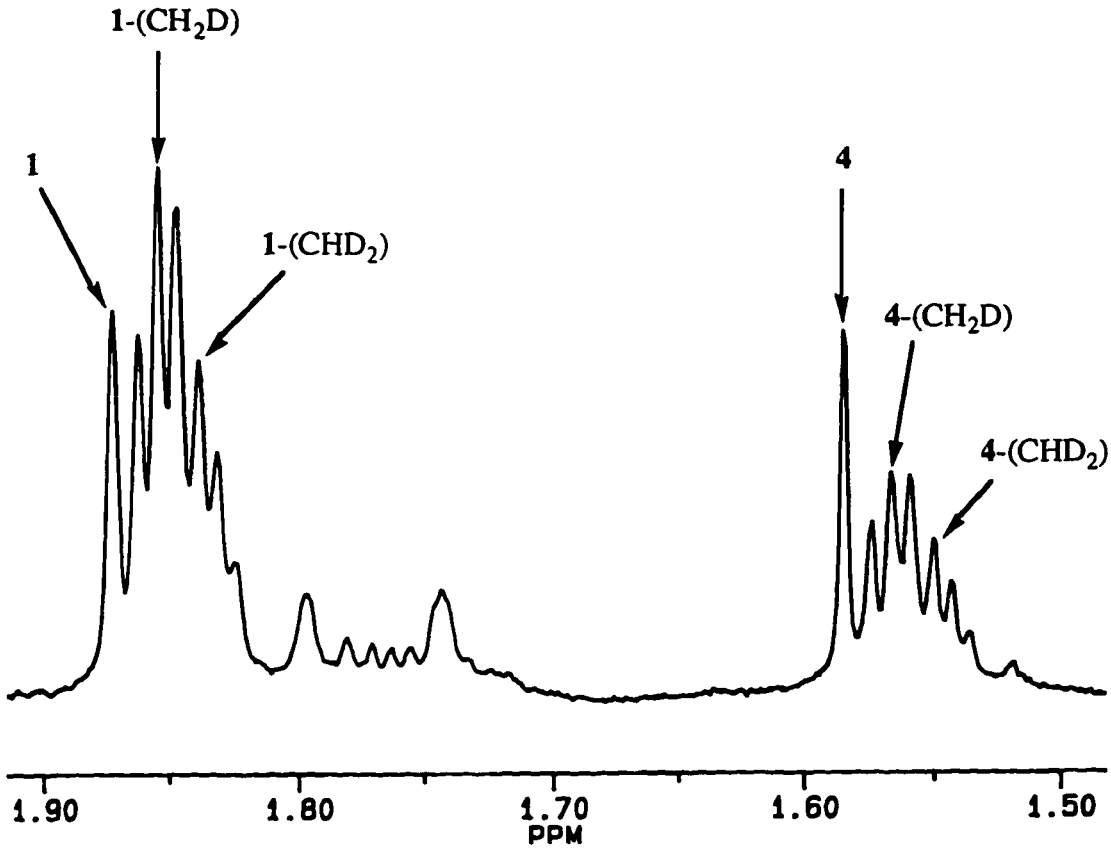

Figure 3.2. Partial ^{1}H NMR (300 MHz) spectrum (Cp* region) of a solution of $[Cp^*Ir(CO)H]_2$ (**3**) in C_6D_6, under H_2 (0.4 atm), heated to 100 °C for 133 days. The small resonances between 1.80 and 1.74 ppm are due to unknown decomposition products. The resonance due to **3** is not shown.

Thermolysis of **3** in methylcyclohexane-d_{14} at 139 °C over the course of several weeks generates primarily **4**, with minor amounts of several unidentified Cp*-bearing species. Significantly, ^{1}H NMR spectra exhibit no resonances attributable to the monomeric dihydride, **1**. There is no indication of deuterium incorporation into any of the Cp* resonances from this solvent. Curiously, neither H_2, nor any new hydride resonances, are detectable in the ^{1}H NMR spectra. A plot of ln [**3**] versus time correlates

well to a linear fit ($R^2 = 0.987$), indicating that the reaction is first order in **3** (Figure 3.3), and yielding the following kinetic parameters: $\Delta G^{\ddagger}_{412} = 35.3 \pm 0.4$ kcal mol^{-1}, $k = (1.61 \pm 0.08) \times 10^{-6}$ s^{-1}, $t_{1/2} = 5.0$ days.

Heating a solid sample of **3** without solvent under static vacuum (10^{-3} torr) to 96 °C causes the compound to sublime as yellow crystals. An X-ray structure determination of one of these crystals was obtained (see Chapter 2). When heated under argon to 120 °C for 7.5 days, **4** is generated in good yield (90% by ^{1}H NMR integration of resonances in Cp* region). No Cp*Ir(CO)H$_2$ (**1**) is observed to form.

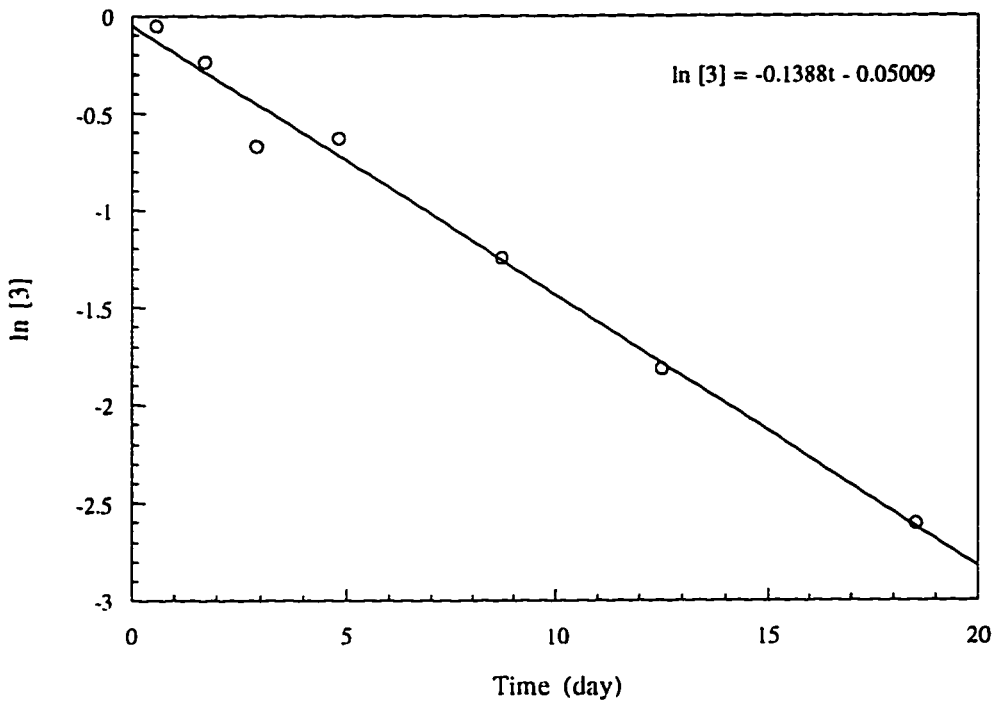

Figure 3.3. First order plot for the thermal decomposition of [Cp*Ir(CO)H]$_2$ (**3**) in methylcyclohexane-d_{14} at 139 °C.

Photolysis

Bright yellow solutions of $[Cp^*Ir(CO)H]_2$ (**3**) in methylene chloride or benzene, when exposed to room light, gradually darken to brown over the course of several days. When the solution is shielded from light, the reaction stops, confirming the photochemical nature of the decomposition. ^1H NMR spectra of **3** in CD_2Cl_2 show clean decomposition to $Cp^*Ir(CO)H_2$ (**1**) and $[Cp^*Ir(\mu\text{-}CO)]_2$ (**4**) in a constant 2:1 molar ratio (1.9 ± 0.2) (eq 3.6). No H_2 is evident. The dark brown color is due to the formation of **4**,

$$\underset{\mathbf{3}}{2\ [Cp^*Ir(CO)H]_2} \xrightarrow{h\nu} \underset{\mathbf{1}}{2\ Cp^*Ir(CO)H_2} + \underset{\mathbf{4}}{[Cp^*Ir(\mu\text{-}CO)]_2} \qquad (3.6)$$

a highly colored compound (the monomer, **1**, is very pale yellow). Addition of triphenylphosphine (10.1 equiv) to a solution of **3** in CD_2Cl_2, shielded from light, shows no reaction after standing for 46 h. When the solution is then exposed to room light, **3** decomposes to generate **1** and $Cp^*Ir(CO)(PPh_3)$[22] in approximately a 1:1 molar ratio (0.85 ± 0.03) (eq 3.7).

$$\underset{\mathbf{3}}{[Cp^*Ir(CO)H]_2} \xrightarrow[PPh_3]{h\nu} \underset{\mathbf{1}}{Cp^*Ir(CO)H_2} + Cp^*Ir(CO)(PPh_3) \qquad (3.7)$$

Irradiation ($\lambda > 360$ nm) of **3** in C_6D_6 or methylcyclohexane-d_{14} rapidly yields **1** and **4**, the same products that result from room light photochemistry. The molar ratio of the products, however, is slightly different: $[Cp^*Ir(CO)H_2]/[Cp^*Ir(\mu\text{-}CO)]_2] \approx 2.5{:}1$. After 1.75 h of photolysis in C_6D_6, **3** makes up only 6.1% of the total Cp^* region integration. After 3.5 h of irradiation, no **3** is detectable. Again, there is no H_2 apparent

by ^{1}H NMR. Further irradiation to a total of 11.5 h produces no change, indicating that both **1** and **4** are stable to light with $\lambda > 360$ nm.

Oxidation

Addition of the oxidant $[Cp_2Fe]BAr'_4$ (0.3 equiv) to a solution of $Cp^*Ir(CO)H_2$ (**1**) in methylene chloride induces proton transfer and generates primarily $\{[Cp^*Ir(CO)H]_2(\mu\text{-}H)\}BAr'_4$ along with Cp_2Fe and some unreacted **1** (eq 3.8).

$$2\ Cp^*Ir(CO)H_2 + [Cp_2Fe]^+ \longrightarrow [Cp^*Ir(CO)H]_2(\mu\text{-}H)^+ + Cp_2Fe + 0.5\ H_2 \qquad (3.8)$$

Similarly, oxidation of $[Cp^*Ir(CO)H]_2$ (**3**) with $[Cp_2Fe]BAr'_4$ (1.0 equiv) in methylene chloride leads to proton transfer and formation of $\{[Cp^*Ir(CO)H]_2(\mu\text{-}H)\}BAr'_4$, though not as cleanly. No free hydrogen is apparent by ^{1}H NMR spectroscopy. The initial, transient deep blue-green color of the solution upon reaction may be indicative of the presence of $[Cp^*Ir(CO)]_2(\mu\text{-}H)^+$ (see Chapter 4).

In contrast, addition of $[Cp_2Fe]BAr'_4$ (1.1 equiv) to a methylene chloride solution of $Cp^*Ir(CO)(CH_3)_2$ (**2**) produces no reaction. When the same reactants are placed in CD_3CN, no new resonances are evident by ^{1}H NMR, but the resonances associated with $Cp^*Ir(CO)(CH_3)_2$ and acetonitrile-d_2 are broadened.

Reaction of $[Cp^*Ir(CO)H]_2$ (3) with CO.

Addition of carbon monoxide (1.6 atm) to a solution of **3** in C_6D_6, shielded from light, effects clean conversion to the biscarbonyl monomer, $Cp^*Ir(CO)_2$,[23] over the course of a week, as determined by ^{1}H NMR spectroscopy. A resonance at 4.47 ppm indicates the presence of free hydrogen.

Discussion

Thermolysis of $Cp^*Ir(CO)R_2$ (R = H (1), Me (2))

The concerted reductive elimination of H_2 from cis monomeric dihydrides of the form L_4MH_2 or $CpM(L)H_2$ is not forbidden by molecular orbital symmetry correlations.[2] Nevertheless, many dihydrides of third row metals are quite stable thermodynamically with respect to thermal reductive elimination, due to the strength of the M-H bonds. There is an entropic driving force for the reductive elimination. Bergman and Hoff estimate[24] a $\Delta S^\circ \approx 30$ eu, which leads to a $T\Delta S^\circ$ contribution to ΔG°_{298} of about 9 kcal mol^{-1}. Hence, if the sum of the two M-H bond dissociation energies (BDE) is greater than the 104 kcal mol^{-1} gained upon H-H bond formation plus the 9 kcal mol^{-1} increase in entropy, then the reductive elimination reaction at room temperature is thermodynamically unfavorable. Two related complexes, $(CO)_4OsH_2$ and $Cp^*Ir(PMe_3)H_2$, possess strong M-H bonds (average BDE[24,25] = 78 and 74 kcal mol^{-1} respectively), and both show significant thermal stability.

The monomeric dihydride, $Cp^*Ir(CO)H_2$ (1), likewise exhibits substantial thermal stability in solution. Extended heating of 1 for over a month in benzene at 100 °C generates only a minimal amount of $[Cp^*Ir(\mu\text{-}CO)]_2$ (4). The effect of different ancillary ligands upon the M-H bond strength is not well understood,[24] though there is some evidence that replacement of a phosphine by a carbonyl leads to a weaker M-H bond.[26]

This thermal stability is in marked contrast to that of the Cp analogue, $CpIr(CO)H_2$, reported by Shapley and co-workers.[27] Heating $CpIr(CO)H_2$ to reflux in benzene for several days affords primarily C_s-$Cp_3Ir_3(CO)_3$, as well as minor products identified as $Cp_4Ir_4(CO)_x$ clusters. The analogous trimer, $Cp^*_3Ir_3(CO)_3$, is not known, presumably due to the greater steric demand of Cp^* versus Cp.[28] Indeed, we chose the Cp^* ligand for our dimer chemistry in part because of its disinclination to form tri- and polynuclear species. Further experiments in the presence of H_2, D_2, and trapping agents

confirm that $CpIr(CO)H_2$ loses H_2 to generate the reactive CpIr(CO) fragment. Interestingly, a footnote in this communication[27] mentions "unpublished results" which indicate that $Cp^*Ir(CO)H_2$ (**1**) is much less reactive than $CpIr(CO)H_2$. A reductive elimination reaction results in a formal reduction of the metal center. All other factors being equal, a less electron rich metal center will be more inclined to undergo reductive elimination. Hence, the greater facility of $CpIr(CO)H_2$ to eliminate H_2 versus **1**, is consistent with the lesser electron-donating ability of Cp versus Cp^*.

Despite its apparent lack of thermal reactivity, the Cp^* methyls and hydride ligands of **1** do undergo H/D exchange with the solvent. The scrambling occurs thermally in benzene-d_6 (apparent after 9 days at 100 °C, shielded from light), but not in methylene chloride-d_2. The incorporation of deuterium from deuterated solvents into the methyl groups of Cp^* ligands in organometallic compounds is not unprecedented, though examples are few. A case involving a molecule closely related to **1** is provided by Jones et al.[29] They report that extended thermolysis (> 178 h) of $Cp^*Rh(PMe_3)(C_6D_5)D$ at 74 °C in C_6D_6 yields new resonances (dt, $J_{Rh\text{-}P}$ = 155 Hz, $^2J_{D\text{-}P}$ = 7 Hz) in the $^{31}P\{^1H\}$ NMR spectrum just upfield (0.21 ppm) of those of the starting material. By 700 hours, four new sets of resonances, each a doublet of 1:1:1 triplets with identical coupling constants, had appeared. These new resonances are attributed to isotopomers of $Cp^*Rh(PMe_3)(C_6D_5)D$, formed by deuterium incorporation into the Cp^* methyl groups. They disclose that the mechanism for this deuterium exchange has not been established.

We invoke intramolecular oxidative addition of a C-H bond of a Cp^* methyl group to form the cyclometallated species as a potential intermediate. Isolated late metal compounds (Mn-Fe-Co-Ni triads) containing cyclometallated Cp^* ligands are rare and include an iridium dimer in which a Cp^* methyl is activated by the adjacent Ir atom to form a bridging methylene-tetramethylcyclopentadienyl ligand.[30] Early metal examples

are somewhat more common and include $Cp^*(\eta^5,\eta^1\text{-}C_5Me_4CH_2)WH$, formed by reductive elimination of RH from $Cp^*_2W(R)H$ ($R = CH_3$, $CH_2C_6H_5$) at ca. 100 °C.[31]

There are several possible mechanisms we can envision for this deuterium scrambling (Scheme 3.1). All initiate with the opening of a coordination site to form a 16-electron intermediate: A) dissociation of CO, B) ring slip (η^5 to η^3), C) metal-to-ring hydrogen transfer, or D) elimination of H_2. The second step involves oxidative addition of the solvent (C_6D_6) to form an Ir(V) (A, B) or Ir(III) (C, D) species. For pathways A, B, and C, reductive elimination of C_6D_5H followed by cyclometallation of the Cp^* ring

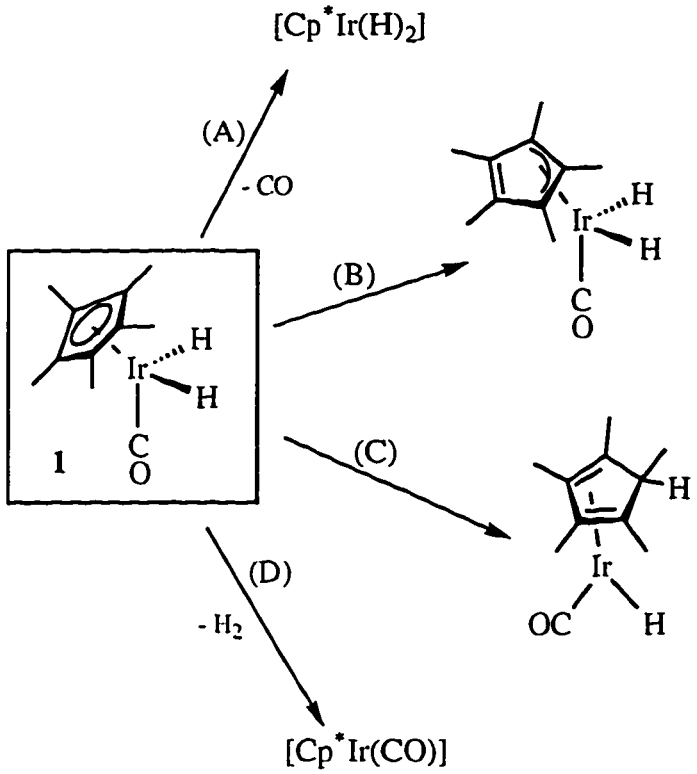

Scheme 3.1

yields another Ir(V) (A, B) or Ir(III) (C) transient (eq 3.9). Reductive elimination of the cyclometallated Cp^* methyl as CH_2D incorporates deuterium into that methyl. The

reverse of the initial step completes the cycle. In the case of pathway D (eq 3.10), direct coupling of the phenyl ligand with a hydrogen of a Cp^* methyl group leads to a cyclometallated species. Again, reversible cyclometallation of the Cp^* ring allows ring deuterium exchange.

$$[Cp^*Ir(H)_2] \xrightarrow{C_6D_6} [Cp^*Ir(C_6D_5)(D)H_2] \xrightarrow{-C_6D_5H} [Cp^*Ir(H)(D)] \longrightarrow$$

(A)

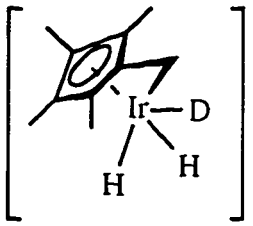

$$\longrightarrow [(Cp^*\text{-}d_1)Ir(H_2)] \qquad (3.9)$$

$$[Cp^*Ir(CO)] \xrightarrow{C_6D_6} [Cp^*Ir(CO)(C_6D_5)(D)] \xrightarrow{-C_6D_5H}$$

(D)

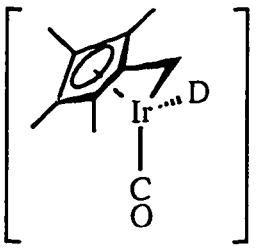

$$\longrightarrow [(Cp^*\text{-}d_1)Ir(CO)] \qquad (3.10)$$

In addition to the mechanisms described above, we cannot rule out the possibility of a radical pathway. Many transition metal hydride complexes are known to undergo hydrogen atom abstraction reactions in the presence of some initiator (e.g. small amounts of oxygen).[26] For example, phosphine substitution of $H_2Os(CO)_4$ to form

$H_2Os(CO)_3(PPh_3)$ was found to proceed via a radical-chain mechanism initiated by H-atom abstraction.[32]

There are now a growing number of stable Ir(V) compounds to support their proposal as suitable intermediates.[33,34] Activation of benzene by a neutral 16-electron species seems plausible based on the work of the Bergman and Graham groups (independently) which suggests that fragments of the form [Cp*IrL] are the active intermediates which oxidatively add a variety of alkanes and arenes. Mechanism A seems somewhat unlikely since it has been reported[35] that $Cp^*Ir(CO)H_2$ (**1**) reacts readily with CO to generate $Cp^*Ir(CO)_2$. We see no evidence for the formation of $Cp^*Ir(CO)_2$ during the thermolysis of **1**. Support for mechanism B is provided by the work of Rerek and Basolo[28] which demonstrated that some compounds of the Co triad, $Cp^*M(CO)_2$ (M = Co, Rh), undergo substitution reactions via a ring-slip pathway. Mechanisms B and C seem a little odd in that cyclometallation of a Cp^* ring that is not bound in an η^5 fashion would be required. Possibilities A, B, and C (as outlined above), for opening a coordination site at iridium, were also proposed by Graham, Rest, and co-workers[36] to explain deuterium isotope scrambling during the photolysis of $CpIr(CO)H_2$. Ultra-violet irradiation of a solution of $CpIr(CO)H_2$ in neopentane afforded the solvent activation product, $CpIr(CO)(CH_2CMe_3)H$, and was presumed to proceed via H_2 loss and formation of [CpIr(CO)]. However, photolysis of $CpIr(CO)D_2$ in unlabelled neopentane evolved HD and H_2 gas, in addition to D_2, and deuterium was incorporated into the methylene of the bound neopentyl ligand. These observations indicate that initial H_2 loss was not *solely* responsible for creating the species capable of C-H bond activation. Note that in this case, there was no evidence for deuterium scrambling into the ring.

Based on the work of Jones and co-workers described above, we favor mechanism D because it proposes the iridium analogue, $Cp^*Ir(CO)(C_6D_5)D$, as an intermediate (the thermal stability of compounds of the form $Cp^*Ir(CO)(R)H$ is discussed below). In

addition, it seems reasonable that $[Cp^*Ir(\mu\text{-}CO)]_2$ (**4**), which is slowly generated during the thermolysis of **1**, would form via dimerization of the $[Cp^*Ir(CO)]$ intermediate. The direct intramolecular coupling of an alkyl or hydride ligand with a hydrogen of an adjacent Cp^* methyl group has been observed in several metallocene compounds.[37,38] For example, Bercaw and co-workers reported[37] that thermolysis of $Cp^*_2Zr(CH_2CDMe_2)D$ did not generate the expected product of simple reductive elimination of the cis alkyl and hydride (deuteride) ligands, CH_2DCDMe_2, but rather CH_3CDMe_2. Further experiments proved that the abstracted hydrogen came from the Cp^* methyl group. In other work by the Bercaw group,[38] the 18-electron dihydride, $Cp^*_2WH_2$, was found to thermally eliminate hydrogen via direct coupling of a hydride ligand with a hydrogen from a Cp^* methyl group. Reductive elimination of methane from the dimethyl derivative, $Cp^*_2WMe_2$, was also postulated to proceed via abstraction of a hydrogen atom from a Cp^* methyl group by a methyl ligand.

Like $Cp^*Ir(CO)H_2$ (**1**), the dimethyl monomer, $Cp^*Ir(CO)(CH_3)_2$ (**2**), is thermally stable with respect to reductive elimination. Unlike **1**, the Cp^* methyl groups of **2** do not undergo H/D exchange with the solvent. Maitlis and co-workers recently reported[39] that thermolysis of **2** under CO (1 atm) requires temperatures as high as 400 °C to effect decomposition. The C-C coupling product, ethane, is only produced in 3% yield; the main product is methane.

The methyl hydride, $Cp^*Ir(CO)(Me)H$, was prepared by Graham et al.[40] via photolysis of $Cp^*Ir(CO)_2$ in perfluorohexane under a methane atmosphere. The thermal stability of $Cp^*Ir(CO)(Me)H$ and the other alkyl hydrides is not well documented, but circumstantial evidence supports a susceptibility to reductive elimination at mild temperatures. The methyl hydride, as well as the other alkyl hydrides, is reported[40] to decompose at room temperature as a concentrated solution or as the isolated oil. Hence, in the $Cp^*Ir(CO)$ system, it appears that the methyl hydride derivative is much less stable

with respect to thermal reductive elimination than the dihydride, which is perhaps slightly less stable than the dimethyl. This trend is typical of related organometallic systems. For example, the approximate decomposition temperature of the *cis*-$(CO)_4Os(R)(R')$ derivatives[1] are as follows: $(CO)_4Os(Me)H$ = 50 °C, $(CO)_4OsH_2$ = 125 °C, and $(CO)_4OsMe_2$ = 160 °C.

Thermolysis of $[Cp^*Ir(CO)H]_2$ (3).

The thermolysis of **3** in the solid state or in methylcyclohexane-d_{14} (C_7D_{14}) generates predominantly the dehydrogenated dimer, $[Cp^*Ir(\mu\text{-}CO)]_2$ (**4**). The reaction in C_7D_{14} demonstrates first order dependence in **3**, which suggests an intramolecular mechanism. However, this result is not sufficient to rule out a bimolecular reaction. Norton et al.[1,41] have shown that elimination of H_2 from $Os(CO)_4H_2$ is a bimolecular reaction despite the first order dependence of the rate on $Os(CO)_4H_2$: the first step, carbonyl dissociation, is unimolecular and rate-determining, the subsequent step is bimolecular and fast. To rigorously exclude an intermolecular mechanism for the thermal reaction of **3** would require an isotope labelling experiment: detection of H_2 and D_2, but not the crossover product HD, from the thermolysis of equimolar quantities of **3** and **3-d_2**. This experiment has not yet been conducted.

The free energy of activation for the thermolysis of **3** in C_7D_{14} is substantial ($\Delta G^{\ddagger}_{412}$ = 35 kcal mol^{-1}), but is still significantly less than that theorized for a concerted 1,2-dinuclear reductive elimination of H_2. Trinquier and Hoffmann[3] used molecular orbital theory to predict a minimum energy barrier of 65 kcal mol^{-1} for the symmetry forbidden dinuclear reductive elimination of H_2 from the hypothetical dimer, $Mn_2(CO)_8H_2^{2-}$, a model compound that is isolobal with **3**. Certainly this is only a theoretical value, but the paucity of complexes which have been proposed to undergo intramolecular dinuclear reductive elimination lends support to the large barrier

predicted. However, in order to simplify their analysis, the authors did not take into account any migration of the carbonyl ligands from terminal to bridging positions during the reaction. The effect of the transformation of terminal carbonyl ligands in the reactant to bridging carbonyl ligands in the product on the theoretical energy barrier for the reductive elimination has not been determined, but it is well established that the molecular orbitals of $[Cp^*Ir(\mu\text{-}CO)]_2$ (**4**) involved in metal-metal bonding (see Chapter 4) are largely delocalized over the bridging carbonyls. Hence, the perturbation due to bridging ligands may be significant. It is interesting to note that almost all the reported examples thus far of compounds believed to undergo intramolecular dinuclear reductive elimination of H_2 contain metal centers bridged by bis-phosphine ligands. It also should be noted that a reaction that is similarly forbidden by orbital symmetry as a concerted process, the extrusion of ethylene from a 1,2-diosmacyclobutane, is nevertheless believed to be concerted.[11,12]

The isolobal osmium carbonyl analogue, $H_2Os_2(CO)_8$, exhibits no tendency for thermal loss of H_2. In fact, the compound can be synthesized in an autoclave at 160-170 °C under CO (140 atm!).[42] The putative product of simple intramolecular reductive elimination, $Os_2(CO)_8$, is presumed to be a high energy species (microsecond lifetime in solution at room temperature),[43] and may give rise to a large thermodynamic barrier for the reaction.

The special role of the bridging carbonyls to stabilize $[Cp^*Ir(\mu\text{-}CO)]_2$ (**4**) and perhaps to facilitate the reductive elimination of H_2 from $[Cp^*Ir(CO)H]_2$ (**3**), is evident when compared to the thermal chemistry of the Cp triphenylphosphite analogue. Previous research[44] in the Heinekey group demonstrated that thermolysis of $[CpIr(P(OPh)_3)H]_2$ in a variety of solvents always furnished a complicated mixture of products. Given the reluctance of monodentate phosphine ligands to bridge metal centers, the putative product of simple reductive elimination of H_2, $[CpIr(P(OPh)_3)]_2$,

would likely possess an unsupported iridium-iridium double bond. This doubly bonded dimer is not a known compound and would most probably be very reactive. We are unaware of any isolable, organometallic, late metal dimers that contain an unsupported metal-metal multiple bond.

Compounds faced with large activation barriers to a reaction often find lower energy alternatives. Two possible alternatives to concerted 1,2-dinuclear reductive elimination of H_2 from **3** include 1,1-reductive elimination, or a radical pathway. Given the facility with which the hydride ligands exchange between the iridium atoms (see Chapter 2), reductive elimination of H_2 from one iridium center (1,1) seems reasonable. Tilset, Vollhardt, and Boese[45] recently reported an example of thermal elimination of H_2 from a dinuclear dihydride that is believed to proceed via radical species (eq 3.11). When a solution of $FvW_2(CO)_6H_2$ (Fv = fulvalene, η^5:η^5-$C_{10}H_8$) in diglyme was heated to 160 °C for 2-4 days, H_2 was generated with concomitant formation of a W-W bond to give $FvW_2(CO)_6$. Irreproducible reaction rates, induction periods, and rate increases upon addition of radical initiators lead them to conclude that a radical mechanism is most likely operative, i.e. that the elimination of H_2 is not concerted. We observe no induction period during the thermal decomposition of **3**.

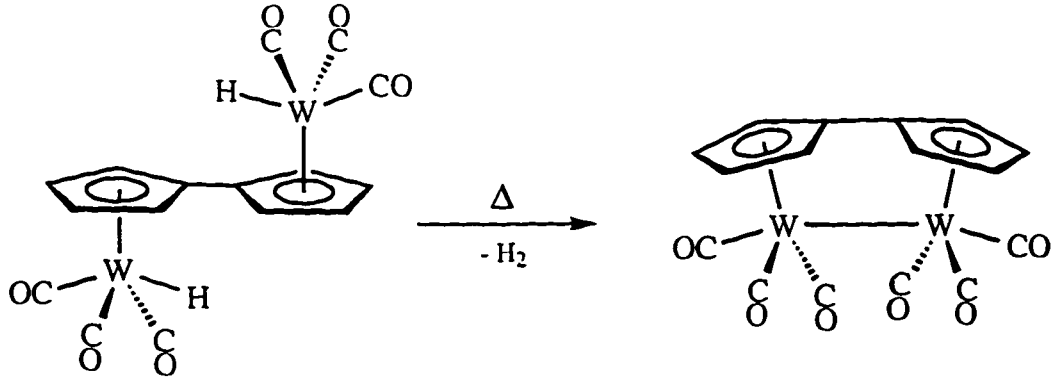

(3.11)

The thermolysis of the dihydride dimer (**3**) in C_6D_6 initially produces the dehydrogenated dimer (**4**) exclusively. However, after continued heating, the dihydride monomer, $Cp^*Ir(CO)H_2$ (**1**), is observed to form. Extended thermolysis of **1** (vide supra) generates only a minor amount of **4**, indicating that the production of **4** during the thermolysis of $[Cp^*Ir(CO)H]_2$ (**3**) does not result (to any great extent) from decomposition of **1**. During the thermolysis of **3** in C_6D_6, deuterium is incorporated from the solvent into the Cp^* ligands of **1**. The isotope scrambling is subsequently observed in the Cp^* ligands of **4**, but not **3**. This result confirms that there is some conversion of **1** to **4**, but indicates that the decomposition reactions of **3** that generate **1** and **4** are irreversible. Consistent with these results, we can postulate three mechanisms for the thermal decomposition of **3** (Scheme 3.2). All three mechanisms include the direct reductive elimination of H_2 from **3** to generate **4**, but invoke different routes for the formation of the monomer (**1**).

The first mechanism (A) posits dimer fragmentation to the monomeric dihydride (**1**) and the 16-electron fragment, $[Cp^*Ir(CO)]$, as an alternate thermal decomposition pathway for **3**. The same dimer fragmentation is believed to occur photochemically (vide infra). The unsaturated $[Cp^*Ir(CO)]$ species is extremely reactive and hence its lifetime would be exceedingly short. Graham and co-workers demonstrated in their fundamental work[40,46] on alkane activation that $[Cp^*Ir(CO)]$, the presumed product of photolysis of $Cp^*Ir(CO)_2$,[47] oxidatively adds the C-H bond of a variety of alkanes and arenes to form $Cp^*Ir(CO)(R)H$. Therefore, we would expect that generation of $[Cp^*Ir(CO)]$ in C_6D_6 would lead to formation of $Cp^*Ir(CO)(C_6D_5)D$. No ^1H NMR resonance in the Cp^* region attributable to $Cp^*Ir(CO)(C_6D_5)D$ is observed during the thermolyses of **3**. As mentioned above, the thermal stability of $Cp^*Ir(CO)(Ph)H$ and the other alkyl hydrides is not well documented. A dilute solution of the neopentyl hydride, $Cp^*Ir(CO)(CH_2CMe_3)H$, in hexane is reported[46] to suffer no noticeable decomposition at

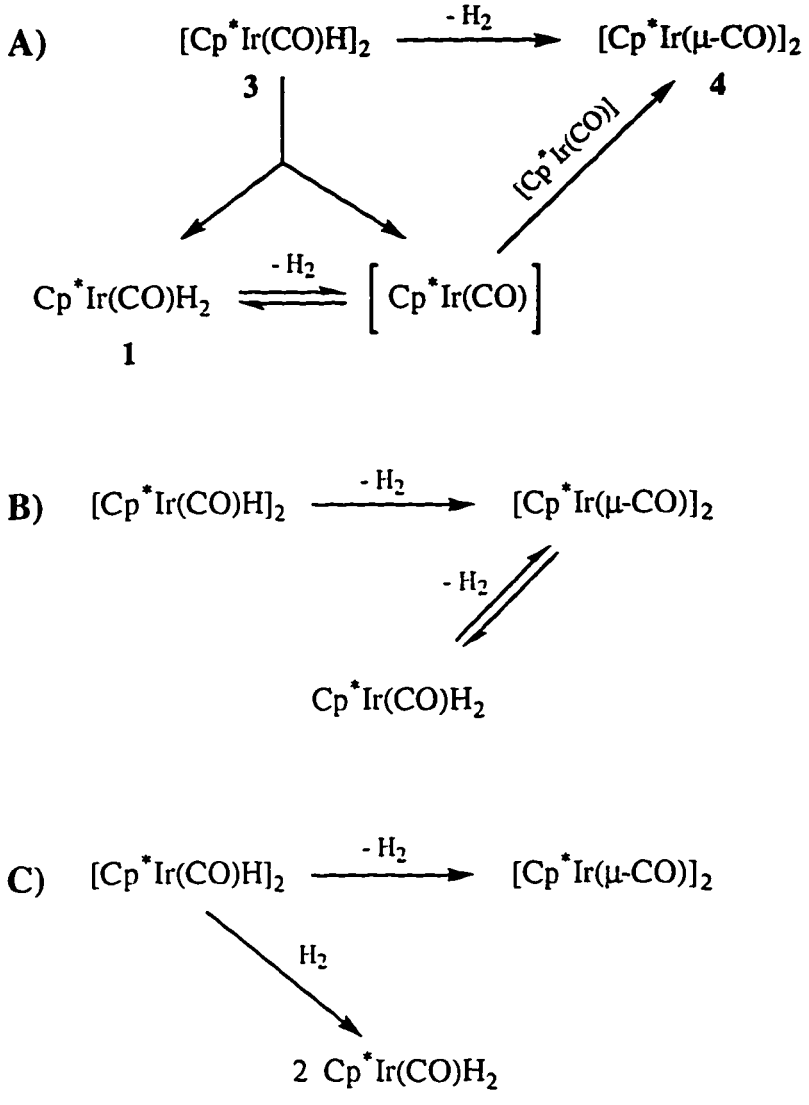

Scheme 3.2

5 °C over two weeks, but slowly decomposes at room temperature as a concentrated solution or as the isolated oil. Certainly at the high temperatures maintained for the thermolyses of **3**, the stability of $Cp^*Ir(CO)(Ph)H$ would be suspect. Moreover, Graham[48] has also demonstrated that $[Cp^*Ir(CO)]$ shows a great preference for oxidative addition of H_2 over activation of the alkane solvent. It is unclear whether this preference is kinetic or thermodynamic in nature. It seems likely that $[Cp^*Ir(CO)]$ formed during

the thermolysis of **3** would react with any H_2 present to form the dihydride, **1**. In the absence of free H_2, [$Cp^*Ir(CO)$] presumably dimerizes to form **4**.

The second postulated mechanism (B) proposes that the free H_2 generated via reductive elimination from the dihydride dimer (**3**), subsequently reacts with the dehydrogenated dimer (**4**) to afford the monomeric dihydride (**1**). In a separate experiment, thermolysis of **4** in C_6D_6 under H_2 (0.4 atm) did generate **1** over the course of several days, although obviously the concentration of hydrogen generated from thermolysis of several milligrams of **3** in an NMR tube would be substantially less. A plausible route might entail slow fragmentation of **4** into two [$Cp^*Ir(CO)$] moieties, which are rapidly trapped by H_2 to form **1**.

A third mechanism (C) invokes direct reaction of H_2 with **3** to generate **1**. The dihydride dimer (**3**) does not react with H_2 (0.4 atm) at room temperature (in the dark), but it is unclear to what extent reaction occurs at the thermolysis temperatures.

Another important question is as follows: why is it that thermolysis of **3** in methylcyclohexane-d_{14} does *not* generate the monomer, **1**? Unfortunately, we are presently unable to reconcile this result with our proposed mechansims. Certainly more experiments are required in order to determine the solvent dependence of the reaction pathway.

Photochemistry

As alluded to in the introduction to this chapter, photo-excited polyhydride dimers have available several avenues of reactivity, including ligand dissociation, metal-metal bond homolysis, and reductive elimination of H_2. The light-sensitive nature of [$Cp^*Ir(CO)H]_2$ (**3**) in solution became apparent during routine NMR analysis of the compound. A bright yellow solution of **3** in CD_2Cl_2 or C_6D_6 in an NMR tube, left standing on the benchtop, begins to darken over the course of several days. If the tube is

kept in the dark the reaction ceases. The decomposition is remarkably clean, generating $Cp^*Ir(CO)H_2$ (**1**) and $[Cp^*Ir(\mu\text{-}CO)]_2$ (**4**) in a 2:1 ratio. Irradiation of solutions of **3** in benzene-d_6 or methylcyclohexane-d_{14} with filtered light ($\lambda > 360$ nm) from a mercury lamp generates the same products, **1** and **4**, though the reaction is complete within a few hours.

There are several mechanisms that we can envisage for this photodecomposition (Scheme 3.3). The first (A) involves homolysis of the metal-metal bond, a reaction pathway well established for a variety of transition metal carbonyl dimers.[49] For example, Norton and Edidin report[32] that irradiation of a benzene solution of the isolobal osmium carbonyl analogue, $H_2Os_2(CO)_8$, generates $Os(CO)_4H^\bullet$. The initial product of bond homolysis is a caged radical pair, which is subject to competing reactions.[50] The caged pair intermediate, $[Cp^*Ir(CO)H^\bullet, Cp^*Ir(CO)H^\bullet]$, formed upon homolysis of the Ir-Ir bond of **3**, could recombine, diffuse into the solvent, or undergo hydrogen atom transfer reactions. At first glance, this pathway, and others that proceed via generation of radical species, might seem somewhat unlikely based upon our observation that the photodecomposition occurs cleanly in methylene chloride. We would expect that formation of the free radical $[Cp^*Ir(CO)H^\bullet]$ would lead to production of $Cp^*Ir(CO)(Cl)H$, and no new Cp^* or hydride resonances are observed in the ^1H NMR spectrum. The hydridochloride, $Cp^*Ir(CO)(Cl)H$, is not a known compound, but it seems improbable that this compound would be unstable at room temperature given the stability of the related compounds, $Cp^*Ir(PMe_3)(Cl)H$[51] and $Cp^*Ir(CO)(Cl)Me$.[40] However, mechanism A can avoid this apparent inconsistency if the rate of hydrogen atom transfer in the caged radical pair is much greater than the rate of chlorine atom abstraction from the solvent by the free radicals. Hydrogen atom transfer between metal atoms is typically very rapid; the rate constant for hydrogen atom transfer from $HSnBu_3$ to $Re(CO)_5^\bullet$ ($k \approx 10^7$ M^{-1} s^{-1}) is within two orders of magnitude of the diffusion controlled limit.[26] Chlorine atom

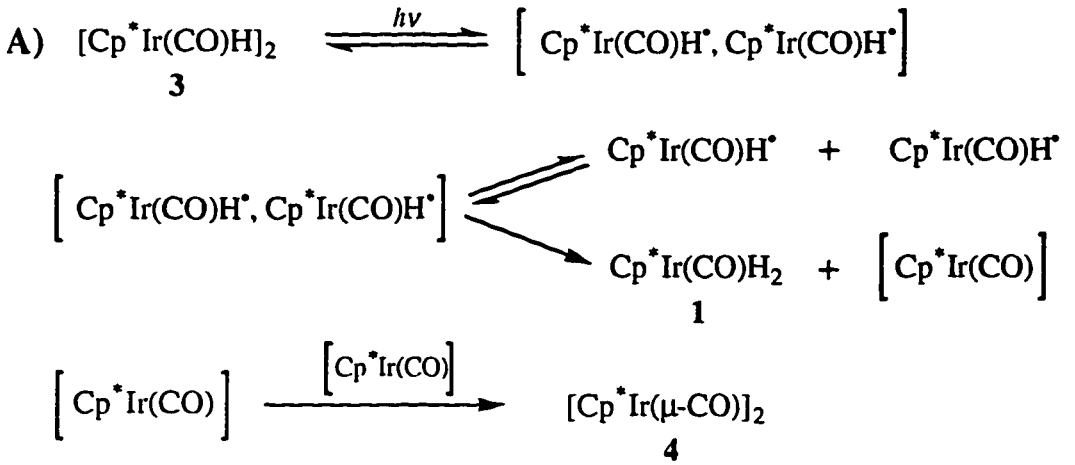

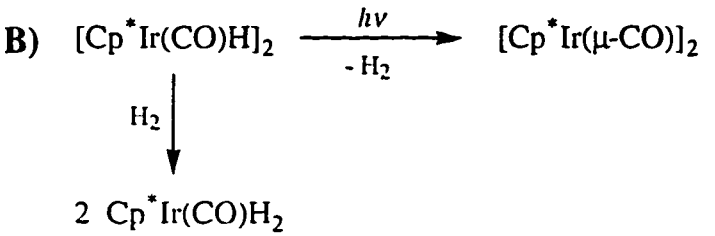

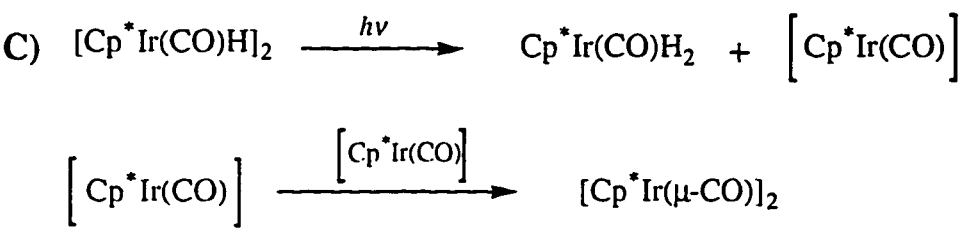

Scheme 3.3

transfer to metal centered radicals can also be quite fast, but the rate is dependent upon the substrate. Laine and Ford determined[52] the rate constants for the abstraction of a chlorine atom by $CpW(CO)_3^{\bullet}$ (generated by photolysis of the dimer) from a variety of

halocarbons. They found that the rate constant for chlorine atom transfer from CH_2Cl_2 ($k < 0.6\ M^{-1}\ s^{-1}$) was relatively small and five orders of magnitude less than that for CCl_4. Therefore, a radical pathway for the photodecomposition of $[Cp^*Ir(CO)H]_2$ (**3**) cannot be discounted.

Photo-induced reductive elimination of H_2 is a second mechanism (B). The concerted 1,2-dinuclear reductive elimination of H_2 as a *photochemical* process is symmetry allowed.[3] An example was reported[18] by Geoffroy and co-workers who observed the elimination of H_2 upon irradiation of platinum A-frame dimers such as $[Pt_2H_2Cl(dppm)_2]^+$. In our system, the subsequent reaction of H_2 with the starting material (**3**) could generate the dihydride monomer (**1**). In a separate experiment, **3** does react with H_2 (0.93 atm) in room light to afford primarily **1**, with some **4**. This pathway is inconsistent though with the photolysis of **3** in the presence of PPh_3, which produces an approximately 1:1 mixture of **1** and $Cp^*Ir(CO)(PPh_3)$. It would be possible to accommodate this discrepancy if **4** could react with PPh_3 to afford $Cp^*Ir(CO)(PPh_3)$. However, previous experiments in the Heinekey group[53] indicate that **4** is unreactive towards phosphines: **4** does not react with $P(OMe)_3$ (4.5 equiv) in benzene at reflux over several days. Hence, we can rule out mechanism B.

A third possibility (C) is similar to the first postulated mechanism (A) in that rupture of the metal-metal bond occurs. However, in this scenario, the dimer fragments into the monomeric dihydride, **1**, and the 16-electron species $[Cp^*Ir(CO)]$. This fragmentation is simply the combination of the first two steps of mechanism one (with hydrogen atom transfer), but precludes the formation of radical species. In this manner, **1** is simply acting as a good leaving group, like the photodissociation of CO from $Cp^*Ir(CO)_2$. The coordinatively unsaturated $[Cp^*Ir(CO)]$ fragment can subsequently react with another $[Cp^*Ir(CO)]$ moiety to form the dimer **4**, or in the presence of PPh_3, can be trapped to generate $Cp^*Ir(CO)(PPh_3)$. A perplexing issue arises however if we

more carefully consider the fate of the [Cp*Ir(CO)] fragment. As discussed above in relation to the thermal decomposition of **3**, we would expect [Cp*Ir(CO)] to oxidatively add the C-D bonds of the benzene-d_6 or methylcyclohexane-d_{14} solvent. No new ^{1}H NMR resonances in the Cp* region attributable to Cp*Ir(CO)(R)D are observed during the photodecomposition of **3**. To circumvent this apparent dilemma, we might propose a fourth pathway (D) that proceeds via a bimolecular reaction (Scheme 3.4). In this mechanism, absorption of radiation by **3** generates an excited state which can then react with a good ligand (e.g. PPh_3), or, in the absence of a good ligand, react with another molecule of **3**. Bimolecular reactions of organometallic excited states are known, though Geoffroy and Wrighton noted[49] in 1979 that we do not yet have "an extensive array of bimolecular reactions."

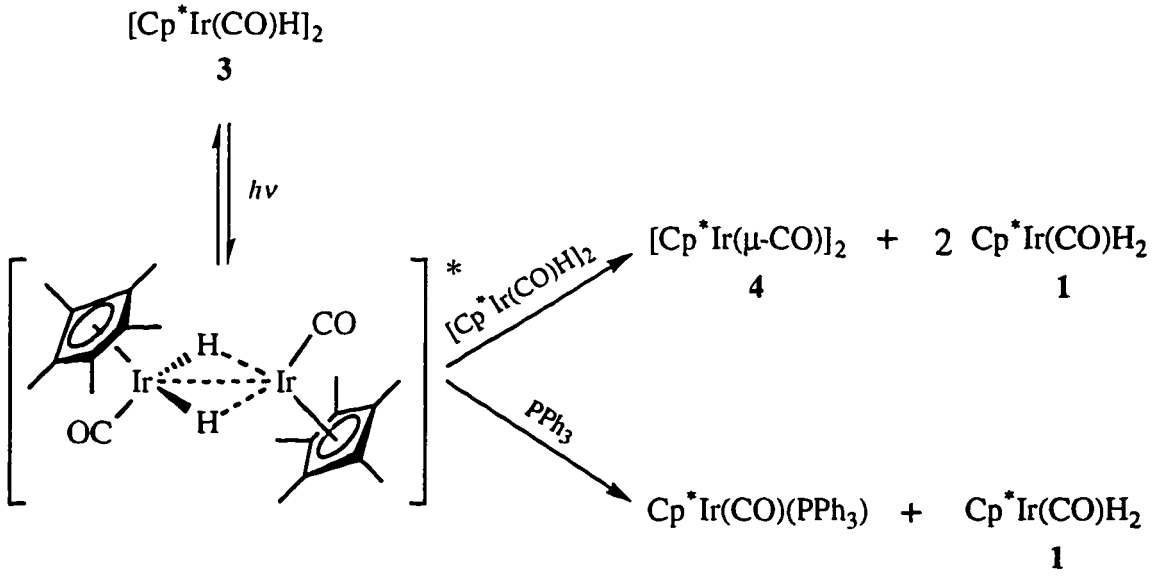

Scheme 3.4

Bergman and Krause report[54] that the related rhodium alkyl, $[Cp^*Rh(\mu\text{-}CO)(Me)]_2$, reacts in a similar fashion when irradiated, generating $[Cp^*Rh(\mu\text{-}CO)]_2$ and $Cp^*Rh(CO)Me_2$. The mechanism for this reaction was not discussed, but the results lend credibility to pathways A, C, or D above. Mechanism B would certainly be improbable in this case, necessitating reaction of $[Cp^*Rh(\mu\text{-}CO)(Me)]_2$ with ethane.

We did not irradiate a solution containing only $Cp^*Ir(CO)H_2$ (**1**). However, **1** was formed during the photolysis of **3** and is stable to room light and irradiation with $\lambda > 360$ nm. It is understandable that **1** is less sensitive to irradiation than **3** since it lacks a metal-metal bond, which typically is subject to cleavage by low energy σ to σ^* transitions. Shorter wavelength irradiation of **1** does lead to H_2 elimination. Poliakoff and co-workers[55] have performed "solvent-free" photochemical reactions in supercritical fluid solutions and find that UV irradiation of **1** is more efficient than irradiation of $Cp^*Ir(CO)_2$ for activating the C-H bonds of alkanes.

Oxidation

Reductive elimination of dihydrogen or alkane from a transition metal center leads to a formal reduction in the oxidation number of the metal and hence is favored by metal centers in a high oxidation state. We would expect that oxidation of a metal complex, whether electrochemical or via a reagent, should enhance that complex's ability to undergo reductive elimination. However, oxidation of transition metal complexes containing hydride ligands also facilitates proton transfer. The thermodynamic acidity of neutral, 18-electron transition metal hydrides increases by 20-25 pKa units upon oxidation by one electron.

Tilset and Pedersen[56] have recently studied the oxidation chemistry of the monomeric phosphine analogues, $Cp^*Ir(PPh_3)(R)(R')$ (R/R' = H/H, H/Me, Me/Me), finding that the reactivity varies greatly between them. Chemical oxidation of

$Cp^*Ir(PPh_3)H_2$ with $[Cp_2Fe]PF_6$ (0.67 equiv) in CH_2Cl_2 affords $Cp^*Ir(PPh_3)H_3^+$ and $[Cp^*Ir(PPh_3)H]_2(\mu\text{-}H)^+$, consistent with a proton transfer reaction. In contrast, addition of $[Cp_2Fe]^+$ (2 equiv) to an acetonitrile solution of $Cp^*Ir(PPh_3)(CH_3)H$ spontaneously induces the intramolecular reductive elimination of CH_4 with quantitative formation of $Cp^*Ir(PPh_3)(NCMe)^{2+}$. This is a large enhancement over the rate of reductive elimination without benefit of an oxidant, as $Cp^*Ir(PPh_3)(CH_3)H$ extrudes CH_4 only after several days in benzene at 110 °C. Oxidation of $Cp^*Ir(PPh_3)(CH_3)_2$ with $[Cp_2Fe]^+$ in acetonitrile slowly produced $Cp^*Ir(PPh_3)(NCMe)(CH_3)^+$ plus CH_4 in an as yet unresolved mechanism.

As in the phosphine system, chemical oxidation of the dihydride, $Cp^*Ir(CO)H_2$ (**1**), results in a spontaneous reaction consistent with a proton transfer mechanism. The predominant Cp^*-bearing product is $[Cp^*Ir(CO)H]_2(\mu\text{-}H)^+$. A proposed mechanism is shown in Scheme 3.5. The first step involves the one electron oxidation of the neutral dihydride to the 17-electron radical cation $Cp^*Ir(CO)H_2^{\bullet+}$. This species transfers a proton to another molecule of **1** to generate the 17-electron neutral radical, $Cp^*Ir(CO)H^\bullet$, and the 18-electron trihydride cation, $Cp^*Ir(CO)H_3^+$. In the phosphine system, $Cp^*Ir(PPh_3)H_3^+$ is stable, but the carbonyl trihydride cation is known to spontaneously decompose at temperatures above -78 °C to form H_2 and 0.5 equiv of $[Cp^*Ir(CO)H]_2(\mu\text{-}H)^+$ (see Chapter 2). The 17-electron $Cp^*Ir(CO)H^\bullet$ is undoubtedly quite reactive and could combine with yet another molecule of the neutral dihydride to afford the radical dimer, $[Cp^*Ir(CO)]_2H_3^\bullet$, which then undergoes one electron oxidation to the cationic product. It is conceivable that $Cp^*Ir(CO)H^\bullet$ could react with a molecule of $Cp^*Ir(CO)H_2^{\bullet+}$ to form $[Cp^*Ir(CO)H]_2(\mu\text{-}H)^+$ directly, but this seems unlikely based upon analogy to the phosphine system. It was observed[56] by cyclic voltammetry that one electron electrochemical oxidation of $Cp^*Ir(PPh_3)H_2$ was chemically irreversible on the

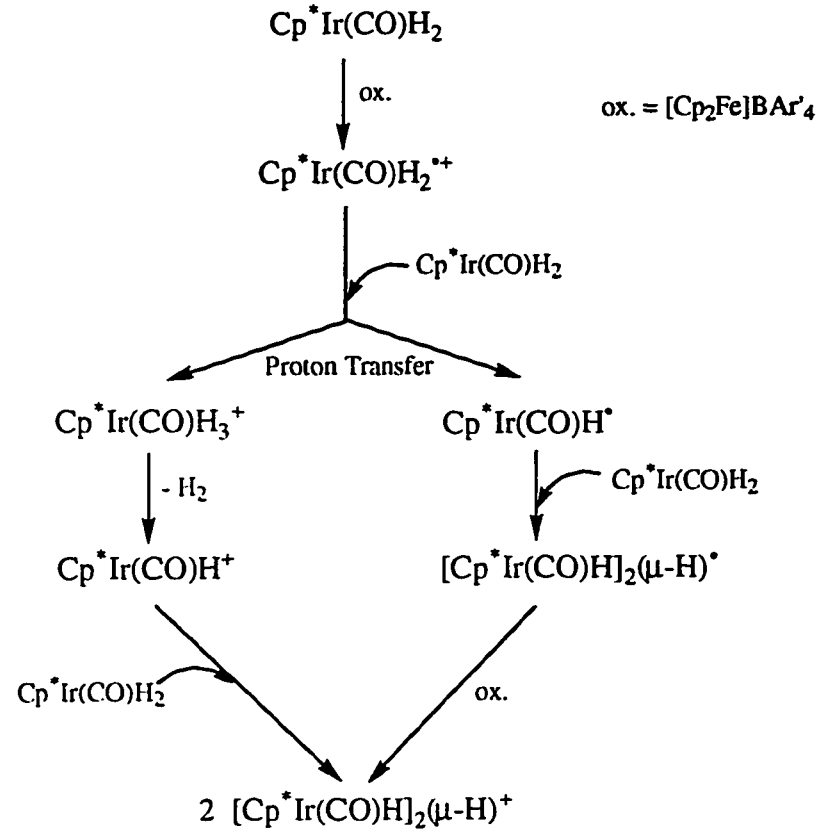

Overall:

$$4\,Cp^*Ir(CO)H_2 + 2\,[Cp_2Fe]^+ \longrightarrow 2\,[Cp^*Ir(CO)H]_2(\mu\text{-}H)^+ + 2\,Cp_2Fe + H_2$$

Scheme 3.5

time scale of the experiment, that is the lifetime of $Cp^*Ir(PPh_3)H_2^{\bullet+}$ was very short ($\tau < 10^{-4}$ s). Hence, if the lifetime of $Cp^*Ir(CO)H_2^{\bullet+}$ is similarly short, then its concentration would be very small relative to that of $Cp^*Ir(CO)H_2$ (**1**).

The stoichiometry of the reaction as proposed would require 0.5 equiv of oxidant. The presence of unreacted **1** at the completion of our experiment confirms that greater than 0.3 equiv of oxidant is required. The reaction appears fairly clean by ^1H NMR and could be of synthetic utility. The dihydride (**1**) is a weak base and can only be protonated cleanly by strong acids (e.g. HOTf). Synthesis of $[Cp^*Ir(CO)H]_2(\mu\text{-}H)^+$ by the oxidation

route would allow it to be prepared with a variety of counterions in addition to OTf^-.

Unlike the phosphine system, the dimethyl complex, $Cp^*Ir(CO)(CH_3)_2$ (**2**), does not react with ferrocenium. This may reflect the greater electron withdrawing ability of the CO ligand, creating a metal center that is less electron rich, and hence more difficult to oxidize. The broadened lines in the ^1H NMR spectrum (in CD_3CN) are most likely due to the presence of a small quantity of the singly oxidized paramagnetic species, $Cp^*Ir(CO)(CH_3)_2^{\bullet+}$, which undergoes a rapid self-exchange reaction with the unoxidized parent compound. Broadened NMR lines are a common manifestation of electron self-exchange reactions.[57,58]

Like monomeric hydrides, the oxidation of dimeric compounds containing hydride ligands should facilitate both reductive elimination and proton transfer reactions. But unlike monomers, electron-poor dimers can stabilize themselves via formation of metal-metal bonds. As in the case of the dihydride monomer (**1**), oxidation of the dimer, $[Cp^*Ir(CO)H]_2$ (**3**), induces proton transfer. The primary product is the trihydride cation, $[Cp^*Ir(CO)H]_2(\mu\text{-}H)^+$, a compound that has been prepared by other routes (see Chapter 2). The proposed mechanism is presented in Scheme 3.6. Single electron oxidation of **3** generates the radical cation dimer, which would have a formal Ir-Ir bond order of 1.5. Proton transfer to a second equivalent of **3** affords $[Cp^*Ir(CO)H]_2(\mu\text{-}H)^+$ and a 33-electron dimer, $[Cp^*Ir(CO)]_2(\mu\text{-}H)^\bullet$. Further oxidation of $[Cp^*Ir(CO)]_2(\mu\text{-}H)^\bullet$ produces the known unsaturated dimer, $[Cp^*Ir(CO)]_2(\mu\text{-}H)^+$ (see Chapter 4), which possesses a formal Ir=Ir double bond. The initial deep blue-green color of the solution is characteristic of $[Cp^*Ir(CO)]_2(\mu\text{-}H)^+$. However, $[Cp^*Ir(CO)]_2(\mu\text{-}H)^+$ is an extremely reactive compound, and under these conditions, reacts further to form unidentified products.

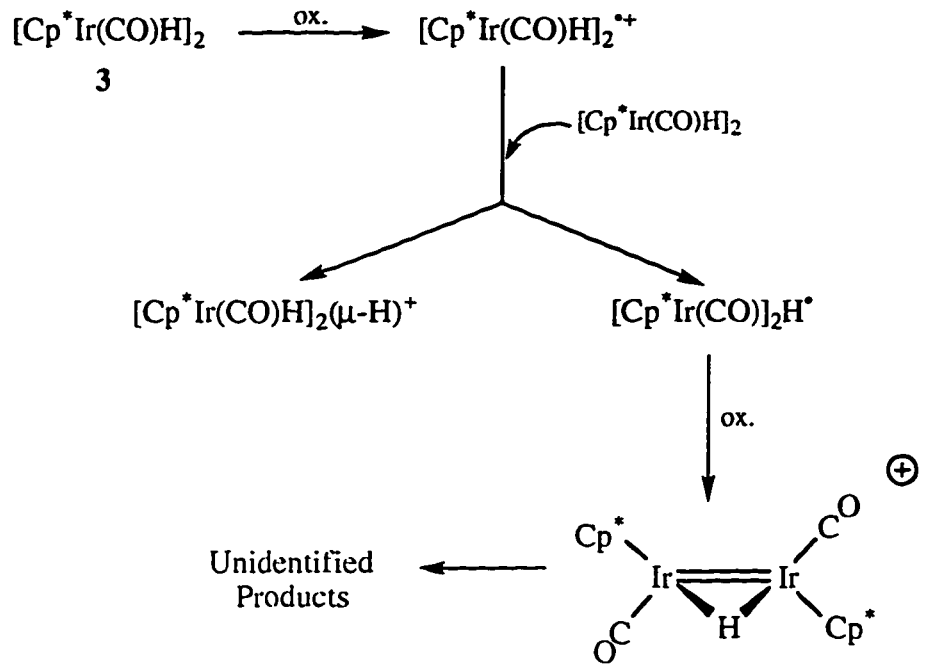

Scheme 3.6

Attempts at Ligand-Induced Reductive Elimination

Bergman and co-workers have shown that reaction of a bis-Cp*, bridging allyl iridium dimer with a variety of soft donor ligands (e.g. tertiary phosphines, isocyanides, carbon monoxide) induces intramolecular reductive elimination of benzene (eq 3.12).[8] We wondered whether reaction of CO with $[Cp^*Ir(CO)H]_2$ (**3**) would similarly effect reductive elimination of H_2 with formation of the known tricarbonyl dimer, $[Cp^*Ir(CO)]_2(\mu\text{-}CO)$.[59,60] However, addition of CO to a benzene solution of **3** (shielded from light) produces solely the monomer, $Cp^*Ir(CO)_2$. We could hypothesize that

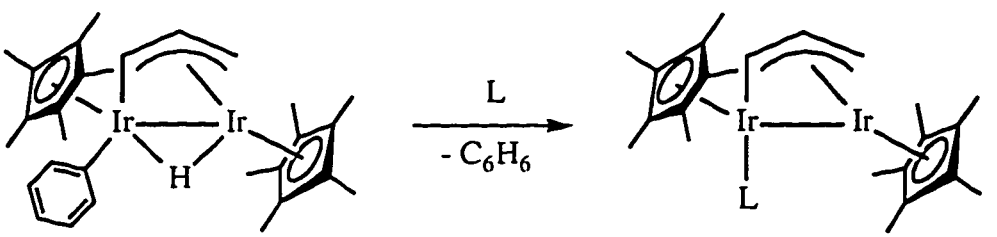

(3.12)

$[Cp^*Ir(CO)]_2(\mu\text{-}CO)$ is initially formed and then rapidly reacts with another equivalent of CO to form two molecules of $Cp^*Ir(CO)_2$, but this is not in accord with the previously published results; $[Cp^*Ir(CO)]_2(\mu\text{-}CO)$ is reported to be stable to excess CO.[59,60] A more likely mechanism proceeds via CO-assisted fragmentation of the dihydride dimer, **3**, to form $Cp^*Ir(CO)_2$ and $Cp^*Ir(CO)H_2$ (**1**), followed by rapid reaction of **1** with CO to provide another molecule of $Cp^*Ir(CO)_2$ and H_2 (eq 3.14). The reaction of **1** with CO is confirmed by Bergman and Gilbert, who find that addition of only 8 equiv of CO to Cp^*IrH_4 initially generates **1**, which subsequently is converted to $Cp^*Ir(CO)_2$.[35] Further support for this pathway is provided by the related rhodium methyl dimer, $[Cp^*Rh(CO)Me]_2$, which is reported[54] to react with CO in a similar fashion to give $Cp^*Rh(CO)_2$ and $Cp^*Rh(CO)Me_2$ in a 1:1 ratio.

$$\underset{\mathbf{3}}{[Cp^*Ir(CO)H]_2} \xrightarrow{CO} Cp^*Ir(CO)_2 + Cp^*Ir(CO)H_2\ (\mathbf{1}) \qquad (3.13)$$

$$Cp^*Ir(CO)H_2\ (\mathbf{1}) \xrightarrow{CO,\ -H_2} Cp^*Ir(CO)_2$$

Surprisingly, triphenylphosphine does not react with **3** when shielded from light, perhaps due to its steric bulk. When exposed to light, reaction does occur (see Photochemistry section above).

Conclusion

The monomers, $Cp^*Ir(CO)H_2$ (**1**) and $Cp^*Ir(CO)Me_2$ (**2**), both exhibit substantial thermal stability. Taken together with the relative thermal instability of the previously reported alkyl hydride derivatives, this reactivity trend is typical of related systems. The dihydride monomer (**1**) does participate in a slow thermal reaction, incorporation of deuterium from C_6D_6 into its Cp^* methyl groups. The mechanism is not known, but we favor the initial loss of H_2, followed by oxidative addition of C_6D_6, and subsequent intramolecular activation of a C-H bond of a Cp^* methyl group.

Thermolysis of the dihydride dimer, $[Cp^*Ir(CO)H]_2$ (**3**), in the solid state or in methylcyclohexane-d_{14}, leads to extrusion of H_2 and exclusive formation of $[Cp^*Ir(\mu\text{-}CO)]_2$ (**4**). Examples of thermal reductive elimination of H_2 from metal dimers are rare. The concerted *1,2*-dinuclear reductive elimination of H_2 is forbidden according to the principles of orbital symmetry conservation. The intramolecular nature of the elimination of H_2 from **3** has not yet been determined. Thermolysis of **3** in C_6D_6 or CD_2Cl_2 is complicated by the generation of the dihydride monomer, **1**, for which several mechanisms have been postulated.

The dimer (**3**) is light sensitive. Photolysis leads to clean fragmentation of the dimer to form **1** and **4** in a 2:1 molar ratio. A plausible mechanism proceeds via Ir-Ir bond homolysis followed by rapid hydrogen atom transfer, however a bimolecular reaction cannot be ruled out.

Chemical oxidation of both the dihydride monomer (**1**) and dimer (**3**) induces proton transfer reactions. The principal product of both reactions is the trihydride cation dimer, $[Cp^*Ir(CO)H]_2(\mu\text{-}H)^+$. The dimethyl monomer, **2**, is not oxidized by $[Cp_2Fe]^+$.

Reaction of **3** with CO causes fragmentation of the dimer to **1** and $Cp^*Ir(CO)_2$, and eventually results in complete conversion to $Cp^*Ir(CO)_2$.

Experimental

General procedures for manipulation and characterization of compounds are presented in Chapter 2. $[Cp_2Fe]BAr'_4$ was prepared by C. E. Radzewich.[61]

Rate Plots. Shortly after a sample solution was prepared, a ^1H NMR spectrum of the solution was acquired. The ratio of the integral of the Cp^* resonance of interest to the integral of the TMS resonance was calculated to give an initial value. Periodically during the experiment, ^1H NMR spectra were collected and the ratio of the Cp^*/TMS integrals was divided by the initial ratio (t = 0) to yield a relative concentration. A long relaxation delay between pulses (typically RD = 60 s) was employed during all ^1H NMR acquisitions.

Photolysis Experiments. Irradiation was furnished by a Hanovia medium pressure mercury lamp set in a cylindrical quartz water jacket and transmitted through a glass filter ($\lambda > 360$ nm). A sample solution in a flame-sealed NMR tube was placed in the path of the filtered light, about 10 cm from the lamp. Solutions were monitored periodically by NMR spectroscopy.

Thermolysis Experiments. A typical thermolysis experiment was performed as follows. An NMR tube fitted with a high vacuum Teflon stopcock was charged with the organometallic solid. Solvent and a trace amount of TMS were vacuum transferred onto the solids. The solution was frozen in a liquid N_2 bath and the NMR tube flame-sealed under vacuum. The sealed tube was completely immersed in a heated oil bath and shielded from light with foil. The tube was removed periodically for analysis by NMR spectroscopy.

Thermolysis of $Cp^*Ir(CO)H_2$ (1). An NMR tube containing 20.3 mg of **1** (57 μmol) and benzene-d_6 (0.5 mL) was heated to 100 °C. After heating for 20 days the pale yellow solution had become dark brown, characteristic of $[Cp^*Ir(\mu\text{-}CO)]_2$ (**4**). ^1H NMR: **1** (96%), **4** (4%). Triplets (1:1:1, J = 2.2 Hz) just upfield (18 ppb) of the Cp^* resonances of **1** and **4** indicate deuterium incorporation from the solvent into the Cp^* methyl groups of both compounds.

Thermolysis of $Cp^*Ir(CO)Me_2$ (2). An NMR tube containing 5.9 mg of **2** (15 μmol) and benzene-d_6 (0.5 mL), but no TMS, was heated to 85 °C for 97 days. No reaction was apparent by ^1H NMR, except for a minor unidentified resonance at 1.41 ppm.

Thermolysis of $[Cp^*Ir(CO)H]_2$ (3) in C_6D_6. An NMR tube containing 5.0 mg of **3** (7.0 μmol) and benzene-d_6 (0.5 mL), was heated to 100 °C. After heating for 90 days the bright yellow solution had become dark brown, characteristic of $[Cp^*Ir(\mu\text{-}CO)]_2$ (**4**). ^1H NMR: **3** (40%), **1** (14%), **4** (46%). Triplets (1:1:1, J = 2.2 Hz) just upfield (18 ppb) of the Cp^* resonances of **1** and **4** indicate deuterium incorporation from the solvent into the Cp^* methyl groups of both compounds.

Thermolysis of $[Cp^*Ir(CO)H]_2$ (3) in Methylcyclohexane-d_{14}. An NMR tube containing 3.4 mg of **3** (4.8 μmol) and methylcyclohexane-d_{14} (0.5 mL), was heated to 139 °C.

Solid State Thermolysis of $[Cp^*Ir(CO)H]_2$ (3). To a screw-cap NMR tube was added 3.1 mg of **3** (4.3 μmol). The tube was evacuated, placed under argon, and the bottom immersed in a sand bath heated to 120 °C. After heating for 7.5 days, the yellow starting material had become brown. Addition of CD_2Cl_2 (0.3 mL) via vacuum transfer yielded a

clear, brown-orange solution. ^{1}H NMR: $[Cp^*Ir(\mu\text{-}CO)]_2$ (**4**) (90%), **3** (2%), and two small, unidentified resonances at 1.94 and 1.90 ppm.

Reaction of $Cp^*Ir(^{13}CO)H_2$ (1*) with $[Cp_2Fe]BAr'_4$. To an NMR tube fitted with a high vacuum Teflon stopcock was added 9.3 mg of **1*** (26 μmol) and 8.2 mg of $[Cp_2Fe]BAr'_4$ (0.78 μmol, 0.30 equiv). Methylene chloride-d_2 (0.5 mL) and a trace amount of TMS were vacuum transferred onto the solids. The NMR tube was sealed under vacuum and ^{1}H NMR spectra acquired. The principal products were $\{[Cp^*Ir(^{13}CO)H]_2(\mu\text{-}H)\}BAr'_4$ (δ 7.72 (br s, BAr'_4, ortho),[62] 7.56 (br s, BAr'_4, para), 2.18 (s, Cp^*), -16.50 (br s, Ir-H), based upon comparison to the chemical shifts of the triflate salt) and Cp_2Fe (δ 4.15). Some of the dihydride (**1***) remained unreacted and no free H_2 was observed. When a spectrum was collected with selective homonuclear decoupling of the Cp^* resonance at 2.18 ppm, the hydride resonance at -16.50 ppm was resolved into a triplet ($J_{C\text{-}H}$ = 3.3 Hz).

Reaction of $Cp^*Ir(CO)Me_2$ (2) with $[Cp_2Fe]BAr'_4$ in CD_2Cl_2. To an NMR tube fitted with a high vacuum Teflon stopcock was added 4.9 mg of **2** (13 μmol) and 13.1 mg of $[Cp_2Fe]BAr'_4$ (12.5 μmol, 0.98 equiv). Methylene chloride-d_2 (0.5 mL) was vacuum transferred onto the solids. The NMR tube was flame-sealed under vacuum. No reaction was evident by ^{1}H NMR.

Reaction of $Cp^*Ir(CO)Me_2$ (2) with $[Cp_2Fe]BAr'_4$ in CD_3CN. To a screw-cap NMR tube was added 4.1 mg of **2** (11 μmol) and 12.2 mg of $[Cp_2Fe]BAr'_4$ (11.6 μmol, 1.1 equiv). CD_3CN (0.4 mL) was vacuum transferred onto the solids. No new signals were apparent by ^{1}H NMR, however the resonances attributed to **2** (δ 1.84, 0.28) were broader

and had shifted slightly downfield (**2** in CD_3CN: δ 1.82, 0.27). Additionally, the acetonitrile-d_2 resonance had broadened as well as increased in intensity.

Reaction of $[Cp^*Ir(CO)H]_2$ (3) with $[Cp_2Fe]BAr'_4$. To an NMR tube fitted with a high vacuum Teflon stopcock was added 4.5 mg of **3** (6.3 μmol) and 6.6 mg of $[Cp_2Fe]BAr'_4$ (6.3 μmol, 1.0 equiv). Methylene chloride-d_2 (0.35 mL) was vacuum transferred onto the solids. The NMR tube was flame-sealed under vacuum. Upon thawing, the solution immediately became deep blue-green and opaque. After standing ca. 30 minutes at room temperature the solution turned orange. The ^1H NMR spectrum revealed the presence of Cp_2Fe (δ 4.15) and $\{[Cp^*Ir(CO)H]_2(\mu\text{-}H)\}BAr'_4$ (δ 2.18 (Cp^*), -16.49 (Ir-H)) and several other unknown species, but no free H_2.

Photolysis of $[Cp^*Ir(CO)H]_2$ (3) in C_6D_6, C_7D_{14}. To an NMR tube fitted with a high vacuum Teflon stopcock was added 3.2 mg of **3** (4.5 μmol). Benzene-d_6 (0.4 mL) and a trace of TMS were vacuum transferred onto the solids. The solution was frozen in a liquid N_2 bath and the NMR tube flame-sealed under vacuum. The solution was irradiated ($\lambda > 360$ nm) for 11.5 hours and monitored periodically by ^1H NMR spectroscopy. After 3.5 hours the starting material was consumed and the reaction was complete by ^1H NMR, yielding the following products: $Cp^*Ir(CO)H_2$ (**1**) (71%, molar basis), $[Cp^*Ir(\mu\text{-}CO)]_2$ (**4**) (29%). Irradiation of **3** in methylcyclohexane-d_{14} was also conducted, with similar results.

Reaction of $[Cp^*Ir(CO)H]_2$ (3) with CO. To a screw-cap NMR tube was added 6.4 mg of **3** (9.0 μmol) and C_6D_6 (0.4 mL) via vacuum transfer. During all further manipulations the solution was shielded from light with foil. The bottom of the tube was immersed in a CO_2/IPA bath, the head space evacuated, and then pressurized to 1185 torr (1.56 atm)

with CO. After standing at room temperature for one week, the starting material was almost entirely (> 96% by ^{1}H NMR) converted to $Cp^*Ir(CO)_2$ (δ 1.78) with concomitant generation of H_2 (δ 4.47).

Reaction of $[Cp^*Ir(CO)H]_2$ (3) with PPh_3. To an NMR tube fitted with a high vacuum Teflon stopcock was added 3.5 mg of **3** (4.9 μmol) and 13.0 mg of PPh_3 (49.6 μmol, 10 equiv). Methylene chloride-d_2 and a trace of TMS were vacuum transferred onto the solids. The tube was shielded from light with foil. The solution was frozen in a liquid N_2 bath and the NMR tube sealed under vacuum. A ^{1}H NMR spectrum taken after standing for 46 h in the dark indicated that no reaction had taken place. The solution was then left exposed to room light. Upon standing for a further 24 h, the products were $Cp^*Ir(CO)H_2$ (**1**) (37% of total Cp^* integration) and $Cp^*Ir(CO)(PPh_3)$ (30%; δ 1.82 (d, $^4J_{H\text{-}P}$ = 1.5 Hz, Cp^*); based upon comparison to the reported[22] chemical shift of the Cp^* resonance) along with unreacted **3** (33%).

Notes to Chapter 3

(1) Norton, J. R. *Acc. Chem. Res.* **1979**, *12*, 139-145.

(2) Hoffmann, R. In *IUPAC Frontiers of Chemistry*; Laidler, K. J., Ed.; Pergamon: Oxford, 1982; pp 247-263.

(3) Trinquier, G.; Hoffmann, R. *Organometallics* **1984**, *3*, 370-380.

(4) Halpern, J. *Inorg. Chim. Acta* **1982**, *62*, 31-37.

(5) Reductive elimination is ligand induced: Hill, R. H.; Puddephatt, R. J. *J. Am. Chem. Soc.* **1983**, *105*, 5797-5804.

(6) Kellenberger, B.; Young, S. J.; Stille, J. K. *J. Am. Chem. Soc.* **1985**, *107*, 6105-6107.

(7) Young, S. J.; Kellenberger, B.; Reibenspies, J. H.; Himmel, S. E.; Manning, M.; Anderson, O. P.; Stille, J. K. *J. Am. Chem. Soc.* **1988**, *110*, 5744-5753.

(8) Reductive elimination is ligand induced: McGhee, W. D.; Hollander, F. J.; Bergman, R. G. *J. Am. Chem. Soc.* **1988**, *110*(25), 8428-8443.

(9) Reports in which *intra*molecular dinuclear reductive elimination is suggested, though not proven, include: (a) Davies, S. G.; Hibberd, J.; Simpson, S. J.; Watts, O. *J. Organomet. Chem.* **1983**, *241*, C31-C33. (b) Sterenberg, B. T.; Hilts, R. W.; Moro, G.; McDonald, R.; Cowie, M. *J. Am. Chem. Soc.* **1995**, *117*, 245-258 .

(10) Pearson, R. G. *Symmetry Rules for Chemical Reactions*; Wiley-Interscience: New York, 1976.

(11) Hembre, R. T.; Scott, C. P.; Norton, J. R. *J. Am. Chem. Soc.* **1987**, *109*, 3468-3470.

(12) Hembre, R. T.; Ramage, D. L.; Scott, C. P.; Norton, J. R. *Organometallics* **1994**, *13*, 2995-3001.

(13) Kelland, J. W.; Norton, J. R. *J. Organomet. Chem.* **1978**, *149*, 185-194.

(14) Norton, J. R.; Carter, W. J.; Kelland, J. W.; Okrasinski, S. J. *Adv. Chem. Ser.* **1978**, *167*, 170-180.

(15) Ball, R. G.; Graham, W. A. G.; Heinekey, D. M.; Hoyano, J. K.; McMaster, A. D.; Mattson, B. M.; Michel, S. T. *Inorg. Chem.* **1990**, *29*, 2023-2025.

(16) Geoffroy, G. L.; Bradley, M. G.; Pierantozzi, R. *Adv. Chem. Ser.* **1978**, *167*, 181-200.

(17) Janowicz, A. H.; Bergman, R. G. *J. Am. Chem. Soc.* **1983**, *105*, 3929-3939.

(18) Foley, H. C.; Morris, R. H.; Targos, T. S.; Geoffroy, G. L. *J. Am. Chem. Soc.* **1981**, *103*, 7337-7339.

(19) Hill, R. H.; de Mayo, P.; Puddephatt, R. J. *Inorg. Chem.* **1982**, *21*, 3642-3646.

(20) Hill, R. H.; Puddephatt, R. J. *Organometallics* **1983**, *2*, 1472-1474.

(21) Davies, S. G.; Hibberd, J.; Simpson, S. J.; Watts, O. *J. Organomet. Chem.* **1983**, *241*, C31-C33.

(22) Glueck, D. S.; Newman Winslow, L. J.; Bergman, R. G. *Organometallics* **1991**, *10*, 1462-1479.

(23) Kang, J. W.; Moseley, K.; Maitlis, P. M. *J. Am. Chem. Soc.* **1969**, *91*, 5970-5977.

(24) Stoutland, P. O.; Bergman, R. G.; Nolan, S. P.; Hoff, C. D. *Polyhedron* **1988**, *7*, 1429-1440.

(25) Calderazzo, R. *Ann. N.Y. Acad. Sci.* **1983**, *415*, 37-46.

(26) Brown, T. L. In *Organometallic Radical Processes*; Trogler, W. C., Ed.; Elsevier: Amsterdam, 1990; pp 67-107, and references therein.

(27) Shapley, J. R.; Adair, P. C.; Lawson, R. J.; Pierpont, C. G. *Inorg. Chem.* **1982**, *21*, 1701-1702.

(28) Rerek, M. E.; Basolo, F. *Organometallics* **1983**, 2(3), 372-376, and references therein.

(29) Selmeczy, A. D.; Jones, W. D.; Partridge, M. G.; Perutz, R. N. *Organometallics* **1994**, *13*, 522-532.

(30) Einstein, F. W. B.; Jones, R. H.; Zhang, X.; Yan, X.; Negelkerke, R.; Sutton, D. *J. Chem. Soc., Chem. Commun.* **1989**, 1424-1426.

(31) Parkin, G.; Bercaw, J. E. *Polyhedron* **1988**, *7*, 2053-2082.

(32) Edidin, R. T.; Norton, J. R. *J. Am. Chem. Soc.* **1986**, *108*, 948-953.

(33) Gilbert, T. M.; Bergman, R. G. *J. Am. Chem. Soc.* **1985**, *107*, 3508-3516, and references therein.

(34) Heinekey, D. M.; Millar, J. M.; Koetzle, T. F.; Payne, N. G.; Zilm, K. W. *J. Am. Chem. Soc.* **1990**, *112*, 909-919.

(35) Gilbert, T. M. Ph.D. Thesis, University of California, Berkeley, 1985.

(36) Bloyce, P. E.; Rest, A. J.; Whitwell, I.; Graham, W. A. G.; Holmes-Smith, R. *J. Chem. Soc., Chem. Commun.* **1988**, 846-848.

(37) McAlister, D. R.; Erwin, D. K.; Bercaw, J. E. *J. Am. Chem. Soc.* **1978**, *100*, 5966-5968.

(38) Parkin, G.; Bercaw, J. E. *Organometallics* **1989**, *8*, 1172-1179.

(39) Maitlis, P. M.; Long, H. C.; Quyoum, R.; Turner, M. L.; Wang, Z.-Q. *J. Chem. Soc., Chem. Commun.* **1996**, 1-8.

(40) Hoyano, J. K.; McMaster, A. D.; Graham, W. A. G. *J. Am. Chem. Soc.* **1983**, *105*, 7190-7191.

(41) Evans, J.; Norton, J. R. *J. Am. Chem. Soc.* **1974**, *96*, 7577-7578.

(42) Moss, J. R.; Graham, W. A. G. *Inorg. Chem.* **1977**, *16*, 75-79.

(43) Grevels, F.-W.; Klotzbücher, W. E.; Seils, F.; Schaffner, K.; Takats, J. *J. Am. Chem. Soc.* **1990**, *112*, 1995-1996.

(44) Michel, S. Ph.D. Thesis, Yale University, Dec. 1989.

(45) Tilset, M.; Vollhardt, K. P. C.; Boese, R. *Organometallics* **1994**, *13*, 3146-3169.

(46) Hoyano, J. K.; Graham, W. A. G. *J. Am. Chem. Soc.* **1982**, *104*, 3723-3725.

(47) Rest, A. J.; Whitwell, I.; Graham, W. A. G.; Hoyano, J. K.; McMaster, A. D. *J. Chem. Soc., Dalton Trans.* **1987**, 1181-1190.

(48) Graham, W. A. G. *J. Organomet. Chem.* **1986**, *300*, 81-91.

(49) Geoffroy, G. L.; Wrighton, M. S. *Organometallic Photochemistry*; Academic: New York, 1979.

(50) Halpern, J. In *Bonding Energetics in Organometallic Compounds*; Marks, T. J., Ed.; American Chemical Society: Washington, DC, 1990; pp 100-112.

(51) Gill, D. S.; Maitlis, P. M. *J. Organomet. Chem.* **1975**, *87*, 359-364.

(52) Laine, R. M.; Ford, P. C. *Inorg. Chem.* **1977**, *16*, 388-391.

(53) Heinekey, D. M.; Michel, S. T. , Yale University, unpublished results.

(54) Krause, M. J.; Bergman, R. G. *Organometallics* **1986**, *5*, 2097-2108.

(55) Banister, J. A.; Cooper, A. I.; Howdle, S. M.; Jobling, M.; Poliakoff, M. *Organometallics* **1996**, *15*, 1804-1812.

(56) Pedersen, A.; Tilset, M. *Organometallics* **1994**, *13*, 4887-4894.

(57) Koval, C. A.; Margerum, D. W. *Inorg. Chem.* **1981**, *20*, 2311-2318.

(58) Voges, M. H. Ph.D. Thesis, University of Washington, 1996.

(59) McGhee, W. D.; Foo, T.; Hollander, F. J.; Bergman, R. G. *J. Am. Chem. Soc.* **1988**, *110*, 8543-8545.

(60) Heinekey, D. M.; Michel, S. T. *Organometallics* **1989**, *8*, 1241-1246.

(61) Radzewich, C. E. Ph.D. Thesis, University of Washington, 1997.

(62) The chemical shifts of the BAr'_4^- protons are essentially independent of the associated cation and as such do not provide meaningful structural information. They are thus not included in the remainder of the experimental section.

CHAPTER 4

Protonation of $[Cp^*Ir(\mu\text{-}CO)]_2$: Formation and Reactions of $[Cp^*Ir(CO)]_2(\mu\text{-}H)^+$

Introduction

There is an extensive body of work devoted to the chemistry of cyclopentadienyl carbonyl dimers containing multiple bonds between the metal atoms.[1] Dimers of the form $[Cp'M(CO)]_2$ (M = Co, Rh, Ir; Cp' = Cp, Cp^*) contain a formal M=M double bond according to electron counting convention, and the carbonyls adopt bridging positions. The CpCo compound was isolated[2] in 1977, but the CpRh[3] and CpIr[4,5] complexes appear to be unstable at room temperature. The Cp^* analogues are easier to prepare and hence have been more extensively studied. $[Cp^*Ir(\mu\text{-}CO)]_2$ was first reported by Graham and co-workers[6] as a byproduct of photolysis reactions of $Cp^*Ir(CO)_2$. An efficient synthesis of $[Cp^*Ir(\mu\text{-}CO)]_2$ was only achieved quite recently,[7] via thermolysis of $Cp^*Ir(CO)_2$ in 1-butanol at reflux.

Hoffmann[8] has used molecular orbital diagrams constructed from combination of fragment valence orbitals to suggest that compounds of the form $[Cp'M(\mu\text{-}CO)]_2$ (M = Co, Rh, Ir; Cp' = Cp, Cp^*) are isolobal with ethylene. Two fragments or molecules are "isolobal" if the number, symmetry, approximate energy, and shape of their frontier orbitals, and the number of electrons in them, are similar.[8] In accord with the isolobal analogy, we would predict that these complexes, $[Cp'M(\mu\text{-}CO)]_2$, will undergo reactions in a similar fashion to ethylene. This approach has been successfully exploited by a number of research groups to prepare new compounds.[9-11] For example, analogous to the cyclopropanation of ethylene, addition of diazoalkanes to these unsaturated metal dimers provides an efficient route to bridging alkylidenes. Heinekey and Michel[12] have shown

that reaction of $[Cp^*Ir(\mu\text{-}CO)]_2$ with CH_2N_2 in THF at 195 K affords the metallacyclopropane complex, $[Cp^*Ir(CO)]_2(\mu\text{-}CH_2)$ (eq 4.1).

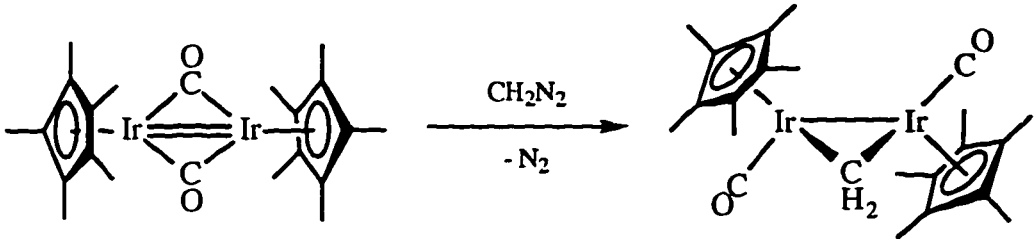

(4.1)

An obvious extension of ethylene chemistry would be reaction of unsaturated Cp' carbonyl metal dimers with electrophiles such as hydrogen halides (or any proton donor) or halogens, though there are surprisingly few examples. Curtis and co-workers[13] performed a variety of electrophilic additions to the Mo-Mo triple bond of $Cp_2Mo_2(CO)_4$. Oxidative addition of HX (X = Cl, I) or I_2 across the Mo-Mo bond generated $Cp_2Mo_2(CO)_4(\mu\text{-}H)(\mu\text{-}X)$ (formal Mo-Mo single bond) and $Cp_2Mo_2(CO)_4(\mu\text{-}I)_2$ (no formal Mo-Mo bond) respectively.

Addition of H_2 to dimers containing metal-metal multiple bonds often leads to cleavage of those bonds with concomitant formation of the corresponding monomeric hydrides. There are relatively few examples of unsaturated metal dimers which undergo oxidative addition of H_2 across the metal-metal multiple bond to generate stable dimeric dihydrides.[14-18] A tungsten dimer reported by Green and Mountford,[16] $[(\eta^5\text{-}C_5H_4{}^iPr)WCl_2]_2$, containing a formal W-W triple bond with no bridging ligands, adds H_2 at room temperature, to generate the doubly hydride bridged $[(\eta^5\text{-}C_5H_4{}^iPr)WCl_2(\mu\text{-}H)]_2$. This was noted as the first, and to our knowledge the only, case in which thermal H_2 addition across M-M multiple bonds is reversible. The concerted *1,2*-oxidative addition of H_2 to a bimetallic compound is forbidden by orbital symmetry arguments,[19] just as it is for the reverse reductive elimination reaction (see

Chapter 3). Hence, these reactions are thought to proceed via initial addition of H_2 to a single metal center.

The Ir=Ir bond of $[Cp^*Ir(\mu\text{-}CO)]_2$ (**1**) is quite strong; an equimolar mixture of isotopically pure $[Cp^*(^{191}Ir)(\mu\text{-}CO)]_2$ and $[Cp^*(^{193}Ir)(\mu\text{-}CO)]_2$ slowly forms a statistical mixture of the isotopomers when heated to reflux in toluene ($t_{1/2} \approx 2$ weeks).[12] Hence, **1** provides a good platform for the preparation of dimeric derivatives. In this chapter, the protonation of **1** with a variety of strong acids is reported, as well as the reactions of the mono-protonated product, $[Cp^*Ir(CO)]_2(\mu\text{-}H)^+$ (**2**). The increased reactivity of the dimer upon protonation is discussed in terms of molecular orbital arguments.

Results

Mono-protonation of $[Cp^*Ir(\mu\text{-}CO)]_2$ (1): Generation of $[Cp^*Ir(CO)]_2(\mu\text{-}H)^+$ (2).

A variety of strong acids protonate $[Cp^*Ir(\mu\text{-}CO)]_2$ ($Cp^* = \eta^5\text{-}C_5Me_5$) (**1**), including HOTf, $HBF_4 \bullet Et_2O$, $HBAr'_4 \bullet (Et_2O)_2$ ($BAr'_4 = B(3,5\text{-}(CF_3)_2C_6H_3)_4^-$), and $H_2C(SO_2CF_3)_2$, but not HCl. Addition of 1.1 equiv of $HBAr'_4 \bullet (Et_2O)_2$ to a solution of **1** in methylene chloride immediately turns the yellow color to an opaque blue-green. ^1H NMR spectroscopy reveals new resonances in the Cp^* (δ 1.95) and hydride regions (δ -17.97) in the ratio 30:1. An IR spectrum of the isolated dark blue solid (Nujol mull) exhibits an absorbance at 1994 cm^{-1}, characteristic of a terminal CO stretch,[20] but no peaks attributable to a terminal or bridging hydride.[21] Significantly, reaction of the dihydride dimer, $[Cp^*Ir(CO)H]_2$, with the hydride abstraction reagent, $[Ph_3C]BAr'_4$ (1.1 equiv), in CD_2Cl_2 similarly results in the bright yellow solution turning deep blue-green. ^1H NMR again displays new resonances at δ 1.95 and -17.97, with concomitant formation of Ph_3CH. Based on these data, and on its subsequent reactivity (vide infra), we formulate the product of these two reactions as $\{[Cp^*Ir(CO)]_2(\mu\text{-}H)\}BAr'_4$ (**2-BAr'$_4$**) (Scheme 4.1).

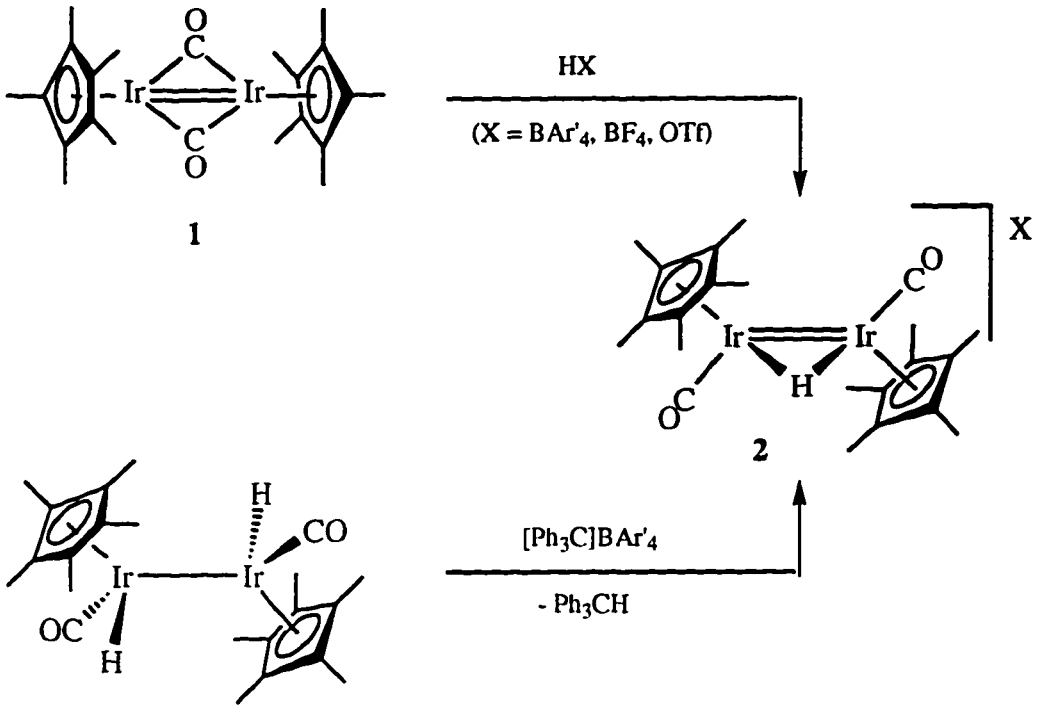

Scheme 4.1

Addition of $HBF_4 \cdot Et_2O$ (1.4 equiv) to a CD_2Cl_2 solution of the dimer **1** results in immediate precipitation of red-orange crystals. A ^1H NMR spectrum of the solution exhibits several resonances in the Cp^* region, none of which belong to the starting material. The two predominant resonances (accounting for 72% of the total Cp^* integrals) are at δ 2.11 and 1.99. The peak at 1.99 ppm (along with its corresponding hydride at -17.94 ppm) is attributed to $\{[Cp^*Ir(CO)]_2(\mu\text{-}H)\}BF_4$ (**2-BF$_4$**) by comparison to that of the BAr'_4^- analogue. The resonance at 2.11 ppm corresponds to a hydride resonance at -14.87 ppm that integrates as 15:1. These resonances are assigned to the dihydride dication, $\{[Cp^*Ir(CO)]_2(\mu\text{-}H)_2\}(BF_4)_2$ (**3-BF$_4$**) (vide infra).

When HOTf (2 equiv) is added to a solution of **1** in CD_2Cl_2, red solids are again produced and the liquid is green. Peak intensities in the ^1H NMR spectrum are weak as the majority of the organometallic product is insoluble. The principal soluble species is

again proposed to be the mono-protonated dimer, {[$Cp^*Ir(CO)]_2(\mu$-H)}OTf (**2-OTf**) (δ 1.98, -17.94). These resonances are somewhat broadened, probably due to intermolecular proton transfer. Several minor species are present, including the dimer fragmentation product, $Cp^*Ir(CO)_2H^+$ (δ 2.41, -13.8).[22]

Addition of the acid $H_2C(SO_2CF_3)_2$ (1.9 equiv) to a CD_2Cl_2 solution of **1** immediately turns the dark blue-green color characteristic of the mono-protonated dimer (**2**), but over the course of the next 10-20 minutes becomes yellow-brown with dark solids. The ^1H NMR spectrum reveals 11 resonances in the Cp^* region and 2 hydride resonances, none of which we attribute to **2**.

Combination of HCl and **1** in CD_2Cl_2 results in neither color change, nor reaction as determined by ^1H NMR spectroscopy.

Di-Protonation of [$Cp^*Ir(\mu$-CO)]$_2$ (1): Generation of [$Cp^*Ir(CO)]_2(\mu$-H)$_2^{2+}$ (3).

The production of red solids upon addition of slightly more than one equiv of HBF_4 or HOTf to solutions of **1** in methylene chloride prompted us to further investigate the nature of these solids. Our observations suggested that the greater the number of equivalents of acid added, the greater the quantity of red precipitate generated, and the less intense the blue color of the liquid. Experiments using an excess of acid were conducted.

Reverse addition of a CH_2Cl_2 solution of **1** to an excess of $HBF_4 \cdot Et_2O$ (9.5 equiv) in CH_2Cl_2 produces a pale orange solution containing a suspension of fine red solids. An IR spectrum of the isolated solid as a Nujol mull exhibits a single strong absorbance in the CO region at 2052 cm^{-1}, which we assign as a terminal ν_{CO} stretch. No peak corresponding to a terminal or bridging Ir-H vibration was observed. NMR spectroscopy of the solid was attempted in a variety of solvents but was generally uninformative due either to the material's insolubility or reactivity with the solvent. The material is

sparingly soluble in CD_2Cl_2; as mentioned above, an NMR tube experiment with addition of 1.4 equiv of $HBF_4 \cdot Et_2O$ to **1** exhibited resonances at 2.11 and -14.87 ppm in a 15:1 ratio.

The reaction of **1** with an excess of $HBAr'_4 \cdot (Et_2O)_2$ (4.3 equiv) in CD_2Cl_2 causes the solution to become deep blue-green upon thawing and subsequently red-brown after shaking for 1-2 minutes. The ^1H NMR spectrum indicates that the starting material is completely consumed and the main product possesses resonances at δ 2.10 and -15.23 in a 15:1 ratio. From this and the IR spectrum of the isolated BF_4^- analogue, we formulate the structure of the product of $[Cp^*Ir(\mu\text{-}CO)]_2$ and excess $HBAr'_4 \cdot (Et_2O)_2$ or $HBF_4 \cdot Et_2O$ as the di-protonated dication, $\{[Cp^*Ir(CO)]_2(\mu\text{-}H)_2\}X_2$ (X = BF_4, BAr'_4) (**3**) (equation 4.2). Addition of proton sponge (1 equiv) to **3-BAr'$_4$** in CD_2Cl_2 regenerates $\{[Cp^*Ir(CO)]_2(\mu\text{-}H)\}BAr'_4$ (**2-BAr'$_4$**), confirming the formulation of the dihydride dication.

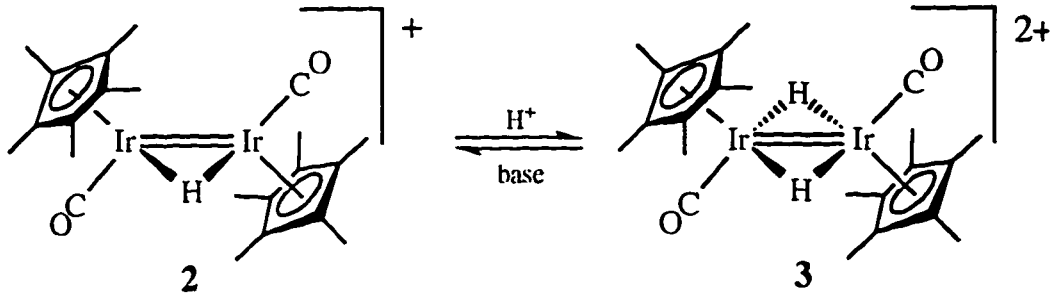

2 **3** (4.2)

We believe that the red solid formed upon addition of HOTf to **1**, as outlined above, is similarly the dication $\{[Cp^*Ir(CO)]_2(\mu\text{-}H)_2\}(OTf)_2$ (**3-OTf**), though it has not been characterized as yet. It appears that the BAr'_4 counterion imparts greater solubility to the dication in methylene chloride than do the BF_4 or OTf anions.

Reactions of $[Cp^*Ir(CO)]_2(\mu\text{-}H)^+$ (2).

Perhaps the strongest evidence for the formulation of the mono-protonated dimer as $[Cp^*Ir(CO)]_2(\mu\text{-}H)^+$ (**2**), is provided by its reactivity with CO, H_2, and Cl^- to generate known compounds (Scheme 4.2). Addition of CO to a solution of $[Cp^*Ir(\mu\text{-}CO)]_2$ (**1**) and $HBAr'_4\bullet(Et_2O)_2$ in CD_2Cl_2 rapidly changes the blue-green color to orange-brown. ^1H NMR spectroscopy reveals a new set of resonances at δ 2.12 and -13.34 in a 30:1 ratio, which is identified as $\{[Cp^*Ir(CO)]_2(\mu\text{-}CO)(\mu\text{-}H)\}BAr'_4$ (**4-BAr'$_4$**), by comparison to the chemical shifts of the $HC(SO_2CF_3)_2^-$ salt.[12] A structural determination of the OTf^- salt was made by single crystal X-ray diffraction (vide infra). The carbonyl and hydride bridged dimer **4** has been prepared previously[12] by the addition of the acid $H_2C(SO_2CF_3)_2$ to $[Cp^*Ir(CO)]_2(\mu\text{-}CO)$ in methylene chloride.

When H_2 is added to CD_2Cl_2 solutions of isolated **2-BAr'$_4$**, or in situ with **1** and $HBAr'_4\bullet(Et_2O)_2$, the dark blue-green color is replaced by a golden yellow. A new pair of resonances appear in the ^1H NMR spectrum at δ 2.19 and -16.50 in a 10:1 ratio. The product is identified as $\{[Cp^*Ir(CO)H]_2(\mu\text{-}H)\}BAr'_4$ (**5**) by comparison to previous spectra. The trihydride cation dimer, **5**, can be prepared independently by reaction of the oxidant $[Cp_2Fe]BAr'_4$ with $Cp^*Ir(CO)H_2$ (see Chapter 3).

Exposure of a solution of **2** in CD_2Cl_2 to ethylene (P = 1.5 atm) causes the blue-green color to immediately become orange. Unfortunately, the reaction is not clean. A ^1H NMR spectrum reveals that the mono-protonated dimer, **2**, has been entirely converted to unidentified products which exhibit three major resonances in the Cp^* region, as well as two upfield resonances in the hydride region.

The addition of [PPN]Cl (PPN = $(PPh_3)_2N^+$) to a CD_2Cl_2 solution of $[Cp^*Ir(CO)]_2(\mu\text{-}H)^+$ (**2**), prepared in situ from $[Cp^*Ir(\mu\text{-}CO)]_2$ (**1**) and $HBAr'_4\bullet(Et_2O)_2$, results in deprotonation of the hydride-bridged dimer and regeneration of **1** along with

formation of HCl (δ 1.55). Deprotonation of **2** by the very weak base Cl^- is consistent with the inability of HCl to protonate $[Cp^*Ir(\mu\text{-}CO)]_2$.

The mono-protonated dimer, **2**, does not react with methane (3.1 atm) in CD_2Cl_2 upon standing for 1 hour.

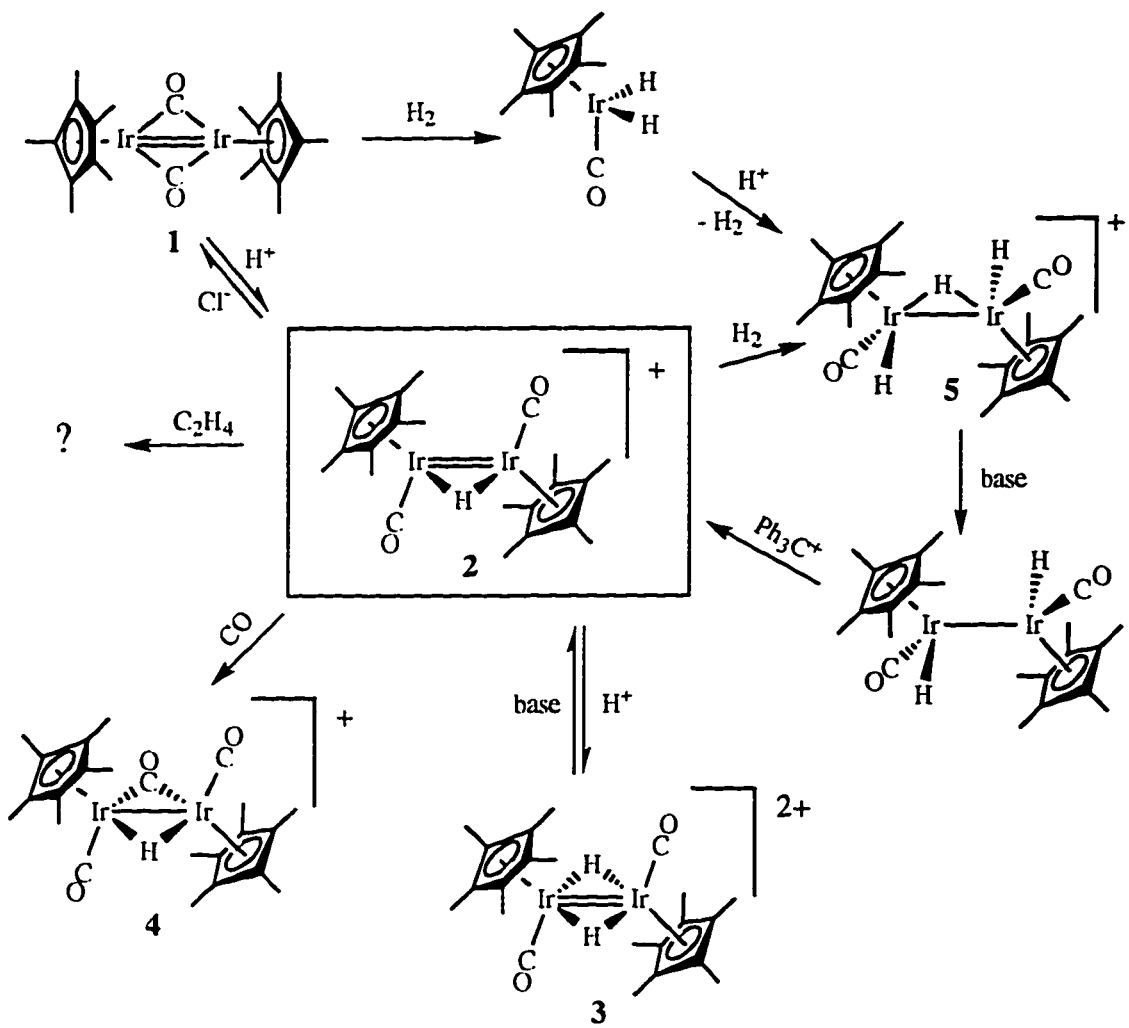

Scheme 4.2

Solid State Structure of {[Cp*Ir(CO)]$_2$(μ-CO)(μ-H)}OTf (4-OTf).

A summary of the crystallographic data is presented in Table 4.1. ORTEP diagrams are shown in Figures 4.1 and 4.5. Selected bond lengths and angles are given in Table 4.2. Tables of atomic coordinates, and isotropic and anisotropic displacement coefficients are presented in the appendix.

Hydrogenation and Halogenation of [Cp*Ir(μ-CO)]$_2$ (1).

Placing a solution of **1** in C_6D_6 under H_2 (2.8 atm) at room temperature slowly breaks apart the dimer to form exclusively Cp*Ir(CO)H_2. No trace of [Cp*Ir(CO)H]$_2$ was detected by ^{1}H NMR.

The dimer **1** reacts rapidly with I_2 in methylene chloride and toluene, and with Cl_2 in methylene chloride. However, several products are formed in each case with new chemical shifts in the Cp* region of the ^{1}H NMR spectrum, and their identities have yet to be determined.

Table 4.1 Summary of Crystal Data for {[Cp*Ir(CO)]$_2$(μ-CO)(μ-H)}OTf (**4**).

Empirical Formula	$C_{24}H_{31}F_3Ir_2O_6S$
Color; Habit	Orange red needle
Crystal Size (mm)	0.1 x 0.1 x 0.1
Crystal System	Monoclinic
Space Group	$P2_1/n$
Unit Cell Dimensions	a = 7.790 (1) Å
	b = 25.572 (3) Å
	c = 14.080 (2) Å
	β = 105.36 (2)°
Volume	2703.1 (14) Å^3
Z	4
Formula Weight	889.0
Density (calc.)	2.182 mg/m^3
Absorption Coefficient	9.970 mm^{-1}
F(000)	1676
Radiation	MoKα (λ = 0.71073 Å)
Temperature (K)	183
Monochromator	Highly oriented graphite crystal
2θ Range	1.0 to 50.0°
Scan Type	ω
Scan Speed	Variable; 1.5 to 5.5°/min. in ω
Scan Range (ω)	0.80 + 0.35(tan θ)°
Reflections Collected	6361
Independent Reflections	4752 (R_{int} = 2.94 %)
Observed Reflections	3515 (F > 4.0σ(F))
Number of Parameters Refined	326
Final R Indices (obs. data)	R = 3.58 %, wR = 4.60 %
R Indices (all data)	R = 5.97 %, wR = 5.14 %
Goodness of Fit	1.14

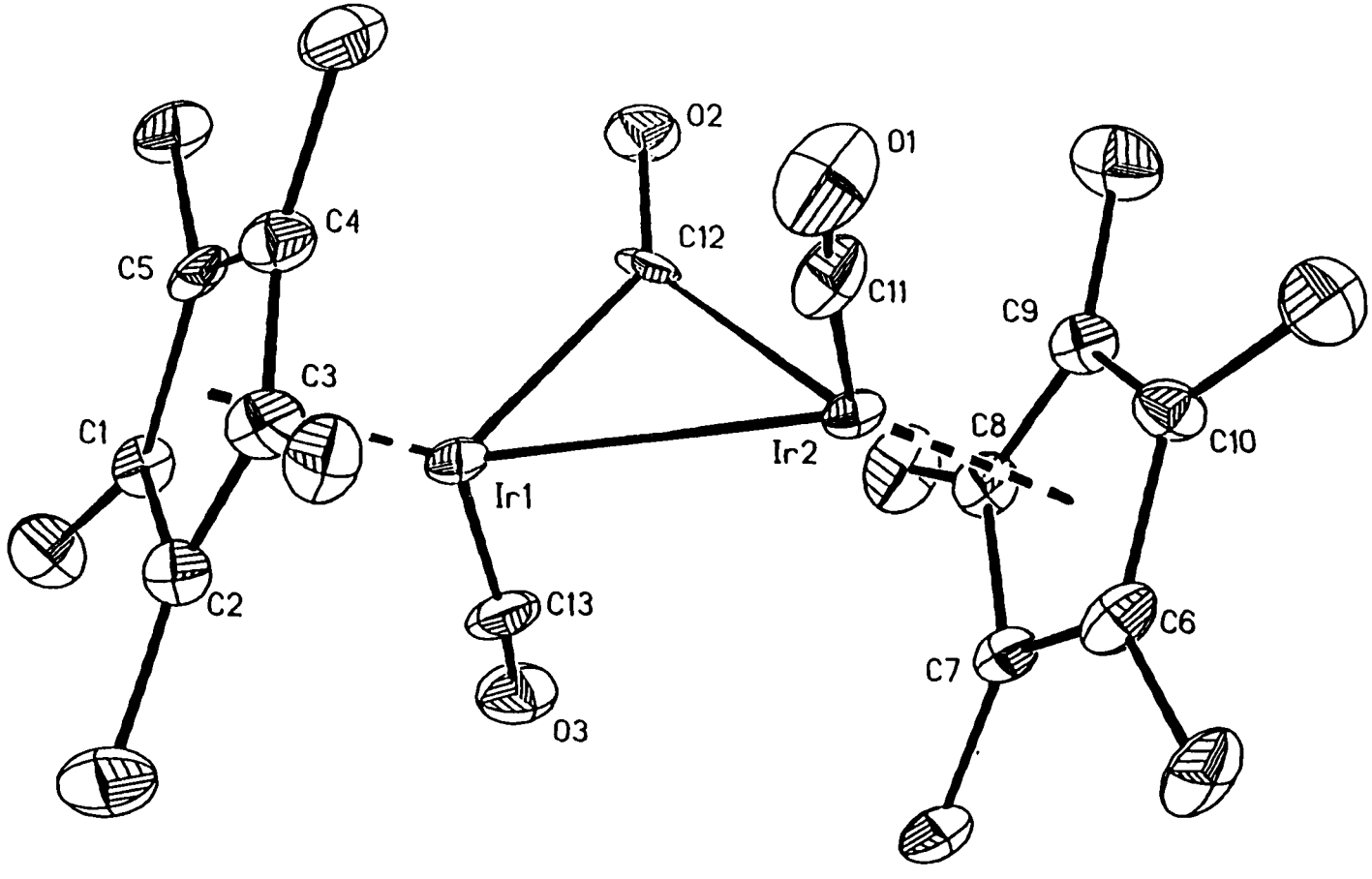

Figure 4.1. ORTEP representation of $\{[Cp^*Ir(CO)]_2(\mu\text{-}CO)(\mu\text{-}H)\}OTf$ (**4**). Thermal ellipsoids are shown at 50% probability. Hydrogen atoms are omitted for clarity. The hydride ligand was not located. The OTf anion is not pictured.

Table 4.2 Selected Bond Distances and Angles for **4**.

Bond Length (Å)			
Ir(1)-Ir(2)	2.831 (1)[b]		
Ir(1)-C(13)	1.857 (12)		
Ir(2)-C(11)	1.869 (13)		
Ir(1)-C(12)	2.034 (9)		
Ir(2)-C(12)	2.028 (9)		
Ir(1)-Cp(1)[a]	1.896		
Ir(2)-Cp(2)	1.895		
C(13)-O(3)	1.148 (15)		
C(11)-O(1)	1.150 (16)		
C(12)-O(2)	1.180 (10)		
Bond Angle (°)			
Ir(1)-Ir(2)-Cp(2)	136.5	Ir(1)-C(12)-O(2)	135.6 (7)
Ir(2)-Ir(1)-Cp(1)	137.1	Ir(2)-C(12)-O(2)	136.1 (8)
Ir(1)-Ir(2)-C(11)	93.5 (3)	Ir(1)-C(13)-O(3)	174.1 (9)
Ir(2)-Ir(1)-C(13)	93.4 (3)	Ir(2)-C(11)-O(1)	175.7 (10)
Ir(1)-Ir(2)-C(12)	45.9 (3)	Cp(1)-Ir(1)-C(13)	129.1
Ir(2)-Ir(1)-C(12)	45.7 (2)	Cp(2)-Ir(2)-C(11)	129.5
C(12)-Ir(1)-C(13)	96.8 (4)	Cp(1)-Ir(1)-C(12)	121.8
C(12)-Ir(2)-C(11)	94.2 (4)	Cp(2)-Ir(2)-C(12)	123.4
Ir(1)-C(12)-Ir(2)	88.4 (3)		
Dihedral Angle (°)			
Cp(1)-Ir(1)-Ir(2)-Cp(2)	172.9		
C(13)-Ir(1)-Ir(2)-C(11)	171.3		

[a]Cp(1) refers to the centroid of Cp attached to Ir(1). [b]Standard deviations in the least significant figures are enclosed in parentheses following the value.

Discussion

Mono-Protonation of $[Cp^*Ir(\mu\text{-}CO)]_2$ (1).

To our knowledge, addition of proton donors to unsaturated Cp carbonyl metal dimers of the form $[Cp'M(CO)]_2$ ($Cp' = Cp, Cp^*$; M = Co, Rh, Ir) has not been previously reported. However, the ability of **1** to react with small electrophiles was not wholly unexpected based on previous work in the Heinekey group. In 1989, it was reported[12] that reaction of Me^+, in the form of MeOTf, with **1** in CD_2Cl_2 at 250 K, added across the Ir=Ir double bond to generate $\{[Cp^*Ir(CO)]_2(\mu\text{-}CH_2)(\mu\text{-}H)\}OTf$ (eq 4.3).

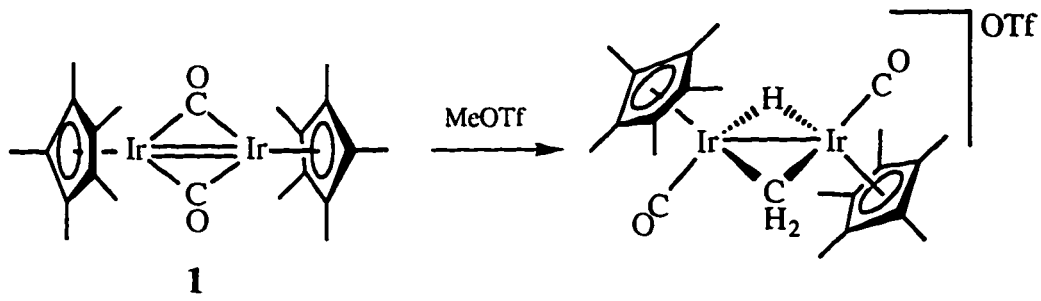

1 (4.3)

Despite possessing a formal Ir=Ir double bond, **1** is not a good base: strong acids are required to effect proton transfer. In fact, **1** is not protonated by HCl. This was confirmed by reaction of $\{[Cp^*Ir(CO)]_2(\mu\text{-}H)\}BAr'_4$ (**2-BAr'$_4$**) with [PPN]Cl, which leads to deprotonation of the dimer and formation of HCl. It was surprising to us that $HBAr'_4$ proved to be a competent acid whereas HCl was not. Hydrogen chloride is listed as the stronger acid in water (Table 4.3), and furthermore appears to be the stronger acid in Et_2O since $HBAr'_4$ is made from $NaBAr'_4$ and HCl in Et_2O.[23] These experiments are a reminder that acid strength is solvent dependent, and imply that in CH_2Cl_2, HCl is a weaker acid than $HBAr'_4 \cdot (Et_2O)_2$. This result is corroborated by Cowie and co-workers[24] who found that protonation of a cationic diphosphine-bridged iridium hydride

dimer, $[Ir_2(H)(CO)_2(\mu\text{-}H)_2(dppm)_2]BF_4$, to generate the tetrahydride dication, can be accomplished by protonated ether ($HBF_4 \bullet Et_2O$), but not by HCl.

Table 4.3 Acid Dissociation Constants (aqueous)

Acid	pKa	Ref.
$HOSO_2CF_3$	< -10	25
HCl	-7	26
$HBF_4 \bullet Et_2O$	-3.5[a]	26
$HBAr'_4 \bullet (Et_2O)_2$	-3.5[a]	26
$H_2C(SO_2CF_3)_2$	-1	27

[a] pKa of $HOEt_2^+$

The molecular orbital description of **1** (Figure 4.2) is consistent with its poor basicity. The electrons of the two HOMOs are not localized between the metal atoms, but instead are stabilized by delocalization over the bridging carbonyls. The two molecular orbitals that are metal-metal bonding ($1a_g$ and $4b_u$) are best described as 4-center-2-electron bonds. The construction of these frontier orbitals was first carried out by Hoffmann and co-workers[28] using extended Hückel calculations, and their shape, symmetry, and relative ordering were confirmed by Griewe and Hall[29] using Fenske-Hall methods. This description is also supported by photoelectron spectroscopy.[29]

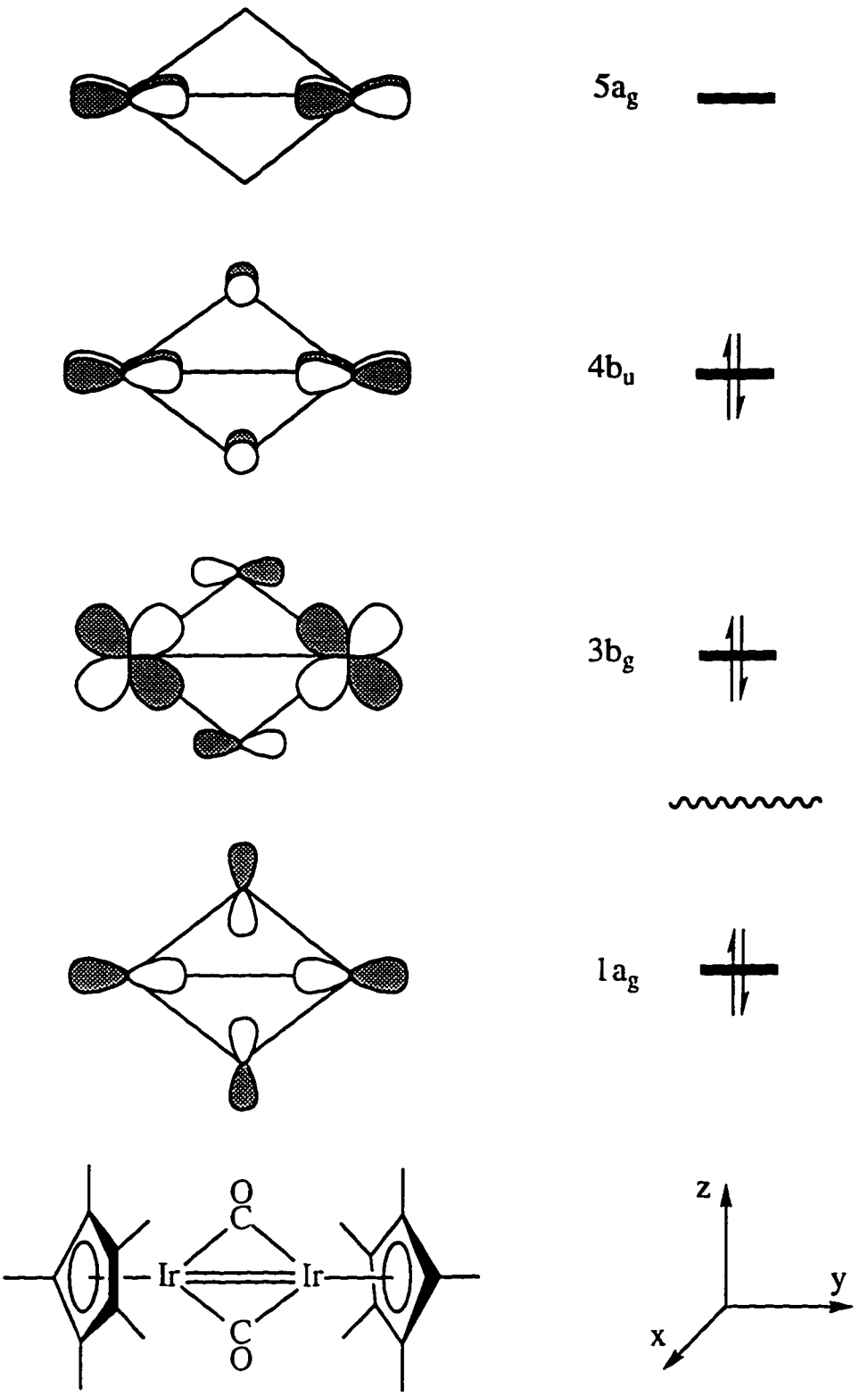

Figure 4.2. Metal-metal bonding and valence orbitals of $[Cp^*Ir(\mu\text{-}CO)]_2$ (**1**).[29] View is of the yz-plane. Only orbitals of the Ir and carbonyl C atoms are shown.

Transfer of a proton to $[Cp^*Ir(\mu\text{-}CO)]_2$ (**1**) greatly enhances the reactivity of the product. Infrared data suggest that the bridging carbonyls have swung open into terminal positions, reducing steric congestion at the Ir-Ir bond, and the hydride adopts a bridging position, forming a 3-center-2-electron bond. The single IR carbonyl stretch is consistent with that predicted by group theory for a trans geometry with idealized C_{2h} symmetry (ignoring the bridging hydride). The independence of the Cp* and hydride ^1H NMR chemical shifts of $\{[Cp^*Ir(CO)]_2(\mu\text{-}H)\}X$ (**2**) with various anions is evidence that the counterion is non-coordinating. The transformation of the carbonyls from bridging to terminal positions upon protonation is well documented in related systems. Bursten and co-workers,[30] in a series of papers on the electronic structure of piano stool dimers, note that dimers of the form $[CpML]_2(\mu\text{-}L)_2$ "seem only able to form μ-H products if the bridging ligands transform to terminal ones." Examples include the protonation of $[CpFe(CO)]_2(\mu\text{-}CO)_2$[31] and $[CpRu(PMe_3)]_2(\mu\text{-}CO)_2$[32] to generate $[CpFe(CO)_2]_2(\mu\text{-}H)^+$ and $[CpRu(CO)(PMe_3)]_2(\mu\text{-}H)^+$ respectively.

The relative stability of the bridged versus unbridged forms of the CpRh analogue, $Cp_2Rh_2(CO)_2$, have been calculated theoretically.[33] Though the bridged form, $[CpRh(\mu\text{-}CO)]_2$, is more stable then the unbridged by 21.7 kcal/mol, the unbridged form is better suited to bind a proton (also CH_2 or CO). Figure 4.3 depicts the interaction of the proton s-orbital with the frontier orbitals of the unbridged $[Cp^*Ir(CO)]_2$. Upon approach of the H^+ in the x-direction, mixing of the σ and π_{xy} orbitals on $[Cp^*Ir(CO)]_2$ generates a filled hybrid orbital pointing directly at an open bridging site in the xy-plane, ready to accept an electrophile. The large orbital stabilization favors formation of the μ-H product.

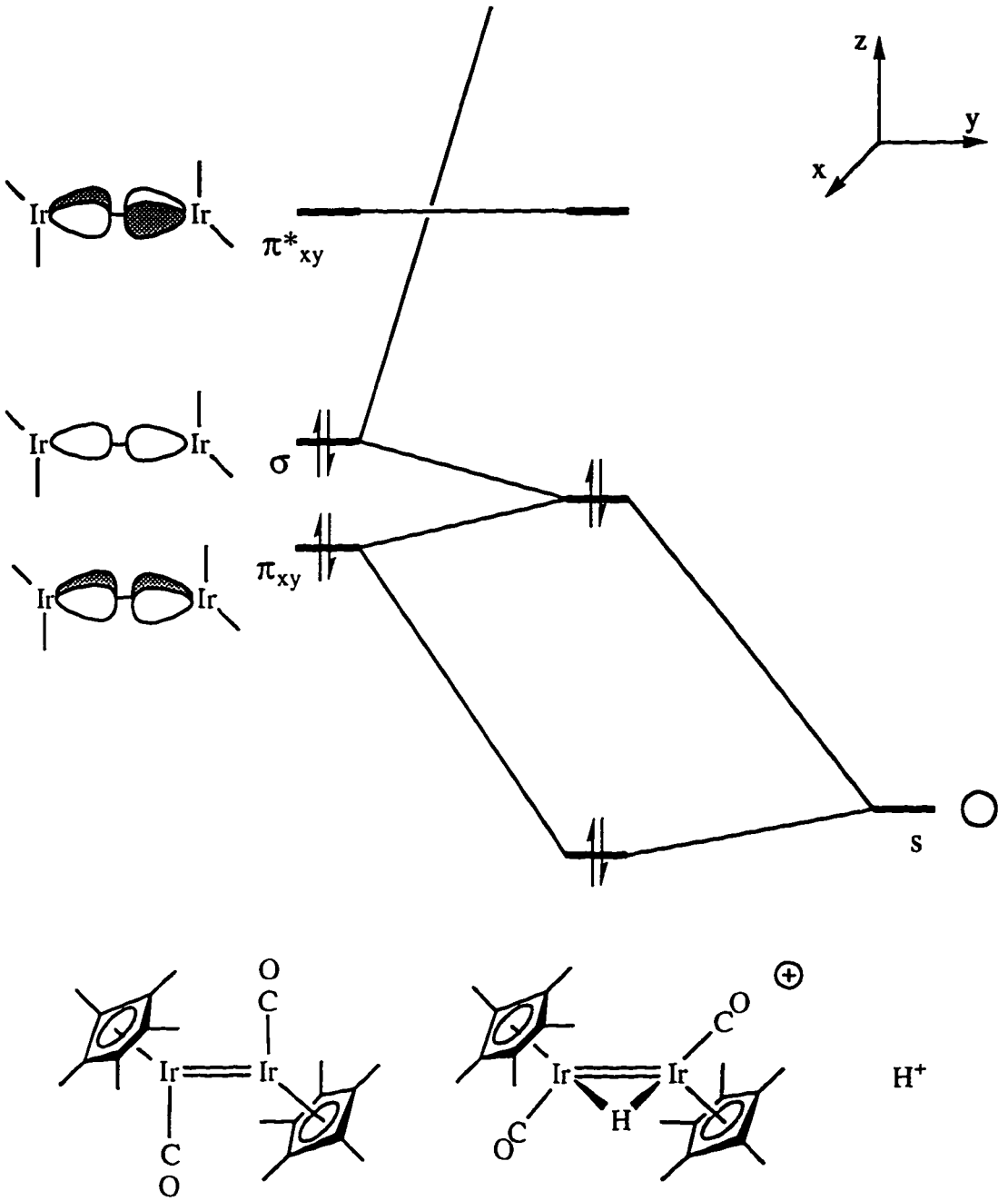

Figure 4.3. Molecular orbital diagram for interaction of valence orbitals of $[Cp^*Ir(CO)]_2$ with a proton approaching in the xy-plane. Valence orbitals of $[Cp^*Ir(CO)]_2$ are those derived for $[CpRh(CO)]_2$.[34]

From the interaction of the $[Cp^*Ir(CO)]_2$ and H^+ fragment orbitals we can construct the frontier orbitals of the product mono-protonated dimer **2** (Figure 4.4), and in so doing the dimer's enhanced reactivity now becomes apparent. The HOMO is a relatively high-lying orbital that is directed towards the empty bridging position, well suited for a σ interaction. The LUMO is a relatively low-lying orbital that is perfectly situated for a π interaction at the empty bridging position. Rapid reaction of CO, H_2, C_2H_4, and even a second H^+, are in accord with this orbital description. Reaction of **2** with a host of other reagents that can bridge metal-metal bonds, such as diazoalkanes, alkynes, and isonitriles, would seem promising.

The protonation of **1** with $HBAr'_4\bullet(Et_2O)_2$, as monitored by ^1H NMR, results in a much cleaner conversion to the mono-protonated dimer **2** than does HOTf, $HBF_4\bullet Et_2O$, or $H_2C(SO_2CF_3)_2$. Some of the side products generated upon protonation of **1** with HOTf, $HBF_4\bullet Et_2O$, or $H_2C(SO_2CF_3)_2$ are most likely due to interaction of the respective conjugate base with the empty bridging site, even though they are relatively poor ligands. The BAr'_4 anion was developed as a truly non-coordinating counterion and its utility is borne out in this chemistry.

Hydride Abstraction.

The formal abstraction of a hydride ligand from $[Cp^*Ir(CO)H]_2$ by $[Ph_3C]BAr'_4$ provides an alternative route to generation of $\{[Cp^*Ir(CO)]_2(\mu\text{-}H)\}BAr'_4$ (**2-BAr'$_4$**). This preparation may have greater synthetic utility than protonation of $[Cp^*Ir(\mu\text{-}CO)]_2$ (**1**) by $HBAr'_4\bullet(Et_2O)_2$ because it avoids the inclusion of any ether.

In an attempt to generate $\{[Cp^*Ir(CO)]_2(\mu\text{-}H)_2\}^{2+}$ (**3**) in the same manner, $[Ph_3C]BAr'_4$ was added to $[Cp^*Ir(CO)H]_2(\mu\text{-}H)^+$ (**5**), but did not result in any reaction. This is not entirely surprising, as **5** is a fairly good acid; in other words, the hydrides are not very "hydridic."

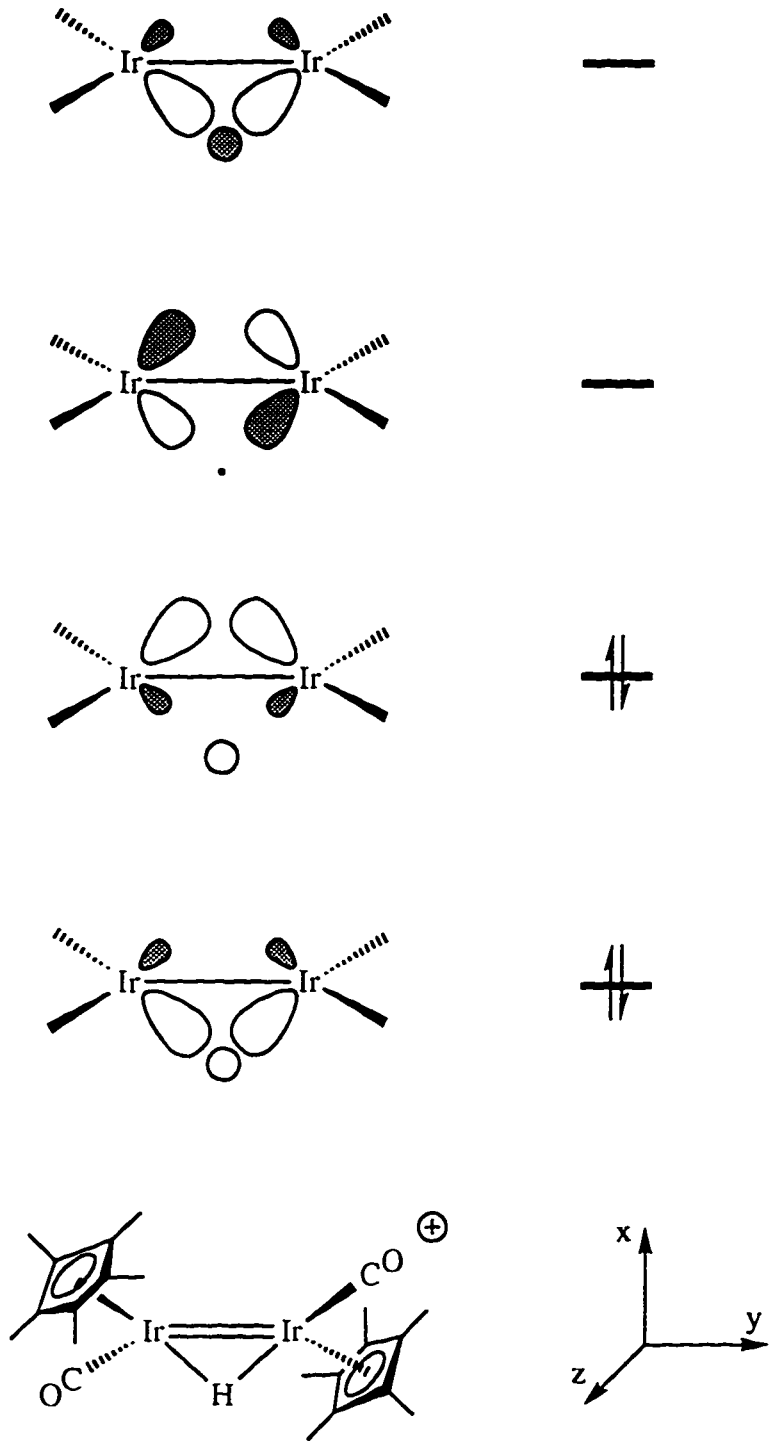

Figure 4.4. Frontier orbitals of $[Cp^*Ir(CO)]_2(\mu\text{-}H)^+$ (**2**). Orbitals are in the xy-plane.

Reactions of {[Cp*Ir(CO)]$_2$(μ-H)}BAr'$_4$ (2-BAr'$_4$).

As mentioned above, protonation of [Cp*Ir(μ-CO)]$_2$ (**1**) greatly increases its subsequent reactivity. An important example is the reaction with hydrogen. The dimer **1** does react with H_2 (P = 2.8 atm), but the reaction is sluggish, occurring over the course of several days. In addition, the Ir=Ir bond is broken, yielding the monomer, Cp*Ir(CO)H_2, as product. By comparison, **2** reacts completely with H_2 in several minutes. Moreover, the metal-metal bond remains intact as H_2 formally adds across the Ir=Ir bond to afford [Cp*Ir(CO)H]$_2$(μ-H)$^+$ (**5**). To our knowledge, this is the first example of H_2 addition across a metal-metal multiple bond in a cationic compound. Of course, the Ir-Ir bond order in **2** is somewhat ambiguous due to the bridging hydride. The M-(μ-H)-M interaction is best described as a delocalized 3-center 2-electron bond.[35] Since **2** can be prepared by addition of a proton (i.e. no electrons) to a compound containing an Ir=Ir double bond (confirmed by the Ir-Ir distance in an X-ray structure determination[7]), it seems reasonable to postulate that multiple bond character is retained. An X-ray structure determination of [Cp*Ir(CO)]$_2$(μ-H)$^+$ furnishing an Ir-Ir bond length would be informative.

Perhaps the closest example to our system is provided by Casey and co-workers,[17] who reported the rapid reaction of H_2 with [Cp*Re(CO)$_2$]$_2$ (formal Re=Re double bond) to form [Cp*Re(CO)$_2$]$_2$(μ-H)$_2$. In this case, the facile addition of H_2 may be attributable to the fact that the carbonyls of [Cp*Re(CO)$_2$]$_2$ are semi-bridging, i.e. that the Re=Re double bond is not entirely protected by bridging carbonyls.

The rapid, one-pot generation of the trihydride dimer **5** from **1**, HBAr'$_4$•(Et$_2$O)$_2$, and H_2 should prove to be a useful synthetic route to the hydride dimers. The starting material, **1**, is an air-stable, thermally robust compound, and this route would eliminate the need to synthesize Cp*Ir(CO)H_2, a compound that is somewhat difficult to prepare and manipulate (see Chapter 2). Further, the BAr'$_4^-$ salt crystallizes better and may be

more stable than the OTf^- salt, which decomposes over time in the solid state, even under argon.

Like hydrogen, CO also reacts more rapidly with the mono-protonated dimer, **2**, than with **1**, though the advantage is less substantial. Carbon monoxide instantaneously adds to **2** to form $[Cp^*Ir(CO)]_2(\mu\text{-}CO)(\mu\text{-}H)^+$ (**4**). Carbonylation of **1** to form $[Cp^*Ir(CO)]_2(\mu\text{-}CO)$ requires 30 minutes for complete reaction.[12,36]

The dicarbonyl bridged dimer, **1**, does not react with ethylene (P = 2.9 atm) at room temperature. The mono-protonated dimer, **2**, reacts immediately with ethylene, though the products have not been characterized. It was hoped that the reaction of **2** with ethylene would generate a μ-*1,2*-ethanyl complex analogous to Norton and co-workers' $(\mu\text{-}C_2H_4)Os_2(CO)_8$.[37]

We speculate that addition of an acid with a non-coordinating anion, such as BAr'_4^-, may prove to be a general route to enhanced reactivity in compounds with carbonyl ligands that bridge a metal-metal multiple bond.

Solid State Structure of $\{[Cp^*Ir(CO)]_2(\mu\text{-}CO)(\mu\text{-}H)\}OTf$ (4-OTf).

The unusual manner in which this crystal was generated warrants comment. The partial decomposition of $\{[Cp^*Ir(CO)H]_2(\mu\text{-}H)\}OTf$ (**5-OTf**) to **4** and two other unidentified products occurs slowly (over the course of several months) in the solid state under argon. A plausible mechanism would involve slow loss of H_2 to form $[Cp^*Ir(CO)]_2(\mu\text{-}H)^+$ (**2**), followed by rapid scavenging of CO from another molecule of **5**. However, subjecting solid **5** to dynamic vacuum overnight produces no observed decomposition by ^1H NMR. A solution of **5-OTf** in $CDCl_2F$ kept in the freezer (-30 °C) for almost 2 years showed essentially no decomposition. It is not clear at this time if the solid state decomposition is thermal or photochemical. Reversible H_2 addition across a

metal-metal multiple bond would be intriguing as we know of only one reported example.[16]

The dimeric nature of **4** was confirmed by an X-ray structure determination (Figure 4.1). The Cp^* ligands are disposed in a trans fashion (Cp^*_c-Ir-Ir-Cp^*_c dihedral angle = 173°, Cp^*_c = ring centroid), as are the terminal carbonyl ligands (C-Ir-Ir-C dihedral angle = 171°). The Ir-C-O angles are reduced slightly from 180° (174° and 176°) and are bent away from the vicinal Cp^* ligand. The Ir atoms, the Cp^* centroids, and the terminal carbonyl carbon atoms are all essentially co-planar (Figure 4.5). The bridging carbonyl makes an angle of approximately 90° with this plane, and is symmetrically positioned between the Ir atoms. Though the hydride was not explicitly located, it seems apparent from the symmetry of the structure that the hydride occupies the empty bridging site opposite the carbonyl. The Ir-Ir bond length (2.831 Å) is consistent with an Ir-Ir single bond, and is longer than that of the unsupported Ir-Ir bond in $[Cp^*Ir(CO)H]_2$ (2.730 Å), but shorter than the hydride bridged Ir-Ir bond in $\{[Cp^*Ir(CO)H]_2(\mu\text{-}H)\}BAr'_4$ (2.935 Å). This suggests that the bridging carbonyl holds the Ir atoms closer together than would be expected for a simple hydride bridged dimer. The SO_3CF_3 anion is non-coordinating: the closest contact is 2.921 Å, between one of its oxygen atoms and a Cp^* methyl hydrogen.

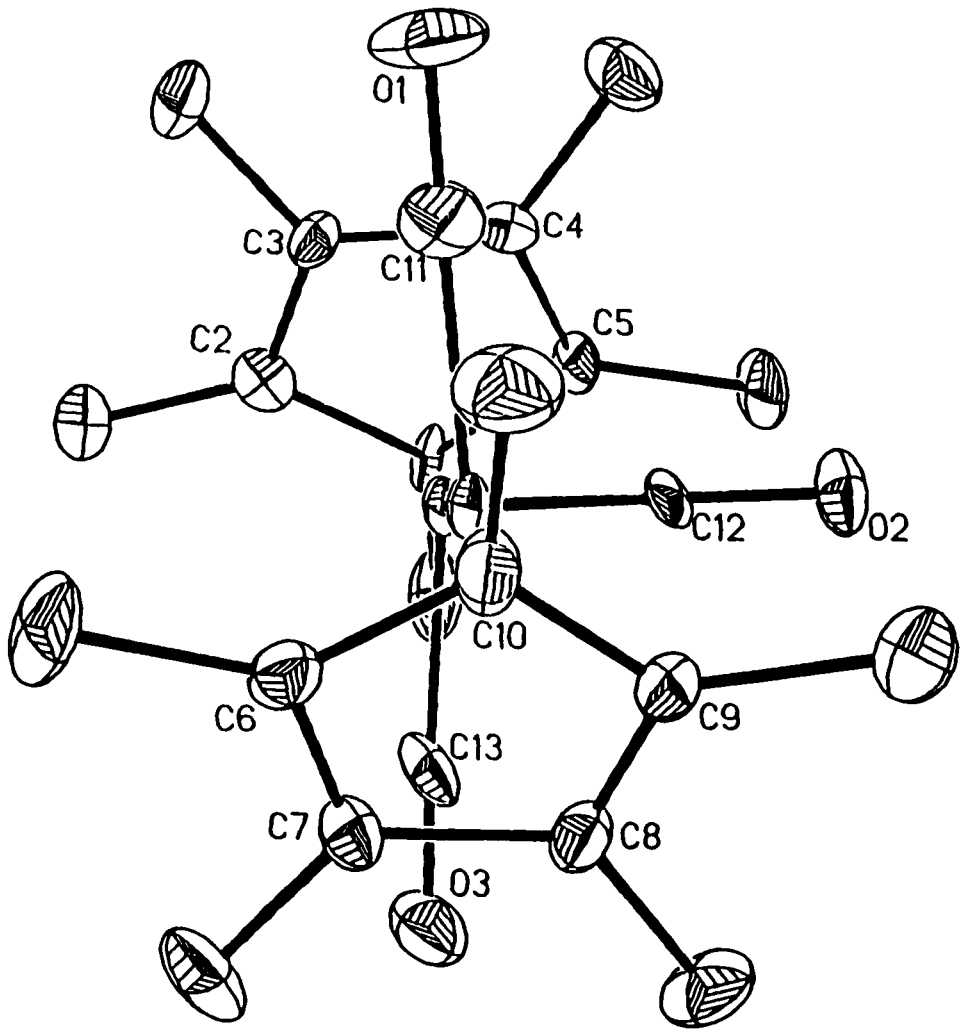

Figure 4.5. ORTEP representation of $\{[Cp^*Ir(CO)]_2(\mu\text{-}CO)(\mu\text{-}H)\}OTf$ (**4**). Projection along the Ir-Ir axis.

Di-Protonation of $[Cp^*Ir(\mu\text{-}CO)]_2$ (1).

The formation of the dihydride dication, $[Cp^*Ir(CO)]_2(\mu\text{-}H)_2^{2+}$ (**3**), from reaction of **1** with greater than 1 equiv of various strong acids, was somewhat surprising since there are few reports of iridium hydride dications in the literature. A closely related example that is air-stable and contains no hydride ligands is $[Cp^*Ir(CO)_2]_2(BF_4)_2$.[38] Most cationic iridium hydride complexes are themselves acidic and hence are not amenable to protonation.

However, the reaction of $[Cp^*Ir(CO)]_2(\mu\text{-}H)^+$ (**2**) with a second proton is not surprising in light of the molecular orbital description (Figure 4.4). The HOMO of **2** points directly at the empty bridging position and is perfectly situated to interact with the incoming proton. The proposed structure of the dihydride dication, **3**, with trans Cp^* ligands, terminal carbonyls and bridging hydrides, would be isostructural to the isoelectronic osmium neutral, $[Cp^*Os(CO)]_2(\mu\text{-}H)_2$.[39] There are many other transition metal dimers with M=M double bonds bridged by two hydride ligands,[40-43] formally "diprotonated double bonds," but none to our knowledge were actually generated by successive protonations of the metal-metal bond.

The ν_{CO} (2052 cm^{-1}) in the IR spectrum of **3-BF_4** is at the high end of the range for terminal CO stretching vibrations (1850-2125 cm^{-1}), and indicates poor back donation to the carbonyls, which is consistent with the dication formulation. In comparison, the terminal CO stretching frequency of the mono-cation (**2**) is 1994 cm^{-1}, and those of the neutral dihydride dimer (Chapter 2), $[Cp^*Ir(CO)H]_2$, are 1971 and 1942 cm^{-1}. The related dication, $[Cp^*Ir(CO)_2]_2(BF_4)_2$, reported by Sutton and co-workers,[38] also exhibits high ν_{CO} at 2073 and 2058 cm^{-1}. The single carbonyl band is again consistent with that predicted by group theory for a trans geometry of C_{2h} symmetry.

The ^1H NMR chemical shift of the hydrides of $\{[Cp^*Ir(CO)]_2(\mu\text{-}H)_2\}X_2$ are somewhat dependent on the nature of X (X = BAr'_4, δ -15.23; = BF_4, δ -14.87) and may indicate some interaction between the counterion and the hydride ligands.

Conclusion

The carbonyl bridged dimer, $[Cp^*Ir(\mu\text{-}CO)]_2$ (**1**) can be protonated by a variety of strong acids. Reaction of **1** with one equiv of acid opens the carbonyl bridges to generate $[Cp^*Ir(CO)]_2(\mu\text{-}H)^+$ (**2**) and substantially increases the reactivity of the dimer. Molecular orbital diagrams depicting the frontier orbitals of **1** and **2** help to explain the difference in reactivity. The mono-protonated dimer, **2**, reacts instantaneously at room temperature with a variety of reagents, including H_2 and CO. Addition of H_2 to **2** to form the trihydride dimer, $[Cp^*Ir(CO)H]_2(\mu\text{-}H)^+$ (**5**), is a rare example of oxidative addition of H_2 across a metal-metal bond resulting in a stable dimeric product. The hydride cation dimer, **2**, can react with a second equivalent of acid to yield the dihydride dication, $[Cp^*Ir(CO)]_2(\mu\text{-}H)_2^{2+}$ (**3**).

Experimental

General procedures for manipulation and characterization of compounds are presented in Chapter 2. The acid $H_2C(SO_2CF_3)_2$ was the generous gift of Dr. Allen Siedle of 3M. $[Cp^*Ir(\mu\text{-}CO)]_2$ was prepared according to the published procedure.[7] Hydrogen (> 99.999%) and ethylene (> 99.7%) were purchased from Airco. $[Ph_3C]BAr'_4$[44] and $HBAr'_4\bullet(Et_2O)_2$[45] were prepared by the reported methods.

$\{[Cp^*Ir(CO)]_2(\mu\text{-}H)\}BAr'_4$ (2) from $[Cp^*Ir(\mu\text{-}CO)]_2$ (1) and $HBAr'_4\bullet(Et_2O)_2$. A Schlenk flask was charged with 20.2 mg of **1** (28.4 μmol). Methylene chloride (12 mL, distilled) was added via cannula to give a clear, yellow-brown solution, and the flask was

immersed in an ice bath. A solution of $HBAr'_4 \cdot (Et_2O)_2$ (29.4 mg, 29.0 μmol, 1.0 equiv) in CH_2Cl_2 (3 mL) was added via cannula immediately creating a deep blue color. The solution was stirred for 30 minutes and the solvent removed in vacuo, leaving a dark blue-green, air-sensitive solid. The protonated dimer, **2**, is insoluble in C_6D_6, decomposes slowly (days) in CD_2Cl_2, and reacts instantly with CD_3NO_2 and acetone-d_6. ^1H NMR (CD_2Cl_2): δ 1.96 (Cp^*, 30 H), -17.96 (Ir-H, 1 H). IR (Nujol): 1994 cm^{-1} (ν_{CO}).

Reaction of $[Cp^*Ir(\mu\text{-}CO)]_2$ (1) with $HBF_4 \cdot Et_2O$. An NMR tube fitted with a high vacuum Teflon stopcock was charged with 2.9 mg of **1** (4.1 μmol). Methylene chloride-d_2 (0.4 mL) was added to the solids via vacuum transfer yielding a yellow solution containing some brown insoluble material. With the solution immersed in a CO_2/IPA bath, ca. 1.0 μL of $HBF_4 \cdot Et_2O$ (85%, 5.8 μmol, 1.4 equiv) was added via syringe against an argon purge. Three freeze/pump/thaw cycles were performed and the tube was sealed under vacuum. Upon thawing, red-orange crystals precipitated from the brown-yellow liquid. A ^1H NMR spectrum revealed that the starting material had been entirely consumed and six new peaks appeared in the Cp^* region as well as two peaks in the hydride region. Two resonances of approximately equal intensity at δ 2.11 and 1.99 account for 72% of the total Cp^* region intensity. The resonances at δ 1.99 (30 H) and -17.94 (1 H) are attributed to the mono-protonated dimer, **2**, by comparison to those of the BAr'_4^- analogue (δ 1.95, -17.97). The resonances at 2.11 ppm (15 H) and -14.87 ppm (1 H) are tentatively assigned to the dication, **3**, by comparison to the BAr'_4^- analogue (δ 2.10, -15.23). The red solid is believed to be the bulk insoluble fraction of **3**.

Reaction of $[Cp^*Ir(\mu\text{-}CO)]_2$ (1) with HOTf. The same procedure was used as that described above for $HBF_4 \cdot Et_2O$. In this case, 4.3 mg of **1** (6.1 μmol) and 1.0 μL of HOTf (2.0 equiv) were employed. The reaction furnished a green liquid over red solids.

A ^1H NMR (CD_2Cl_2) spectrum displayed weak signal intensities, indicating that the majority of organometallic product is insoluble. The major soluble product is the mono-protonated dimer, **2-OTf** (δ 1.98, -17.94). These peaks are somewhat broadened, presumably due to intermolecular proton transfer. $[Cp^*Ir(CO)_2H]OTf$ (δ 2.41, -13.8) is present as a minor product, as well as several unidentified species.

Reaction of $[Cp^*Ir(\mu\text{-}CO)]_2$ (1) with $H_2C(SO_2CF_3)_2$. To a screw-cap NMR tube charged with **1** (5.8 mg, 8.2 μmol) was added 4.4 mg of $H_2C(SO_2CF_3)_2$ (15.7 μmol, 1.9 equiv). Methylene chloride-d_2 (0.4 mL) was added to the solids via vacuum transfer. Upon thawing, the solution immediately was deep blue-green. Over the course of 10-20 minutes, the solution became yellow-brown with dark solids. ^1H NMR spectroscopy revealed 11 new resonances in the Cp^* region and 2 hydride resonances, none of which were attributable to the mono-protonated dimer, **2**.

Reaction of $[Cp^*Ir(\mu\text{-}CO)]_2$ (1) with HCl. The same procedure was used as that described above for $HBF_4 \cdot Et_2O$. In this case, 3.3 mg of **1** (4.6 μmol) and 9 μL of anhydrous HCl (1.0 M in Et_2O, 2 equiv) were employed. No color change was observed and a ^1H NMR spectrum indicated that no reaction had occurred upon standing for 3 days.

Reaction of $\{[Cp^*Ir(CO)]_2(\mu\text{-}H)\}BAr'_4$ (2) with [PPN]Cl. The protonated dimer, **2**, was generated in situ, as follows. To an NMR tube fitted with a high vacuum Teflon stopcock was added 3.1 mg of **1** (4.4 μmol) and 4.9 mg of $HBAr'_4 \cdot (Et_2O)_2$ (4.8 μmol, 1.1 equiv) in the glove box. Methylene chloride was vacuum transferred onto the solids and the solution immediately became a deep blue-green color upon warming to room temperature. After standing at room temperature for 5-10 minutes, the tube was

immersed in an ice bath and the solvent was removed in vacuo. In the glove box, 2.9 mg of [PPN]Cl (5.0 μmol, 1.2 equiv) was added to the dark blue-green residue. CD_2Cl_2 was added to the solids via vacuum transfer yielding an orange solution with some dark solids. The tube was sealed under vacuum and a ^1H NMR spectrum acquired. The primary Cp*-bearing product is **1** (δ 1.76). A peak at 1.55 ppm is assigned to HCl. There are four other small unidentified resonances in the Cp* region.

{[Cp*Ir(CO)]$_2$(μ-H)}BAr'$_4$ (2) from [Cp*Ir(CO)H]$_2$ and [Ph$_3$C]BAr'$_4$. To an NMR tube fitted with a high vacuum Teflon stopcock was added 4.5 mg of [Cp*Ir(CO)H]$_2$ (6.3 μmol) and 7.7 mg of [Ph$_3$C]BAr'$_4$ (7.0 μmol, 1.1 equiv) in the glove box. Methylene chloride-d_2 (0.4 mL) was vacuum transferred onto the solids. The NMR tube was sealed under vacuum. The solution immediately became a deep blue-green color upon warming to room temperature. The major products were identified by ^1H NMR as **2** (δ 1.95 (Cp*), -17.97 (Ir-H)), and Ph$_3$CH (δ 5.55 (Ph$_3$C*H*)). A small quantity of [Cp*Ir(CO)H]$_2$(μ-H)$^+$ (**5**) was also formed. Several small resonances (δ 1.97, 1.94, -18.05) were unidentified.

Reaction of {[Cp*Ir(CO)H]$_2$(μ-H)}BAr'$_4$ (2) with CO. The protonated dimer, **2**, was generated in situ, as follows. To a screw-cap NMR tube charged with **1** (6.3 mg, 8.9 μmol) was added 9.7 mg of HBAr'$_4$•(Et$_2$O)$_2$ (9.6 μmol, 1.1 equiv) in the glove box. Methylene chloride-d_2 (0.5 mL) was added to the solids via vacuum transfer yielding a dark blue-green solution. The NMR tube was immersed in a liquid N_2 bath and the frozen solution degassed. The entire NMR tube was immersed in a CO_2/IPA bath and pressurized to 1000 torr (1.3 atm) with CO. Upon warming to room temperature (P_{298K} = 2.0 atm) the solution immediately became orange-brown. The major product was identified as {[Cp*Ir(CO)]$_2$(μ-CO)(μ-H)}BAr'$_4$ (**4**) based upon comparison to the ^1H

NMR of **4**-$CH(SO_2CF_3)_2$ ((CD_2Cl_2) δ: 2.13, -13.26). ^1H NMR (CD_2Cl_2) δ: 2.12 (s, Cp^*, 30 H), -13.34 (s, Ir-H, 1 H).

X-ray Structure Determination of {[$Cp^*Ir(CO)]_2(\mu$-CO)(μ-H)}OTf (4).

A crystal of **4** was generated unintentionally in an attempt to grow X-ray diffraction quality crystals of {[$Cp^*Ir(CO)H]_2(\mu$-H)}OTf (**5**). A 5 mm glass tube sealed at one end and equipped with a high vacuum Teflon stopcock was charged with 15.3 mg of **5**. This sample of **5** had been standing in the glove box for five months and had decomposed slightly, as indicated by its color change from pale to dark brown and by a ^1H NMR (CD_2Cl_2) spectrum which exhibited three new resonances of weak intensity in the Cp^* region, one of which we attribute to **4**. A small quantity of acetone was added to the trihydride, **5**, via vacuum transfer yielding a clear brown solution. A greater quantity of pentane was layered onto the solution via vacuum transfer and the tube was sealed under vacuum. Crystals of **4** were formed amidst brown amorphous solids after standing for a week in the dark.

A clear orange-red crystal of dimensions 0.1 x 0.1 x 0.1 mm was mounted in a stream of nitrogen gas at 183 K on an Enraf-Nonius CAD-4 diffractometer using Mo Kα radiation with a graphite monochromator (λ = 0.71073 Å). Systematic absences were consistent with the monoclinic space group $P2_1/n$. A total of 4752 independent reflections were collected with $2\theta \leq 50°$, of which 3515 with $I > 4\sigma(I)$ were used in the refinement. The structure was solved by direct methods which gave the location of the Ir atoms. The remaining non-hydrogen atoms were located from difference Fourier maps. The hydrogen atoms were placed at calculated positions. The hydride bound to iridium was not located. The final R factor was 3.58%.

Reaction of {[Cp*Ir(CO)H]$_2$(μ-H)}BAr'$_4$ (2) with H_2. The protonated dimer, **2**, was generated in situ, as follows. A screw-cap NMR tube was loaded with 3.6 mg of **1** (5.1 μmol) and 5.4 mg of HBAr'$_4$•(Et$_2$O)$_2$ (5.3 μmol, 1.1 equiv) in the glove box. Methylene chloride-d_2 (0.4 mL) was added to the solid via vacuum transfer and the solution was kept frozen. With the NMR tube completely immersed in a liquid N_2 bath, the head space was evacuated and subsequently pressurized to 561 torr (0.74 atm) with H_2. The NMR tube was warmed to room temperature (P_{298K} = 2.9 atm), and the solution immediately became dark blue-green. After 5-10 minutes of gentle shaking the solution became golden yellow. The predominant product was the trihydride cation dimer, **5**, as determined by comparison to previous ^{1}H NMR spectra (see Chapter 3). A minor impurity at δ 1.79 was unidentified.

Reaction of {[Cp*Ir(CO)H]$_2$(μ-H)}BAr'$_4$ (2) with Ethylene. The protonated dimer, **2**, was generated in situ, as follows. An NMR tube attached to a high vacuum Teflon stopcock was loaded with 5.3 mg of **1** (7.5 μmol) and 7.4 mg of HBAr'$_4$•(Et$_2$O)$_2$ (7.3 μmol, 1.0 equiv) in the glove box. Methylene chloride-d_2 (0.4 mL) was added to the solid via vacuum transfer and then thawed in a CO_2/IPA bath and shaken, yielding a deep blue-green solution. With the bottom of the NMR tube immersed in the CO_2/IPA bath, the head space was evacuated and then pressurized to 1145 torr (1.5 atm) with C_2H_4. The contents of the NMR tube were frozen in a liquid N_2 bath and the tube was flame-sealed under vacuum. Upon thawing, the solution immediately became yellow-brown, with some dark solid present. A ^{1}H NMR spectrum revealed the following unidentified resonances: δ 2.88 (d, J = 6.8 Hz), 2.10, 2.05, 2.02 (w), 1.93 (w), 1.90 (w), 1.84, -14.57 (w), -15.81 (w). Upon standing for three days, the resonance at 2.10 ppm became predominant (80% of Cp* region intensity) and the peak at -14.57 ppm disappeared. The resonances at δ 2.10 and -15.81 integrate in a 30:1 ratio.

$[Cp^*Ir(CO)H]_2(BF_4)_2$ (3). A Schlenk flask was charged with 21.6 mg of **1** (30.4 μmol). Methylene chloride (10 mL, distilled) was added via cannula to give a yellow-brown solution containing some undissolved solid. In a separate Schlenk flask a solution of 50 μL of $HBF_4 \cdot Et_2O$ (85%, 9.5 equiv) in 5-10 mL of CH_2Cl_2 was prepared. The acid solution was subjected to 3 freeze/pump/thaw cycles and the flask then immersed in an ice bath. The iridium solution was transferred via cannula to an addition funnel and added dropwise to the cold stirring acid solution. The addition produced a suspension of fine red solids in the pale orange liquid. The solution was allowed to stand overnight at -30 °C to encourage solid formation. The supernatant was removed via cannula and the red solid washed with 2 x 5 mL of cold CH_2Cl_2 (washings were pale blue indicating some deprotonation of the product, presumably by adventitious water). Despite drying the air-sensitive product in vacuo for several hours, it was found to be sticky and difficult to manipulate, precluding a yield measurement. The product is insoluble in C_6D_6, and 1,2-difluorobenzene, slightly soluble in CD_2Cl_2, and reacts with CD_3NO_2 and $(CD_3)_2CO$. ^1H NMR (CD_2Cl_2): δ 2.11 (Cp^*, 30 H), -14.87 (Ir-H, 2 H). IR (Nujol): 2052 cm^{-1} (ν_{CO})

Reaction of $[Cp^*Ir(\mu\text{-}CO)]_2$ (1) with excess $HBAr'_4 \cdot (Et_2O)_2$. To a screw-cap NMR tube charged with **1** (3.5 mg, 4.9 μmol) was added 21.7 mg of $HBAr'_4 \cdot (Et_2O)_2$ (21.4 μmol, 4.3 equiv) in the glove box. Methylene chloride-d_2 (0.4 mL) was added to the solids via vacuum transfer. Upon thawing, a deep blue-green solution was immediately formed. After shaking for 1-2 minutes, the color became red-brown. The principal product was the dication, **3**. ^1H NMR: δ 2.01 (Cp^*, 30 H), -15.23 (Ir-H, 2 H). A small peak at δ 1.95 is attributed to **2** (the hydride could not be detected). Two other minor

resonances in the Cp^* region at δ 1.90 and 1.78 are unidentified. The dihydride dication, **3**, completely decomposed upon standing in CD_2Cl_2 at room temperature overnight.

Reaction of $\{[Cp^*Ir(CO)]_2(\mu\text{-}H)_2\}(BAr'_4)_2$ (3) with Proton Sponge. The di-protonated dimer, **3**, was generated in situ, as follows A screw-cap NMR tube was loaded with 4.5 mg of **1** (6.3 μmol) and 25.8 mg of $HBAr'_4{\bullet}(Et_2O)_2$ (25.5 μmol, 4.0 equiv) in the glove box. Methylene chloride (0.6 mL) was added to the solid via vacuum transfer. Upon thawing, the solution immediately became dark blue-green and then deep red-brown after several minutes of shaking. The NMR tube was allowed to stand in an ice bath for one hour yielding a clear deep red solution. The volatiles were removed in vacuo leaving an oily, red-orange residue. In the glove box, Proton Sponge (19.1 μmol) was added to the residue. Methylene chloride-d_2 was added via vacuum transfer yielding a deep green solution. The predominant organometallic product, as determined by ^1H NMR, was the mono-protonated dimer, **2** (δ 1.95, -17.96), along with formation of the protonated Proton Sponge.

Reaction of $[Cp^*Ir(\mu\text{-}CO)]_2$ (1) with H_2. The dimer, **1** (7.8 mg), was dissolved in 1 mL of C_6D_6. The deep yellow solution was transferred via syringe through a 0.2 μm nylon filter into an NMR tube attached to a high vacuum Teflon stopcock. The solution was subjected to three freeze-pump-thaw cycles and a trace amount of TMS was added via vacuum transfer. The NMR tube was completely immersed in a liquid N_2 bath and pressurized to 551 torr (0.72 atm) with H_2 (P_{298K} = 2.8 atm). The NMR tube was sealed at this pressure and analyzed by ^1H NMR. A spectrum acquired within several hours of the reaction exhibited resonances due only to starting material and H_2. After standing at room temp. for 8 days, a new spectrum showed that **1** had been converted (ca. 90%) to $Cp^*Ir(CO)H_2$.

Notes to Chapter 4

(1) For a recent review see: Winter, M. J. *Adv. Organomet. Chem.* **1989**, *29*, 101-162.

(2) Lee, W. S.; Brintzinger, H. H. *J. Organomet. Chem.* **1977**, *127*, 87-92.

(3) Anderson, F. R.; Wrighton, M. S. *Inorg. Chem.* **1986**, *25*, 112-114.

(4) Bloyce, P. E.; Rest, A. J.; Whitwell, I.; Graham, W. A. G.; Holmes-Smith, R. *J. Chem. Soc., Chem. Commun.* **1988**, 846-848.

(5) Rest, A. J.; Whitwell, I.; Graham, W. A. G.; Hoyano, J. K.; McMaster, A. D. *J. Chem. Soc., Dalton Trans.* **1987**, 1181-1190.

(6) Graham, W. A. G.; Hoyano, J. K.; McMaster, A. D. Presented at the 23rd International Conference on Coordination Chemistry, Boulder, CO, 1984; TH51-02.

(7) Ball, R. G.; Graham, W. A. G.; Heinekey, D. M.; Hoyano, J. K.; McMaster, A. D.; Mattson, B. M.; Michel, S. T. *Inorg. Chem.* **1990**, *29*, 2023-2025.

(8) Hoffmann, R. *Angew. Chem. Int. Ed. Engl.* **1982**, *21*, 711-724.

(9) Herrmann, W. A.; Krüger, C.; Goddard, R.; Bernal, I. *Angew. Chem. Int. Ed. Engl.* **1977**, *16*, 334.

(10) Clauss, A. D.; Dimas, P. A.; Shapley, J. R. *J. Organomet. Chem.* **1980**, *201*, C31-C34.

(11) Green, M.; Mills, R. M.; Pain, G. N.; Stone, F. G. A.; Woodward, P. *J. Chem. Soc., Dalton Trans.* **1982**, *7*, 1309-1319.

(12) Heinekey, D. M.; Michel, S. T. *Organometallics* **1989**, *8*, 1241-1246.

(13) Curtis, M. D.; Fotinos, N. A.; Han, K. R.; Butler, W. M. *J. Am. Chem. Soc.* **1983**, *105*, 2686-2694.

(14) Sattelberger, A. P.; Wilson Jr., R. B.; Huffman, J. C. *J. Am. Chem. Soc.* **1980**, *102*, 7111-7113.

(15) Ting, C. T.; Baenziger, N. C.; Messerle, L. *J. Chem. Soc., Chem. Commun.* **1988,** 1133-1135.

(16) Green, M. L.; Mountford, P. *J. Chem. Soc., Chem. Commun.* **1989,** 732-734.

(17) Casey, C. P.; Sakaba, H.; Hazin, P. N.; Powell, D. R. *J. Am. Chem. Soc.* **1991,** *113*, 8165-8166.

(18) Chaudret, B.; Dahan, F.; Sabo, S. *Organometallics* **1985,** *4*, 1490-1492.

(19) Trinquier, G.; Hoffmann, R. *Organometallics* **1984,** *3*, 370-380.

(20) Collman, J. P.; Hegedus, L. S.; Norton, J. R.; Finke, R. G. *Principles and Applications of Organotransition Metal Chemistry*; University Science Books: Mill Valley, California, 1987.

(21) Terminal hydride ligands give rise to IR bands that are sharper, stronger, and at higher energy (2200-1600 cm^{-1}) than the corresponding bands of bridging hydrides (1400-800 cm^{-1}): Kaesz, H. D.; Saillant, R. B. *Chem. Rev.* **1972,** *72*, 231-281.

(22) Plank, J.; Riedel, D.; Herrmann, W. A. *Angew. Chem. Int. Ed. Engl.* **1980,** *19*, 937-938.

(23) This reaction could be driven by the precipitation of NaCl.

(24) McDonald, R.; Sutherland, B. R.; Cowie, M. *Inorg. Chem.* **1987,** *26*, 3333-3339.

(25) Triflic acid is a stronger aqueous acid than perchloric acid: Cox, R. A.; Krull, U. J.; Thompson, M.; Yates, K. *Anal. Chim. Acta* **1979,** *106*, 51-57.

(26) Gordon, A. J.; Ford, R. A. In *The Chemist's Companion*; John Wiley & Sons: New York, 1972.

(27) Siedle, A. R.; Newmark, R. A.; Pignolet, L. H.; Howells, R. D. *J. Am. Chem. Soc.* **1984,** *106*, 1510-1511.

(28) Pinhas, A. R.; Hoffmann, R. *Inorg. Chem.* **1979,** *18*(3), 654-658.

(29) Griewe, G. L.; Hall, M. B. *Organometallics* **1988,** *7*, 1923-1930.

(30) Bursten, B. E.; Cayton, R. H. *J. Am. Chem. Soc.* **1987,** *109*, 6053-6059.

(31) Legdzins, P.; Martin, D. T.; Nurse, C. R.; Wassink, B. *Organometallics* **1983**, *2*, 1238-1244.

(32) Chinn, M. S. Ph.D. Thesis, Yale University, 1989.

(33) Pinhas, A. R.; Albright, T. A.; Hofmann, P.; Hoffmann, R. *Helv. Chim. Acta* **1980**, *63*(4), 29-49.

(34) Hofmann, P. *Angew. Chem. Int. Ed. Engl.* **1979**, *18*(7), 554-556.

(35) Bau, R.; Teller, R. G.; Kirtley, S. W.; Koetzle, T. F. *Acc. Chem. Res.* **1979**, *12*, 176-183.

(36) McGhee, W. D.; Foo, T.; Hollander, F. J.; Bergman, R. G. *J. Am. Chem. Soc.* **1988**, *110*, 8543-8545.

(37) Motyl, K. M.; Norton, J. R.; Schauer, C. K.; Anderson, O. P. *J. Am. Chem. Soc.* **1982**, *104*, 7325-7327.

(38) Einstein, F. W. B.; Jones, R. H.; Zhang, X.; Yan, X.; Negelkerke, R.; Sutton, D. *J. Chem. Soc., Chem. Commun.* **1989**, 1424-1426.

(39) Hoyano, J. K.; Graham, W. A. G. *J. Am. Chem. Soc.* **1982**, *104*, 3722-3723.

(40) Alt, H. G.; Mahmoud, K. A.; Rest, A. J. *Angew. Chem. Int. Ed. Engl.* **1983**, *22*, 544-545.

(41) Mahmoud, K. A.; Rest, A. J.; Alt, H. G. *J. Chem. Soc., Dalton Trans.* **1985**, 1365-1374.

(42) Legdzins, P.; Martin, J. T.; Oxley, J. C. *Organometallics* **1985**, *4*, 1263-1271.

(43) Dahl, L. F. *Ann. N.Y. Acad. Sci.* **1983**, 1-26, and references therein.

(44) Bahr, S. R.; Boudjouk, P. *J. Org. Chem.* **1992**, *57*, 5545-5547.

(45) Brookhart, M.; Grant, B.; Volpe Jr., A. F. *Organometallics* **1992**, *11*, 3920-3922.

CHAPTER 5

Preparation of Methyl Derivatives of Cp^* Carbonyl Monomers and Dimers of Iridium

Introduction

One of the objectives of our research has been to compare the thermal and photochemical reactivity of the dihydride dimer, $[Cp^*Ir(CO)H]_2$, with that of the dihydride monomer, $Cp^*Ir(CO)H_2$, specifically with respect to the facility to undergo reductive elimination of H_2 (see Chapter 3). Another goal has been to prepare monomeric and dimeric alkyl derivatives in order to compare their ability to undergo reductive elimination reactions with that of their hydride analogues. As is the case for monomeric alkyl hydrides,[1] $L_nM(R)H$, we might expect that the dimeric alkyl hydrides, $R(L_n)M\text{-}M(L_n)H$, would exhibit less thermal stability than the corresponding dihydride and dialkyl complexes. Given that the bond dissociation energy (BDE) of an M-C bond is typically less than that of the corresponding M-H bond,[2] and that the BDE of CH_4 is about equal to the BDE of H_2,[3] then the enthalpy of reaction for the reductive elimination of methane from $Me(L_n)M\text{-}M(L_n)H$ will be less than that for the loss of H_2 from $H(L_n)M\text{-}M(L_n)H$. In addition, given that the absolute entropy of methane is greater than that of hydrogen,[4] and assuming that the starting methyl hydride and dihydride dimers have comparable entropies, then the entropy of reaction should also favor the reductive elimination of methane from $Me(L_n)M\text{-}M(L_n)H$ over loss of H_2 from $H(L_n)M\text{-}M(L_n)H$. Hence, the methyl hydride dimer should be subject to a greater *thermodynamic* driving force for reductive elimination than the corresponding dihydride dimer.

The thermodynamic driving force for reductive elimination of ethane from $Me(L_n)M\text{-}M(L_n)Me$ relative to reductive elimination from the dihydride or alkyl hydride dimer is more difficult to predict. But, as in the case for the monomeric analogues, a

1,2-dimethyl dimer would be expected to have a greater *kinetic* barrier to intramolecular reductive elimination, due to the activation energy for the required re-orientation of the directional methyl carbon sp^3 orbitals.

The only series of dimers for which the dihydride, methyl hydride, and dimethyl derivatives are all known compounds, is the isolobal osmium carbonyl system examined by Norton and co-workers.[1,5-7] As predicted above, the alkyl hydrides, which are described as "unstable colorless oils,"[7] appear to exhibit the greatest thermal reactivity; thermolysis of $Me(CO)_4Os$-$Os(CO)_4H$ at 74 °C generates methane. It is important to note, however, that all evidence indicates that this reaction is not the result of simple *intra*molecular reductive elimination, but rather proceeds (at least for the most part) by an *inter*molecular process.[1] In other words, $Me(CO)_4Os$-$Os(CO)_4H$ may have access to a lower energy reaction pathway unavailable to its dihydride and dimethyl counterparts, and hence is less stable due to kinetic considerations.

Aside from the examination of the reactivity of $[Cp^*Ir(CO)]_2(Me)H$ and $[Cp^*Ir(CO)Me]_2$, an additional point of interest would be the determination of their structure. As noted in Chapter 2, the structure of the dihydride dimer, $[Cp^*Ir(CO)H]_2$, is unusual in that both the hydride and carbonyl ligands adopt terminal positions, i.e. the Ir-Ir bond is unsupported by bridging ligands. However, the related rhodium dimethyl dimer, $[Cp^*Rh(\mu\text{-}CO)Me]_2$, possesses a Rh-Rh bond bridged by the carbonyl ligands.[8] The structure of these dimers may play an important role in their ability to undergo reductive elimination reactions.

This chapter describes attempts to prepare and isolate $[Cp^*Ir(CO)]_2(Me)H$ and $[Cp^*Ir(CO)Me]_2$, as well as a new method for the synthesis of $Cp^*Ir(CO)Me_2$.

Results

Addition of excess MeLi to a solution of $Cp^*Ir(CO)Cl_2$ in Et_2O affords the dimethyl monomer, $Cp^*Ir(CO)Me_2$. The sublimed product of this reaction often is contaminated with small amounts of yellow $Cp^*Ir(CO)(Me)Cl$. Purification of the colorless, air-stable $Cp^*Ir(CO)Me_2$ is achieved by chromatography or successive recrystallizations from cold pentane. The dimethyl monomer is a weak base; $Cp^*Ir(CO)Me_2$ is not protonated by $[Et_3NH]Cl$, but reacts cleanly with one equiv of HCl to generate $Cp^*Ir(CO)(Me)Cl$ and methane.

A variety of methods were employed in attempts to synthesize the dimethyl dimer, $[Cp^*Ir(CO)Me]_2$. The most successful procedure involved the Na/K alloy reduction of $[Cp^*Ir(\mu\text{-}CO)]_2$ in THF, presumably forming the dianion $[Cp^*Ir(\mu\text{-}CO)]_2^{2-}$, followed by reaction with MeCl (eq 5.1). The reaction was performed in an H-tube under static vacuum or argon to minimize exposure to air. A ^1H NMR spectrum of the solid products in CD_2Cl_2 revealed two pairs of singlet resonances (δ 1.83, -0.55; 1.85, -0.21), with each pair integrating in a 5:1 ratio. The two sets of resonances are tentatively assigned to cis and trans isomers (relative to the metal-metal bond) of $[Cp^*Ir(CO)Me]_2$ respectively, by analogy to $[Cp^*Rh(\mu\text{-}CO)Me]_2$.[8] Upon standing for several days, the pair of resonances at 1.83 and -0.55 ppm disappeared. An IR spectrum of a different sample containing only what is believed to be the trans isomer, exhibited a single absorbance in the ν_{CO} range at 1745 cm^{-1}, characteristic of a bridging CO stretch.[9] Unfortunately, in all attempts, a significant quantity of $[Cp^*Ir(\mu\text{-}CO)]_2$ remained at the end of the reaction. Sublimation, chromatography, and recrystallization were employed in efforts to separate $[Cp^*Ir(CO)Me]_2$ from $[Cp^*Ir(\mu\text{-}CO)]_2$, with limited success.

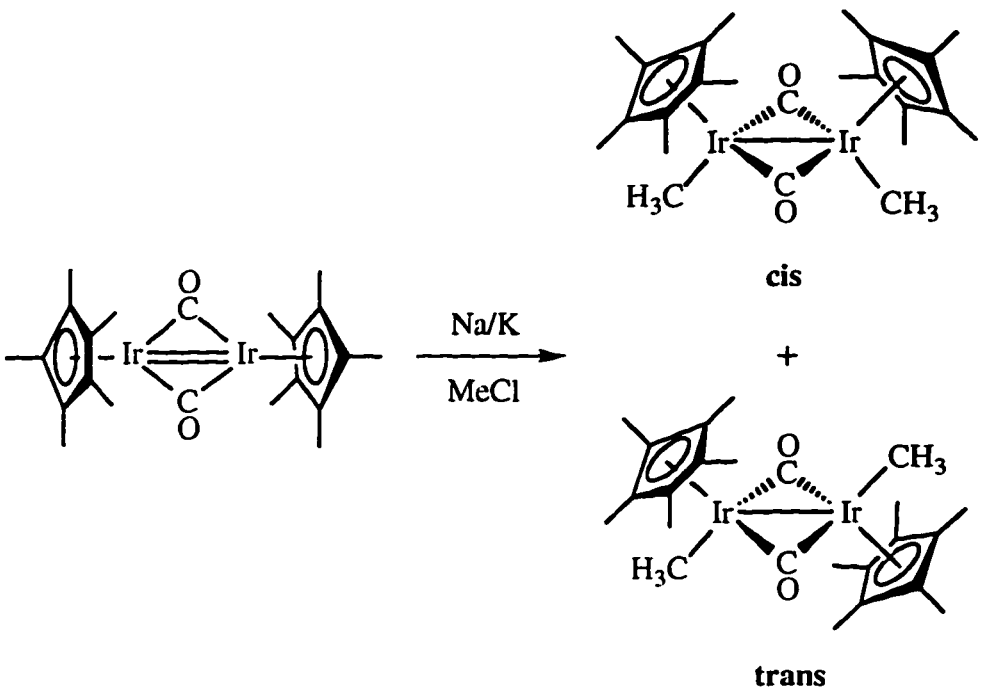

(5.1)

A second route, deprotonation of $[Cp^*Ir(CO)H]_2$ with two equiv of a strong base (*n*BuLi or MeLi), followed by addition of MeCl, also generated *cis*- and *trans*-$[Cp^*Ir(CO)Me]_2$, along with a substantial amount of unreacted $[Cp^*Ir(CO)H]_2$, and again accompanied by $[Cp^*Ir(\mu\text{-}CO)]_2$. A third route attempted to synthesize the unknown dichloride dimer, $[Cp^*Ir(CO)Cl]_2$, which perhaps could then be converted to $[Cp^*Ir(CO)Me]_2$. The dihydride dimer, $[Cp^*Ir(CO)H]_2$, does react rapidly at room temperature with CCl_4 or N-chlorosuccinimide, but the reaction is not clean (as determined by ^1H NMR), and no attempt was made to isolate the various products. Attempts were also made to generate $[Cp^*Ir(CO)Me]_2$ in a stepwise fashion via addition of Me^- (MeLi or MeMgBr) and subsequently Me^+ (MeCl or MeI) to $[Cp^*Ir(\mu\text{-}CO)]_2$. No reaction between Me^- and $[Cp^*Ir(\mu\text{-}CO)]_2$ occurred, even in the presence of the lithium sequestering agent, PMDT. Finally, $Cp^*Ir(CO)Me_2$ was protonated under H_2 in an effort to generate a dimethyl hydride cation dimer, $[Cp^*Ir(CO)Me]_2(\mu\text{–}H)^+$, with the expectation that it could subsequently be deprotonated to yield the neutral dimethyl

dimer. However, the principal products of this reaction were $[Cp^*Ir(CO)]_2(\mu\text{-}CH_2)(\mu\text{-}H)^+$[10]and $[Cp^*Ir(CO)H]_2(\mu\text{-}H)^+$ (see Chapter 2).

Several attempts were also made to prepare the methyl hydride dimer, $[Cp^*Ir(CO)]_2(Me)H$. Thermolysis of an equimolar solution of $Cp^*Ir(CO)H_2$ and $Cp^*Ir(CO)Me_2$ produced no reaction apart from incorporation of deuterium from the solvent into the Cp^* methyl groups of $Cp^*Ir(CO)H_2$. In another experiment, an acid was added to a solution of $Cp^*Ir(CO)H_2$ and $Cp^*Ir(CO)Me_2$ in an effort to generate a dimeric complex with one methyl and two hydride ligands, $[Cp^*Ir(CO)H]_2(Me)^+$, which presumably could be deprotonated to the neutral methyl hydride dimer. However, the principal product was the trihydride cation dimer, $[Cp^*Ir(CO)H]_2(\mu\text{-}H)^+$. The dark blue-green color of the resultant solution is characteristic of the presence of the unsaturated dimer, $[Cp^*Ir(CO)]_2(\mu\text{-}H)^+$ (see Chapter 4). A third attempt, exposure of a CD_2Cl_2 solution of $[Cp^*Ir(CO)]_2(\mu\text{-}CH_2)$[10] to an atmosphere of H_2 (3.0 atm), produced no reaction.

Discussion

Synthesis of $Cp^*Ir(CO)Me_2$, $Cp^*Ir(CO)(Me)Cl$.

The dimethyl monomer, $Cp^*Ir(CO)Me_2$, was first reported[11] in 1983 by Maitlis and co-workers as a minor byproduct (2% yield) of the reaction of $[Cp^*IrCl]_2$ with Al_2Me_6 in benzene under a CO atmosphere. Two years later, Maitlis et al. detailed[12] a superior route to $Cp^*Ir(CO)Me_2$ via reaction of the dimethylsulfoxide complex,[13] $Cp^*Ir(Me_2SO)Me_2$, with either CO or acetaldehyde (eq 5.2). Yields were reportedly "good," though no values were given. Curiously, the initial preparation was not mentioned in the later publication.

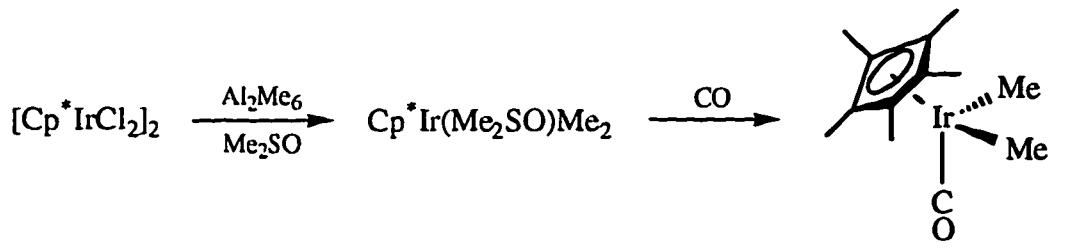

(5.2)

We sought a route to $Cp^*Ir(CO)Me_2$ that did not involve the use of Al_2Me_6, a pyrophoric reagent. Direct reaction of MeLi with $Cp^*Ir(CO)Cl_2$ efficiently generates $Cp^*Ir(CO)Me_2$. If the reaction mixture is not extracted with water, $Cp^*Ir(CO)Me_2$ will not sublime from the resulting solids, presumably due to the formation of LiCl adducts. A similar difficulty was encountered by Graham, Heinekey and co-workers,[14] who found that the bis-carbonyl, $Cp^*Ir(CO)_2$, when prepared from reaction of $Cp^*Ir(CO)Cl_2$ with zinc metal in methylene chloride, does not sublime unless the reaction mixture is extracted by water. They surmise that a $Cp^*Ir(CO)_2 \cdot ZnCl_2$ adduct is generated which requires hydrolysis prior to sublimation.

Addition of one equiv of HCl to $Cp^*Ir(CO)Me_2$ cleanly affords methane and $Cp^*Ir(CO)(Me)Cl$. Graham and co-workers previously reported[15] the preparation of $Cp^*Ir(CO)(Me)Cl$ from $Cp^*Ir(CO)(Me)H$ and CCl_4, as a means of characterizing the thermally unstable methyl hydride. More recently, Maitlis et al.[16] found that reaction of $Cp^*Ir(Me_2SO)(Me)Cl$ with CO also affords $Cp^*Ir(CO)(Me)Cl$.

Synthesis of $[Cp^*Ir(CO)Me]_2$.

Our initial attempts to synthesize $[Cp^*Ir(CO)Me]_2$ were guided by the methods reported[8] by Bergman and Krause for the preparation of the rhodium analogue, $[Cp^*Rh(\mu\text{-}CO)Me]_2$. They found that the most efficient route to $[Cp^*Rh(\mu\text{-}CO)Me]_2$ (59% yield) involved stepwise addition of MeLi and MeI to $[Cp^*Rh(\mu\text{-}CO)]_2$. Reduction of $[Cp^*Rh(\mu\text{-}CO)]_2$ to $[Cp^*Rh(\mu\text{-}CO)]_2^{2-}$ with Na/K alloy, followed by addition of MeI,

was observed to generate $[Cp^*Rh(\mu\text{-}CO)Me]_2$, but in only a 3% yield, and with $[Cp^*Rh(\mu\text{-}CO)]_2$ as a side product. They were able to separate $[Cp^*Rh(\mu\text{-}CO)Me]_2$ from $[Cp^*Rh(\mu\text{-}CO)]_2$ via chromatography. In addition, they were able to isolate $[Cp^*Rh(\mu\text{-}CO)]_2^{2-}$ as the potassium salt.

We were unable to effect any reaction of MeLi or MeMgBr with $[Cp^*Ir(\mu\text{-}CO)]_2$. This was somewhat curious considering that previous work[17] in our group suggested that MeLi did indeed react with $[Cp^*Ir(\mu\text{-}CO)]_2$. A report[18] by Bergman and Gilbert of increased reaction rates by addition of the lithium chelating agent, PMDT, to alkyl lithium reactions of related compounds, prompted us to apply it to our system. However, addition of PMDT to a THF solution of MeLi and $[Cp^*Ir(\mu\text{-}CO)]_2$ produces no reaction.

In contrast to the rhodium analogue, the most effective route to $[Cp^*Ir(CO)Me]_2$ proved to be via Na/K alloy reduction of $[Cp^*Ir(\mu\text{-}CO)]_2$ with subsequent addition of MeCl. Initial attempts by this route succeeded only in recovering the reactant dimer, $[Cp^*Ir(\mu\text{-}CO)]_2$. Since there is no color change in this reaction, it was unclear whether the putative dianion, $[Cp^*Ir(\mu\text{-}CO)]_2^{2-}$, was generated but was re-oxidized by the MeCl, or whether $[Cp^*Ir(\mu\text{-}CO)]_2$ was not reduced in the first place. Subsequently, it became clear that the reduction of $[Cp^*Ir(\mu\text{-}CO)]_2$ is slow (requiring overnight mixing), and that the initial experiments had not allowed enough mixing time prior to addition of Me^+. By comparison, reduction of $[Cp^*Rh(\mu\text{-}CO)]_2$ to $[Cp^*Rh(\mu\text{-}CO)]_2^{2-}$ requires only 1-2 hours, and fortuitously is accompanied by a marked color change. Even with long mixing times, yields of $[Cp^*Ir(CO)Me]_2$ by this route are inconsistent.

Bergman and Krause found that reaction of $[Cp^*Rh(\mu\text{-}CO)]_2$ with MeLi followed by MeI at 0 °C generates a single isomer of $[Cp^*Rh(\mu\text{-}CO)Me]_2$, believed to be the cis geometrical isomer. Allowing a solution of *cis*-$[Cp^*Rh(\mu\text{-}CO)Me]_2$ to stand at room temperature slowly produces an equilibrium mixture of the cis and trans isomers, with the thermodynamic product, the trans isomer, predominating. An IR spectrum of the cis

isomer shows two bands in the carbonyl region, while that of the trans isomer displays one band. This is in agreement with group theory which predicts that a cis geometry with C_{2v} symmetry should exhibit two bands due to the carbonyl ligands, whereas a trans structure with C_{2h} symmetry should exhibit one band. Similarly, $[Cp^*Ir(CO)Me]_2$ appears to exist as two isomers, with one isomer predominating over time in solution. An IR spectrum of the predominant isomer exhibits a single absorbance in the CO region at 1745 cm^{-1}, characteristic of bridging carbonyls, and consistent with a trans geometry.

Further indirect evidence that the dimethyl dimer, $[Cp^*Ir(CO)Me]_2$, is the principal product of the reduction/alkylation reaction of $[Cp^*Ir(\mu\text{-}CO)]_2$ is provided by an independent synthetic route. Double deprotonation of $[Cp^*Ir(CO)H]_2$ followed by alkylation with MeCl affords products with the same ^1H NMR chemical shifts as are observed to result from the reduction/alkylation pathway and are again attributed to formation of *cis*- and *trans*-$[Cp^*Ir(CO)Me]_2$.

Both synthetic routes are complicated by the presence of significant quantities of $[Cp^*Ir(\mu\text{-}CO)]_2$ as byproduct. Unlike the rhodium system, we have been unable to separate $[Cp^*Ir(\mu\text{-}CO)]_2$ from $[Cp^*Ir(CO)Me]_2$ by chromatography. The best means of purification of $[Cp^*Ir(CO)Me]_2$ at this point appears to be successive recrystallizations from cold heptane. Due to the difficulty in obtaining a pure sample of $[Cp^*Ir(CO)Me]_2$, we have not yet tested its thermal stability at elevated temperatures. The rhodium dimethyl dimer, $[Cp^*Rh(\mu\text{-}CO)Me]_2$, is observed to be "thermally quite stable" and decomposes slowly at temperatures above 50 °C.[8]

An additional attempt to generate $[Cp^*Ir(CO)Me]_2$ utilized a modification of the monomer condensation methodology that was used previously to prepare the trihydride cation dimer, $[Cp^*Ir(CO)H]_2(\mu\text{-}H)^+$ (see Chapter 2). It was thought that protonation of $Cp^*Ir(CO)Me_2$ with 0.5 equiv of acid under H_2 might lead to $[Cp^*Ir(CO)Me]_2(\mu\text{-}H)^+$ by the series of steps outlined in Scheme 5.1, which could then presumably be deprotonated

to the neutral dimethyl dimer. Note in this scheme that a potential side-product, $Cp^*Ir(CO)H_3^+$, is unstable with respect to reductive elimination of H_2 at room temperature.[19]

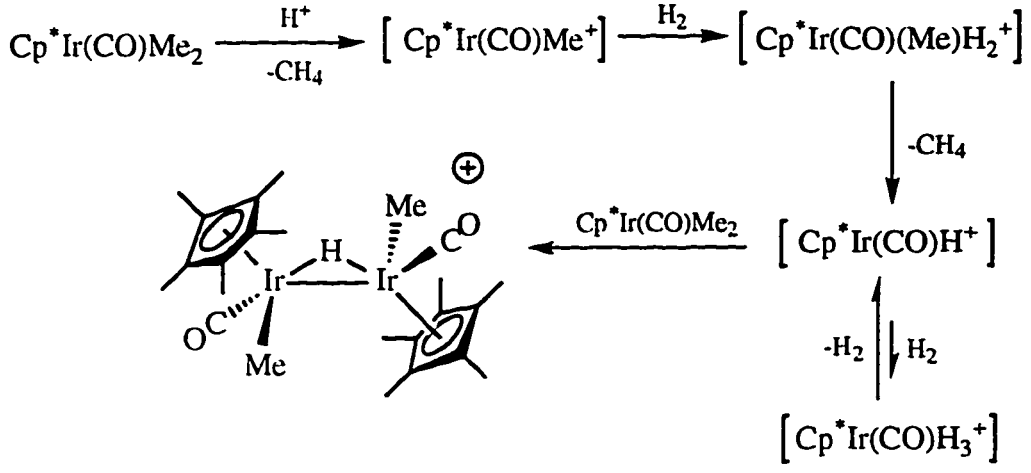

Scheme 5.1

The primary organometallic product of the reaction however was *trans*-$[Cp^*Ir(CO)]_2(\mu\text{-}CH_2)(\mu\text{-}H)^+$, along with a lesser amount of $[Cp^*Ir(CO)H]_2(\mu\text{-}H)^+$; methane was also produced. It seems probable that $[Cp^*Ir(CO)Me]_2(\mu\text{-}H)^+$ was indeed generated, but that it is unstable with respect to reductive elimination of methane (Scheme 5.2). Loss of methane from $[Cp^*Ir(CO)Me]_2(\mu\text{-}H)^+$ would be expected to initially form $[Cp^*Ir(CO)]_2(Me)^+$. Heinekey and co-workers[10] have shown that addition of Me^+ (MeOTf) to $[Cp^*Ir(\mu\text{-}CO)]_2$ affords a mixture of *cis*- and *trans*-$[Cp^*Ir(CO)]_2(\mu\text{-}CH_2)(\mu\text{-}H)^+$ and is proposed to proceed via intramolecular oxidative addition of a C-H bond of the methyl group of $[Cp^*Ir(CO)]_2(Me)^+$. The pathway for the formation of the minor product, $[Cp^*Ir(CO)H]_2(\mu\text{-}H)^+$, is unclear at this point. We might anticipate that $[Cp^*Ir(CO)]_2(\mu\text{-}CH_2)(\mu\text{-}H)^+$ could react with H_2 to generate $[Cp^*Ir(CO)H]_2(Me)^+$, which itself is unstable with respect to reductive elimination of methane (see following section).

The unsaturated product, $[Cp^*Ir(CO)]_2(\mu\text{-}H)^+$, would then add H_2 to form $[Cp^*Ir(CO)H]_2(\mu\text{-}H)^+$ (see Chapter 4). However, under these conditions, *trans*-$[Cp^*Ir(CO)]_2(\mu\text{-}CH_2)(\mu\text{-}H)^+$ seems to be stable in the presence of excess H_2. A possible explanation might be that *cis*-$[Cp^*Ir(CO)]_2(\mu\text{-}CH_2)(\mu\text{-}H)^+$ reacts with H_2 , whereas the *trans* isomer does not. *cis*-$[Cp^*Ir(CO)]_2(\mu\text{-}CH_2)(\mu\text{-}H)^+$ was demonstrated by Heinekey et al.[10] to be in rapid equilibrium with an agostic methyl tautomer, though the *trans* isomer shows no such interconversion. Reaction of isolated $[Cp^*Ir(CO)]_2(\mu\text{-}CH_2)(\mu\text{-}H)^+$ with H_2 has not yet been performed.

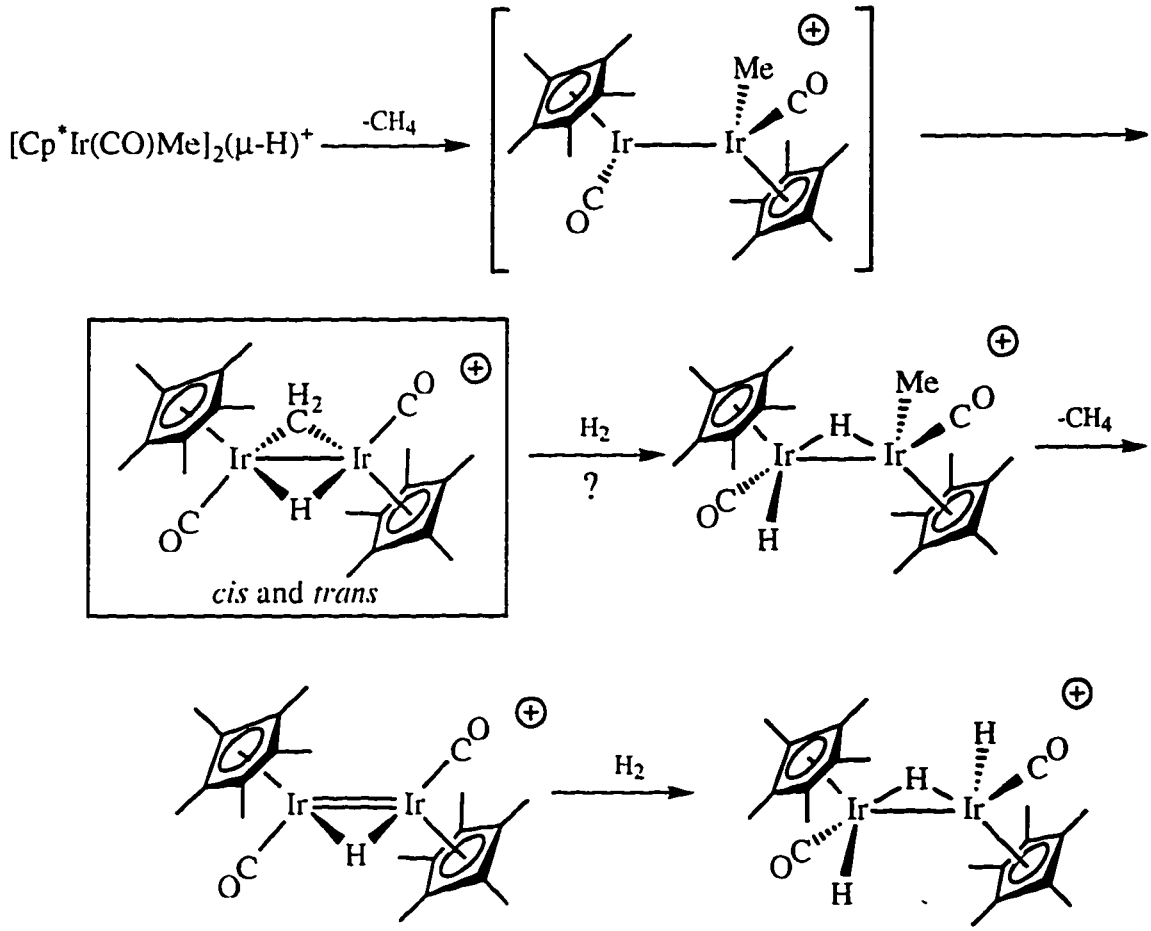

Scheme 5.2

Efforts to Prepare $[Cp^*Ir(CO)]_2(Me)H$.

For a synthetic route to the methyl hydride dimer, we could not look to the rhodium system for examples. Bergman and Krause report[8] that reaction of $[Cp^*Rh(\mu\text{-}CO)]_2$ with MeLi followed by either H_2O or MeOH at -78 °C results in isolation of only $[Cp^*Rh(\mu\text{-}CO)]_2$. This reaction suggests that perhaps $[Cp^*Rh(CO)]_2(Me)H$ is formed, but that it is thermally unstable with respect to reductive elimination of methane. Norton and co-workers[7] generated a methyl hydride dimer, $MeOs_2(CO)_8H$, via thermolysis of $Os(CO)_4H_2$ and $Os(CO)_4Me_2$ at 85 °C in C_6D_6. Unfortunately, thermolysis of $Cp^*Ir(CO)H_2$ and $Cp^*Ir(CO)Me_2$ at 85 °C in C_6D_6 does not result in any reaction. The difference between the reactivity of the two systems may lie in the greater facility with which a methyl group of $Os(CO)_4Me_2$ can migrate to one of the carbonyls to open up a site of coordinative unsaturation.

For an alternate route to $[Cp^*Ir(CO)]_2(Me)H$, we again attempted to utilize a modification of the monomer condensation methodology. It was hoped that reaction of $Cp^*Ir(CO)Me_2$ with one equiv of H^+ would generate methane and the 16-electron species $[Cp^*Ir(CO)Me]^+$, which in the presence of excess $Cp^*Ir(CO)H_2$ would form $[Cp^*Ir(CO)H]_2Me^+$. Subsequent deprotonation of $[Cp^*Ir(CO)H]_2Me^+$ would give the neutral methyl hydride dimer. Instead, the principal product was $[Cp^*Ir(CO)H]_2(\mu\text{-}H)^+$, along with unreacted $Cp^*Ir(CO)Me_2$ and methane. This result indicates that some of the acid ($HBAr'_4\bullet(Et_2O)_2$) was consumed by proton transfer to $Cp^*Ir(CO)H_2$. A possible mechanism for this reaction is presented in Scheme 5.3. The blue-green color of the solution is consistent with the presence of the unsaturated protonated dimer, $[Cp^*Ir(CO)]_2(\mu\text{-}H)^+$. However, no resonances attributable to $[Cp^*Ir(CO)]_2(\mu\text{-}H)^+$ were evident in the ^1H NMR spectrum of the solution. Since even dilute solutions of $[Cp^*Ir(CO)]_2(\mu\text{-}H)^+$ are deeply colored, it seems reasonable that there might be a trace

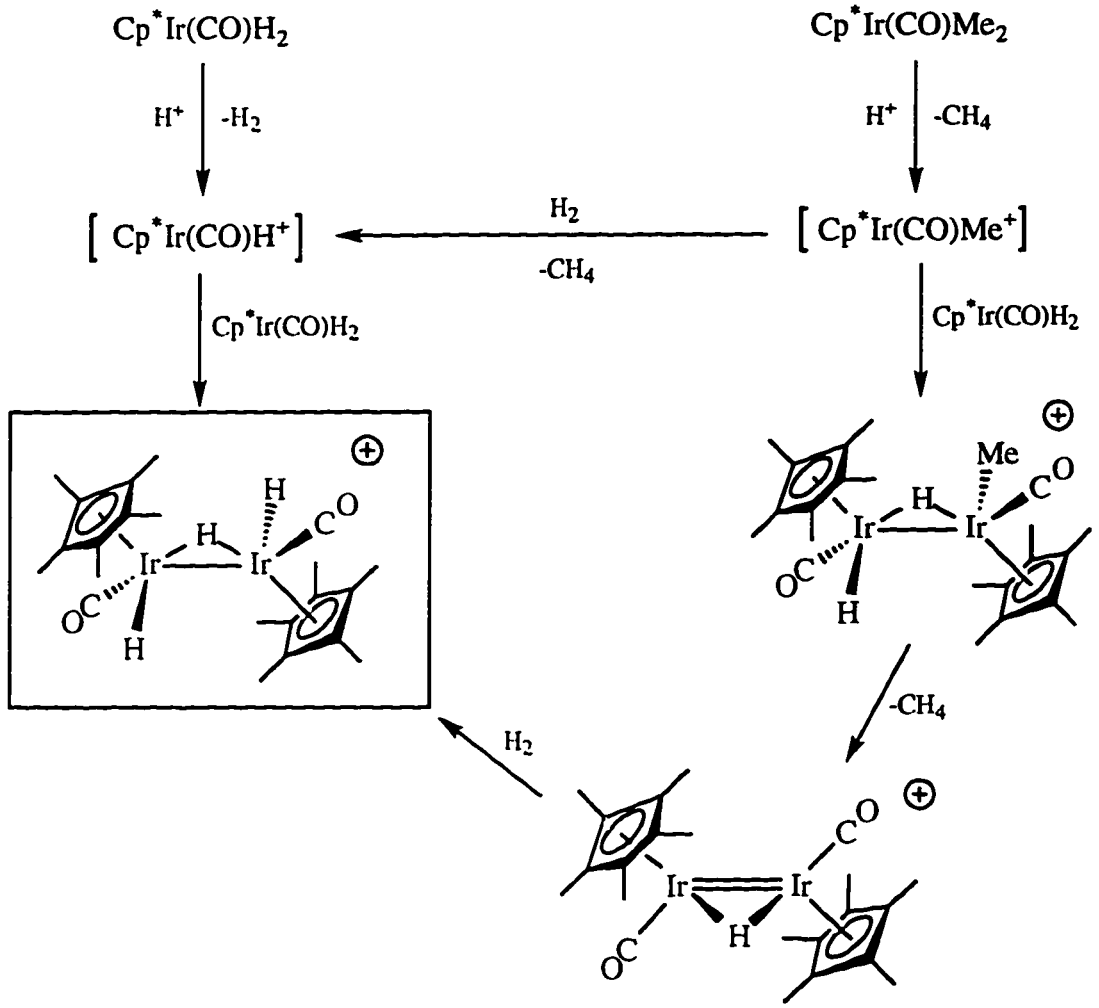

Scheme 5.3

amount of the mono-protonated dimer present. This suggests that $[Cp^*Ir(CO)H]_2(Me)^+$ was indeed generated, but that it is unstable with respect to reductive elimination of methane.

The instability of the putative methyl hydride cation dimers, $[Cp^*Ir(CO)Me]_2(\mu\text{-}H)^+$ and $[Cp^*Ir(CO)H]_2(Me)^+$, with respect to reductive elimination of methane is not entirely surprising given the general instability of monomeric alkyl hydrides. A recently reported[20] cationic dimer with methyl and hydride ligands bound to

the same metal center was also observed to be unstable with respect to elimination of methane above 0 °C (eq 5.3). Presumably, if an acid were used that was of sufficient strength to protonate $Cp^*Ir(CO)Me_2$ but not $Cp^*Ir(CO)H_2$, then the primary product of the reaction would be $[Cp^*Ir(CO)]_2(\mu\text{-}H)^+$.

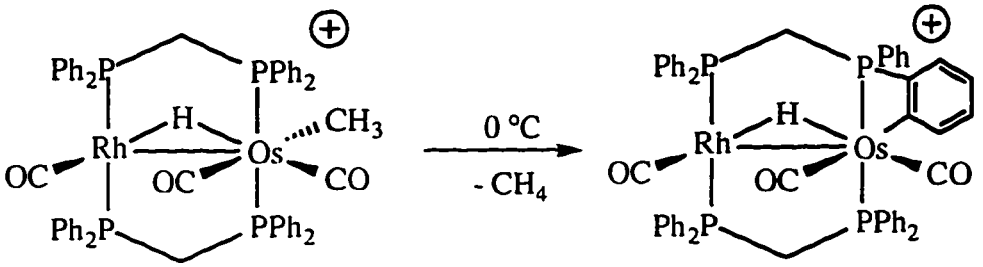

(5.3)

It is interesting to speculate as to which structure $[Cp^*Ir(CO)]_2(Me)H$ might adopt: a geometry with all ligands bound in a terminal fashion, like $[Cp^*Ir(CO)H]_2$, or a geometry with carbonyls bridging the Ir-Ir bond, as in $[Cp^*Ir(CO)Me]_2$. The factors which influence these structural changes are not apparent at this time, but are obviously subtle.

Conclusion

A new and efficient synthesis of $Cp^*Ir(CO)Me_2$ has been developed. A promising route to $Cp^*Ir(CO)(Me)Cl$ has also been discovered.

The dimethyl dimer, $[Cp^*Ir(CO)Me]_2$, was generated by two different routes, the most successful of which involved reduction with Na/K alloy followed by alkylation with MeCl. Like the rhodium analogue, $[Cp^*Rh(CO)Me]_2$, but unlike the dihydride dimer, $[Cp^*Ir(CO)H]_2$, the carbonyl ligands of $[Cp^*Ir(CO)Me]_2$ bridge the Ir-Ir bond. Again, like the rhodium analogue, $[Cp^*Ir(CO)Me]_2$ appears to exist as cis and trans isomers.

Unfortunately, efforts to separate $[Cp^*Ir(CO)Me]_2$ from the persistent byproduct $[Cp^*Ir(\mu\text{-}CO)]_2$ have found limited success.

Several strategies were employed in efforts to synthesize the methyl hydride dimer, $[Cp^*Ir(CO)]_2(Me)H$, but were unsuccessful. It is proposed that cationic dimers with methyl and hydride ligands bound to the same iridium center are unstable at room temperature with respect to reductive elimination of methane.

Experimental

General procedures for manipulation and characterization of compounds are presented in the experimental section of Chapter 2.

An "H-tube" is an all glass apparatus that consists of two cylindrical chambers connected in the middle by a horizontal tube that contains a glass frit. Each chamber is topped by a ground glass joint.

$Cp^*Ir(CO)Cl_2$ was prepared with slight modification to the published procedure.[21] The syntheses of $Cp^*Ir(CO)H_2$ and $[Cp^*Ir(CO)H]_2$ are outlined in Chapter 2. $[Cp^*Ir(\mu\text{-}CO)]_2$ was prepared by the reported method.[14] N ,N ,N' ,N", N"-Pentamethyl-diethylenetriamine (PMDT) was distilled under reduced pressure from sodium and stored under argon over molecular sieves (4Å). All other reagents were used as received.

$Cp^*Ir(CO)(CH_3)_2$. To a straight-side Schlenk flask containing $Cp^*Ir(CO)Cl_2$ (259 mg, 0.607 mmol) was added 30 mL of Et_2O via cannula. With the flask immersed in a CO_2/IPA bath, 4.3 mL of MeLi solution (1.4 M in Et_2O, 10 equiv) was added to the stirring, bright yellow suspension dropwise via syringe. After 1.5 h, the clear, pale orange solution was transferred to an ice/NaCl bath and left to stir overnight. To the then cloudy, yellow solution was added 20 mL of deionized water (argon sparged) via cannula at room temperature. After stirring for 0.5 h, the Et_2O layer was transferred via cannula

into a Schlenk flask containing oven-dried $MgSO_4$. The aqueous phase was extracted with 2 x 5 mL of Et_2O and the extracts combined with the Et_2O layer. The mixture was stirred for an hour and the yellow-brown liquid transferred via filter cannula into a 200 mL round-bottom Schlenk flask. The $MgSO_4$ was washed with Et_2O and this liquid was combined with the previous extracts. The solvent was removed in vacuo leaving a yellow-brown residue. A very pale yellow solid was recovered by sublimation (25 °C, dynamic vacuum). The sublimed material contained a small quantity (≈ 3%) of yellow $Cp^*Ir(CO)(CH_3)Cl$. The colorless, air-stable product was isolated by chromatography through a silica gel column with methylene chloride as eluent. Yield = 108 mg (46%). Successive recrystallizations from pentane at -30 °C were also successful in purification of $Cp^*Ir(CO)(CH_3)_2$. ^1H NMR ($CDCl_3$) is consistent with literature data.[12] ^1H NMR (CD_2Cl_2) δ: 1.82 (s, Cp^*, 15 H), 0.29 (s, CH_3, 6 H). ^1H NMR (C_6D_6) δ: 1.48 (Cp^*), 0.73 (CH_3).

Reaction of $Cp^*Ir(CO)(CH_3)_2$ with HCl. To a screw-cap NMR tube charged with 5.2 mg of $Cp^*Ir(CO)(CH_3)_2$ (14 μmol) was added methylene chloride-d_2 (0.5 mL) via vacuum transfer yielding a clear, colorless solution. A 1.0 M solution of HCl in Et_2O (anhydrous, 14 μL, 1.1 equiv) was added via syringe causing the solution to immediately become yellow. The only products, as determined by ^1H NMR, were $Cp^*Ir(CO)(CH_3)Cl$ and methane. ^1H NMR (CD_2Cl_2) δ: (reported[15]) 1.88 (s, Cp^*, 15 H), 1.05 (s, CH_3, 3 H); (found) 1.85 (s, 15 H), 0.99 (s, 3 H).

Reaction of $Cp^*Ir(CO)(CH_3)_2$ with $HBAr'_4{\bullet}(Et_2O)_2$ under H_2. A screw-cap NMR tube was charged with 5.1 mg of $Cp^*Ir(CO)(CH_3)_2$ (13 μmol) and 6.9 mg of $HBAr'_4{\bullet}(Et_2O)_2$ (6.8 μmol, 0.52 equiv). Methylene chloride-d_2 (0.5 mL) was vacuum transferred onto the solids and the contents were kept frozen by complete immersion of

the NMR tube in a liquid N_2 bath. The head space was evacuated and pressurized with H_2 (0.74 atm). The solution was thawed in a CO_2/IPA bath yielding orange solid in a bright yellow liquid. Upon thawing to room temperature (P_{H2} = 2.9 atm), the solid dissolved to give an orange-brown solution. A ^1H NMR spectrum revealed the formation of methane and several organometallic products (four resonances in the Cp* region and five hydride region resonances), in addition to unreacted $Cp^*Ir(CO)Me_2$ and excess H_2. No new resonances in the methyl region were observed. The major resonance in the Cp* region (δ 2.16) was unidentified, but two of the minor products were characterized as $[Cp^*Ir(CO)H]_2(\mu\text{-}H)^+$ and *trans*-$[Cp^*Ir(CO)]_2(\mu\text{-}CH_2)(\mu\text{-}H)^+$.[10] After standing for five days, the resonance at 2.16 ppm disappeared and the concentration of *trans*-$[Cp^*Ir(CO)]_2(\mu\text{-}CH_2)(\mu\text{-}H)^+$ increased to become the principal product.

Reaction of $Cp^*Ir(^{13}CO)H_2$ with $Cp^*Ir(CO)(CH_3)_2$ and $HBAr'_4\bullet(Et_2O)_2$. An NMR tube fitted with a high vacuum Teflon stopcock was charged with 3.6 mg of $Cp^*Ir(CO)(CH_3)_2$ (9.3 μmol). In a glove box, 10.0 mg of $HBAr'_4\bullet(Et_2O)_2$ (9.88 μmol, 1.1 equiv based upon dimethyl) and 11.4 mg of $Cp^*Ir(^{13}CO)H_2$ (31.8 μmol) were added. Methylene chloride-d_2 (0.5 mL) was vacuum transferred onto the solids, the contents frozen in a liquid N_2 bath, and the NMR tube flame-sealed under vacuum. The NMR tube was thawed in a CO_2/IPA bath for one hour generating a yellow-brown solution. Upon warming to room temperature, the solution immediately became dark blue-green. A ^1H NMR spectrum revealed the presence of only $\{[Cp^*Ir(CO)H]_2(\mu\text{-}H)\}BAr'_4$, $Cp^*Ir(CO)(CH_3)_2$, and CH_4. The NMR tube was slowly cooled to -30 °C overnight generating green crystals of $\{[Cp^*Ir(CO)H]_2(\mu\text{-}H)\}BAr'_4$, one of which was used for an X-ray structure determination (see Chapter 2).

Thermolysis of $Cp^*Ir(CO)H_2$ with $Cp^*Ir(CO)(CH_3)_2$. To an NMR tube fitted with a high vacuum Teflon stopcock were added 5.5 mg of $Cp^*Ir(CO)H_2$ (15 μmol) and 5.4 mg of $Cp^*Ir(CO)(CH_3)_2$ (14 μmol). Benzene-d_6 (0.5 mL) was vacuum transferred onto the solids. The NMR tube was flame-sealed under vacuum and placed in an oil bath heated to 47 °C. After 5 days, no reaction was apparent by ^1H NMR, and the bath temperature was increased to 85 °C. After two weeks of further heating, still no reaction between the starting materials had occurred, although $Cp^*Ir(CO)H_2$ had incorporated deuterium from the solvent into its Cp^* methyl groups (see Chapter 3 for further discussion of this topic).

$[Cp^*Ir(CO)(CH_3)]_2$ from $[Cp^*Ir(\mu\text{-}CO)]_2$. One side of an H-tube reactor was charged with 42 mg of $[Cp^*Ir(\mu\text{-}CO)]_2$ (59 μmol) and19 mg of a Na/K alloy (1:1 molar basis, 31 μmol K, 5.2 equiv K). Further manipulations were performed while shielded from light. THF (10 mL) was vacuum transferred onto the solids and the solution was left to stir overnight. The deep red-brown solution was filtered through the H-tube frit and methyl chloride (0.74 mmol) was condensed in. After stirring for 3.5 h with no apparent color change, the solvent was removed under vacuum leaving an oily brown residue. The residue was extracted with pentane (2 x 8 mL) and the orange-brown extracts passed through a medium frit. The pentane was removed under vacuum yielding heterogeneous brown-yellow solids. The major species present, as determined by ^1H NMR, were the cis and trans isomers of $[Cp^*Ir(CO)(CH_3)]_2$ (by comparison to the Rh analogues), which accounted for 52% (based upon total Cp^* region integrals) of the products. Also present were $[Cp^*Ir(\mu\text{-}CO)]_2$ and an unidentified resonance at δ 2.07. Recrystallization of a small sample of the crude solid from heptane at -30 °C produced *trans*-$[Cp^*Ir(CO)(CH_3)]_2$ as an orange microcrystalline solid. Attempts to purify $[Cp^*Ir(CO)(CH_3)]_2$ via chromatography were unsuccessful. *cis*-$[Cp^*Ir(CO)(CH_3)]_2$: ^1H NMR (CD_2Cl_2) δ: 1.83 (Cp^*, 30 H), -0.55 (CH_3, 6 H). *trans*-$[Cp^*Ir(CO)(CH_3)]_2$: ^1H

NMR (CD_2Cl_2) δ: 1.85 (Cp^*, 30 H), -0.21 (CH_3, 6 H); ^1H NMR (C_6D_6) δ: 1.68 (Cp^*), 0.40 (CH_3); IR (heptane): 1745 cm^{-1} (ν_{CO}).

$[Cp^*Ir(CO)(CH_3)]_2$ from $[Cp^*Ir(CO)H]_2$. An NMR tube fitted with a high vacuum Teflon stopcock was charged with 4.8 mg of $[Cp^*Ir(CO)H]_2$ (6.7 μmol). THF-d_8 (0.4 mL) was added via vacuum transfer yielding a clear, bright yellow solution. With the bottom of the tube immersed in a CO_2/IPA bath, 10 μL of *n*BuLi (1.6 M in hexanes, 2.4 equiv) was added via syringe. The solution was subjected to three freeze/pump/thaw (thaw to -60 °C) cycles and became orange-yellow. The solution was allowed to stand at -60 to -50 °C for 1.75 h with occasional shaking. Methyl chloride (49 μmol) was condensed in and the tube was flame-sealed. The predominant products are *cis*- and *trans*-$[Cp^*Ir(CO)(CH_3)]_2$, $[Cp^*Ir(\mu\text{-}CO)]_2$, and an unidentified compound with resonances at 2.06 (d, J = 0.9 Hz) and -19.83 ppm. A substantial quantity of $[Cp^*Ir(CO)H]_2$ remained unreacted. This reaction was also performed with MeLi (1.4 M in Et_2O) in place of *n*BuLi, with similar results.

Notes to Chapter 5

(1) Norton, J. R. *Acc. Chem. Res.* **1979**, *12*, 139-145.

(2) Stoutland, P. O.; Bergman, R. G.; Nolan, S. P.; Hoff, C. D. *Polyhedron* **1988**, *7*, 1429-1440.

(3) Morrison, R. T.; Boyd, R. N. *Organic Chemistry*; Allyn and Bacon: Boston, 1973.

(4) *Handbook of Chemistry and Physics*; 71st ed.; Lide, D. R., Ed.; CRC: Boca Raton, 1990.

(5) Norton, J. R.; Carter, W. J.; Kelland, J. W.; Okrasinski, S. J. *Adv. Chem. Ser.* **1978**, *167*, 170-180.

(6) Kelland, J. W.; Norton, J. R. *J. Organomet. Chem.* **1978**, *149*, 185-194.

(7) Carter, W. J.; Kelland, J. W.; Okrasinski, S. J.; Warner, K. E.; Norton, J. R. *Inorg. Chem.* **1982**, *21*, 3955-3960.

(8) Krause, M. J.; Bergman, R. G. *Organometallics* **1986**, *5*, 2097-2108.

(9) Collman, J. P.; Hegedus, L. S.; Norton, J. R.; Finke, R. G. *Principles and Applications of Organotransition Metal Chemistry*; University Science Books: Mill Valley, California, 1987.

(10) Heinekey, D. M.; Michel, S. T. *Organometallics* **1989**, *8*, 1241-1246.

(11) Isobe, K.; Vázquez de Miguel, A.; Maitlis, P. M. *J. Organomet. Chem.* **1983**, *250*, C25-C27.

(12) Gómez, M.; Kisenyi, J. M.; Sunley, G. J.; Maitlis, P. M. *J. Organomet. Chem.* **1985**, *296*, 197-207.

(13) Vázquez de Miguel, A.; Gómez, M.; Isobe, K.; Taylor, B. F.; Mann, B. E.; Maitlis, P. M. *Organometallics* **1983**, *2*, 1724-1730.

(14) Ball, R. G.; Graham, W. A. G.; Heinekey, D. M.; Hoyano, J. K.; McMaster, A. D.; Mattson, B. M.; Michel, S. T. *Inorg. Chem.* **1990**, *29*, 2023-2025.

(15) Hoyano, J. K.; McMaster, A. D.; Graham, W. A. G. *J. Am. Chem. Soc.* **1983**, *105*, 7190-7191.

(16) Monti, D.; Frachey, G.; Bassetti, M.; Haynes, A.; Sunley, G. J.; Maitlis, P. M.; Cantoni, A.; Bocelli, G. *Inorg. Chim. Acta* **1995**, *240*, 485-493.

(17) Heinekey, D. M.; Michel, S. T. , Yale University, unpublished results.

(18) Gilbert, T. M.; Bergman, R. G. *J. Am. Chem. Soc.* **1985**, *107*, 3502-3507.

(19) Heinekey, D. M.; Harper, T. G. P. , Yale University, unpublished results.

(20) Sterenberg, B. T.; Hilts, R. W.; Moro, G.; McDonald, R.; Cowie, M. *J. Am. Chem. Soc.* **1995**, *117*, 245-258.

(21) Kang, J. W.; Maitlis, P. M. *J. Organomet. Chem.* **1971**, *26*, 393-399.

Bibliography

Adams, R. D.; Cotton, F. A. In *Dynamic Nuclear Magnetic Resonance Spectroscopy*; Jackman, L. M. and Cotton, F. A., Eds.; Academic: New York, 1975; pp 489-522.

Alt, H. G.; Mahmoud, K. A.; Rest, A. J. *Angew. Chem. Int. Ed. Engl.* **1983**, *22*, 544-545.

Anderson, F. R.; Wrighton, M. S. *Inorg. Chem.* **1986**, *25*, 112-114.

Angoletta, M.; Ciani, G.; Manassero, M.; Sansoni, M. *J. Chem. Soc., Chem. Commun.* **1973**, 789-790.

Bahr, S. R.; Boudjouk, P. *J. Org. Chem.* **1992**, *57*, 5545-5547.

Ball, R. G.; Graham, W. A. G.; Heinekey, D. M.; Hoyano, J. K.; McMaster, A. D.; Mattson, B. M.; Michel, S. T. *Inorg. Chem.* **1990**, *29*, 2023-2025.

Banister, J. A.; Cooper, A. I.; Howdle, S. M.; Jobling, M.; Poliakoff, M. *Organometallics* **1996**, *15*, 1804-1812.

Bau, R.; Teller, R. G.; Kirtley, S. W.; Koetzle, T. F. *Acc. Chem. Res.* **1979**, *12*, 176-183.

Beringhelli, T.; Ciani, G.; D'Alfonso, G.; Garlaschelli, L.; Moret, M.; Sironi, A. *J. Chem. Soc., Dalton Trans.* **1992**, 1865-1866.

Bertrand, J. A.; Cotton, F. A.; Dollase, W. A. *J. Am. Chem. Soc.* **1963**, *85*, 1349-1350.

Bloyce, P. E.; Rest, A. J.; Whitwell, I.; Graham, W. A. G.; Holmes-Smith, R. *J. Chem. Soc., Chem. Commun.* **1988**, 846-848.

Brookhart, M.; Grant, B.; Volpe Jr., A. F. *Organometallics* **1992**, *11*, 3920-3922.

Brosset, C. *Nature* **1935**, *135*, 874.

Brosset, C. *Arkiv for Kemi, Miner. Geol.* **1946**, *A22*(11).

Brown, T. L. In *Organometallic Radical Processes*; Trogler, W. C., Ed.; Elsevier: Amsterdam, 1990; pp 67-107.

Brunner, H. *Adv. Organomet. Chem.* **1980**, *18*, 151-206.

Buchanan, M. J.; Stryker, J. M.; Bergman, R. G. *J. Am. Chem. Soc.* **1986**, *108*, 1537-1550.

Burns, C. J.; Rutherford, N. M.; Berg, D. J. *Acta Crystallog. Sect. C: Cryst. Struct. Commun.* **1987**, *43*, 229-231.

Bursten, B. E.; Cayton, R. H. *J. Am. Chem. Soc.* **1987**, *109*, 6053-6059.

Calderazzo, R. *Ann. N.Y. Acad. Sci.* **1983**, *415*, 37-46.

Carter, W. J.; Kelland, J. W.; Okrasinski, S. J.; Warner, K. E.; Norton, J. R. *Inorg. Chem.* **1982**, *21*, 3955-3960.

Casey, C. P.; Sakaba, H.; Hazin, P. N.; Powell, D. R. *J. Am. Chem. Soc.* **1991**, *113*, 8165-8166.

Chaudret, B.; Dahan, F.; Sabo, S. *Organometallics* **1985**, *4*, 1490-1492.

Chinn, M. S. Ph.D. Thesis, Yale University, 1989.

Reactivity of Metal-Metal Bonds; Chisholm, M. H., Ed.; ACS Symposium Series 155; American Chemical Society: Washington, D.C., 1981.

Churchill, M. R.; Deboer, B. G.; Rotella, F. J. *Inorg. Chem.* **1976**, *15*, 1843-1853.

Churchill, M. R. *Adv. Chem. Ser.* **1978**, *167*, 36-60.

Ciriano, M. A.; Sebastian, S.; Oro, L. A.; Tiripicchio, A.; Tiripicchio Camellini, M.; Lahoz, F. J. *Angew. Chem. Int. Ed. Engl.* **1988**, *27*, 402-403.

Clauss, A. D.; Dimas, P. A.; Shapley, J. R. *J. Organomet. Chem.* **1980**, *201*, C31-C34.

Collman, J. P.; Hegedus, L. S.; Norton, J. R.; Finke, R. G. *Principles and Applications of Organotransition Metal Chemistry*; University Science Books: Mill Valley, California, 1987.

Cotton, F. A.; DeBoer, B. G.; LaPrade, M. D.; Pipal, J. R.; Ucko, D. A. *J. Am. Chem. Soc.* **1970**, *92*, 2926-2927.

Cotton, F. A.; Walton, R. A. *Multiple Bonds between Metal Atoms;* 2nd ed.; Clarendon: Oxford, 1993.

Cox, R. A.; Krull, U. J.; Thompson, M.; Yates, K. *Anal. Chim. Acta* **1979**, *106*, 51-57.

Crabtree, R. H.; Quirk, J. M. *Synth. React. Inorg. Met.-Org. Chem.* **1982**, *12*(4), 407-413.

Curtis, M. D.; Fotinos, N. A.; Han, K. R.; Butler, W. M. *J. Am. Chem. Soc.* **1983**, *105*, 2686-2694.

Dahl, L. F. *Ann. N.Y. Acad. Sci.* **1983**, 1-26.

Davies, S. G.; Hibberd, J.; Simpson, S. J.; Watts, O. *J. Organomet. Chem.* **1983**, *241*, C31-C33.

Transition Metal Hydrides; Dedieu, A., Ed.; VCH: New York, 1992.

Dooley, T.; Fairhurst, G.; Chalk, C. D.; Tabatabaian, K.; White, C. *Transition Met. Chem.* **1978**, *3*, 299-302.

Edidin, R. T.; Norton, J. R. *J. Am. Chem. Soc.* **1986**, *108*, 948-953.

Einstein, F. W. B.; Jones, R. H.; Zhang, X.; Yan, X.; Negelkerke, R.; Sutton, D. *J. Chem. Soc., Chem. Commun.* **1989**, 1424-1426.

El Amouri, H.; Gruselle, M.; Jaouen, G. *Synth. React. Inorg. Met.-Org. Chem.* **1994**, *24*(3), 395-400.

Evans, J.; Norton, J. R. *J. Am. Chem. Soc.* **1974**, *96*, 7577-7578.

Evans, J.; Okrasinski, S. J.; Pribula, A. J.; Norton, J. R. *J. Am. Chem. Soc.* **1976**, *98*, 4000-4001.

Faller, J. W.; Anderson, A. S. *J. Am. Chem. Soc.* **1970**, *92*, 5852-5860.

Foley, H. C.; Morris, R. H.; Targos, T. S.; Geoffroy, G. L. *J. Am. Chem. Soc.* **1981**, *103*, 7337-7339.

Galakhov, M. V.; Gil, A.; de Jesús, E.; Royo, P. *Organometallics* **1995**, *14*, 3746-3750.

Geoffroy, G. L.; Bradley, M. G.; Pierantozzi, R. *Adv. Chem. Ser.* **1978**, *167*, 181-200.

Geoffroy, G. L.; Wrighton, M. S. *Organometallic Photochemistry*; Academic: New York, 1979.

Gilbert, T. M.; Bergman, R. G. *J. Am. Chem. Soc.* **1985**, *107*, 3502-3507.

Gilbert, T. M. Ph.D. Thesis, University of California, Berkeley, 1985.

Gilbert, T. M.; Bergman, R. G. *J. Am. Chem. Soc.* **1985**, *107*, 3508-3516.

Gill, D. S.; Maitlis, P. M. *J. Organomet. Chem.* **1975**, *87*, 359-364.

Glueck, D. S.; Newman Winslow, L. J.; Bergman, R. G. *Organometallics* **1991**, *10*, 1462-1479.

Gordon, A. J.; Ford, R. A. In *The Chemist's Companion*; John Wiley & Sons: New York, 1972.

Gómez, M.; Kisenyi, J. M.; Sunley, G. J.; Maitlis, P. M. *J. Organomet. Chem.* **1985**, *296*, 197-207.

Graham, W. A. G.; Hoyano, J. K.; McMaster, A. D. Presented at the 23rd International Conference on Coordination Chemistry, Boulder, CO, 1984; TH51-02.

Graham, W. A. G. *J. Organomet. Chem.* **1986**, *300*, 81-91.

Green, M.; Mills, R. M.; Pain, G. N.; Stone, F. G. A.; Woodward, P. *J. Chem. Soc., Dalton Trans.* **1982**, *7*, 1309-1319.

Green, M. L.; Mountford, P. *J. Chem. Soc., Chem. Commun.* **1989**, 732-734.

Grevels, F.-W.; Klotzbücher, W. E.; Seils, F.; Schaffner, K.; Takats, J. *J. Am. Chem. Soc.* **1990**, *112*, 1995-1996.

Griewe, G. L.; Hall, M. B. *Organometallics* **1988**, *7*, 1923-1930.

Halpern, J. *Inorg. Chim. Acta* **1982**, *62*, 31-37.

Halpern, J. In *Bonding Energetics in Organometallic Compounds*; Marks, T. J., Ed.; American Chemical Society: Washington, DC, 1990; pp 100-112.

Hamilton, D. G.; Crabtree, R. H. *J. Am. Chem. Soc.* **1988**, *110*, 4126-4133.

Heinekey, D. M.; Michel, S. T. *Organometallics* **1989**, *8*, 1241-1246.

Heinekey, D. M.; Millar, J. M.; Koetzle, T. F.; Payne, N. G.; Zilm, K. W. *J. Am. Chem. Soc.* **1990**, *112*, 909-919.

Heinekey, D. M.; Fine, D. A.; Harper, T. G. P.; Michel, S. T. *Can. J. Chem.* **1995**, *73*, 1116-1125.

Hembre, R. T.; Scott, C. P.; Norton, J. R. *J. Am. Chem. Soc.* **1987**, *109*, 3468-3470.

Hembre, R. T.; Ramage, D. L.; Scott, C. P.; Norton, J. R. *Organometallics* **1994**, *13*, 2995-3001.

Herrmann, W. A.; Krüger, C.; Goddard, R.; Bernal, I. *Angew. Chem. Int. Ed. Engl.* **1977**, *16*, 334.

Herrmann, W. A.; Plank, J.; Riedel, D.; Ziegler, M. L.; Weidenhammer, K.; Guggolz, E.; Balbach, B. *J. Am. Chem. Soc.* **1981**, *103*, 63-75.

Hill, R. H.; de Mayo, P.; Puddephatt, R. J. *Inorg. Chem.* **1982**, *21*, 3642-3646.

Hill, R. H.; Puddephatt, R. J. *Organometallics* **1983**, 2, 1472-1474.

Hill, R. H.; Puddephatt, R. J. *J. Am. Chem. Soc.* **1983**, *105*, 5797-5804.

Hoffmann, R. *Angew. Chem. Int. Ed. Engl.* **1982**, *21*, 711-724.

Hoffmann, R. In *IUPAC Frontiers of Chemistry*; Laidler, K. J., Ed.; Pergamon: Oxford, 1982; pp 247-263.

Hofmann, P. *Angew. Chem. Int. Ed. Engl.* **1979**, *18*(7), 554-556.

Hoyano, J. K.; Graham, W. A. G. *J. Am. Chem. Soc.* **1982**, *104*, 3722-3723.

Hoyano, J. K.; Graham, W. A. G. *J. Am. Chem. Soc.* **1982**, *104*, 3723-3725.

Hoyano, J. K.; McMaster, A. D.; Graham, W. A. G. *J. Am. Chem. Soc.* **1983**, *105*, 7190-7191.

Isobe, K.; Vázquez de Miguel, A.; Maitlis, P. M. *J. Organomet. Chem.* **1983**, *250*, C25-C27.

Janowicz, A. H.; Bergman, R. G. *J. Am. Chem. Soc.* **1982**, *104*, 352-354.

Janowicz, A. H.; Bergman, R. G. *J. Am. Chem. Soc.* **1983**, *105*, 3929-3939.

Jesson, J. P.; Meakin, P. *Acc. Chem. Res.* **1973**, *6*, 269-275.

Kaesz, H. D.; Saillant, R. B. *Chem. Rev.* **1972**, *72*, 231-281.

Kang, J. W.; Moseley, K.; Maitlis, P. M. *J. Am. Chem. Soc.* **1969**, *91*, 5970-5977.

Kang, J. W.; Maitlis, P. M. *J. Organomet. Chem.* **1971**, *26*, 393-399.

Kauffman, G. B.; Meyers, R. D. *Inorg. Synth.* **1978**, *18*, 131-133.

Kelland, J. W.; Norton, J. R. *J. Organomet. Chem.* **1978**, *149*, 185-194.

Kellenberger, B.; Young, S. J.; Stille, J. K. *J. Am. Chem. Soc.* **1985**, *107*, 6105-6107.

King Jr., W. R.; Garner, C. S. *J. Chem. Phys.* **1950**, *18*, 689-691.

Koval, C. A.; Margerum, D. W. *Inorg. Chem.* **1981**, *20*, 2311-2318.

Krause, M. J.; Bergman, R. G. *Organometallics* **1986**, *5*, 2097-2108.

Krusic, P. J.; Jones, D. J.; Roe, D. C. *Organometallics* **1986**, *5*, 456-460.

Laine, R. M.; Ford, P. C. *Inorg. Chem.* **1977**, *16*, 388-391.

Lee, W. S.; Brintzinger, H. H. *J. Organomet. Chem.* **1977**, *127*, 87-92.

Legdzins, P.; Martin, D. T.; Nurse, C. R.; Wassink, B. *Organometallics* **1983**, *2*, 1238-1244.

Legdzins, P.; Martin, J. T.; Oxley, J. C. *Organometallics* **1985**, *4*, 1263-1271.

Handbook of Chemistry and Physics; 71st ed.; Lide, D. R., Ed.; CRC: Boca Raton, 1990.

Mahmoud, K. A.; Rest, A. J.; Alt, H. G. *J. Chem. Soc., Dalton Trans.* **1985**, 1365-1374.

Maitlis, P. M.; White, C.; Oliver, A. J. *J. Chem. Soc., Dalton Trans.* **1973**, 1901-1907.

Maitlis, P. M.; Long, H. C.; Quyoum, R.; Turner, M. L.; Wang, Z.-Q. *J. Chem. Soc., Chem. Commun.* **1996**, 1-8.

Marks, T. *Acc. Chem. Res.* **1992**, *25*, 57-65.

McAlister, D. R.; Erwin, D. K.; Bercaw, J. E. *J. Am. Chem. Soc.* **1978**, *100*, 5966-5968.

McDonald, R.; Sutherland, B. R.; Cowie, M. *Inorg. Chem.* **1987**, *26*, 3333-3339.

McGhee, W. D.; Foo, T.; Hollander, F. J.; Bergman, R. G. *J. Am. Chem. Soc.* **1988**, *110*, 8543-8545.

McGhee, W. D.; Hollander, F. J.; Bergman, R. G. *J. Am. Chem. Soc.* **1988**, *110*(25), 8428-8443.

Michel, S. Ph.D. Thesis, Yale University, Dec. 1989.

Monti, D.; Frachey, G.; Bassetti, M.; Haynes, A.; Sunley, G. J.; Maitlis, P. M.; Cantoni, A.; Bocelli, G. *Inorg. Chim. Acta* **1995**, *240*, 485-493.

Morrison, R. T.; Boyd, R. N. *Organic Chemistry*; Allyn and Bacon: Boston, 1973.

Moss, J. R.; Graham, W. A. G. *J. Chem. Soc., Dalton Trans.* **1977**, 89-94.

Moss, J. R.; Graham, W. A. G. *Inorg. Chem.* **1977**, *16*, 75-79.

Motyl, K. M.; Norton, J. R.; Schauer, C. K.; Anderson, O. P. *J. Am. Chem. Soc.* **1982**, *104*, 7325-7327.

Transition Metal Hydrides; Muetterties, E. L., Ed.; Marcel Dekker: New York, 1971.

Muetterties, E. L.; Rhodin, T. N.; Band, E.; Brucker, C. F.; Pretzer, W. R. *Chem. Rev.* **1979**, *79*, 91-137.

Muetterties, E. L.; Krause, M. J. *Angew. Chem. Int. Ed. Engl.* **1983**, *22*, 135-148.

Norton, J. R.; Carter, W. J.; Kelland, J. W.; Okrasinski, S. J. *Adv. Chem. Ser.* **1978**, *167*, 170-180.

Norton, J. R. *Acc. Chem. Res.* **1979**, *12*, 139-145.

Ogilvy, A. E.; Rauchfuss, T. B. *Organometallics* **1988**, *7*, 1884-1885.

Parkin, G.; Bercaw, J. E. *Polyhedron* **1988**, *7*, 2053-2082.

Parkin, G.; Bercaw, J. E. *Organometallics* **1989**, *8*, 1172-1179.

Pearson, R. G. *Symmetry Rules for Chemical Reactions*; Wiley-Interscience: New York, 1976.

Pedersen, A.; Tilset, M. *Organometallics* **1994**, *13*, 4887-4894.

Pinhas, A. R.; Hoffmann, R. *Inorg. Chem.* **1979**, *18*(3), 654-658.

Pinhas, A. R.; Albright, T. A.; Hofmann, P.; Hoffmann, R. *Helv. Chim. Acta* **1980**, *63*(4), 29-49.

Plank, J.; Riedel, D.; Herrmann, W. A. *Angew. Chem. Int. Ed. Engl.* **1980**, *19*, 937-938.

Radzewich, C. E. Ph.D. Thesis, University of Washington, 1997.

Rasmussen, P. G.; Anderson, J. E.; Bailey, O. H.; Tamres, M. *J. Am. Chem. Soc.* **1985**, *107*, 279-281.

Rerek, M. E.; Basolo, F. *Organometallics* **1983**, *2*(3), 372-376.

Rest, A. J.; Whitwell, I.; Graham, W. A. G.; Hoyano, J. K.; McMaster, A. D. *J. Chem. Soc., Dalton Trans.* **1987**, 1181-1190.

Robinson, W. T.; Fergusson, J. E.; Penfold, B. R. *Proc. Chem. Soc.* **1963**, 116.

Sattelberger, A. P.; Wilson Jr., R. B.; Huffman, J. C. *J. Am. Chem. Soc.* **1980**, *102*, 7111-7113.

Selmeczy, A. D.; Jones, W. D.; Partridge, M. G.; Perutz, R. N. *Organometallics* **1994**, *13*, 522-532.

Shanan-Atidi, H.; Bar-Eli, K. H. *J. Phys. Chem.* **1970**, *74*(4), 961-963.

Shapley, J. R.; Adair, P. C.; Lawson, R. J.; Pierpont, C. G. *Inorg. Chem.* **1982**, *21*, 1701-1702.

Siedle, A. R.; Newmark, R. A.; Pignolet, L. H.; Howells, R. D. *J. Am. Chem. Soc.* **1984**, *106*, 1510-1511.

Siegel, J. S.; Anet, F. A. L. *J. Org. Chem.* **1988**, *53*, 2629-2630.

Sloan, T. E. In *Topics in Inorganic and Organometallic Stereochemistry*; Geoffroy, G. L., Ed.; Wiley: New York, 1981; Vol. 12; pp 1-36.

Somorjai, G. A. *Pure Appl. Chem.* **1988**, *60*, 1499-1516.

Somorjai, G. A. In *Perspectives in Catalysis*; Thomas, J. M. and Zamaraev, K. I., Eds.; Blackwell Scientific: Oxford, 1992; pp 147-167.

Sterenberg, B. T.; Hilts, R. W.; Moro, G.; McDonald, R.; Cowie, M. *J. Am. Chem. Soc.* **1995**, *117*, 245-258.

Stoutland, P. O.; Bergman, R. G.; Nolan, S. P.; Hoff, C. D. *Polyhedron* **1988**, *7*, 1429-1440.

Sweet, J. R. Ph.D. Thesis, University of Alberta, 1981.

Threlkel, R. S.; Bercaw, J. E.; Seidler, P. F.; Stryker, J. M.; Bergman, R. G. *Org. Synth.* **1987**, *65*, 42-45.

Tilset, M.; Vollhardt, K. P. C.; Boese, R. *Organometallics* **1994**, *13*, 3146-3169.

Ting, C. T.; Baenziger, N. C.; Messerle, L. *J. Chem. Soc., Chem. Commun.* **1988**, 1133-1135.

Trinquier, G.; Hoffmann, R. *Organometallics* **1984**, *3*, 370-380.

Van Geet, A. L. *Anal. Chem.* **1970**, *42*(6), 679-680.

Vázquez de Miguel, A.; Gómez, M.; Isobe, K.; Taylor, B. F.; Mann, B. E.; Maitlis, P. M. *Organometallics* **1983**, *2*, 1724-1730.

Venanzi, L. M. *Coord. Chem. Rev.* **1982**, *43*, 251-274.

Voges, M. H. Ph.D. Thesis, University of Washington, 1996.

Werner, H.; Wolf, J. *Angew. Chem. Int. Ed. Engl.* **1982**, *21*(4), 296-297.

Werner, H.; Treiber, M.; Nessel, A.; Lippert, F.; Betz, P.; Kruger, C. *Chem. Ber.* **1992**, *125*, 337-346.

Winter, M. J. *Adv. Organomet. Chem.* **1989**, *29*, 101-162.

Young, S. J.; Kellenberger, B.; Reibenspies, J. H.; Himmel, S. E.; Manning, M.; Anderson, O. P.; Stille, J. K. *J. Am. Chem. Soc.* **1988**, *110*, 5744-5753.

Appendix A

Supplementary X-ray Data for {[$Cp^*Ir(CO)H]_2(\mu$-H)}BAr'_4

Table 1. Atomic coordinates ($x10^5$) and equivalent isotropic displacement coefficients ($Å^2 x10^4$)

	x	y	z	U(eq)
Ir(1)	-8521(3)	19686(2)	54601(2)	320(2)
Ir(2)	8350(3)	28245(2)	47801(2)	302(2)
C(1)	-10450(108)	20164(70)	46085(71)	563(63)
O(1)	-11584(100)	20495(65)	41137(48)	968(64)
C(2)	13371(95)	19625(67)	47685(52)	427(51)
O(2)	16632(76)	14602(45)	47486(42)	594(41)
C(3)	-16781(83)	10839(53)	60896(51)	313(43)
C(3M)	-26617(92)	8534(71)	59229(64)	552(60)
C(4)	-6255(87)	8222(53)	60253(55)	349(45)
C(4M)	-2700(117)	2866(71)	57486(72)	658(69)
C(5)	218(76)	11156(53)	62971(51)	301(42)
C(5M)	12084(87)	9481(69)	63853(65)	503(59)
C(6)	-5990(79)	15784(56)	65188(53)	326(45)
C(6M)	-2263(101)	19668(66)	68860(60)	512(55)
C(7)	-16552(79)	15354(57)	64143(47)	331(43)
C(7M)	-25979(87)	18782(65)	66461(64)	523(55)
C(8)	14205(90)	38565(61)	45003(57)	433(49)
C(8M)	21412(104)	40515(70)	48813(69)	610(64)
C(9)	16957(80)	36056(54)	40051(50)	332(42)
C(9M)	27936(97)	35199(76)	37655(63)	639(62)
C(10)	7718(92)	35566(59)	37141(56)	419(49)
C(10M)	7359(112)	33434(72)	31427(60)	578(61)
C(11)	-1123(77)	37271(54)	40570(51)	311(43)
C(11M)	-12207(91)	38036(71)	38710(66)	574(59)
C(12)	2661(97)	39157(55)	45442(54)	412(47)
C(12M)	-3981(109)	41740(61)	49846(59)	533(56)
B(1)	-53715(88)	-4474(66)	75224(61)	290(50)
C(1S)	-59016(73)	-11686(52)	76649(46)	251(41)
C(2S)	-69626(79)	-11448(58)	75485(53)	332(46)
C(3S)	-74514(84)	-17323(61)	76549(54)	358(49)
C(4S)	-68970(86)	-23888(61)	78881(52)	368(49)
C(5S)	-58556(83)	-24102(53)	80240(49)	302(43)
C(6S)	-53820(77)	-18178(54)	79087(49)	272(42)
C(7S)	-85884(90)	-16706(74)	75142(73)	494(64)
F(1)	-88068(69)	-19925(82)	71839(61)	1413(92)
F(2)	-91353(72)	-20243(79)	80636(62)	1412(83)
F(3)	-90306(75)	-11064(53)	73162(95)	1963(111)
C(8S)	-52359(108)	-30795(59)	82735(66)	474(56)
F(4)	-48413(151)	-32647(71)	78386(64)	2028(104)
F(5)	-44637(73)	-31245(40)	86253(48)	917(47)
F(6)	-57405(89)	-35959(50)	86293(96)	1853(102)
C(9S)	-40830(76)	-5516(49)	75316(49)	250(40)
C(10S)	-34778(84)	-2609(51)	78407(49)	295(41)
C(11S)	-23960(77)	-3724(54)	78275(52)	306(44)
C(12S)	-18727(76)	-7614(59)	75094(56)	358(46)
C(13S)	-24558(80)	-10457(55)	72087(51)	326(44)
C(14S)	-35570(78)	-9256(53)	71886(49)	293(41)
C(15S)	-17770(91)	-671(71)	81635(60)	438(57)
F(7)	-22055(100)	-571(88)	87020(66)	1575(102)
F(8)	-9095(86)	-3899(72)	83819(81)	1679(105)
F(9)	-15939(132)	5395(55)	78625(58)	1784(83)
C(16S)	-19287(91)	-14691(69)	68835(61)	464(55)
F(10)	-11570(81)	-18814(64)	71980(56)	1236(68)
F(11)	-14180(103)	-11120(61)	63311(57)	1325(72)

F(12)	-25302(60)	-18196(52)	66918(55)	935(59)
C(17S)	-58673(74)	-2192(49)	81137(48)	238(39)
C(18S)	-66757(76)	2998(51)	80381(51)	275(42)
C(19S)	-70631(73)	4513(51)	85563(50)	260(41)
C(20S)	-67306(77)	915(53)	91935(51)	287(43)
C(21S)	-59388(77)	-4495(53)	92747(48)	268(41)
C(22S)	-55145(76)	-6005(53)	87473(49)	280(41)
C(23S)	-79218(90)	10055(64)	84531(60)	428(54)
F(13)	-77215(73)	14292(43)	87483(46)	862(46)
F(14)	-88337(61)	7813(45)	86858(53)	970(49)
F(15)	-80410(51)	14285(36)	78416(34)	533(31)
C(24S)	-55128(82)	-8788(60)	99340(50)	330(48)
F(16)	-60609(57)	-7497(40)	104106(31)	570(32)
F(17)	-45317(50)	-7711(36)	99829(31)	494(29)
F(18)	-55200(52)	-15415(32)	100790(30)	462(28)
C(25S)	-56751(76)	926(56)	68162(51)	303(44)
C(26S)	-59477(78)	-1142(56)	63081(50)	305(44)
C(27S)	-61798(78)	3697(60)	56770(52)	331(47)
C(28S)	-61515(75)	10817(54)	55085(52)	292(43)
C(29S)	-58853(73)	12877(51)	59923(47)	257(40)
C(30S)	-56557(72)	8149(56)	66185(46)	274(42)
C(31S)	-65025(94)	1157(63)	51928(54)	415(53)
F(19)	-59398(53)	-4675(35)	52217(33)	490(31)
F(20)	-63962(59)	5634(40)	45772(32)	583(34)
F(21)	-74937(53)	-192(41)	52826(37)	596(37)
C(32S)	-59170(86)	20223(60)	58739(55)	379(49)
F(22)	-60752(56)	24433(33)	52402(31)	519(29)
F(23)	-67139(58)	22298(33)	61962(35)	553(31)
F(24)	-50578(57)	21968(35)	60222(37)	613(33)
Ir(3)	-9741(3)	24656(2)	93583(2)	291(2)
Ir(4)	8629(3)	24312(2)	100807(2)	302(2)
C(13)	433(89)	25220(55)	87005(58)	360(48)
O(13)	6185(66)	25599(45)	82856(39)	498(37)
C(14)	10211(86)	15611(72)	100571(57)	439(55)
O(14)	11642(84)	10026(48)	100623(47)	681(47)
C(15)	-16590(82)	14310(53)	96096(53)	312(44)
C(15M)	-11454(94)	7746(63)	96037(68)	526(59)
C(16)	-21595(78)	19954(57)	90692(50)	299(46)
C(16M)	-22632(103)	19843(68)	84067(60)	511(59)
C(17)	-26775(74)	24744(54)	92877(53)	294(44)
C(17M)	-33947(89)	31031(63)	89177(63)	526(56)
C(18)	-24214(75)	22637(59)	99682(47)	295(44)
C(18M)	-28520(101)	25843(72)	104306(66)	566(65)
C(19)	-18188(77)	16073(55)	101519(54)	321(45)
C(19M)	-14861(96)	11786(64)	108327(56)	468(53)
C(20)	15923(78)	34013(51)	93935(50)	282(41)
C(20M)	13782(90)	38173(57)	86964(51)	396(46)
C(21)	23762(74)	28478(54)	96134(48)	267(42)
C(21M)	31120(88)	25921(66)	91922(61)	464(55)
C(22)	23907(75)	25987(54)	103244(52)	293(44)
C(22M)	31871(88)	20687(62)	107558(60)	471(53)
C(23)	16480(85)	30271(55)	105225(49)	337(44)
C(23M)	14889(113)	30199(75)	111813(60)	600(65)
C(24)	11091(79)	34907(51)	99411(53)	312(43)
C(24M)	3069(103)	40606(64)	99108(68)	573(60)
B(2)	45435(83)	48810(55)	73225(54)	197(43)
C(33S)	58164(73)	47801(50)	74134(48)	265(39)
C(34S)	64651(73)	45039(51)	70471(49)	261(40)
C(35S)	75633(84)	44052(53)	71225(50)	317(43)

C(36S)	80214(80)	45988(58)	75549(54)	338(46)
C(37S)	73959(81)	49049(52)	78952(51)	298(42)
C(38S)	63026(75)	49985(49)	78360(50)	263(40)
C(39S)	82271(89)	40837(67)	67349(61)	433(55)
F(25)	77086(56)	39363(65)	63245(53)	1119(71)
F(26)	89599(54)	44698(41)	63866(35)	619(35)
F(27)	87556(60)	34943(39)	71319(41)	669(38)
C(40S)	78378(89)	50886(66)	84156(64)	431(57)
F(28)	75650(72)	57478(45)	83024(48)	869(49)
F(29)	75684(78)	47213(55)	90036(38)	936(51)
F(30)	88711(54)	50383(49)	83853(41)	742(46)
C(41S)	39176(70)	49866(48)	79504(46)	204(37)
C(42S)	42220(75)	45656(50)	85812(50)	258(40)
C(43S)	37058(84)	46126(49)	91210(48)	296(41)
C(44S)	28135(81)	50759(52)	90714(51)	304(44)
C(45S)	24952(73)	54713(50)	84392(48)	234(40)
C(46S)	30266(77)	54359(52)	78977(50)	284(42)
C(47S)	41279(94)	41699(71)	97785(53)	441(56)
F(31)	34827(75)	41927(54)	102517(35)	1048(49)
F(32)	50290(67)	43596(41)	98720(39)	782(39)
F(33)	43091(61)	35205(35)	98762(34)	578(32)
C(48S)	15335(84)	59541(61)	83811(59)	386(51)
F(34)	6683(49)	56266(39)	85412(51)	814(46)
F(35)	15108(55)	63056(37)	87583(37)	583(34)
F(36)	14098(56)	64255(37)	77782(34)	588(32)
C(49S)	43456(67)	55612(51)	66476(47)	229(40)
C(50S)	43270(70)	62368(51)	66153(49)	254(41)
C(51S)	41794(76)	68126(50)	60472(49)	267(41)
C(52S)	40646(79)	67547(52)	54627(50)	293(42)
C(53S)	41048(79)	60802(57)	54761(50)	315(44)
C(54S)	42492(75)	55110(51)	60437(47)	257(40)
C(55S)	41413(97)	74980(59)	60397(56)	415(51)
F(37)	39132(84)	80071(35)	55046(37)	848(43)
F(38)	34869(76)	75986(39)	64869(45)	833(44)
F(39)	50731(76)	76394(45)	61960(59)	1025(60)
C(56S)	40067(115)	60136(64)	48513(58)	504(56)
F(40)	35648(100)	54549(48)	49121(40)	1076(55)
F(41)	35267(83)	65278(42)	43999(39)	897(45)
F(42)	49169(89)	59403(65)	45709(46)	1131(64)
C(57S)	40770(71)	42221(50)	72835(45)	217(38)
C(58S)	45716(75)	35642(50)	75020(46)	248(40)
C(59S)	40914(78)	30071(51)	74869(47)	269(40)
C(60S)	30941(79)	30771(51)	72707(48)	274(41)
C(61S)	25663(76)	37406(52)	70553(51)	284(43)
C(62S)	30545(74)	42845(50)	70777(46)	245(39)
C(63S)	46970(87)	23136(58)	77203(59)	382(51)
F(43)	56186(58)	23349(39)	74099(40)	668(37)
F(44)	49226(63)	20932(37)	83498(35)	647(34)
F(45)	42144(62)	18397(37)	76466(47)	750(42)
C(64S)	14724(83)	38608(61)	68414(53)	364(48)
F(46)	7974(50)	40308(43)	72307(35)	590(36)
F(47)	11212(52)	33313(36)	67627(40)	591(35)
F(48)	13757(52)	43966(38)	62567(32)	555(31)

* Equivalent isotropic U defined as one third of the trace of the orthogonalized U_{ij} tensor

Table 2. Bond lengths (Å)

Ir(1)-Ir(2)	2.935 (1)	Ir(1)-C(1)	1.897 (17)
Ir(1)-C(3)	2.195 (10)	Ir(1)-C(4)	2.256 (10)
Ir(1)-C(5)	2.284 (9)	Ir(1)-C(6)	2.214 (11)
Ir(1)-C(7)	2.208 (9)	Ir(2)-C(2)	1.883 (14)
Ir(2)-C(8)	2.230 (13)	Ir(2)-C(9)	2.213 (9)
Ir(2)-C(10)	2.282 (10)	Ir(2)-C(11)	2.256 (9)
Ir(2)-C(12)	2.214 (11)	C(1)-O(1)	1.099 (20)
C(2)-O(2)	1.119 (17)	C(3)-C(3M)	1.520 (19)
C(3)-C(4)	1.430 (15)	C(3)-C(7)	1.413 (19)
C(4)-C(4M)	1.512 (22)	C(4)-C(5)	1.384 (18)
C(5)-C(5M)	1.538 (15)	C(5)-C(6)	1.419 (17)
C(6)-C(6M)	1.497 (21)	C(6)-C(7)	1.411 (15)
C(7)-C(7M)	1.518 (17)	C(8)-C(8M)	1.486 (22)
C(8)-C(9)	1.417 (19)	C(8)-C(12)	1.479 (17)
C(9)-C(9M)	1.500 (16)	C(9)-C(10)	1.421 (17)
C(10)-C(10M)	1.517 (22)	C(10)-C(11)	1.428 (16)
C(11)-C(11M)	1.484 (16)	C(11)-C(12)	1.424 (19)
C(12)-C(12M)	1.491 (19)	B(1)-C(1S)	1.650 (18)
B(1)-C(9S)	1.650 (15)	B(1)-C(17S)	1.651 (19)
B(1)-C(25S)	1.589 (14)	C(1S)-C(2S)	1.398 (14)
C(1S)-C(6S)	1.379 (14)	C(2S)-C(3S)	1.386 (18)
C(3S)-C(4S)	1.409 (16)	C(3S)-C(7S)	1.497 (16)
C(4S)-C(5S)	1.384 (16)	C(5S)-C(6S)	1.381 (16)
C(5S)-C(8S)	1.469 (15)	C(7S)-F(1)	1.245 (26)
C(7S)-F(2)	1.363 (17)	C(7S)-F(3)	1.193 (17)
C(8S)-F(4)	1.247 (23)	C(8S)-F(5)	1.277 (18)
C(8S)-F(6)	1.290 (16)	C(9S)-C(10S)	1.401 (18)
C(9S)-C(14S)	1.405 (17)	C(10S)-C(11S)	1.388 (14)
C(11S)-C(12S)	1.387 (18)	C(11S)-C(15S)	1.476 (21)
C(12S)-C(13S)	1.361 (19)	C(13S)-C(14S)	1.414 (14)
C(13S)-C(16S)	1.456 (20)	C(15S)-F(7)	1.301 (21)
C(15S)-F(8)	1.263 (16)	C(15S)-F(9)	1.238 (17)
C(16S)-F(10)	1.290 (15)	C(16S)-F(11)	1.346 (16)
C(16S)-F(12)	1.321 (20)	C(17S)-C(18S)	1.398 (14)
C(17S)-C(22S)	1.404 (13)	C(18S)-C(19S)	1.372 (17)
C(19S)-C(20S)	1.396 (14)	C(19S)-C(23S)	1.483 (15)
C(20S)-C(21S)	1.414 (14)	C(21S)-C(22S)	1.405 (17)
C(21S)-C(24S)	1.498 (13)	C(23S)-F(13)	1.357 (20)
C(23S)-F(14)	1.314 (14)	C(23S)-F(15)	1.318 (13)
C(24S)-F(16)	1.344 (14)	C(24S)-F(17)	1.325 (13)
C(24S)-F(18)	1.314 (14)	C(25S)-C(26S)	1.441 (19)
C(25S)-C(30S)	1.422 (16)	C(26S)-C(27S)	1.410 (13)
C(27S)-C(28S)	1.411 (17)	C(27S)-C(31S)	1.480 (20)
C(28S)-C(29S)	1.387 (18)	C(29S)-C(30S)	1.394 (12)
C(29S)-C(32S)	1.471 (17)	C(31S)-F(19)	1.346 (15)
C(31S)-F(20)	1.342 (12)	C(31S)-F(21)	1.324 (14)
C(32S)-F(22)	1.362 (12)	C(32S)-F(23)	1.353 (15)
C(32S)-F(24)	1.302 (15)	Ir(3)-Ir(4)	2.921 (1)
Ir(3)-C(13)	1.887 (12)	Ir(3)-C(15)	2.302 (11)
Ir(3)-C(16)	2.164 (13)	Ir(3)-C(17)	2.205 (10)
Ir(3)-C(18)	2.220 (9)	Ir(3)-C(19)	2.306 (10)
Ir(4)-C(14)	1.856 (16)	Ir(4)-C(20)	2.291 (9)
Ir(4)-C(21)	2.252 (10)	Ir(4)-C(22)	2.172 (11)
Ir(4)-C(23)	2.227 (13)	Ir(4)-C(24)	2.200 (11)
C(13)-O(13)	1.135 (15)	C(14)-O(14)	1.175 (19)
C(15)-C(15M)	1.481 (18)	C(15)-C(16)	1.452 (13)

C(15)-C(19)	1.400	(19)	C(16)-C(16M)	1.505	(19)
C(16)-C(17)	1.386	(18)	C(17)-C(17M)	1.511	(14)
C(17)-C(18)	1.457	(15)	C(18)-C(18M)	1.497	(21)
C(18)-C(19)	1.439	(15)	C(19)-C(19M)	1.497	(15)
C(20)-C(20M)	1.487	(14)	C(20)-C(21)	1.412	(13)
C(20)-C(24)	1.410	(17)	C(21)-C(21M)	1.504	(18)
C(21)-C(22)	1.467	(15)	C(22)-C(22M)	1.507	(14)
C(22)-C(23)	1.420	(17)	C(23)-C(23M)	1.470	(19)
C(23)-C(24)	1.450	(13)	C(24)-C(24M)	1.487	(17)
B(2)-C(33S)	1.644	(14)	B(2)-C(41S)	1.657	(16)
B(2)-C(49S)	1.640	(12)	B(2)-C(57S)	1.613	(17)
C(33S)-C(34S)	1.379	(16)	C(33S)-C(38S)	1.405	(17)
C(34S)-C(35S)	1.417	(14)	C(35S)-C(36S)	1.371	(19)
C(35S)-C(39S)	1.482	(19)	C(36S)-C(37S)	1.360	(17)
C(37S)-C(38S)	1.407	(14)	C(37S)-C(40S)	1.520	(21)
C(39S)-F(25)	1.314	(20)	C(39S)-F(26)	1.321	(14)
C(39S)-F(27)	1.356	(13)	C(40S)-F(28)	1.331	(17)
C(40S)-F(29)	1.288	(14)	C(40S)-F(30)	1.323	(13)
C(41S)-C(42S)	1.396	(13)	C(41S)-C(46S)	1.391	(13)
C(42S)-C(43S)	1.376	(16)	C(43S)-C(44S)	1.410	(14)
C(43S)-C(47S)	1.499	(14)	C(44S)-C(45S)	1.393	(13)
C(45S)-C(46S)	1.379	(16)	C(45S)-C(48S)	1.498	(15)
C(47S)-F(31)	1.319	(15)	C(47S)-F(32)	1.321	(17)
C(47S)-F(33)	1.305	(17)	C(48S)-F(34)	1.332	(13)
C(48S)-F(35)	1.323	(18)	C(48S)-F(36)	1.335	(12)
C(49S)-C(50S)	1.404	(16)	C(49S)-C(54S)	1.409	(17)
C(50S)-C(51S)	1.382	(12)	C(51S)-C(52S)	1.377	(17)
C(51S)-C(55S)	1.443	(18)	C(52S)-C(53S)	1.414	(17)
C(53S)-C(54S)	1.374	(12)	C(53S)-C(56S)	1.472	(19)
C(55S)-F(37)	1.284	(12)	C(55S)-F(38)	1.336	(16)
C(55S)-F(39)	1.363	(18)	C(56S)-F(40)	1.324	(19)
C(56S)-F(41)	1.289	(14)	C(56S)-F(42)	1.319	(18)
C(57S)-C(58S)	1.381	(13)	C(57S)-C(62S)	1.396	(14)
C(58S)-C(59S)	1.403	(16)	C(59S)-C(60S)	1.371	(15)
C(59S)-C(63S)	1.500	(14)	C(60S)-C(61S)	1.407	(14)
C(61S)-C(62S)	1.390	(17)	C(61S)-C(64S)	1.478	(15)
C(63S)-F(43)	1.335	(14)	C(63S)-F(44)	1.338	(15)
C(63S)-F(45)	1.303	(17)	C(64S)-F(46)	1.316	(15)
C(64S)-F(47)	1.330	(17)	C(64S)-F(48)	1.359	(11)

Table 3. Bond angles (°)

Ir(2)-Ir(1)-C(1)	80.9(4)	Ir(2)-Ir(1)-C(3)	161.4(3)
C(1)-Ir(1)-C(3)	104.2(5)	Ir(2)-Ir(1)-C(4)	124.3(3)
C(1)-Ir(1)-C(4)	101.5(5)	C(3)-Ir(1)-C(4)	37.5(4)
Ir(2)-Ir(1)-C(5)	101.6(3)	C(1)-Ir(1)-C(5)	128.6(5)
C(3)-Ir(1)-C(5)	61.1(4)	C(4)-Ir(1)-C(5)	35.5(5)
Ir(2)-Ir(1)-C(6)	108.7(3)	C(1)-Ir(1)-C(6)	162.8(5)
C(3)-Ir(1)-C(6)	62.3(4)	C(4)-Ir(1)-C(6)	61.3(5)
C(5)-Ir(1)-C(6)	36.8(4)	Ir(2)-Ir(1)-C(7)	142.5(3)
C(1)-Ir(1)-C(7)	136.4(5)	C(3)-Ir(1)-C(7)	37.4(5)
C(4)-Ir(1)-C(7)	61.9(4)	C(5)-Ir(1)-C(7)	61.2(4)
C(6)-Ir(1)-C(7)	37.2(4)	Ir(1)-Ir(2)-C(2)	77.8(4)
Ir(1)-Ir(2)-C(8)	144.4(3)	C(2)-Ir(2)-C(8)	137.5(5)
Ir(1)-Ir(2)-C(9)	160.2(3)	C(2)-Ir(2)-C(9)	107.0(5)
C(8)-Ir(2)-C(9)	37.2(5)	Ir(1)-Ir(2)-C(10)	123.5(3)
C(2)-Ir(2)-C(10)	105.0(5)	C(8)-Ir(2)-C(10)	61.7(5)
C(9)-Ir(2)-C(10)	36.8(4)	Ir(1)-Ir(2)-C(11)	99.7(3)
C(2)-Ir(2)-C(11)	131.3(5)	C(8)-Ir(2)-C(11)	63.1(4)
C(9)-Ir(2)-C(11)	62.4(4)	C(10)-Ir(2)-C(11)	36.7(4)
Ir(1)-Ir(2)-C(12)	108.4(3)	C(2)-Ir(2)-C(12)	166.6(4)
C(8)-Ir(2)-C(12)	38.9(4)	C(9)-Ir(2)-C(12)	63.1(4)
C(10)-Ir(2)-C(12)	61.6(5)	C(11)-Ir(2)-C(12)	37.1(5)
Ir(1)-C(1)-O(1)	179.4(15)	Ir(2)-C(2)-O(2)	177.6(10)
Ir(1)-C(3)-C(3M)	126.2(7)	Ir(1)-C(3)-C(4)	73.6(6)
C(3M)-C(3)-C(4)	126.6(12)	Ir(1)-C(3)-C(7)	71.8(6)
C(3M)-C(3)-C(7)	125.2(10)	C(4)-C(3)-C(7)	107.7(10)
Ir(1)-C(4)-C(3)	69.0(5)	Ir(1)-C(4)-C(4M)	126.1(8)
C(3)-C(4)-C(4M)	126.7(12)	Ir(1)-C(4)-C(5)	73.4(6)
C(3)-C(4)-C(5)	108.0(11)	C(4M)-C(4)-C(5)	125.2(11)
Ir(1)-C(5)-C(4)	71.1(5)	Ir(1)-C(5)-C(5M)	128.3(7)
C(4)-C(5)-C(5M)	126.6(12)	Ir(1)-C(5)-C(6)	68.9(5)
C(4)-C(5)-C(6)	108.7(9)	C(5M)-C(5)-C(6)	124.6(12)
Ir(1)-C(6)-C(5)	74.3(7)	Ir(1)-C(6)-C(6M)	126.8(7)
C(5)-C(6)-C(6M)	126.4(10)	Ir(1)-C(6)-C(7)	71.2(6)
C(5)-C(6)-C(7)	107.8(11)	C(6M)-C(6)-C(7)	125.3(11)
Ir(1)-C(7)-C(3)	70.8(6)	Ir(1)-C(7)-C(6)	71.6(6)
C(3)-C(7)-C(6)	107.7(10)	Ir(1)-C(7)-C(7M)	125.9(7)
C(3)-C(7)-C(7M)	126.1(11)	C(6)-C(7)-C(7M)	126.0(12)
Ir(2)-C(8)-C(8M)	126.1(7)	Ir(2)-C(8)-C(9)	70.7(7)
C(8M)-C(8)-C(9)	127.1(11)	Ir(2)-C(8)-C(12)	70.0(7)
C(8M)-C(8)-C(12)	126.5(12)	C(9)-C(8)-C(12)	106.3(11)
Ir(2)-C(9)-C(8)	72.1(6)	Ir(2)-C(9)-C(9M)	127.4(7)
C(8)-C(9)-C(9M)	124.1(12)	Ir(2)-C(9)-C(10)	74.2(6)
C(8)-C(9)-C(10)	109.2(10)	C(9M)-C(9)-C(10)	126.1(12)
Ir(2)-C(10)-C(9)	68.9(6)	Ir(2)-C(10)-C(10M)	125.4(8)
C(9)-C(10)-C(10M)	125.4(11)	Ir(2)-C(10)-C(11)	70.7(6)
C(9)-C(10)-C(11)	108.7(12)	C(10M)-C(10)-C(11)	125.9(11)
Ir(2)-C(11)-C(10)	72.7(6)	Ir(2)-C(11)-C(11M)	130.3(8)
C(10)-C(11)-C(11M)	125.9(12)	Ir(2)-C(11)-C(12)	69.9(6)
C(10)-C(11)-C(12)	107.7(10)	C(11M)-C(11)-C(12)	125.7(11)
Ir(2)-C(12)-C(8)	71.2(7)	Ir(2)-C(12)-C(11)	73.0(6)
C(8)-C(12)-C(11)	107.9(11)	Ir(2)-C(12)-C(12M)	124.8(7)
C(8)-C(12)-C(12M)	126.6(13)	C(11)-C(12)-C(12M)	125.3(11)
C(1S)-B(1)-C(9S)	112.7(9)	C(1S)-B(1)-C(17S)	102.9(8)
C(9S)-B(1)-C(17S)	112.0(10)	C(1S)-B(1)-C(25S)	109.3(10)
C(9S)-B(1)-C(25S)	106.2(8)	C(17S)-B(1)-C(25S)	113.8(9)
B(1)-C(1S)-C(2S)	119.5(9)	B(1)-C(1S)-C(6S)	125.1(9)

C(2S)-C(1S)-C(6S)	115.4(10)	C(1S)-C(2S)-C(3S)	122.2(10)
C(2S)-C(3S)-C(4S)	121.3(10)	C(2S)-C(3S)-C(7S)	119.6(10)
C(4S)-C(3S)-C(7S)	119.1(12)	C(3S)-C(4S)-C(5S)	116.0(11)
C(4S)-C(5S)-C(6S)	121.6(10)	C(4S)-C(5S)-C(8S)	118.8(11)
C(6S)-C(5S)-C(8S)	119.6(10)	C(1S)-C(6S)-C(5S)	123.3(10)
C(3S)-C(7S)-F(1)	114.5(13)	C(3S)-C(7S)-F(2)	110.5(11)
F(1)-C(7S)-F(2)	97.6(13)	C(3S)-C(7S)-F(3)	117.1(14)
F(1)-C(7S)-F(3)	110.5(15)	F(2)-C(7S)-F(3)	104.4(14)
C(5S)-C(8S)-F(4)	113.7(11)	C(5S)-C(8S)-F(5)	116.0(12)
F(4)-C(8S)-F(5)	104.1(14)	C(5S)-C(8S)-F(6)	115.7(12)
F(4)-C(8S)-F(6)	102.6(15)	F(5)-C(8S)-F(6)	103.1(12)
B(1)-C(9S)-C(10S)	123.5(11)	B(1)-C(9S)-C(14S)	118.7(11)
C(10S)-C(9S)-C(14S)	117.8(9)	C(9S)-C(10S)-C(11S)	120.1(11)
C(10S)-C(11S)-C(12S)	122.4(12)	C(10S)-C(11S)-C(15S)	119.0(11)
C(12S)-C(11S)-C(15S)	118.6(10)	C(11S)-C(12S)-C(13S)	117.8(10)
C(12S)-C(13S)-C(14S)	121.8(12)	C(12S)-C(13S)-C(16S)	119.0(10)
C(14S)-C(13S)-C(16S)	119.1(12)	C(9S)-C(14S)-C(13S)	119.9(11)
C(11S)-C(15S)-F(7)	114.1(12)	C(11S)-C(15S)-F(8)	116.3(15)
F(7)-C(15S)-F(8)	98.9(13)	C(11S)-C(15S)-F(9)	116.9(12)
F(7)-C(15S)-F(9)	102.6(15)	F(8)-C(15S)-F(9)	105.7(14)
C(13S)-C(16S)-F(10)	114.5(13)	C(13S)-C(16S)-F(11)	114.0(12)
F(10)-C(16S)-F(11)	99.1(10)	C(13S)-C(16S)-F(12)	116.3(10)
F(10)-C(16S)-F(12)	108.5(13)	F(11)-C(16S)-F(12)	102.5(13)
B(1)-C(17S)-C(18S)	124.5(9)	B(1)-C(17S)-C(22S)	118.4(9)
C(18S)-C(17S)-C(22S)	116.9(10)	C(17S)-C(18S)-C(19S)	121.2(9)
C(18S)-C(19S)-C(20S)	123.9(9)	C(18S)-C(19S)-C(23S)	119.3(9)
C(20S)-C(19S)-C(23S)	116.8(11)	C(19S)-C(20S)-C(21S)	115.0(11)
C(20S)-C(21S)-C(22S)	121.9(9)	C(20S)-C(21S)-C(24S)	120.5(10)
C(22S)-C(21S)-C(24S)	117.6(9)	C(17S)-C(22S)-C(21S)	121.0(9)
C(19S)-C(23S)-F(13)	111.0(10)	C(19S)-C(23S)-F(14)	114.0(10)
F(13)-C(23S)-F(14)	105.9(12)	C(19S)-C(23S)-F(15)	114.1(11)
F(13)-C(23S)-F(15)	103.0(10)	F(14)-C(23S)-F(15)	108.0(10)
C(21S)-C(24S)-F(16)	112.5(9)	C(21S)-C(24S)-F(17)	112.0(8)
F(16)-C(24S)-F(17)	106.6(11)	C(21S)-C(24S)-F(18)	112.6(11)
F(16)-C(24S)-F(18)	106.2(8)	F(17)-C(24S)-F(18)	106.4(8)
B(1)-C(25S)-C(26S)	122.4(10)	B(1)-C(25S)-C(30S)	123.5(12)
C(26S)-C(25S)-C(30S)	114.0(9)	C(25S)-C(26S)-C(27S)	121.8(11)
C(26S)-C(27S)-C(28S)	121.8(12)	C(26S)-C(27S)-C(31S)	118.3(11)
C(28S)-C(27S)-C(31S)	119.9(9)	C(27S)-C(28S)-C(29S)	117.0(9)
C(28S)-C(29S)-C(30S)	121.8(10)	C(28S)-C(29S)-C(32S)	120.6(9)
C(30S)-C(29S)-C(32S)	117.4(11)	C(25S)-C(30S)-C(29S)	123.6(12)
C(27S)-C(31S)-F(19)	112.7(9)	C(27S)-C(31S)-F(20)	113.3(11)
F(19)-C(31S)-F(20)	105.4(10)	C(27S)-C(31S)-F(21)	111.2(10)
F(19)-C(31S)-F(21)	106.7(11)	F(20)-C(31S)-F(21)	107.1(9)
C(29S)-C(32S)-F(22)	113.2(11)	C(29S)-C(32S)-F(23)	112.8(9)
F(22)-C(32S)-F(23)	103.9(8)	C(29S)-C(32S)-F(24)	113.7(9)
F(22)-C(32S)-F(24)	104.8(8)	F(23)-C(32S)-F(24)	107.6(12)
Ir(4)-Ir(3)-C(13)	82.0(4)	Ir(4)-Ir(3)-C(15)	116.2(3)
C(13)-Ir(3)-C(15)	105.4(5)	Ir(4)-Ir(3)-C(16)	153.7(3)
C(13)-Ir(3)-C(16)	99.9(5)	C(15)-Ir(3)-C(16)	37.8(4)
Ir(4)-Ir(3)-C(17)	151.0(3)	C(13)-Ir(3)-C(17)	127.0(5)
C(15)-Ir(3)-C(17)	61.9(4)	C(16)-Ir(3)-C(17)	37.0(5)
Ir(4)-Ir(3)-C(18)	113.3(3)	C(13)-Ir(3)-C(18)	162.9(5)
C(15)-Ir(3)-C(18)	61.6(4)	C(16)-Ir(3)-C(18)	63.0(4)
C(17)-Ir(3)-C(18)	38.4(4)	Ir(4)-Ir(3)-C(19)	99.2(3)
C(13)-Ir(3)-C(19)	136.6(5)	C(15)-Ir(3)-C(19)	35.4(5)
C(16)-Ir(3)-C(19)	61.4(4)	C(17)-Ir(3)-C(19)	61.9(3)
C(18)-Ir(3)-C(19)	37.0(4)	Ir(3)-Ir(4)-C(14)	78.5(4)
Ir(3)-Ir(4)-C(20)	101.3(3)	C(14)-Ir(4)-C(20)	128.0(5)

Ir(3)-Ir(4)-C(21)	124.1(3)	C(14)-Ir(4)-C(21)	101.4(5)
C(20)-Ir(4)-C(21)	36.2(3)	Ir(3)-Ir(4)-C(22)	162.6(3)
C(14)-Ir(4)-C(22)	105.3(5)	C(20)-Ir(4)-C(22)	62.7(4)
C(21)-Ir(4)-C(22)	38.7(4)	Ir(3)-Ir(4)-C(23)	143.2(3)
C(14)-Ir(4)-C(23)	138.1(4)	C(20)-Ir(4)-C(23)	62.2(4)
C(21)-Ir(4)-C(23)	62.9(4)	C(22)-Ir(4)-C(23)	37.6(4)
Ir(3)-Ir(4)-C(24)	108.7(3)	C(14)-Ir(4)-C(24)	163.0(4)
C(20)-Ir(4)-C(24)	36.5(4)	C(21)-Ir(4)-C(24)	61.8(4)
C(22)-Ir(4)-C(24)	63.4(4)	C(23)-Ir(4)-C(24)	38.2(4)
Ir(3)-C(13)-O(13)	176.8(11)	Ir(4)-C(14)-O(14)	176.6(11)
Ir(3)-C(15)-C(15M)	129.5(8)	Ir(3)-C(15)-C(16)	66.0(6)
C(15M)-C(15)-C(16)	127.0(12)	Ir(3)-C(15)-C(19)	72.5(7)
C(15M)-C(15)-C(19)	126.4(9)	C(16)-C(15)-C(19)	106.5(10)
Ir(3)-C(16)-C(15)	76.2(7)	Ir(3)-C(16)-C(16M)	126.2(8)
C(15)-C(16)-C(16M)	123.9(11)	Ir(3)-C(16)-C(17)	73.1(7)
C(15)-C(16)-C(17)	109.7(10)	C(16M)-C(16)-C(17)	125.4(9)
Ir(3)-C(17)-C(16)	69.9(6)	Ir(3)-C(17)-C(17M)	124.7(7)
C(16)-C(17)-C(17M)	128.5(11)	Ir(3)-C(17)-C(18)	71.3(6)
C(16)-C(17)-C(18)	107.4(9)	C(17M)-C(17)-C(18)	124.0(12)
Ir(3)-C(18)-C(17)	70.2(5)	Ir(3)-C(18)-C(18M)	128.6(9)
C(17)-C(18)-C(18M)	127.6(9)	Ir(3)-C(18)-C(19)	74.7(6)
C(17)-C(18)-C(19)	106.5(11)	C(18M)-C(18)-C(19)	124.9(9)
Ir(3)-C(19)-C(15)	72.1(6)	Ir(3)-C(19)-C(18)	68.3(5)
C(15)-C(19)-C(18)	109.4(9)	Ir(3)-C(19)-C(19M)	128.5(8)
C(15)-C(19)-C(19M)	126.9(10)	C(18)-C(19)-C(19M)	123.6(12)
Ir(4)-C(20)-C(20M)	128.9(9)	Ir(4)-C(20)-C(21)	70.4(5)
C(20M)-C(20)-C(21)	123.8(10)	Ir(4)-C(20)-C(24)	68.2(6)
C(20M)-C(20)-C(24)	128.0(9)	C(21)-C(20)-C(24)	108.1(9)
Ir(4)-C(21)-C(20)	73.4(6)	Ir(4)-C(21)-C(21M)	127.4(9)
C(20)-C(21)-C(21M)	126.1(9)	Ir(4)-C(21)-C(22)	67.7(5)
C(20)-C(21)-C(22)	107.6(10)	C(21M)-C(21)-C(22)	126.2(8)
Ir(4)-C(22)-C(21)	73.6(6)	Ir(4)-C(22)-C(22M)	127.4(8)
C(21)-C(22)-C(22M)	125.6(10)	Ir(4)-C(22)-C(23)	73.3(6)
C(21)-C(22)-C(23)	108.0(8)	C(22M)-C(22)-C(23)	125.5(11)
Ir(4)-C(23)-C(22)	69.1(7)	Ir(4)-C(23)-C(23M)	127.6(9)
C(22)-C(23)-C(23M)	126.7(10)	Ir(4)-C(23)-C(24)	69.9(7)
C(22)-C(23)-C(24)	106.3(10)	C(23M)-C(23)-C(24)	126.9(11)
Ir(4)-C(24)-C(20)	75.2(7)	Ir(4)-C(24)-C(23)	71.9(7)
C(20)-C(24)-C(23)	109.5(9)	Ir(4)-C(24)-C(24M)	128.0(8)
C(20)-C(24)-C(24M)	124.5(9)	C(23)-C(24)-C(24M)	125.1(12)
C(33S)-B(2)-C(41S)	111.5(9)	C(33S)-B(2)-C(49S)	104.7(7)
C(41S)-B(2)-C(49S)	111.8(8)	C(33S)-B(2)-C(57S)	113.4(8)
C(41S)-B(2)-C(57S)	104.4(8)	C(49S)-B(2)-C(57S)	111.2(9)
B(2)-C(33S)-C(34S)	120.7(10)	B(2)-C(33S)-C(38S)	122.5(10)
C(34S)-C(33S)-C(38S)	116.6(9)	C(33S)-C(34S)-C(35S)	121.7(11)
C(34S)-C(35S)-C(36S)	120.8(11)	C(34S)-C(35S)-C(39S)	119.8(12)
C(36S)-C(35S)-C(39S)	119.4(10)	C(35S)-C(36S)-C(37S)	118.2(10)
C(36S)-C(37S)-C(38S)	122.1(12)	C(36S)-C(37S)-C(40S)	121.1(10)
C(38S)-C(37S)-C(40S)	116.5(10)	C(33S)-C(38S)-C(37S)	120.5(11)
C(35S)-C(39S)-F(25)	114.1(10)	C(35S)-C(39S)-F(26)	113.2(12)
F(25)-C(39S)-F(26)	106.0(11)	C(35S)-C(39S)-F(27)	110.3(10)
F(25)-C(39S)-F(27)	107.8(13)	F(26)-C(39S)-F(27)	104.8(9)
C(37S)-C(40S)-F(28)	109.8(10)	C(37S)-C(40S)-F(29)	115.2(11)
F(28)-C(40S)-F(29)	108.7(13)	C(37S)-C(40S)-F(30)	110.8(12)
F(28)-C(40S)-F(30)	104.6(11)	F(29)-C(40S)-F(30)	107.2(10)
B(2)-C(41S)-C(42S)	119.8(8)	B(2)-C(41S)-C(46S)	123.9(8)
C(42S)-C(41S)-C(46S)	116.0(9)	C(41S)-C(42S)-C(43S)	122.3(9)
C(42S)-C(43S)-C(44S)	122.0(9)	C(42S)-C(43S)-C(47S)	118.6(9)
C(44S)-C(43S)-C(47S)	119.4(10)	C(43S)-C(44S)-C(45S)	114.9(10)

C(44S)-C(45S)-C(46S)	123.1(9)	C(44S)-C(45S)-C(48S)	115.4(10)
C(46S)-C(45S)-C(48S)	121.5(9)	C(41S)-C(46S)-C(45S)	121.6(9)
C(43S)-C(47S)-F(31)	112.2(10)	C(43S)-C(47S)-F(32)	111.6(9)
F(31)-C(47S)-F(32)	107.4(12)	C(43S)-C(47S)-F(33)	114.0(12)
F(31)-C(47S)-F(33)	105.8(10)	F(32)-C(47S)-F(33)	105.4(10)
C(45S)-C(48S)-F(34)	112.1(10)	C(45S)-C(48S)-F(35)	114.6(10)
F(34)-C(48S)-F(35)	104.8(10)	C(45S)-C(48S)-F(36)	112.3(10)
F(34)-C(48S)-F(36)	106.8(10)	F(35)-C(48S)-F(36)	105.5(10)
B(2)-C(49S)-C(50S)	123.1(10)	B(2)-C(49S)-C(54S)	122.2(10)
C(50S)-C(49S)-C(54S)	114.5(8)	C(49S)-C(50S)-C(51S)	123.5(11)
C(50S)-C(51S)-C(52S)	121.2(11)	C(50S)-C(51S)-C(55S)	121.6(11)
C(52S)-C(51S)-C(55S)	117.2(8)	C(51S)-C(52S)-C(53S)	116.7(8)
C(52S)-C(53S)-C(54S)	121.7(11)	C(52S)-C(53S)-C(56S)	117.0(9)
C(54S)-C(53S)-C(56S)	121.3(12)	C(49S)-C(54S)-C(53S)	122.3(11)
C(51S)-C(55S)-F(37)	118.0(12)	C(51S)-C(55S)-F(38)	113.5(9)
F(37)-C(55S)-F(38)	105.5(10)	C(51S)-C(55S)-F(39)	112.4(10)
F(37)-C(55S)-F(39)	103.3(10)	F(38)-C(55S)-F(39)	102.6(12)
C(53S)-C(56S)-F(40)	112.9(9)	C(53S)-C(56S)-F(41)	116.6(12)
F(40)-C(56S)-F(41)	107.5(13)	C(53S)-C(56S)-F(42)	113.1(12)
F(40)-C(56S)-F(42)	103.0(13)	F(41)-C(56S)-F(42)	102.5(10)
B(2)-C(57S)-C(58S)	125.1(9)	B(2)-C(57S)-C(62S)	119.3(9)
C(58S)-C(57S)-C(62S)	115.3(10)	C(57S)-C(58S)-C(59S)	121.9(9)
C(58S)-C(59S)-C(60S)	122.3(9)	C(58S)-C(59S)-C(63S)	118.2(9)
C(60S)-C(59S)-C(63S)	119.5(11)	C(59S)-C(60S)-C(61S)	116.9(11)
C(60S)-C(61S)-C(62S)	119.9(9)	C(60S)-C(61S)-C(64S)	120.8(11)
C(62S)-C(61S)-C(64S)	119.2(9)	C(57S)-C(62S)-C(61S)	123.7(9)
C(59S)-C(63S)-F(43)	111.3(8)	C(59S)-C(63S)-F(44)	111.5(11)
F(43)-C(63S)-F(44)	105.4(9)	C(59S)-C(63S)-F(45)	113.7(10)
F(43)-C(63S)-F(45)	107.2(12)	F(44)-C(63S)-F(45)	107.4(9)
C(61S)-C(64S)-F(46)	114.1(11)	C(61S)-C(64S)-F(47)	114.3(10)
F(46)-C(64S)-F(47)	106.6(9)	C(61S)-C(64S)-F(48)	110.0(8)
F(45)-C(64S)-F(48)	105.1(9)	F(47)-C(64S)-F(48)	106.0(10)

Table 4. Anisotropic displacement coefficients ($Å^2 x 10^4$)

	U_{11}	U_{22}	U_{33}	U_{12}	U_{13}	U_{23}
Ir(1)	285(2)	370(3)	276(2)	-24(2)	-20(2)	-92(2)
Ir(2)	269(2)	314(3)	282(2)	10(2)	-15(2)	-80(2)
C(1)	638(91)	514(87)	516(93)	-314(71)	-73(72)	-101(72)
O(1)	1451(112	1248(105	309(57)	-662(87)	-192(63)	-254(62)
C(2)	497(76)	471(81)	205(59)	94(63)	76(53)	-60(57)
O(2)	842(69)	358(52)	516(57)	164(50)	133(50)	-172(46)
C(3)	372(65)	234(58)	299(60)	-28(49)	-24(49)	-62(50)
C(3M)	389(73)	676(95)	530(82)	-219(67)	-52(63)	-119(73)
C(4)	428(69)	203(58)	406(66)	58(51)	-26(55)	-125(53)
C(4M)	791(104	567(93)	675(97)	52(79)	45(82)	-342(81)
C(5)	219(56)	270(59)	338(61)	30(47)	5(48)	-51(51)
C(5M)	334(69)	632(89)	611(85)	25(62)	5(61)	-332(74)
C(6)	259(59)	348(65)	354(63)	3(50)	-84(49)	-114(54)
C(6M)	564(82)	497(80)	412(74)	-3(65)	-28(63)	-115(64)
C(7)	267(60)	423(69)	150(52)	-35(50)	94(45)	42(50)
C(7M)	296(66)	465(78)	587(84)	115(58)	67(60)	-12(67)
C(8)	371(69)	397(71)	363(68)	-15(55)	-86(55)	41(58)
C(8M)	595(88)	542(89)	674(95)	-81(71)	-277(76)	-171(77)
C(9)	255(59)	277(60)	270(60)	32(47)	15(48)	87(50)
C(9M)	461(80)	747(103	397(76)	2(72)	99(63)	89(72)
C(10)	449(74)	355(69)	371(68)	68(56)	56(58)	-88(57)
C(10M)	725(96)	612(92)	382(74)	86(75)	-185(68)	-189(69)
C(11)	242(58)	290(61)	337(62)	1(47)	-21(49)	-56(51)
C(11M)	368(74)	610(91)	548(84)	96(65)	-72(63)	-40(72)
C(12)	607(81)	214(60)	294(63)	93(55)	-7(57)	-1(51)
C(12M)	823(100	328(70)	410(73)	147(68)	-53(69)	-147(61)
B(1)	185(61)	384(75)	339(70)	-36(54)	-67(53)	-169(61)
C(1S)	230(55)	327(62)	227(54)	-29(47)	-11(44)	-138(49)
C(2S)	258(60)	414(69)	362(64)	-59(51)	6(49)	-186(55)
C(3S)	327(63)	496(76)	358(64)	-122(57)	88(52)	-272(59)
C(4S)	387(69)	475(75)	302(62)	-105(57)	-18(52)	-198(57)
C(5S)	385(65)	288(63)	243(56)	2(51)	-53(48)	-114(49)
C(6S)	279(57)	347(65)	262(56)	-33(49)	-4(46)	-193(50)
C(7S)	243(65)	660(95)	769(98)	-165(66)	59(67)	-460(84)
F(1)	512(56)	2953(172	1660(110	124(78)	-433(64)	-1863(127)
F(2)	462(58)	2399(161	1254(98)	-398(77)	63(62)	-520(102)
F(3)	539(61)	537(65)	4212(256	48(52)	-1123(104	-143(102)
C(8S)	736(94)	231(67)	532(80)	-40(64)	-188(74)	-206(64)
F(4)	3557(231	1383(116	1186(100	1822(149	-1353(132	-877(98)
F(5)	1072(70)	446(49)	1239(80)	227(47)	-848(66)	-293(52)
F(6)	941(82)	387(59)	3361(231	-154(57)	-506(110	305(92)
C(9S)	259(56)	201(54)	309(58)	-14(44)	-13(46)	-119(48)
C(10S)	413(67)	184(54)	257(57)	23(47)	-46(49)	-58(47)
C(11S)	222(58)	320(62)	366(63)	-39(48)	-97(49)	-106(54)
C(12S)	140(52)	405(68)	430(67)	-40(49)	-74(50)	-43(58)
C(13S)	267(60)	335(63)	320(61)	136(50)	-43(49)	-104(53)
C(14S)	278(59)	302(61)	264(57)	30(48)	8(46)	-90(50)
C(15S)	338(70)	675(96)	362(70)	-68(64)	-105(57)	-246(69)
F(7)	1297(100	2845(187	1439(113	-976(113	130(87)	-1576(129)
F(8)	968(82)	1921(133	3013(189	646(87)	-1313(110	-1907(143)
F(9)	3218(190	783(74)	1174(92)	-1155(103	-1431(114	250(69)
C(16S)	333(69)	590(86)	452(76)	10(66)	34(61)	-200(69)
F(10)	1044(78)	1676(109	1291(92)	930(81)	-590(72)	-1088(88)
F(11)	1857(118	1324(96)	1253(95)	-815(90)	1065(93)	-979(84)
F(12)	465(47)	1224(79)	1746(101	-130(49)	250(55)	-1281(82)

C(17S)	224(53)	215(54)	282(57)	-10(43)	-9(44)	-107(47)
C(18S)	252(56)	257(58)	370(63)	-31(46)	-57(48)	-170(51)
C(19S)	192(52)	229(56)	356(63)	27(43)	-6(47)	-122(50)
C(20S)	253(56)	313(61)	349(62)	-76(48)	-7(48)	-173(52)
C(21S)	278(57)	309(60)	248(57)	-72(47)	-65(46)	-122(49)
C(22S)	241(56)	303(60)	262(59)	-13(46)	-8(46)	-75(50)
C(23S)	341(70)	468(77)	472(78)	140(59)	-11(59)	-224(68)
F(13)	1074(71)	682(57)	986(67)	500(53)	-342(56)	-592(55)
F(14)	465(51)	662(58)	1384(88)	71(43)	333(54)	-44(57)
F(15)	476(42)	504(44)	493(45)	223(35)	-68(34)	-115(37)
C(24S)	308(64)	475(77)	251(60)	-21(53)	-47(49)	-187(56)
F(16)	640(47)	737(53)	307(37)	74(40)	-27(34)	-206(37)
F(17)	420(40)	595(46)	387(38)	-176(34)	-188(31)	-46(34)
F(18)	588(44)	333(40)	335(36)	-85(32)	-124(32)	38(31)
C(25S)	227(56)	368(67)	311(61)	-4(48)	-1(47)	-133(53)
C(26S)	274(58)	387(66)	277(60)	21(49)	-1(47)	-167(53)
C(27S)	230(57)	498(75)	313(62)	-39(51)	32(47)	-211(57)
C(28S)	199(54)	310(63)	375(63)	-9(45)	93(47)	-159(53)
C(29S)	225(54)	264(58)	233(56)	1(44)	-42(44)	-43(48)
C(30S)	164(51)	444(69)	190(54)	21(47)	-23(42)	-106(51)
C(31S)	469(79)	496(79)	293(68)	55(63)	-118(56)	-176(61)
F(19)	551(42)	536(44)	533(43)	155(36)	-174(34)	-398(37)
F(20)	747(52)	686(51)	339(41)	50(41)	-87(36)	-241(39)
F(21)	428(45)	820(57)	693(51)	-34(39)	-101(37)	-452(46)
C(32S)	318(65)	411(71)	380(69)	-124(54)	-35(54)	-96(59)
F(22)	703(48)	325(38)	409(41)	-14(34)	-186(35)	4(33)
F(23)	702(49)	305(38)	634(48)	-22(34)	162(40)	-192(36)
F(24)	652(50)	394(42)	711(52)	-111(37)	-321(41)	-66(38)
Ir(3)	253(2)	323(3)	320(2)	-62(2)	12(2)	-148(2)
Ir(4)	253(2)	353(3)	254(2)	-32(2)	-30(2)	-80(2)
C(13)	363(67)	274(63)	398(72)	-25(51)	-146(60)	-64(55)
O(13)	497(52)	633(60)	286(45)	-36(44)	126(43)	-114(43)
C(14)	278(63)	587(92)	384(70)	-63(59)	-182(53)	-82(65)
O(14)	1007(81)	370(57)	680(67)	30(53)	-315(58)	-200(51)
C(15)	357(62)	263(60)	373(65)	-123(49)	83(51)	-174(54)
C(15M)	397(72)	477(80)	694(92)	-93(61)	47(66)	-210(72)
C(16)	267(57)	468(71)	325(62)	-209(52)	103(48)	-299(58)
C(16M)	632(86)	577(86)	495(79)	-152(69)	-52(66)	-362(70)
C(17)	165(52)	328(61)	455(68)	-135(45)	7(48)	-196(55)
C(17M)	327(68)	482(80)	602(85)	165(59)	-168(62)	-56(68)
C(18)	187(53)	523(74)	215(55)	-117(50)	46(44)	-172(53)
C(18M)	505(81)	694(96)	658(93)	-43(70)	122(70)	-455(82)
C(19)	212(56)	327(63)	410(67)	-79(48)	18(49)	-117(55)
C(19M)	504(77)	496(78)	391(71)	-233(63)	-29(59)	-106(62)
C(20)	286(57)	220(56)	315(60)	-173(47)	153(49)	-62(49)
C(20M)	474(71)	335(66)	289(62)	-96(55)	-84(54)	3(53)
C(21)	227(55)	368(63)	273(57)	-91(48)	34(45)	-186(50)
C(21M)	380(69)	586(83)	530(77)	-102(61)	126(60)	-333(68)
C(22)	189(54)	343(63)	394(65)	-107(47)	-44(47)	-167(54)
C(22M)	360(69)	454(77)	522(78)	92(58)	-176(59)	-116(64)
C(23)	419(67)	320(64)	219(57)	-75(53)	5(50)	-39(51)
C(23M)	781(100	705(99)	421(78)	-28(79)	14(71)	-346(74)
C(24)	299(59)	195(56)	408(66)	-110(46)	59(51)	-67(51)
C(24M)	625(88)	427(78)	661(91)	200(67)	19(73)	-270(71)
B(2)	213(60)	186(60)	252(62)	63(47)	-59(49)	-162(52)
C(33S)	174(52)	210(55)	291(58)	-31(43)	-54(45)	44(48)
C(34S)	173(53)	258(57)	327(59)	13(44)	-35(46)	-91(49)
C(35S)	404(67)	276(61)	278(58)	-68(51)	-56(50)	-96(50)
C(36S)	266(59)	395(67)	382(66)	-45(51)	37(51)	-185(57)

C(37S)	342(63)	237(58)	316(60)	-129(48)	-31(50)	-80(49)
C(38S)	242(56)	170(53)	364(62)	38(43)	-88(48)	-90(48)
C(39S)	306(66)	586(86)	501(77)	33(63)	-125(62)	-313(70)
F(25)	322(43)	2329(126	1593(95)	132(58)	-83(52)	-1773(101)
F(26)	429(43)	812(57)	516(45)	48(41)	163(37)	-197(42)
F(27)	636(50)	547(49)	875(59)	83(41)	189(44)	-394(46)
C(40S)	337(71)	507(82)	568(86)	-106(58)	-162(60)	-297(69)
F(28)	1006(68)	718(61)	1192(78)	154(52)	-522(60)	-691(59)
F(29)	1195(78)	1392(89)	355(48)	-573(68)	10(48)	-372(54)
F(30)	372(44)	1303(79)	840(60)	-154(45)	-99(40)	-694(59)
C(41S)	166(50)	218(53)	238(54)	-24(41)	-54(41)	-93(46)
C(42S)	246(54)	230(56)	314(60)	-27(44)	-60(46)	-114(49)
C(43S)	458(67)	158(53)	223(57)	-55(49)	-51(50)	-9(46)
C(44S)	350(62)	251(59)	361(65)	-78(49)	-3(51)	-160(52)
C(45S)	223(53)	235(55)	291(58)	-64(43)	13(45)	-143(48)
C(46S)	277(58)	268(59)	326(61)	-76(47)	16(48)	-126(50)
C(47S)	468(75)	654(95)	219(62)	-116(66)	-29(56)	-170(63)
F(31)	1177(79)	1368(88)	230(41)	654(69)	7(46)	-107(48)
F(32)	928(62)	675(55)	661(53)	-334(48)	-511(48)	-34(44)
F(33)	859(56)	316(41)	478(44)	-87(37)	-292(40)	-18(35)
C(48S)	288(64)	440(73)	488(76)	-52(55)	-26(55)	-235(67)
F(34)	180(37)	526(48)	1657(93)	-22(34)	95(45)	-353(54)
F(35)	580(47)	550(47)	654(49)	191(37)	29(38)	-338(42)
F(36)	595(47)	549(47)	468(44)	265(38)	-32(36)	-111(39)
C(49S)	92(47)	317(61)	286(58)	-40(42)	25(41)	-124(49)
C(50S)	124(49)	290(61)	349(61)	-32(43)	33(44)	-126(52)
C(51S)	260(56)	217(58)	290(60)	-4(44)	29(46)	-70(49)
C(52S)	311(59)	236(59)	309(61)	2(46)	16(48)	-91(49)
C(53S)	274(58)	404(69)	258(60)	48(50)	-66(47)	-130(54)
C(54S)	249(55)	275(59)	220(56)	45(45)	-61(44)	-76(48)
C(55S)	538(80)	317(71)	354(68)	30(59)	85(60)	-122(61)
F(37)	1720(95)	206(39)	502(50)	72(48)	-148(55)	-33(38)
F(38)	1231(77)	423(47)	943(67)	-71(48)	279(50)	-412(48)
F(39)	923(69)	607(59)	1824(113	-109(51)	-302(72)	-730(70)
C(56S)	812(100	366(76)	274(68)	99(72)	-146(69)	-81(60)
F(40)	2174(122	698(62)	487(51)	-544(71)	-344(64)	-221(47)
F(41)	1604(91)	598(54)	514(50)	253(57)	-606(57)	-250(45)
F(42)	1255(87)	1773(115	692(63)	85(50)	105(61)	-902(74)
C(57S)	200(52)	278(58)	191(50)	-7(44)	-11(41)	-113(45)
C(58S)	287(57)	256(59)	219(54)	12(47)	-27(44)	-117(47)
C(59S)	324(61)	233(58)	219(54)	-27(47)	10(46)	-57(47)
C(60S)	317(60)	245(58)	246(55)	-32(47)	14(47)	-80(47)
C(61S)	249(56)	283(61)	366(62)	-92(48)	-4(48)	-159(52)
C(62S)	263(57)	266(58)	202(52)	18(46)	-33(44)	-93(46)
C(63S)	337(66)	320(68)	520(80)	-43(53)	27(58)	-198(61)
F(43)	551(48)	561(48)	837(59)	116(38)	209(43)	-284(44)
F(44)	866(58)	482(46)	447(45)	309(41)	-126(40)	-99(37)
F(45)	692(53)	337(43)	1274(78)	93(38)	-310(52)	-364(48)
C(64S)	287(62)	466(74)	302(63)	-67(54)	-7(52)	-100(59)
F(46)	320(38)	994(63)	533(45)	22(38)	-64(34)	-393(45)
F(47)	433(41)	458(43)	1001(61)	-14(34)	-353(41)	-370(44)
F(48)	470(41)	631(49)	416(41)	-95(36)	-230(33)	2(37)

The anisotropic displacement exponent takes the form:

$-2\pi^2(h^2a^{*2}U_{11} + \ldots + 2hka^*b^*U_{12})$

Table 5. H-Atom coordinates ($x10^4$) and isotropic displacement coefficients ($Å^2 x10^3$)

	x	y	z	U
H(3MA)	-2859	451	6281	80
H(3MB)	-3215	1216	5842	80
H(3MC)	-2535	749	5543	80
H(4MA)	-246	-163	6090	80
H(4MB)	-745	313	5423	80
H(4MC)	415	371	5558	80
H(5MA)	1342	558	6784	80
H(5MB)	1519	845	6029	80
H(5MC)	1505	1338	6401	80
H(6MA)	-183	1676	7339	80
H(6MB)	451	2113	6722	80
H(6MC)	-709	2362	6831	80
H(7MA)	-2798	1582	7077	80
H(7MB)	-2422	2305	6650	80
H(7MC)	-3168	1965	6359	80
H(8MA)	2270	4525	4657	80
H(8MB)	1832	3984	5301	80
H(8MC)	2789	3768	4933	80
H(9MA)	2957	3941	3420	80
H(9MB)	3252	3418	4121	80
H(9MC)	2882	3153	3612	80
H(10A)	712	3748	2748	80
H(10B)	1345	3043	3134	80
H(10C)	121	3110	3181	80
H(11A)	-1399	4257	3553	80
H(11B)	-1309	3469	3692	80
H(11C)	-1668	3725	4247	80
H(12A)	-539	4663	4767	80
H(12B)	-1045	3964	5088	80
H(12C)	-31	4072	5377	80
H(15A)	-1641	436	9733	80
H(15B)	-891	850	9171	80
H(15C)	-572	615	9897	80
H(16A)	-2848	1735	8416	80
H(16B)	-2386	2450	8100	80
H(16C)	-1643	1770	8280	80
H(17A)	-4100	2981	8957	80
H(17B)	-3357	3451	9089	80
H(17C)	-3181	3277	8468	80
H(18A)	-3496	2399	10623	80
H(18B)	-2356	2490	10766	80
H(18C)	-2976	3072	10199	80
H(19A)	-1995	861	11053	80
H(19B)	-826	928	10817	80
H(19C)	-1414	1471	11062	80
H(20A)	1811	4193	8545	80
H(20B)	1537	3536	8449	80
H(20C)	657	3994	8645	80
H(21A)	3688	2873	9064	80
H(21B)	3366	2123	9433	80
H(21C)	2764	2623	8812	80
H(22A)	3789	2294	10769	80
H(22B)	2899	1859	11187	80
H(22C)	3388	1722	10585	80

H(23A)	1937	3328	11235	80
H(23B)	774	3167	11243	80
H(23C)	1658	2563	11496	80
H(24A)	629	4469	9852	80
H(24B)	-141	4151	9553	80
H(24C)	-99	3922	10308	80

Appendix B

Supplementary X-ray Data for $[Cp^*Ir(CO)H]_2$

Table 1. Atomic coordinates ($x10^5$) and equivalent isotropic displacement coefficients ($Å^2 x10^4$)

	x	y	z	U(eq)
Ir(1)	16815(3)	17635(4)	15211(3)	233(2)
Ir(2)	18164(3)	2836(3)	22494(3)	220(2)
C(1)	7982(94)	19868(90)	21814(99)	336(51)
O(1)	2439(68)	21360(69)	26083(64)	410(39)
C(2)	9029(101)	-411(92)	16445(81)	296(48)
O(2)	3415(67)	-2691(77)	12615(64)	452(41)
C(3)	24671(90)	25366(95)	7462(81)	285(46)
C(3H)	31726(97)	31831(107)	9586(105)	454(58)
C(4)	26461(94)	17041(106)	5655(80)	320(49)
C(4H)	35156(94)	12496(114)	5629(98)	423(59)
C(5)	18568(98)	13376(85)	2982(75)	273(44)
C(5H)	17691(107)	4700(89)	-404(91)	400(55)
C(6)	11789(91)	19306(94)	3171(79)	279(47)
C(6H)	2285(107)	18188(128)	398(101)	560(68)
C(7)	15612(86)	26794(97)	5997(81)	268(46)
C(7H)	11112(104)	35138(102)	6612(87)	407(58)
C(8)	14271(88)	1462(94)	34895(78)	263(44)
C(8H)	4809(92)	2088(108)	38102(96)	406(56)
C(9)	20328(88)	7899(87)	34476(77)	234(42)
C(9H)	19549(99)	16572(88)	37257(80)	298(47)
C(10)	28383(96)	4586(88)	31277(89)	287(48)
C(10H)	37008(95)	9446(93)	30658(80)	294(47)
C(11)	27253(89)	-4267(86)	30000(78)	246(45)
C(11H)	34275(101)	-10041(98)	27693(90)	409(55)
C(12)	18396(98)	-5984(96)	31888(77)	281(45)
C(12H)	14441(122)	-14690(94)	32129(108)	458(61)

* Equivalent isotropic U defined as one third of the trace of the orthogonalized U_{ij} tensor

Table 2. Bond lengths (Å)

Ir(1)-Ir(2)	2.730 (1)	Ir(1)-C(1)	1.817 (16)
Ir(1)-C(3)	2.210 (15)	Ir(1)-C(4)	2.246 (14)
Ir(1)-C(5)	2.304 (14)	Ir(1)-C(6)	2.296 (14)
Ir(1)-C(7)	2.221 (15)	Ir(2)-C(2)	1.829 (15)
Ir(2)-C(8)	2.301 (14)	Ir(2)-C(9)	2.314 (14)
Ir(2)-C(10)	2.219 (15)	Ir(2)-C(11)	2.236 (14)
Ir(2)-C(12)	2.202 (14)	C(1)-O(1)	1.158 (19)
C(2)-O(2)	1.150 (18)	C(3)-C(3H)	1.540 (22)
C(3)-C(4)	1.410 (23)	C(3)-C(7)	1.412 (19)
C(4)-C(4H)	1.505 (21)	C(4)-C(5)	1.414 (21)
C(5)-C(5H)	1.533 (20)	C(5)-C(6)	1.403 (20)
C(6)-C(6H)	1.529 (21)	C(6)-C(7)	1.433 (21)
C(7)-C(7H)	1.514 (22)	C(8)-C(8H)	1.543 (20)
C(8)-C(9)	1.388 (20)	C(8)-C(12)	1.458 (21)
C(9)-C(9H)	1.492 (20)	C(9)-C(10)	1.447 (20)
C(10)-C(10H)	1.526 (21)	C(10)-C(11)	1.459 (20)
C(11)-C(11H)	1.472 (21)	C(11)-C(12)	1.407 (20)
C(12)-C(12H)	1.529 (22)		

Table 3. Bond angles (°)

Ir(2)-Ir(1)-C(1)	85.4(5)	Ir(2)-Ir(1)-C(3)	138.9(4)
C(1)-Ir(1)-C(3)	133.5(6)	Ir(2)-Ir(1)-C(4)	106.0(4)
C(1)-Ir(1)-C(4)	168.0(6)	C(3)-Ir(1)-C(4)	36.9(6)
Ir(2)-Ir(1)-C(5)	100.4(3)	C(1)-Ir(1)-C(5)	139.3(6)
C(3)-Ir(1)-C(5)	60.9(5)	C(4)-Ir(1)-C(5)	36.2(5)
Ir(2)-Ir(1)-C(6)	125.0(4)	C(1)-Ir(1)-C(6)	110.0(6)
C(3)-Ir(1)-C(6)	61.6(5)	C(4)-Ir(1)-C(6)	60.5(5)
C(5)-Ir(1)-C(6)	35.5(5)	Ir(2)-Ir(1)-C(7)	160.6(4)
C(1)-Ir(1)-C(7)	106.7(6)	C(3)-Ir(1)-C(7)	37.2(5)
C(4)-Ir(1)-C(7)	61.2(5)	C(5)-Ir(1)-C(7)	60.5(5)
C(6)-Ir(1)-C(7)	37.0(5)	Ir(1)-Ir(2)-C(2)	85.1(5)
Ir(1)-Ir(2)-C(8)	121.6(4)	C(2)-Ir(2)-C(8)	110.3(6)
Ir(1)-Ir(2)-C(9)	98.1(4)	C(2)-Ir(2)-C(9)	138.9(6)
C(8)-Ir(2)-C(9)	35.0(5)	Ir(1)-Ir(2)-C(10)	106.1(4)
C(2)-Ir(2)-C(10)	168.2(6)	C(8)-Ir(2)-C(10)	60.7(5)
C(9)-Ir(2)-C(10)	37.2(5)	Ir(1)-Ir(2)-C(11)	141.4(4)
C(2)-Ir(2)-C(11)	132.1(6)	C(8)-Ir(2)-C(11)	62.0(5)
C(9)-Ir(2)-C(11)	62.7(5)	C(10)-Ir(2)-C(11)	38.2(5)
Ir(1)-Ir(2)-C(12)	158.6(4)	C(2)-Ir(2)-C(12)	106.0(6)
C(8)-Ir(2)-C(12)	37.7(5)	C(9)-Ir(2)-C(12)	61.5(5)
C(10)-Ir(2)-C(12)	62.2(5)	C(11)-Ir(2)-C(12)	37.0(5)
Ir(1)-C(1)-O(1)	179.0(16)	Ir(2)-C(2)-O(2)	177.8(13)
Ir(1)-C(3)-C(3H)	127.0(11)	Ir(1)-C(3)-C(4)	72.9(9)
C(3H)-C(3)-C(4)	124.8(13)	Ir(1)-C(3)-C(7)	71.8(8)
C(3H)-C(3)-C(7)	127.2(14)	C(4)-C(3)-C(7)	107.4(13)
Ir(1)-C(4)-C(3)	70.2(8)	Ir(1)-C(4)-C(4H)	126.1(11)
C(3)-C(4)-C(4H)	129.3(14)	Ir(1)-C(4)-C(5)	74.2(8)
C(3)-C(4)-C(5)	108.4(13)	C(4H)-C(4)-C(5)	122.0(15)
Ir(1)-C(5)-C(4)	69.6(8)	Ir(1)-C(5)-C(5H)	129.6(10)
C(4)-C(5)-C(5H)	126.1(13)	Ir(1)-C(5)-C(6)	71.9(8)
C(4)-C(5)-C(6)	108.7(13)	C(5H)-C(5)-C(6)	124.9(13)
Ir(1)-C(6)-C(5)	72.6(8)	Ir(1)-C(6)-C(6H)	126.8(10)
C(5)-C(6)-C(6H)	126.6(14)	Ir(1)-C(6)-C(7)	68.7(8)
C(5)-C(6)-C(7)	106.9(12)	C(6H)-C(6)-C(7)	126.3(14)
Ir(1)-C(7)-C(3)	71.0(8)	Ir(1)-C(7)-C(6)	74.4(9)
C(3)-C(7)-C(6)	108.5(13)	Ir(1)-C(7)-C(7H)	125.2(10)
C(3)-C(7)-C(7H)	124.6(13)	C(6)-C(7)-C(7H)	126.6(12)
Ir(2)-C(8)-C(8H)	126.0(10)	Ir(2)-C(8)-C(9)	73.0(8)
C(8H)-C(8)-C(9)	125.6(13)	Ir(2)-C(8)-C(12)	67.4(8)
C(8H)-C(8)-C(12)	125.9(13)	C(9)-C(8)-C(12)	108.5(12)
Ir(2)-C(9)-C(8)	72.0(8)	Ir(2)-C(9)-C(9H)	129.0(10)
C(8)-C(9)-C(9H)	129.4(13)	Ir(2)-C(9)-C(10)	67.9(8)
C(8)-C(9)-C(10)	107.4(12)	C(9H)-C(9)-C(10)	123.1(12)
Ir(2)-C(10)-C(9)	75.0(8)	Ir(2)-C(10)-C(10H)	127.5(10)
C(9)-C(10)-C(10H)	123.8(13)	Ir(2)-C(10)-C(11)	71.5(8)
C(9)-C(10)-C(11)	109.0(12)	C(10H)-C(10)-C(11)	126.4(13)
Ir(2)-C(11)-C(10)	70.2(8)	Ir(2)-C(11)-C(11H)	126.9(10)
C(10)-C(11)-C(11H)	125.5(13)	Ir(2)-C(11)-C(12)	70.2(8)
C(10)-C(11)-C(12)	105.5(12)	C(11H)-C(11)-C(12)	128.8(13)
Ir(2)-C(12)-C(8)	74.9(8)	Ir(2)-C(12)-C(11)	72.8(8)
C(8)-C(12)-C(11)	109.4(13)	Ir(2)-C(12)-C(12H)	127.7(11)
C(8)-C(12)-C(12H)	125.6(13)	C(11)-C(12)-C(12H)	124.0(14)

Table 4. Anisotropic displacement coefficients ($Å^2 x 10^4$)

	U_{11}	U_{22}	U_{33}	U_{12}	U_{13}	U_{23}
Ir(1)	266(3)	252(3)	181(3)	24(3)	7(3)	5(3)
Ir(2)	249(3)	240(3)	172(3)	4(3)	-5(3)	1(2)
C(1)	306(80)	202(78)	500(104	-83(64)	-183(83)	51(73)
O(1)	327(59)	516(74)	386(71)	145(55)	126(55)	16(59)
C(2)	392(84)	316(87)	181(78)	84(67)	32(70)	-76(67)
O(2)	278(55)	582(80)	497(76)	-88(58)	-53(55)	-216(67)
C(3)	273(69)	338(90)	244(79)	-64(71)	61(67)	-67(68)
C(3H)	353(85)	478(104	532(113	-10(89)	33(83)	-28(94)
C(4)	339(80)	394(96)	227(79)	8(77)	62(66)	104(76)
C(4H)	268(79)	547(115	453(107	165(79)	55(72)	95(94)
C(5)	424(82)	210(76)	187(73)	22(67)	93(71)	-66(60)
C(5H)	521(96)	334(93)	345(96)	-16(78)	33(85)	-98(74)
C(6)	288(73)	383(95)	168(76)	90(66)	-39(63)	137(71)
C(6H)	451(100	834(141	396(110	106(110	-198(87)	49(109)
C(7)	247(71)	341(88)	217(80)	54(65)	-55(61)	-45(68)
C(7H)	403(91)	581(122	236(86)	253(83)	64(72)	5(81)
C(8)	291(72)	395(89)	103(68)	-7(64)	-2(61)	88(72)
C(8H)	277(79)	463(105	479(106	44(77)	160(75)	69(94)
C(9)	308(72)	270(77)	123(70)	-7(61)	40(62)	61(63)
C(9H)	425(84)	255(81)	214(76)	-54(69)	38(64)	-197(64)
C(10)	322(75)	229(85)	309(87)	99(62)	-63(69)	58(69)
C(10H)	293(77)	386(92)	202(77)	-155(70)	2(64)	-65(73)
C(11)	306(77)	235(82)	197(75)	72(61)	-24(61)	47(64)
C(11H)	484(97)	386(98)	357(93)	196(76)	-101(85)	-134(82)
C(12)	349(81)	374(84)	120(69)	20(71)	-66(66)	66(62)
C(12H)	564(107	271(89)	541(117	-28(77)	99(93)	89(86)

The anisotropic displacement exponent takes the form:

$-2\pi^2(h^2a^{*2}U_{11} + \ldots + 2hka^*b^*U_{12})$

Table 5. H-Atom coordinates ($x10^4$) and isotropic displacement coefficients ($Å^2 x10^3$)

	x	y	z	U
H(3HA)	3405	3419	506	80
H(3HB)	2911	3611	1258	80
H(3HC)	3643	2925	1234	80
H(4HA)	3805	1330	89	80
H(4HB)	3887	1455	957	80
H(4HC)	3407	671	639	80
H(5HA)	1889	479	-568	80
H(5HB)	2174	99	203	80
H(5HC)	1173	285	42	80
H(6HA)	209	1921	-490	80
H(6HB)	25	1267	140	80
H(6HC)	-145	2209	293	80
H(7HA)	1156	3794	189	80
H(7HB)	499	3434	785	80
H(7HC)	1390	3841	1043	80
H(8HA)	489	118	4342	80
H(8HB)	263	755	3708	80
H(8HC)	102	-192	3577	80
H(9HA)	2088	1660	4252	80
H(9HB)	2366	2008	3467	80
H(9HC)	1363	1857	3648	80
H(10A)	4024	931	3528	80
H(10B)	4052	700	2676	80
H(10C)	3563	1508	2938	80
H(11A)	3720	-1236	3198	80
H(11B)	3169	-1441	2477	80
H(11C)	3849	-708	2469	80
H(12A)	1549	-1725	3690	80
H(12B)	818	-1424	3129	80
H(12C)	1705	-1799	2824	80
H(1IR)	1157	1582	1426	50
H(2IR)	1422	-119	2220	50

Appendix C

Supplementary X-ray Data for [Cp^Ir(CO)H]2

Table 1. Atomic coordinates ($x10^5$) and equivalent isotropic displacement coefficients ($Å^2 x10^4$)

	x	y	z	U(eq)
Ir(1)	3640(1)	9429(3)	19884(2)	157(1)
C(1)	-1483(32)	28936(89)	14965(43)	252(24)
O(1)	-4808(31)	40972(57)	11731(41)	411(24)
C(3)	12572(32)	5623(91)	15562(49)	262(26)
C(3M)	12628(39)	11982(102)	7393(48)	339(30)
C(4)	10236(31)	-10389(78)	17012(45)	232(25)
C(4M)	7182(36)	-24117(90)	10180(50)	376(30)
C(5)	11856(32)	-11588(79)	26356(46)	229(24)
C(5M)	10945(38)	-27234(89)	30781(52)	343(28)
C(6)	15531(27)	3737(87)	30761(40)	193(21)
C(8E)	18955(34)	6889(97)	40798(44)	293(26)
C(9E)	26702(35)	-137(109)	45574(48)	387(29)
C(7)	15915(30)	14400(85)	24341(42)	207(23)
C(7M)	19686(35)	31308(92)	25962(53)	371(29)

* Equivalent isotropic U defined as one third of the trace of the orthogonalized U_{ij} tensor

Table 2. Bond lengths (Å)

Ir(1)-C(1)	1.828 (7)	Ir(1)-C(3)	2.256 (8)
Ir(1)-C(4)	2.249 (7)	Ir(1)-C(5)	2.244 (6)
Ir(1)-C(6)	2.293 (5)	Ir(1)-C(7)	2.276 (6)
Ir(1)-Ir(1A)	2.724 (1)	C(1)-O(1)	1.146 (8)
C(3)-C(3M)	1.458 (12)	C(3)-C(4)	1.411 (10)
C(3)-C(7)	1.473 (10)	C(4)-C(4M)	1.486 (9)
C(4)-C(5)	1.441 (11)	C(5)-C(5M)	1.495 (11)
C(5)-C(6)	1.434 (9)	C(6)-C(8E)	1.509 (9)
C(6)-C(7)	1.394 (10)	C(8E)-C(9E)	1.500 (9)
C(7)-C(7M)	1.501 (10)		

Table 3. Bond angles (°)

C(1)-Ir(1)-C(3)	110.0(3)	C(1)-Ir(1)-C(4)	139.6(3)
C(3)-Ir(1)-C(4)	36.5(3)	C(1)-Ir(1)-C(5)	169.0(3)
C(3)-Ir(1)-C(5)	61.9(3)	C(4)-Ir(1)-C(5)	37.4(3)
C(1)-Ir(1)-C(6)	133.8(2)	C(3)-Ir(1)-C(6)	61.5(2)
C(4)-Ir(1)-C(6)	61.5(2)	C(5)-Ir(1)-C(6)	36.8(2)
C(1)-Ir(1)-C(7)	108.0(3)	C(3)-Ir(1)-C(7)	37.9(2)
C(4)-Ir(1)-C(7)	61.5(2)	C(5)-Ir(1)-C(7)	61.0(2)
C(6)-Ir(1)-C(7)	35.5(2)	C(1)-Ir(1)-Ir(1A)	85.5(3)
C(3)-Ir(1)-Ir(1A)	161.3(2)	C(4)-Ir(1)-Ir(1A)	132.9(2)
C(5)-Ir(1)-Ir(1A)	101.2(2)	C(6)-Ir(1)-Ir(1A)	100.3(2)
C(7)-Ir(1)-Ir(1A)	128.4(2)	Ir(1)-C(1)-O(1)	178.5(5)
Ir(1)-C(3)-C(3M)	127.4(5)	Ir(1)-C(3)-C(4)	71.5(5)
C(3M)-C(3)-C(4)	128.2(7)	Ir(1)-C(3)-C(7)	71.8(4)
C(3M)-C(3)-C(7)	124.7(6)	C(4)-C(3)-C(7)	106.8(7)
Ir(1)-C(4)-C(3)	72.0(4)	Ir(1)-C(4)-C(4M)	126.5(4)
C(3)-C(4)-C(4M)	125.2(7)	Ir(1)-C(4)-C(5)	71.1(4)
C(3)-C(4)-C(5)	108.5(6)	C(4M)-C(4)-C(5)	126.0(6)
Ir(1)-C(5)-C(4)	71.5(3)	Ir(1)-C(5)-C(5M)	128.1(5)
C(4)-C(5)-C(5M)	124.8(6)	Ir(1)-C(5)-C(6)	73.5(3)
C(4)-C(5)-C(6)	107.7(6)	C(5M)-C(5)-C(6)	126.8(6)
Ir(1)-C(6)-C(5)	69.7(3)	Ir(1)-C(6)-C(8E)	128.5(5)
C(5)-C(6)-C(8E)	124.9(6)	Ir(1)-C(6)-C(7)	71.6(3)
C(5)-C(6)-C(7)	108.5(6)	C(8E)-C(6)-C(7)	126.4(6)
C(6)-C(8E)-C(9E)	111.1(7)	Ir(1)-C(7)-C(3)	70.3(4)
Ir(1)-C(7)-C(6)	72.9(3)	C(3)-C(7)-C(6)	108.5(6)
Ir(1)-C(7)-C(7M)	126.9(5)	C(3)-C(7)-C(7M)	124.1(7)
C(6)-C(7)-C(7M)	127.2(6)		

Table 4. Anisotropic displacement coefficients ($Å^2 x 10^4$)

	U_{11}	U_{22}	U_{33}	U_{12}	U_{13}	U_{23}
Ir(1)	146(2)	220(2)	160(2)	11(1)	116(1)	7(1)
C(1)	273(29)	327(36)	275(33)	-41(30)	228(25)	-34(33)
O(1)	464(31)	317(29)	464(35)	171(23)	226(27)	97(24)
C(3)	172(28)	380(36)	333(39)	40(28)	201(27)	-43(36)
C(3M)	257(35)	660(56)	148(33)	-57(31)	134(29)	-3(33)
C(4)	161(29)	353(38)	231(35)	15(24)	133(26)	-97(28)
C(4M)	342(35)	391(43)	408(41)	18(31)	186(31)	-157(37)
C(5)	145(27)	290(35)	273(35)	54(25)	114(25)	1(30)
C(5M)	365(34)	299(34)	397(40)	69(31)	204(31)	55(36)
C(6)	82(23)	296(30)	231(32)	93(24)	97(22)	44(30)
C(8E)	225(31)	510(44)	170(33)	24(29)	113(27)	11(33)
C(9E)	258(32)	607(54)	267(37)	24(33)	98(28)	-13(38)
C(7)	166(27)	283(32)	194(32)	1(26)	103(24)	-28(30)
C(7M)	293(32)	422(46)	420(42)	-55(32)	183(30)	-10(37)

The anisotropic displacement exponent takes the form:

$-2\pi^2(h^2a^{*2}U_{11} + \ldots + 2hka^*b^*U_{12})$

Table 5. H-Atom coordinates ($x10^4$) and isotropic displacement coefficients ($Å^2 x10^3$)

	x	y	z	U
H(1H)	-6971(2395)	9505(3181)	3411(3164	2288(313)
H(3MA)	1716	859	734	50
H(3MB)	846	707	231	50
H(3MC)	1222	2409	704	50
H(4MA)	1118	-3086	1033	50
H(4MB)	398	-3108	1160	50
H(4MC)	438	-1938	426	50
H(5MA)	1532	-3415	3282	50
H(5MB)	1027	-2379	3587	50
H(5MC)	668	-3360	2667	50
H(8EA)	1586	213	4317	50
H(8EB)	1925	1887	4184	50
H(9EA)	2876	217	5192	50
H(9EB)	2641	-1215	4462	50
H(9ED)	2983	475	4328	50
H(7MD)	2490	2984	2782	50
H(7MA)	1746	3776	2047	50
H(7MB)	1906	3720	3059	50

Appendix D

Supplementary X-ray Data for {[$Cp^*Ir(CO)]_2(\mu\text{-}CO)(\mu\text{-}H)$}OTf

Table 1. Atomic coordinates ($x10^5$) and equivalent isotropic displacement coefficients ($Å^2 x10^4$)

	x	y	z	U(eq)
Ir(1)	26013(5)	1604(2)	72773(3)	153(1)
C(1)	22091(126)	-6764(39)	69251(64)	169(30)
C(1M)	28200(152)	-9697(44)	61444(78)	308(38)
C(2)	31858(139)	-6567(42)	79554(74)	226(34)
C(2M)	49137(147)	-9298(50)	84086(83)	332(40)
C(3)	20606(134)	-3896(41)	84457(72)	224(34)
C(3M)	24474(144)	-3135(40)	95382(69)	244(36)
C(4)	4378(136)	-2622(40)	77648(75)	219(34)
C(4M)	-11879(142)	-415(45)	79904(85)	296(39)
C(5)	4989(124)	-4445(39)	68099(69)	183(31)
C(5M)	-9839(137)	-4288(44)	58863(77)	287(36)
C(11)	15289(153)	10554(42)	88970(85)	288(39)
O(1)	7805(116)	9953(34)	94912(56)	398(32)
C(12)	10181(121)	7981(37)	68664(71)	171(32)
O(2)	-3206(89)	8877(29)	62624(50)	259(25)
C(13)	41107(136)	2896(43)	64805(83)	270(37)
O(3)	49601(102)	3387(31)	59329(56)	318(29)
Ir(2)	27331(5)	12076(2)	79451(3)	153(1)
C(6)	49026(143)	18081(39)	85262(74)	233(35)
C(6M)	62766(165)	18299(42)	94988(79)	326(40)
C(7)	51780(131)	16183(40)	76375(74)	207(33)
C(7M)	68627(141)	13748(44)	75378(93)	336(41)
C(8)	36030(140)	17255(39)	68580(71)	206(33)
C(8M)	33495(167)	16275(47)	57692(75)	328(41)
C(9)	23918(132)	19925(42)	72652(72)	203(33)
C(9M)	6564(161)	22348(48)	66884(90)	369(43)
C(10)	31444(138)	20420(42)	82955(75)	222(33)
C(10M)	23772(168)	23563(47)	89990(84)	348(43)
S(1)	17898(37)	18443(11)	30146(20)	271(9)
O(1S)	27663(124)	23293(36)	31434(63)	472(35)
O(2S)	28447(119)	13699(37)	31877(64)	469(34)
O(3S)	2864(117)	18356(32)	34075(63)	399(33)
C(1S)	8240(172)	18161(48)	16791(93)	381(45)
F(1)	20602(118)	18348(31)	11984(54)	555(33)
F(2)	-2866(114)	22082(34)	13745(59)	638(33)
F(3)	-1045(117)	13884(31)	14088(55)	578(32)

* Equivalent isotropic U defined as one third of the trace of the orthogonalized U_{ij} tensor

Table 2. Bond lengths (Å)

Ir(1)-C(1)	2.199 (10)	Ir(1)-C(2)	2.292 (11)
Ir(1)-C(3)	2.287 (11)	Ir(1)-C(4)	2.257 (11)
Ir(1)-C(5)	2.222 (10)	Ir(1)-C(12)	2.034 (9)
Ir(1)-C(13)	1.857 (12)	Ir(1)-Ir(2)	2.831 (1)
C(1)-C(1M)	1.508 (16)	C(1)-C(2)	1.450 (12)
C(1)-C(5)	1.428 (14)	C(2)-C(2M)	1.501 (15)
C(2)-C(3)	1.425 (16)	C(3)-C(3M)	1.500 (14)
C(3)-C(4)	1.408 (13)	C(4)-C(4M)	1.496 (17)
C(4)-C(5)	1.436 (15)	C(5)-C(5M)	1.494 (12)
C(11)-O(1)	1.150 (16)	C(11)-Ir(2)	1.869 (13)
C(12)-O(2)	1.180 (10)	C(12)-Ir(2)	2.028 (9)
C(13)-O(3)	1.148 (15)	Ir(2)-C(6)	2.270 (10)
Ir(2)-C(7)	2.314 (11)	Ir(2)-C(8)	2.260 (11)
Ir(2)-C(9)	2.209 (11)	Ir(2)-C(10)	2.194 (11)
C(6)-C(6M)	1.499 (14)	C(6)-C(7)	1.410 (16)
C(6)-C(10)	1.450 (15)	C(7)-C(7M)	1.492 (16)
C(7)-C(8)	1.439 (13)	C(8)-C(8M)	1.514 (15)
C(8)-C(9)	1.404 (16)	C(9)-C(9M)	1.513 (15)
C(9)-C(10)	1.419 (14)	C(10)-C(10M)	1.516 (18)
S(1)-O(1S)	1.441 (10)	S(1)-O(2S)	1.449 (10)
S(1)-O(3S)	1.422 (11)	S(1)-C(1S)	1.832 (12)
C(1S)-F(1)	1.316 (18)	C(1S)-F(2)	1.319 (15)
C(1S)-F(3)	1.311 (15)		

Table 3. Bond angles (°)

C(1)-Ir(1)-C(2)	37.6(3)	C(1)-Ir(1)-C(3)	61.5(4)
C(2)-Ir(1)-C(3)	36.3(4)	C(1)-Ir(1)-C(4)	62.1(4)
C(2)-Ir(1)-C(4)	61.2(4)	C(3)-Ir(1)-C(4)	36.1(3)
C(1)-Ir(1)-C(5)	37.7(4)	C(2)-Ir(1)-C(5)	62.5(3)
C(3)-Ir(1)-C(5)	61.5(3)	C(4)-Ir(1)-C(5)	37.4(4)
C(1)-Ir(1)-C(12)	132.7(3)	C(2)-Ir(1)-C(12)	152.6(4)
C(3)-Ir(1)-C(12)	119.0(4)	C(4)-Ir(1)-C(12)	91.4(4)
C(5)-Ir(1)-C(12)	97.5(4)	C(1)-Ir(1)-C(13)	96.3(4)
C(2)-Ir(1)-C(13)	109.0(4)	C(3)-Ir(1)-C(13)	144.2(4)
C(4)-Ir(1)-C(13)	155.8(4)	C(5)-Ir(1)-C(13)	118.7(4)
C(12)-Ir(1)-C(13)	96.8(4)	C(1)-Ir(1)-Ir(2)	170.3(3)
C(2)-Ir(1)-Ir(2)	137.6(3)	C(3)-Ir(1)-Ir(2)	109.9(3)
C(4)-Ir(1)-Ir(2)	108.4(3)	C(5)-Ir(1)-Ir(2)	135.7(3)
C(12)-Ir(1)-Ir(2)	45.7(2)	C(13)-Ir(1)-Ir(2)	93.4(3)
Ir(1)-C(1)-C(1M)	126.6(7)	Ir(1)-C(1)-C(2)	74.7(6)
C(1M)-C(1)-C(2)	124.3(9)	Ir(1)-C(1)-C(5)	72.0(6)
C(1M)-C(1)-C(5)	126.1(8)	C(2)-C(1)-C(5)	109.0(9)
Ir(1)-C(2)-C(1)	67.7(5)	Ir(1)-C(2)-C(2M)	131.2(8)
C(1)-C(2)-C(2M)	125.7(10)	Ir(1)-C(2)-C(3)	71.7(6)
C(1)-C(2)-C(3)	105.9(8)	C(2M)-C(2)-C(3)	127.9(9)
Ir(1)-C(3)-C(2)	72.1(6)	Ir(1)-C(3)-C(3M)	129.3(7)
C(2)-C(3)-C(3M)	125.2(9)	Ir(1)-C(3)-C(4)	70.8(6)
C(2)-C(3)-C(4)	109.7(9)	C(3M)-C(3)-C(4)	124.7(10)
Ir(1)-C(4)-C(3)	73.1(6)	Ir(1)-C(4)-C(4M)	128.8(7)
C(3)-C(4)-C(4M)	126.9(10)	Ir(1)-C(4)-C(5)	70.0(6)
C(3)-C(4)-C(5)	108.4(9)	C(4M)-C(4)-C(5)	124.2(8)
Ir(1)-C(5)-C(1)	70.3(5)	Ir(1)-C(5)-C(4)	72.6(6)
C(1)-C(5)-C(4)	106.8(8)	Ir(1)-C(5)-C(5M)	125.3(7)
C(1)-C(5)-C(5M)	126.4(9)	C(4)-C(5)-C(5M)	126.6(9)
O(1)-C(11)-Ir(2)	175.7(10)	Ir(1)-C(12)-O(2)	135.6(7)
Ir(1)-C(12)-Ir(2)	88.4(3)	O(2)-C(12)-Ir(2)	136.1(8)
Ir(1)-C(13)-O(3)	174.1(9)	Ir(1)-Ir(2)-C(11)	93.5(3)
Ir(1)-Ir(2)-C(12)	45.9(3)	C(11)-Ir(2)-C(12)	94.2(4)
Ir(1)-Ir(2)-C(6)	135.9(3)	C(11)-Ir(2)-C(6)	110.5(4)
C(12)-Ir(2)-C(6)	154.1(4)	Ir(1)-Ir(2)-C(7)	109.1(3)
C(11)-Ir(2)-C(7)	145.4(4)	C(12)-Ir(2)-C(7)	120.4(4)
C(6)-Ir(2)-C(7)	35.8(4)	Ir(1)-Ir(2)-C(8)	108.7(3)
C(11)-Ir(2)-C(8)	154.9(4)	C(12)-Ir(2)-C(8)	93.0(4)
C(6)-Ir(2)-C(8)	61.3(4)	C(7)-Ir(2)-C(8)	36.7(3)
Ir(1)-Ir(2)-C(9)	136.5(3)	C(11)-Ir(2)-C(9)	118.3(4)
C(12)-Ir(2)-C(9)	99.5(4)	C(6)-Ir(2)-C(9)	62.2(3)
C(7)-Ir(2)-C(9)	61.1(4)	C(8)-Ir(2)-C(9)	36.6(4)
Ir(1)-Ir(2)-C(10)	170.0(3)	C(11)-Ir(2)-C(10)	96.4(5)
C(12)-Ir(2)-C(10)	134.3(4)	C(6)-Ir(2)-C(10)	37.9(4)
C(7)-Ir(2)-C(10)	61.5(4)	C(8)-Ir(2)-C(10)	62.0(4)
C(9)-Ir(2)-C(10)	37.6(4)	Ir(2)-C(6)-C(6M)	129.6(8)
Ir(2)-C(6)-C(7)	73.8(6)	C(6M)-C(6)-C(7)	125.7(10)
Ir(2)-C(6)-C(10)	68.3(6)	C(6M)-C(6)-C(10)	126.3(10)
C(7)-C(6)-C(10)	107.4(8)	Ir(2)-C(7)-C(6)	70.4(6)
Ir(2)-C(7)-C(7M)	128.0(7)	C(6)-C(7)-C(7M)	124.8(9)
Ir(2)-C(7)-C(8)	69.6(6)	C(6)-C(7)-C(8)	108.2(9)
C(7M)-C(7)-C(8)	126.9(10)	Ir(2)-C(8)-C(7)	73.7(6)
Ir(2)-C(8)-C(8M)	127.4(7)	C(7)-C(8)-C(8M)	126.6(10)
Ir(2)-C(8)-C(9)	69.7(6)	C(7)-C(8)-C(9)	108.1(9)
C(8M)-C(8)-C(9)	124.9(9)	Ir(2)-C(9)-C(8)	73.6(6)
Ir(2)-C(9)-C(9M)	126.3(8)	C(8)-C(9)-C(9M)	125.5(9)

Ir(2)-C(9)-C(10)	70.6(6)	C(8)-C(9)-C(10)	108.7(8)
C(9M)-C(9)-C(10)	125.5(10)	Ir(2)-C(10)-C(6)	73.9(6)
Ir(2)-C(10)-C(9)	71.8(6)	C(6)-C(10)-C(9)	107.6(10)
Ir(2)-C(10)-C(10M)	127.1(8)	C(6)-C(10)-C(10M)	125.8(9)
C(9)-C(10)-C(10M)	126.0(9)	O(1S)-S(1)-O(2S)	116.3(5)
O(1S)-S(1)-O(3S)	115.2(6)	O(2S)-S(1)-O(3S)	114.2(6)
O(1S)-S(1)-C(1S)	102.9(5)	O(2S)-S(1)-C(1S)	101.5(5)
O(3S)-S(1)-C(1S)	104.0(6)	S(1)-C(1S)-F(1)	111.6(8)
S(1)-C(1S)-F(2)	111.1(9)	F(1)-C(1S)-F(2)	108.1(11)
S(1)-C(1S)-F(3)	112.1(9)	F(1)-C(1S)-F(3)	107.7(11)
F(2)-C(1S)-F(3)	106.0(10)		

Table 4. Anisotropic displacement coefficients ($Å^2 x 10^4$)

	U_{11}	U_{22}	U_{33}	U_{12}	U_{13}	U_{23}
Ir(1)	98(2)	224(2)	108(2)	-10(2)	-27(2)	-13(1)
C(1)	174(50)	209(51)	61(43)	-9(40)	-81(37)	-36(37)
C(1M)	298(62)	328(65)	214(58)	49(50)	-82(49)	-101(46)
C(2)	200(52)	222(55)	255(55)	1(44)	59(46)	-8(42)
C(2M)	243(59)	464(74)	249(60)	14(54)	-9(49)	42(52)
C(3)	206(54)	269(55)	176(52)	-5(45)	13(44)	111(43)
C(3M)	280(59)	239(59)	165(54)	-35(45)	-25(45)	28(40)
C(4)	183(52)	265(58)	222(55)	-21(42)	74(45)	30(41)
C(4M)	187(55)	375(69)	331(64)	-64(48)	76(49)	-73(50)
C(5)	123(47)	213(51)	167(50)	-76(41)	-41(40)	-7(38)
C(5M)	170(53)	361(63)	249(59)	-49(48)	-85(45)	-34(47)
C(11)	290(61)	256(62)	310(64)	-117(47)	66(53)	16(46)
O(1)	493(53)	536(55)	249(44)	-205(45)	244(42)	-100(38)
C(12)	93(47)	172(52)	254(53)	78(37)	56(43)	81(40)
O(2)	173(37)	320(43)	227(39)	32(32)	-49(32)	-13(32)
C(13)	105(49)	349(66)	321(62)	-45(44)	-4(48)	-34(47)
O(3)	224(41)	429(52)	323(45)	2(35)	108(37)	-50(35)
Ir(2)	113(2)	222(2)	88(2)	-10(2)	-33(1)	-6(2)
C(6)	220(56)	295(61)	167(53)	-93(45)	22(44)	37(42)
C(6M)	369(69)	356(68)	160(55)	-95(52)	-94(50)	-24(44)
C(7)	153(50)	238(54)	208(53)	-29(42)	9(43)	-8(41)
C(7M)	148(54)	329(66)	510(76)	-75(47)	53(53)	-23(54)
C(8)	212(54)	243(55)	141(51)	-9(43)	10(43)	33(40)
C(8M)	428(72)	428(71)	137(55)	-82(57)	91(52)	-22(47)
C(9)	196(52)	220(55)	186(53)	1(43)	37(44)	68(41)
C(9M)	351(67)	367(69)	390(70)	88(57)	100(57)	174(56)
C(10)	203(52)	264(57)	179(52)	52(45)	17(44)	16(42)
C(10M)	378(69)	419(75)	282(62)	-16(55)	150(55)	-66(50)
S(1)	204(14)	391(17)	203(14)	34(12)	29(11)	14(11)
O(1S)	491(57)	520(59)	365(50)	-121(45)	44(44)	-138(43)
O(2S)	413(54)	633(63)	375(49)	254(45)	129(42)	211(45)
O(3S)	374(51)	492(58)	360(49)	53(40)	150(41)	-5(38)
C(1S)	312(69)	465(80)	313(68)	-49(57)	-9(56)	-27(55)
F(1)	590(54)	816(64)	292(41)	-1(43)	176(40)	10(37)
F(2)	620(55)	617(55)	504(50)	244(44)	-156(43)	51(41)
F(3)	716(58)	499(49)	413(45)	-279(43)	-36(41)	-66(36)

The anisotropic displacement exponent takes the form:

$-2\pi^2(h^2a^{*2}U_{11} + \ldots + 2hka^*b^*U_{12})$

Table 5. H-Atom coordinates ($x10^4$) and isotropic displacement coefficients ($Å^2 x10^3$)

	x	y	z	U
H(1MA)	2477	-1330	6144	50
H(1MB)	2282	-818	5512	50
H(1MC)	4092	-946	6281	50
H(2MA)	4668	-1270	8627	50
H(2MB)	5554	-965	7916	50
H(2MC)	5619	-735	8957	50
H(3MA)	2082	-620	9826	50
H(3MB)	3699	-258	9815	50
H(3MC)	1798	-16	9673	50
H(4MA)	-1855	-319	8184	50
H(4MB)	-840	207	8517	50
H(4MC)	-1912	129	7415	50
H(5MA)	-1741	-729	5847	50
H(5MB)	-1674	-116	5866	50
H(5MC)	-462	-431	5341	50
H(6MA)	6995	2137	9524	50
H(6MB)	5708	1840	10026	50
H(6MC)	7017	1525	9566	50
H(7MA)	7608	1650	7409	50
H(7MB)	7470	1194	8129	50
H(7MC)	6599	1134	6996	50
H(8MA)	3874	1905	5483	50
H(8MB)	3875	1300	5664	50
H(8MC)	2091	1617	5466	50
H(9MA)	854	2583	6484	50
H(9MB)	196	2020	6118	50
H(9MC)	-185	2245	7078	50
H(10A)	2743	2716	9024	50
H(10B)	1102	2337	8786	50
H(10C)	2789	2203	9642	50

David Andrew Fine was born October 12, 1962 in Los Angeles, California. He attended Revelle College of the University of California at San Diego (UCSD). He spent the 1983/84 academic year in the Chemistry and Biochemistry programs at Birmingham University, England, as part of the Education Abroad Program. He graduated from UCSD with a Bachelor of Arts in Chemistry and a minor in Visual Arts in June of 1985. He worked from 1985 to 1987 for Calvert Environmental Equipment, Inc., supervising and executing field performance tests of air pollution control pilot systems. From 1988 through 1991 he was employed as Senior Chemist, and then promoted to Associate Scientist for Metanetix, Inc., assisting in the research and development of new technologies for removal of heavy metals from industrial process streams. In the fall of 1991, he began graduate work in chemistry at the University of Washington. Under the guidance of Professor D. M. Heinekey, he earned a Doctor of Philosophy in Inorganic Chemistry in November of 1996.